

In vitro and *in vivo* analyses of mono- and mixed-species biofilms
formed by microbial pathogens

Inauguraldissertation

zur

Erlangung des akademischen Grades eines

Doktors der Naturwissenschaften
(Dr. rer. nat.)

der

Mathematisch-Naturwissenschaftlichen Fakultät

der

Universität Greifswald

vorgelegt von
Alexander Christian Graf
geboren am 16.08.1989
in Frankenberg/Sa

Greifswald, Oktober 2021

Dekan: Prof. Dr. Gerald Kerth

1. Gutachter: Prof. Dr. Riedel
2. Gutachter: Prof. Dr. Otto (Boston)

Tag der Promotion: 31.01.2022

Table of Contents

1	ZUSAMMENFASSUNG.....	1
2	SUMMARY	3
3	INTRODUCTION	5
3.1	MICROBIAL BIOFILMS	5
3.1.1	Definition, Scientific History, and Characteristics of Microbial Biofilms.....	5
3.1.2	The Biofilm Life Cycle	6
3.1.3	The Extracellular Matrix	8
3.2	THE ROLE OF MICROBIAL BIOFILMS IN INDUSTRY AND HEALTH CARE	12
3.2.1	Harmful Microbial Biofilms in Industry.....	12
3.2.2	The Burden of Microbial Biofilms in Health Care	13
3.2.3	Cystic Fibrosis.....	15
3.3	<i>STAPHYLOCOCCUS AUREUS</i>	17
3.3.1	<i>S. aureus</i> Infections	17
3.3.2	Methicillin-resistant <i>Staphylococcus aureus</i> (MRSA)	18
3.3.3	Virulence Factors of <i>S. aureus</i>	19
3.3.4	<i>S. aureus</i> Biofilm Formation.....	20
3.4	<i>CANDIDA ALBICANS</i>	22
3.5	STRATEGIES COMBATING MICROBIAL BIOFILMS.....	23
3.5.1	Preventing the Initial Step of Biofilm Formation	23
3.5.2	Eradicating Established Biofilms.....	24
3.5.3	Nonthermal Plasma as a new Antibiofilm weapon.....	26
4	ARTICLE I: VIRULENCE FACTORS PRODUCED BY <i>STAPHYLOCOCCUS AUREUS</i> BIOFILMS HAVE A MOONLIGHTING FUNCTION CONTRIBUTING TO BIOFILM INTEGRITY.....	28
5	ARTICLE II: AN INNOVATIVE PROTOCOL FOR METAPROTEOMIC ANALYSES OF MICROBIAL PATHOGENS IN CYSTIC FIBROSIS SPUTUM.....	48
6	ARTICLE III: NONTHERMAL PLASMA JET TREATMENT NEGATIVELY AFFECTS THE VIABILITY AND STRUCTURE OF <i>CANDIDA ALBICANS</i> SC5314 BIOFILMS	67
7	ARTICLE IV: ANTIMICROBIAL EFFECTS OF MICROWAVE-INDUCED PLASMATORCH (MINIMIP) TREATMENT ON <i>CANDIDA ALBICANS</i> BIOFILMS.....	83

8	CONCLUSIONS	99
9	REFERENCES	101
10	EIGENSTÄNDIGKEITSERKLÄRUNG	107
11	<i>CURRICULUM VITAE</i>	108
12	LIST OF PUBLICATIONS	110
12.1	PEER-REVIEWED PUBLICATIONS.....	110
12.2	ORAL PRESENTATIONS	110
12.3	POSTER PRESENTATIONS.....	111
13	ACKNOWLEDGEMENTS	112

Abbreviations

AFM	Atomic force microscopy
CF	Cystic fibrosis
CFU	Colony forming unit
CLSM	Confocal laser scanning microscopy
ECM	Extracellular matrix
EDTA	Ethylenediaminetetraacetic acid
EPS	Extracellular polymeric substances
Ica	Intercellular adhesion
LC-MS/MS	Liquid chromatography tandem mass-spectrometry
MSCRAMMs	Microbial surface components recognizing adhesive matrix molecules
NTPs	Nonthermal plasmas
PIA	Polysaccharide intercellular adhesin
WHO	World Health Organization

1 Zusammenfassung

Mikrobielle Biofilme sind ubiquitär verbreitete, multizelluläre Aggregate, welche in eine selbst-produzierte, extrazelluläre Matrix (ECM) eingebettet sind. Diese extrazelluläre Matrix besteht hauptsächlich aus polymeren Substanzen wie beispielsweise Proteinen und extrazellulärer DNA. Im infektionsbiologischen Kontext sind insbesondere Patienten, die ein medizinisches Implantat erhalten haben oder an Mukoviszidose leiden, anfällig für Biofilm-Infektionen. Sobald sich ein Biofilm etabliert hat, ist eine quantitative Entfernung der biofilm-assoziierten Zellen durch mechanische, chemische, enzymatische oder antibiotische Behandlung nahezu unmöglich, wodurch oftmals eine Entfernung des betroffenen Implantats oder Körperteils die letzte Behandlungsoption darstellt. Dies kann durch eine reduzierte metabolische Aktivität der Zellen (bis hin zur metabolischen Inaktivität von sog. Persister-Zellen) sowie durch den Schutz der extrazellulären Matrix, die als effektive (Diffusions-) Barriere gegen Antibiotika und das Immunsystem wirkt, bedingt sein. Diese Schlüsseleigenschaften verleihen Biofilm-assoziierten Zellen eine massiv erhöhte Toleranz gegenüber Antibiotika, machen Biofilme zu einer der größten Infektions-assoziierten Belastungen und Gefahren im Gesundheitswesen und verursachen weltweit jährliche Behandlungskosten in Milliardenhöhe. Dies unterstreicht die Notwendigkeit, die Struktur und Funktion mikrobieller Biofilme besser zu verstehen, um so innovative Behandlungsstrategien entwickeln zu können. Daher war es das Ziel dieser Arbeit, grundlegende strukturelle sowie patho-physiologische Eigenschaften wichtiger bakterieller und fungaler Biofilm-Bildner *in vitro* und *in vivo* zu untersuchen, sowie die Wirksamkeit einer neuen Behandlungsstrategie durch Niedertemperaturplasmen *in vitro* zu evaluieren.

In Publikation I wurde das intrazelluläre sowie das Proteom der extrazellulären Matrix von einem der wichtigsten Biofilm-Bildner – *Staphylococcus aureus* – mittels Flüssigkeits-chromatographie-gekoppelter Tandem-Massenspektrometrie (LC-MS/MS) analysiert. Hierfür wurden die Biofilme *in vitro* in einem Durchflussreaktor kultiviert. Struktur und Zusammensetzung des Biofilms wurden mit Hilfe globaler Proteom- und Metabolomanalysen sowie mikroskopischen Untersuchungen charakterisiert. Es konnte gezeigt werden, dass der anaerobe Metabolismus der Biofilm-assoziierten Zellen durch die Sekretion organischer Säuren zu einer Absenkung des pH-Werts der ECM führt. Diese Ansäuerung wiederum führt zur Protonierung alkalischer ECM Proteine, darunter vornehmlich ribosomale Proteine, die durch Zellyse freigesetzt werden sowie aktiv sekretierte Virulenzfaktoren. Diese positiv geladenen, alkalischen Proteine akkumulieren in der Folge in der ECM und bilden ein elektrostatisches Netzwerk mit negativ-geladenen Zelloberflächen, eDNA und Metaboliten, was gesamtheitlich zur Biofilmstabilität beiträgt.

In Publikation II wurde die Zusammensetzung und der physiologische Zustand mikrobieller Biofilme aus Sputum-Proben von Mukoviszidose-Patienten mittels Metaproteom-Analysen untersucht. Diese Multispezies-Biofilme spielen eine entscheidende Rolle für das Fortschreiten der Krankheit, konnten bisher jedoch auf Proteomebene aufgrund ihrer Komplexität nur schwer analysiert werden. Daher wurde erstmals ein Aufarbeitungsprotokoll etabliert, das es erlaubt, Mikroorganismen aus Sputum-Proben mit geringem Volumen anzureichern, Proteine zu extrahieren und mittels Metaproteom-Analysen zu charakterisieren. Zusätzlich konnten aus derselben Sputum-Probe 16S Sequenzierungen, Messungen der extrazelluläre Metabolite sowie mikroskopische Analysen durchgeführt werden. Durch die Anwendung dieses Protokolls war es möglich, die Anzahl identifizierter Proteine signifikant zu erhöhen, sodass erste Einblicke in die Pathophysiologie von Schlüsselkeimen der CF-Lunge auf Proteom-Ebene gewonnen werden konnten. Diese ersten Metaproteom-Daten zeigen, dass der Arginin-Deaminase-Stoffwechselweg sowie mikrobielle Proteasen eine bisher unterschätzte Rolle im Infektionsgeschehen spielen könnten.

In Publikation III und IV wurde eine innovative Strategie zur Bekämpfung von Biofilmen des pathogenen Pilzes *Candida albicans* mittels Niedertemperatur-Plasmen evaluiert. Hierfür wurden *C. albicans* Biofilme mit zwei verschiedenen Plasmaquellen (mit dem sog. Nonthermal Plasma Jet "kINPen09" sowie der sog. Microwave-induced plasma torch "MiniMIP") behandelt. Der Effekt auf das Wachstum, Überleben und die Vitalität wurden mittels Bestimmung der Kolonie-bildenden Einheiten (engl. CFU), Zellproliferations-Assays, sowie Lebend-Tot-Färbung kombiniert mit Fluoreszenz- und konfokaler Laser-Scanning-Mikroskopie (engl. CLSM) bestimmt. Strukturelle Auswirkungen auf behandelte *C. albicans* Biofilme wurden zudem mittels Rasterkraftmikroskopie (engl. AFM) untersucht. Diese Experimente zeigten, dass die Behandlung mit beiden Plasma-Quellen jeweils einen starken Inaktivierungs-Effekt auf *C. albicans* Biofilme hat – vornehmlich auf der Unterseite der Biofilme – was das große Potential dieser beiden Plasma-Quellen im Kampf gegen mikrobielle Biofilme aufzeigt.

2 Summary

Microbial biofilms can be defined as multicellular clusters of microorganisms embedded in a self-produced extracellular matrix (ECM), which is primarily composed of polymeric biomolecules. Biofilms represent one of the most severe burdens in both industry and healthcare worldwide, causing billions of dollars of treatment costs annually because biofilms are inherently difficult to prevent, treat, and eradicate. In health care settings, patients suffering from cystic fibrosis, or patients with medical implants are highly susceptible to biofilm infections. Once a biofilm is formed, it is almost impossible to quantitatively eradicate it by mechanical, enzymatical, chemical, or antimicrobial treatment. Often the only remaining option to fully eradicate the biofilm is removing of the infected implant or body part. The primary reasons for the inherent resistance of biofilms against all forms of antimicrobial treatment are (I) a reduced metabolic activity of biofilm-embedded cells climaxing in the presence of metabolic inactive persister cells, as well as (II) the protective nature of the biofilm matrix acting as a (diffusion) barrier against antimicrobials and the host immune system. Consequently, there is an urgent need to better understand microbial biofilms from a structural and (patho-) physiological point of view in order to be able to develop new treatment strategies.

Therefore, the aims of this study were to investigate fundamental physiological properties of different clinically relevant single and multi-species biofilms, both *in vitro* and *in vivo*. Furthermore, the effectiveness of a novel treatment strategy using cold atmospheric pressure plasma was evaluated *in vitro* to treat biofilms of the pathogenic fungus *C. albicans*.

In article I, the intracellular and ECM protein inventory of *Staphylococcus aureus* during *in vitro* biofilm growth in a flow reactor was analyzed by liquid-chromatography coupled to tandem mass-spectrometry (LC-MS/MS) analysis combined with metabolic footprint analysis. This analysis showed that anaerobiosis within biofilms releases organic acids lowering the ECM pH. This, in turn, leads to protonation of alkaline proteins – mostly ribosomal proteins originating from cell lysis as well as actively secreted virulence factors – resulting in a positive net charge of these proteins. As a consequence, these proteins accumulate within the ECM and form an electrostatic network with negatively charged cell surfaces, eDNA, and metabolites contributing to the overall biofilm stability.

In article II, the *in vivo* metaproteome of the multi-species biofilm community in cystic fibrosis sputum was investigated. To this end, an innovative protocol was developed allowing the enrichment of microbial cells, the extraction of proteins from a small amount of cystic fibrosis sputum, and subsequent metaproteome analysis. This protocol also allows 16S sequencing, metabolic footprint analysis, and microscopy of the same sample to complement the metaproteome data. Applying this protocol, we were able to significantly enhance microbial

protein coverage providing first insights into important physiological pathways during CF lung infection. A key finding was that the arginine deaminase pathway as well as microbial proteases play a so far underappreciated role in CF pathophysiology.

In articles III and IV, a novel treatment strategy for biofilms formed by the important fungal pathogen *Candida albicans* was evaluated *in vitro*. Biofilms were treated with two different sources of nonthermal plasma (with the Nonthermal Plasma Jet “kINPen09” as well as with the Microwave-induced plasma torch “MiniMIP”) and the effect on growth, survival, and viability was assessed by counting colony-forming units (CFU), by cell proliferation assays, as well as by live/dead staining combined with fluorescence microscopy, confocal laser scanning microscopy, (CLSM) and atomic force microscopy (AFM). These tests revealed that biofilms were effectively inactivated mostly on the bottom side of biofilms, indicating a great potential of these two plasma sources to fight biofilms.

3 Introduction

3.1 Microbial Biofilms

3.1.1 Definition, Scientific History, and Characteristics of Microbial Biofilms

The vast majority of microorganisms in nature grow as biofilms, which can be defined as polymicrobial aggregates embedded in a primarily self-produced, hydrated extracellular matrix (ECM) composed of diverse polymeric substances. Frequently, these aggregates form on interphases as mats, flocs, sludge, or biofilms (1). Historically, Van Leeuwenhoek first observed microorganisms sticking to the surfaces of teeth and therewith could be considered being the discoverer of microbial biofilms (2, 3). Also, Louis Pasteur described and sketched bacterial aggregates derived from acetic wine (2). Other early publications mentioning the concept of biofilms were published by Angst in 1923 describing biofouling of ship bottoms by bacteria and by Henrici in 1933, stating that “for the most part water bacteria are not free-floating organisms, but grow upon submerged surfaces” (3-5). In the 1940s, Hekelekian and Heller, as well as Zobell published that bacterial growth in aquatic environments was enhanced on surfaces these bacteria attached to and that the bacterial load in the surrounding medium was substantially lower compared to the colonies on surfaces (6-8). The nowadays established designation “biofilm” was introduced by Costerton, one of the most important pioneers of biofilm research, when the phenomenon of bacterial biofilm formation was scientifically described in more detail for the first time back in 1978 (9-12).

The fact that microbial cells rarely live as free-floating (planktonic) cells but rather form polymicrobial aggregates represents a survival strategy, which is evolutionarily advantageous since microbial communities obtain multiple benefits from the formation of biofilms. Notably, the biofilm matrix acts as a protective shield against environmental, chemical, and mechanical stresses like desiccation, shear forces, protozoan grazing, antimicrobial compounds, and the host immune system (9, 10). Another characteristic of the biofilm mode of existence is the complex community behavior in mono- and mixed-species biofilms, which even lead to the comparisons of biofilms with “multicellular organisms” or “tissues of higher organisms” (11, 12). This advantageous community behavior ranges from (I) mutualism, e.g. by profiting from a shared ECM serving as a nutrient reservoir and an external digestion system dividing the metabolic burden, (II) commensalism, e.g. of aerobic and obligate anaerobic microorganisms in mixed-species biofilms, (III) eased horizontal gene transfer (e.g. of antibiotic resistance genes) due to close cell-to-cell proximity, and even (IV) altruism, where cells exhibit a behavior

comparable to programmed cell death in higher organisms (12, 13).

The ability to form biofilms is considered to be a nearly ubiquitous microbial feature, both spatially and taxonomically, and is seen to be the default mode of growth among microbes representing a fundamental survival strategy. In fact, biofilms are formed by the vast majority of microorganisms, including Gram-positive and Gram-negative, motile and non-motile, aerobic and anaerobic bacteria, as well as single-celled eukaryotes like yeast (14). Biofilms can be found in nearly every abiotic and biotic, nutrient-sufficient environment on earth, rendering them the most widely distributed and most successful form of life (8, 11, 12).

3.1.2 The Biofilm Life Cycle

The formation of complex, three-dimensional biofilm architectures is a highly coordinated and dynamic process. In general, biofilm formation can be described as a life cycle involving the following four simplified phases, regardless of the enormous diversity of biofilm-forming species, biofilm-formation kinetics, and morphologies (15): (I) attachment of single, planktonic cells to a surface, which is initially reversible, then irreversible due to first ECM production, (II) formation of a mono-layer/microcolonies, (III) biofilm growth/maturation forming the three-dimensional architecture, (IV) dispersal triggered by internal and external signals releasing cell aggregates and single cells for the colonization of novel niches (3, 11, 16) (Figure 1). Notably, each phase of the biofilm life-cycle is characterized by an individual gene expression pattern (17).

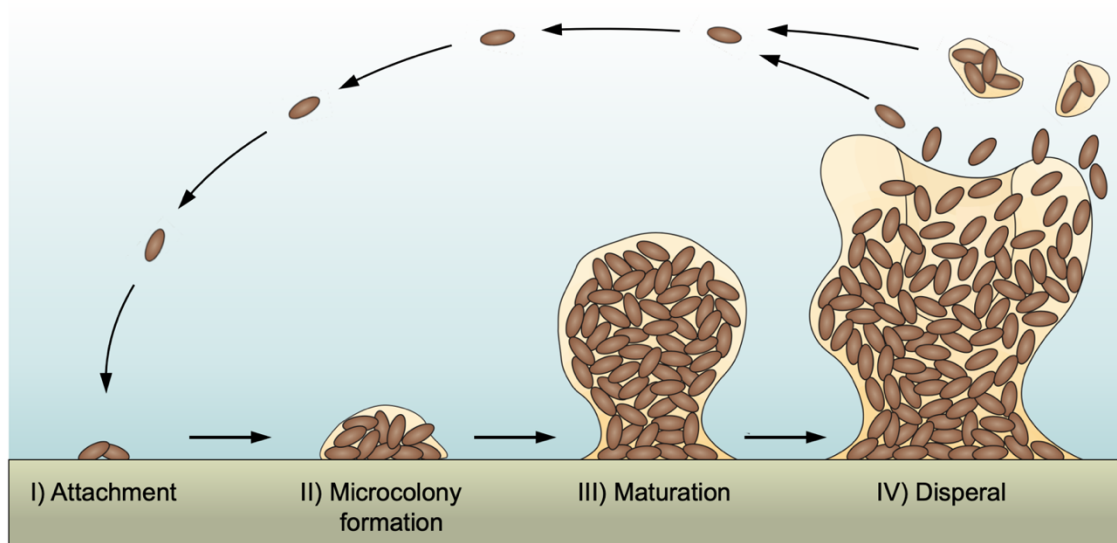


Figure 1: Illustration of the biofilm life cycle, modified from McDougald et al., 2011 (18).

The biofilm life cycle contains four simplified steps: (I) attachment of planktonic cells (first

reversible, then irreversible attachment due to first ECM production), (II) microcolony formation with formation of a mono-layer/microcolonies, (III) biofilm growth/maturation, which forms three-dimensional structures, (IV) dispersal releasing cell aggregates and single cells for the colonization of novel niches.

Before the biofilm life cycle starts with the initial attachment of single planktonic cells, surfaces in contact with an aqueous environment get inevitably coated by organic polymers forming a so-called “conditioning film” (8). The formation of these conditioning films can be observed in nature, e.g. on surfaces exposed to seawater or in the human host, e.g. on surfaces of medical implants exposed to blood, urine, or saliva. For example, the conditioning film forming on teeth (“acquired pellicle”) represents a proteinaceous coating composed of albumin, lysozyme, phosphoproteins, glycoproteins, lipids, and more (8). The coating of surfaces with such a conditioning film affects the physicochemical surface properties and thus significantly influences the degree of microbial attachment (8).

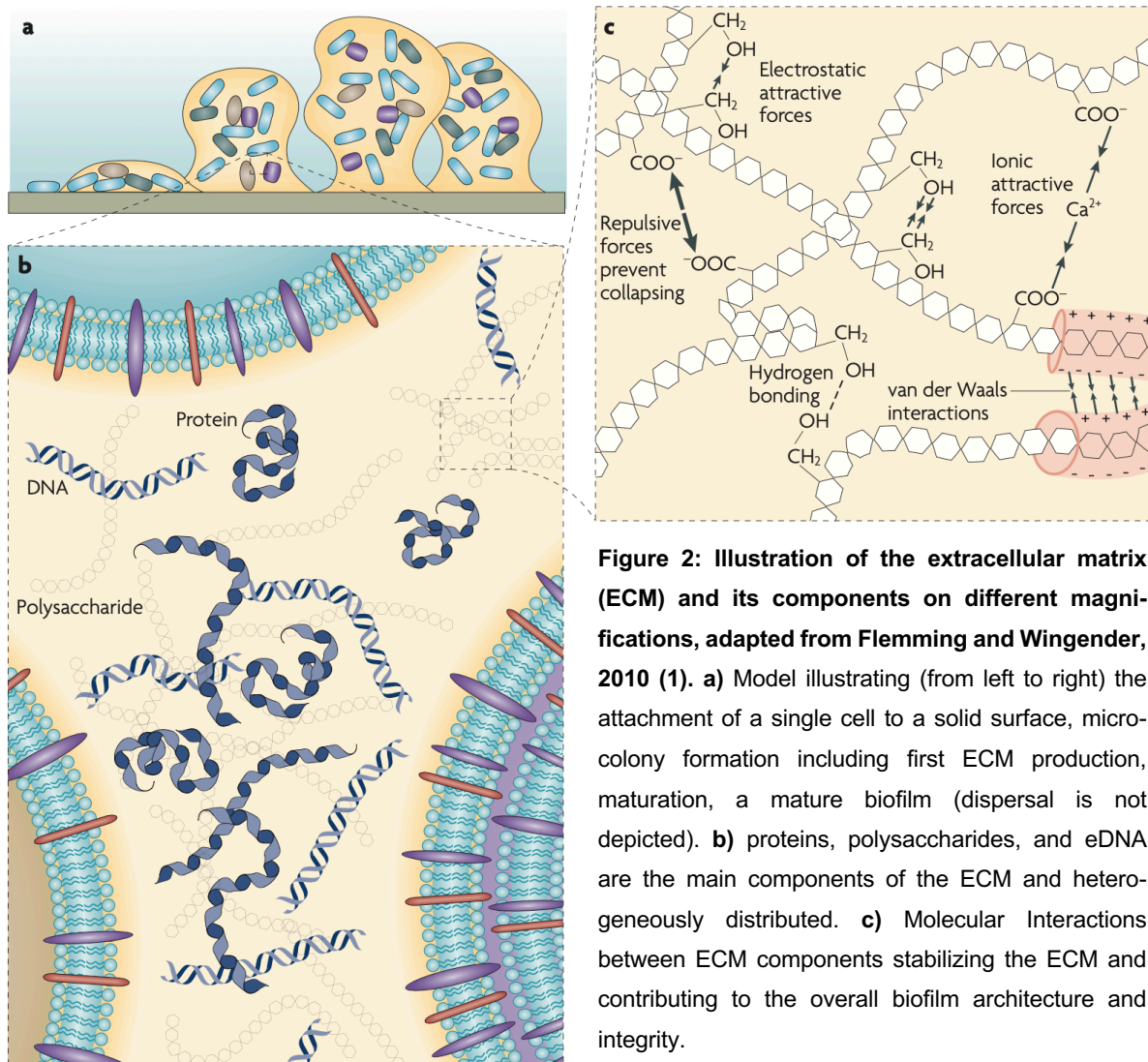
Prior to the first (reversible) attachment of planktonic cells to a (conditioned) surface, cells sense environmental characteristics like nutrient concentrations, temperature, pH, and osmolarity, triggering a sessile lifestyle (3), which is initially affected by Brownian motion, bacterial motility as well as by gravitational and hydrodynamic forces (8, 19). On a molecular level, the initial attachment is mediated by electrostatic and hydrophobic interactions of the substratum and several adhesive bacterial surface structures. These structures include pili, flagella e.g. found on *Pseudomonas aeruginosa* cells, or teichoic acids, and adhesion proteins like the group of microbial surface components recognizing adhesive matrix molecules (MSCRAMMs) e.g. found on *Staphylococcus aureus* cells (15, 20, 21). Interestingly, substratum properties like roughness and hydrophobicity do influence bacterial adhesion, but only to a minor extent. This means that bacteria are able to efficiently colonize both smooth surfaces as well as rough surfaces (17, 22). Thus, there is currently no biocompatible material available, which is able to resist microbial attachment due to its surface properties (20). The immediate transition from planktonic to biofilm growth within minutes after initial attachment to a solid surface is mediated by a broad regulatory network orchestrating changes in gene expression. These changes e.g. affect the expression of genes encoding surface proteins, proteins for nutrient utilization, and virulence factors preparing the cell to survive under hostile environmental conditions (19). Therefore, the gene expression profile of biofilm cells differs greatly from the profile of their planktonic counterparts with up to 70% (20). After the initial reversible attachment of single cells, they attach irreversibly to the substratum due to the first production of ECM components, which starts to tighten cell-to-cell and cell-to-surface contacts. However, there is also evidence that bacteria frequently detach before they phenotypically

switch to ECM production and irreversible attachment (15, 20). In the second step of biofilm formation – monolayer and microcolony formation, respectively - motile microorganisms like *P. aeruginosa* use type IV pili (after flagellum-mediated initial attachment) for lateral twitching motility and the building of first microcolony structures. However, nonmotile microorganisms like *S. aureus* form monolayers and build biofilm structures by clonal growth. During biofilm maturation, three-dimensional structures are formed by cell division and excessive production of ECM components (see 3.1.3) like polysaccharides (e.g. alginate, Psl, Pel in *P. aeruginosa*), proteins (ribosomal proteins and virulence factors of *S. aureus*), amyloid fibers (e.g. curli in *Escherichia coli*, or TasA in *Bacillus subtilis*), as well as eDNA in multiple species (1, 23). After maturation, biofilms reach a steady-state phase and release single cells or cell clumps from the community to colonize new niches. Here, release mechanisms can be divided into desorption, detachment, and dispersion (17). Desorption primarily occurs during earlier phases of the biofilm life cycle and describes the direct transfer of biofilm cells into the environment. Detachment is mediated by external forces, including abrasion by elevated shear forces, grazing, and erosion, which are able to disrupt biofilm integrity. In contrast to desorption and detachment as passive release mechanisms, dispersion is an active process involving gene expression changes, which mediate cellular release from biofilms e.g. by the secretion of nucleases, proteases, surfactants, D-amino acids, or by cell death (17, 19). Such gene expression changes, which lead to dispersal, are triggered by internal and external environmental signals like levels of oxygen, nitric oxide, and carbon and energy sources (24).

3.1.3 The Extracellular Matrix

The extracellular matrix (ECM) encapsulates biofilm-grown cells as a mostly self-produced scaffold, thereby significantly contributing to the three-dimensional biofilm architecture (1). The ECM accounts for more than 90% of the dry mass, which emphasizes its importance for microbial biofilms (1, 11). To a large extent, the ECM consists of extracellular polymeric substances (EPS), which were formerly called “the dark matter of biofilms” due to their great variety and the lack of proper analytical methods in the past. In the early days of biofilm research, EPS was mistakenly used as an abbreviation for “extracellular polysaccharides” but was renamed when other biopolymers were discovered as essential components of the ECM (1). Today, the main components of the ECM are generally well described. However, the composition is very dynamic, heterogeneous and depends on the biofilm-forming species, growth conditions, and environmental factors like shear forces, temperature and nutrient concentrations (1). In general, the scientific consensus states polysaccharides, proteins, extracellular nucleic acids (primarily eDNA, but also eRNA), and lipids being the main

components of the ECM (1, 11, 25). In addition, structures like pili, flagella, adhesive fibers, outer membrane vesicles, and humic substances have also been described as important ECM components (19, 26). Besides these polymeric substances, also metabolites, metal ions, and water play a crucial role (1, 19, 27). Indeed, in early reports, biofilms were designated as “stiff water” (1). Depending on the environment, also abiotic materials like mineral crystals, corrosion particles, clay, or split particles can be found within the ECM (8). In infection settings, also blood components and other host proteins were described as parts of the biofilm ECM (8). As mentioned above, the ECM is primarily responsible for the architectural properties of biofilms. Specifically, it defines the density of biofilm areas, pores and water channels within the biofilm. It furthermore accounts for morphological characteristics like thickness, roughness, porosity, or the formation of mushroom-like microcolonies (1). Structural properties and biofilm stability are attributable to molecular interactions between the ECM components, including van der Waals interactions, hydrogen bonds, as well as attractive and repulsive electrostatic forces (Figure 2, adapted from Flemming and Wingender, 2010 (1)).



However, the ECM composition changes dynamically and can be actively influenced in response to environmental cues like nutrient limitation or elevated shear stress. This is accomplished by the secretion of enzymes (e.g. proteases, nucleases), or the release e.g. of proteins and DNA into the ECM by cell lysis, but also via active secretion processes (28). Thus, biofilm architecture and ECM composition can be adjusted according to environmental conditions (19). For example, biofilms under high shear stress conditions are mechanically more stable than biofilms of the same species grown under low shear stress (22).

The complex and dynamic composition of the ECM furthermore leads to physicochemical heterogeneities within the biofilm manifesting as gradients of nutrients, oxygen, signaling molecules, waste products, and pH, which form e.g. depending on the biofilm depth (12, 18). These gradients lead to physiological heterogeneities of subpopulations e.g. represented by respiring microbes using oxygen as the terminal electron acceptor in oxygen-rich biofilm areas close to the surface vs. fermenting microbes in oxygen-depleted, deeper biofilm levels. Moreover, there are even metabolically inactive, non-dividing persister cells described within biofilms, which are genotypically identical to the remaining population, but dramatically more tolerant against antimicrobial therapy since most antibiotics target bacterial processes relevant for growth or cell division (19, 28). These persister cells as reservoirs of the disease and their potential to reactivate into an infectious state when antibiotic treatment ends are reasons why biofilms are so challenging to treat and such a significant healthcare burden (28, 29).

Structure and function of the biofilm ECM are in close relation. The highly hydrated but robust structure encapsulating biofilm-embedded cells fulfills a broad spectrum of functions. Most intuitively, the biofilm ECM confers stability to the entire biofilm. As mentioned above, biofilm stability thereby increases with elevating shear forces. The stability is mediated by attracting intermolecular interactions between ECM components, cellular surface components as well as surface molecules of the substratum. In consequence, the ECM plays an essential role in the adhesion of the entire biofilm. This is especially important during the early stages of biofilm development after the first attachment of single cells, which start expressing and secreting ECM components within minutes after the first surface contact (20). The adhesive character of the ECM also mediates an important cell-to-cell-contact within the biofilm, which enables efficient quorum sensing signaling as well as an eased horizontal gene transfer (1, 19, 29). In fact, the ECM acts as a reservoir for great amounts of genetic material, which facilitates a quick spread e.g. of antibiotic resistance genes further complicating biofilm treatment. Moreover, the ECM not only represents a reservoir for genetic information but also binds nutrients and enzymes, which are derived from cell lysis or are actively secreted. This renders the ECM an “external digestion” system containing “common goods”, which makes nutrients available to a great number of cells embedded in multi-species biofilm – even those lacking the genetic

information for the utilization of particular nutrients. However, one of the most important features of the ECM is its protective function against a variety of different environmental factors. These e.g. include protection from desiccation, radiation, oxidants, protozoan grazing, the host immune system, antimicrobials, and other harmful agents (19) and can mainly be explained by the ECM acting as a diffusion barrier. In fact, biofilm-grown cells are up to 1000 times more tolerant against antibiotics compared to their planktonic counterparts (30). A summary of the most essential ECM functions is modified from Flemming and Wingender (1) and provided in Table 1.

In summary, the ECM is the outstanding hallmark of biofilms fulfilling a great variety of different functions – each inheriting a great individual importance, which in total reasons the immense evolutionary success of the biofilm mode of growth.

Table 1: ECM functions in biofilms modified from Flemming and Wingender, 2010 (1)

Function	Relevance for biofilms	Involved EPS components
Adhesion	Allows the initial steps in the colonization of abiotic and biotic surfaces by planktonic cells, and the long-term attachment of whole biofilms to surfaces 123	Polysaccharides, proteins, DNA and amphiphilic molecules
Aggregation of bacterial cells	Enables bridging between cells, the temporary immobilization of bacterial populations, the development of high cell densities and cell–cell recognition 123	Polysaccharides, proteins and DNA
Cohesion of biofilms	Forms a hydrated polymer network (the biofilm matrix), mediating the mechanical stability of biofilms (often in conjunction with multivalent cations) and, through the EPS structure (capsule, slime or sheath), determining biofilm architecture, as well as allowing cell–cell communication 123	Neutral and charged polysaccharides, proteins (such as amyloids and lectins), and DNA
Retention of water	Maintains a highly hydrated microenvironment around biofilm organisms, leading to their tolerance of dessication in water-deficient environments 123	Hydrophilic polysaccharides and, possibly, proteins
Protective barrier	Confers resistance to nonspecific and specific host defences during infection, and confers tolerance to various antimicrobial agents (for example, disinfectants and antibiotics), as well as protecting cyanobacterial nitrogenase from the harmful effects of oxygen and protecting against some grazing protozoa 123	Polysaccharides and proteins
Sorption of organic compounds	Allows the accumulation of nutrients from the environment and the sorption of xenobiotics (thus contributing to environmental detoxification)	Charged or hydrophobic polysaccharides and proteins

	123	
Sorption of inorganic ions	Promotes polysaccharide gel formation, ion exchange, mineral formation and the accumulation of toxic metal ions (thus contributing to environmental detoxification)	Charged polysaccharides and proteins, including inorganic substituents such as phosphate and sulphate 123
Enzymatic activity	Enables the digestion of exogenous macromolecules for nutrient acquisition and the degradation of structural EPS, allowing the release of cells from biofilms 123	Proteins
Nutrient source	Provides a source of carbon-, nitrogen- and phosphorus-containing compounds for utilization by the biofilm community 123	Potentially all EPS components
Exchange of genetic information	Faciliates horizontal gene transfer between biofilm cells 123	DNA
Export of cell components	Releases cellular material as a result of metabolic turnover	Membrane vesicles containing nucleic acids, enzymes, lipopolysaccharides and phospholipids 123
Binding of enzymes	Results in the accumulation, retention and stabilization of enzymes through their interaction with polysaccharides 123	Polysaccharides and enzymes

3.2 The Role of Microbial Biofilms in Industry and Health Care

3.2.1 Harmful Microbial Biofilms in Industry

The earliest report of biofilms dates back to 1923, describing biofouling of ship bottoms (7). The term “Biofouling” generally outlines the attachment and growth of micro- and macroorganisms on surfaces leading to major problems and financial losses in a great variety of industrial, medical, and marine devices and applications (31). In marine industrial environments, biofouling can be ubiquitously observed, which includes underwater structures like the aforementioned ship hulls, but also offshore structures, oil installations, cables, marinas, and many more (32). The biofouling-induced increase in ship friction, for example, leads to a significantly decreased speed, as well as an increase in mechanical engine stress, fuel consumption, and emission of greenhouse gases. In fact, it is reported that a biofilm of

1 mm thickness on ship hulls increases the ship drag by 80% and consequently lowers ship speed by 15% (32). Moreover, also in other water-associated industrial environments, biofouling and biofilms, respectively, cause huge problems and economic losses. Examples include power plant cooling systems affected by malfunctioning heat exchange facilities, water-treatment systems affected by blocked pipes and decreased membrane flux, and food-, beverage-, and dairy-associated industries suffering from microbial contamination of equipment and products (31-33). Another dilemma going hand in hand with biofouling is the corrosion of surfaces e.g. made of stainless steel, or aluminum, due to microbial acid production within the biofilms (11, 31, 33, 34). However, the most severe dangers of industrial biofilms originate from diseases transmitted by food, which is contaminated by pathogenic microbes. Some of the most prominent foodborne pathogens include *Salmonella*, *Listeria*, *Campylobacter*, *Yersinia enterocolitica*, *S. aureus*, and *Candida albicans* (31, 35). These contributed to 49,950 foodborne outbreaks in Europe in 2016, which led to 3869 hospitalizations and ultimately to 20 deaths (European Centre for Disease Prevention and Control & European Food Safety Authority, 2017) (36). Of note, in the same year, 99,392 outbreaks were reported in the United States, which led to 2625 hospitalizations and ultimately to 115 deaths (Centers for Disease Control and Prevention, 2016).

3.2.2 The Burden of Microbial Biofilms in Health Care

Besides the health risks originating from food contamination, the by far more severe health burden originates from biofilm-associated infections. Notably, in the past years, it has been recognized that biofilms are responsible for most bacterial diseases (12). It is estimated that approximately 80% of all human infections and 65% of all nosocomial infections are caused by biofilms (11, 37). Here, biofilm-forming pathogenic microbes cause severe, recalcitrant infections, especially in immunocompromised patients. Once opportunistic pathogens establish biofilm-associated infections in these individuals, the infections often become chronic and frequently lead to severe symptoms and ultimately to death (19). More precisely, in the USA, 17 million patients are affected by biofilm-associated infections leading to approximately 550,000 deaths and billions of dollars of treatment costs annually (38). Among the most harmful biofilm-forming pathogens are the ESKAPE organisms *Enterococcus faecalis*, *S. aureus*, *Klebsiella pneumoniae*, *Acinetobacter baumannii*, *P. aeruginosa*, and *Enterobacter spp.*, which are categorized as most clinically relevant and multi-drug-resistant by the World Health Organization (WHO). But also other microbial pathogens are widely recognized as dangerous causative agents of biofilm infections e.g. including *E. coli*, *Proteus mirabilis*, *Streptococcus spp.*, *Staphylococcus epidermidis*, and *C. albicans*. The spectrum of biofilm-associated diseases caused by these pathogens is tremendous, ranging from device-related

infections on urinary catheters, prosthetic joints, central vascular catheters, prosthetic cardiac valves, pacemakers, and contact lenses to tissue-related infections like endocarditis, osteomyelitis, chronic wounds, urinary tract infections, dental caries, otitis media and lung infections in cystic fibrosis (CF) patients and many more (11, 12, 19, 28, 35, 39) (Figure 3).

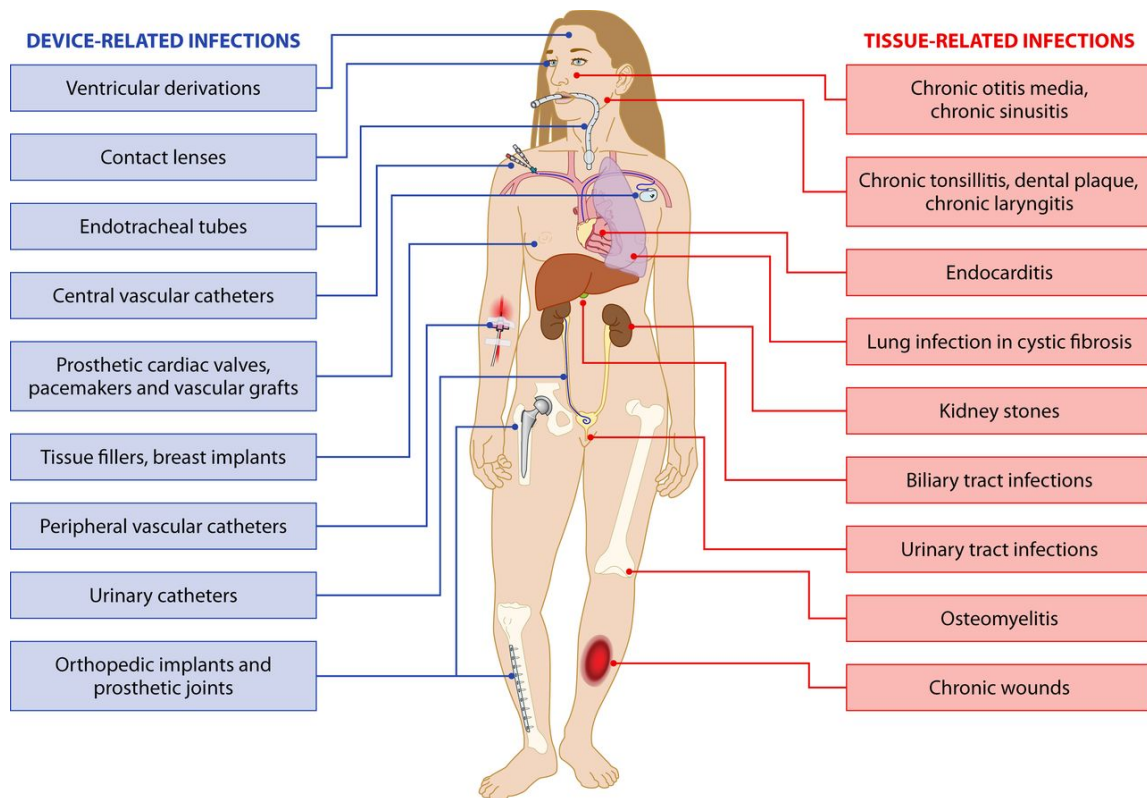


Figure 3: Examples of biofilm infections related to medical devices (left) and tissues (right). Modified from Lebeaux et al., 2014 (39).

The sheer number of annual biofilm-related infections stated above, as well as the great variety of types of biofilm infections, which can be caused by various different species, is alarming. These infection numbers can be explained by a hallmark of microbial biofilm infections: their inherent resistance towards many treatment strategies. Although a large number of biofilm-associated infections occur in immunocompromised patients, even in immunocompetent individuals, the host defense mechanisms are not able to effectively fight and clear biofilm infections (11). This is mainly due to the protective nature of the ECM discussed in section 3.1.3, which shields biofilm bacteria from opsonization and phagocytosis. Moreover, besides the ineffective clearance of biofilms by the immune system, it can be observed that recruited immune cells cause damage to surrounding tissues (11), releasing new nutrients for biofilm-associated microbes. The protective ECM not only avoids clearance by the host immune system, it simultaneously confers tolerance against antimicrobial agents acting as a diffusion barrier (23, 30). Another tolerance mechanism of biofilms is the occurrence of metabolically

inactive, non-dividing subpopulations, so-called persister cells, as already mentioned in section 3.1.3. Since most antimicrobial agents target bacterial growth or cell division processes, persister cells are naturally more tolerant against antibiotics (19, 28). These phenotypical tolerance mechanisms of biofilms are further enhanced by genetically encoded specific antibiotic resistance mechanisms. The impaired diffusion within biofilms leads to decreasing concentrations of antimicrobials in deeper biofilm layers, and this, in turn, supports the development of resistant microbes and the concomitant interspecies spread of resistance genes via horizontal gene transfer (36, 40).

The combination of tolerance and resistance of biofilm-embedded cells is referred to as “recalcitrance” (30), which translates into survival of 10 to 1000-times increased concentrations of antimicrobial agents compared to their planktonic counterparts (12, 23, 30). In consequence, antimicrobial treatment never entirely eradicates the biofilm. Relapse of the biofilm infection after weeks often demands surgical removal of the affected medical device or tissue (11), (12). Consequently, novel treatment strategies are urgently needed.

3.2.3 Cystic Fibrosis

CF patients are suffering from a genetic disorder, which is particularly prevalent among the Caucasian population. More precisely, mutations in a gene encoding the cystic fibrosis transmembrane conductance regulator, an anion channel localized in epithelial cells of the respiratory and gastrointestinal tract, occur with an incidence of approx. one in 3,000 births, thereby causing the CF phenotype (41, 42). More than 1,500 mutations have been identified, which lead to the CF phenotype manifesting in impaired ion homeostasis. The most common mutation (affecting up to 66% of all CF patients) is a deletion of three nucleotides encoding phenylalanine (F508), resulting in an impaired CFTR protein processing and trafficking (43). This, in turn, leads to a dehydrated, viscous, sticky mucous within the CF lung, impairing the mucociliary clearance mechanism, which renders the mucous an ideal growth substrate for the colonization by inhaled opportunistic microbial pathogens (43, 44). Typically, CF patients are already colonized during infancy by *S. aureus* and *Haemophilus influenzae*, followed by other opportunistic pathogens like *P. aeruginosa*, *Burkholderia cepacia* complex, and *Stenotrophomonas maltophilia* (45, 46) (Figure 4). In addition, fungal pathogens like *Aspergillus fumigatus* and *C. albicans*, and viruses (e.g. influenza and respiratory syncytial virus) frequently contribute to the CF lung microbiota and pathophysiology. Here, microbial pathogens are prevalently acquired from environmental reservoirs but can also be transmitted from patient to patient (47). Over the past years, new “core genera” have been identified within the CF airways, which can be attributed to the development of innovative culture-independent

diagnostic methods. These genera e.g. include *Neisseria* and *Streptococcus*, but interestingly also obligate anaerobic bacterial genera like *Prevotella*, *Veilonella*, and *Catonella* (44, 45). Importantly, the polymicrobial communities within the CF airways change dynamically and differ greatly both spatially and from patient to patient. However, it is still under debate if some microbes, which were formerly characterized as pathogenic CF community members, could be part of the normal microbiota rather than being pathogenic, like *S. maltophilia* or *Streptococcus pneumoniae* (45).

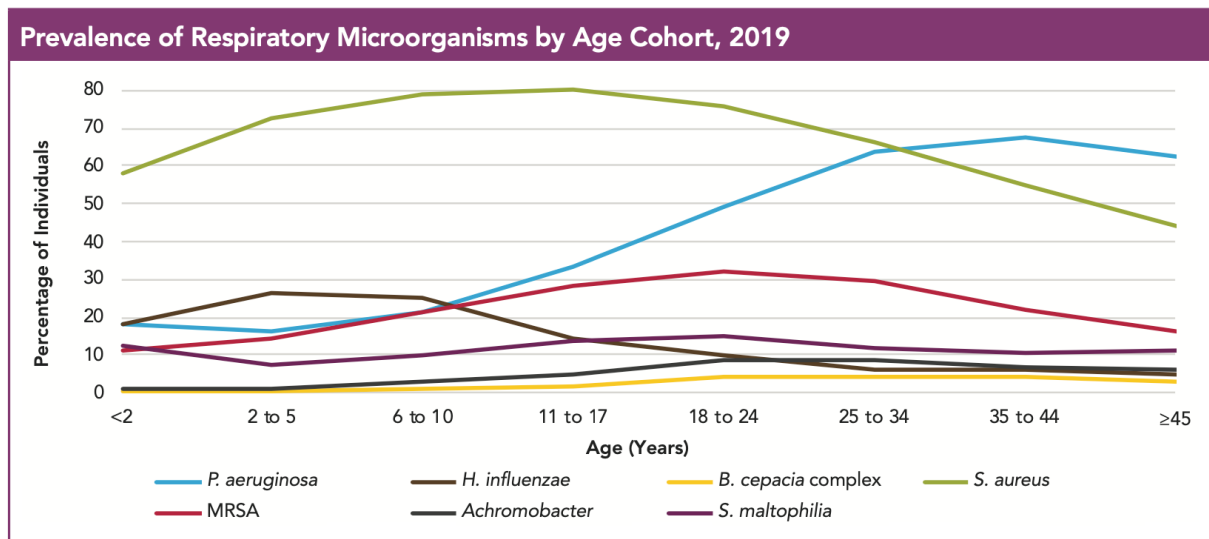


Figure 4: Prevalence of microorganisms colonizing the respiratory tract of CF patients. Taken from Cystic Fibrosis Foundation Annual Data Report 2019 (46)

The colonization by some key microbial pathogens like *P. aeruginosa* and the concomitant establishment of chronic biofilm infections is considered the main reason for CF mortality. This is due to the production of virulence factors and the host immune response leading to an inflammatory milieu, destroyed lung tissue, reduced lung function, and ultimately to death (45, 48, 49). In fact, between 60 to 70% of all CF patients are actually colonized with *P. aeruginosa* already by the age of 20, underlining the importance of this CF key pathogen (49). Furthermore, another CF key pathogen, *S. aureus*, represents one of the earliest colonizing bacteria being frequently detected in infants and children with CF (50). Despite aggressive antibiotic treatment of CF patients starting early in childhood, there is currently no drug available, which is able to cure CF lung infections. This is mainly due to the formation of polymicrobial biofilms and multicellular clusters acting as a naturally drug-shielded reservoir for recalcitrant, recurrent infections (28, 51). Moreover, both synergistic and antagonistic microbial interactions have been described within the CF lung, harboring the potential to exacerbate these severe lung infections. For example, it has been observed that some bacterial species with a limited capability to attach to surfaces and to form biofilms are suppor-

ted by the interaction with the existing polymicrobial community facilitating efficient attachment and biofilm formation (40). Moreover, *P. aeruginosa* is able to sequester exoproducts, enhancing the formation of *S. aureus* small colony variants (SCVs, 3.3.3) with reduced metabolic activity and enhanced resistance against antimicrobial agents providing a survival advantage of *S. aureus* in mixed-species biofilms with *P. aeruginosa* (50).

Taken together, it needs to be emphasized that the role of each single species colonizing the CF airway and the interplay between community members is still poorly understood but nevertheless dramatically important for CF pathophysiology and disease progression. Thus, deeper *in vivo* insights into the CF lung microbiome to shed light on the pathophysiology and polymicrobial interactions within polymicrobial CF biofilms are urgently needed for the development of novel antimicrobial, antibiofilm therapies – a problem, which has been addressed by article II of this thesis: “An innovative protocol for metaproteomic *in vivo* analyses of microbial pathogens in cystic fibrosis sputum”.

3.3 *Staphylococcus aureus*

3.3.1 *S. aureus* Infections

S. aureus is a Gram-positive, nonmotile, opportunistic bacterial pathogen, which is the causative agent of a broad spectrum of diseases. It asymptotically colonizes approximately 20 to 40% of the healthy population on the nasal mucosa but can also be isolated as a commensal from various niches like the anterior nares, pharynx, perineum, or skin (52, 53). However, in immunocompromised patients, *S. aureus* is able to cause infections ranging from (minor) skin and soft tissue infections like folliculitis, impetigo, cutaneous abscesses, and infections in chronic wounds to life-threatening diseases like sepsis and pneumonia. Furthermore, *S. aureus* is responsible for several toxin-associated diseases like toxic-shock syndrome and staphylococcal food-borne diseases (54). The arguably most disease-promoting traits of *S. aureus* are the formation of biofilms on various biotic and abiotic surfaces and the consequent causation of many biofilm-associated infections. *S. aureus* and its close relative *S. epidermidis* are recognized as two of the most frequent causative agents of biofilm-related infections (21, 46). Staphylococcal biofilm-induced pathologies include i.e. osteomyelitis, endocarditis, cystic fibrosis, or chronic wound infections. But also the implantation of medical devices results in biofilm infections e.g. of prosthetic joints, artificial heart valves, pacemakers, or catheters (50, 55-57). In particular, *S. epidermidis* leads to biofilm-formation on indwelling devices. Thus, it is not surprising that *S. aureus* would

infections are considered one of the most feared complications that can occur post-surgery. Collectively, *S. aureus* infections represent one of the most significant health care burdens worldwide and account for 490,000 hospitalizations and more than 20,000 deaths in the USA annually (58, 59). Consequently, due to its immense health care risks and multi-drug resistances (discussed below), *S. aureus* was classified as one of the most dangerous pathogens by the WHO, including it into the list of ESKAPE organisms.

3.3.2 Methicillin-resistant *Staphylococcus aureus* (MRSA)

Increasing the challenges associated with the treatment of *S. aureus* soft-tissue and biofilm infections is the rapid worldwide emergence of multi-drug resistant *S. aureus* strains. From a historical point of view, *S. aureus* infections have been considered highly fatal over the first half of the 20th century, until penicillin became available to treat *S. aureus* infections. However, the first resistances mediated by the β -lactamase gene *blaZ* have been observed very quickly after the first clinical usage of penicillin around 1940 (60). The first semi-synthetic β -lactamase-resistant penicillins, such as methicillin, were developed in 1960. This was followed by the emergence of the first methicillin-resistant *S. aureus* (MRSA) strains within one year of methicillin usage (60). The spread of methicillin resistance is mediated via horizontal gene transfer of a specific mobile genetic element, the staphylococcal cassette chromosome *mec* (SCC*mec*) (60). Acquiring this mobile genetic element confers resistance by the expression of an additional penicillin-binding protein (PBP2A), which has a very low affinity to β -lactam antibiotics. Consequently, these strains are not only resistant towards methicillin but an entire class of β -lactam antibiotics, and the term “multi-resistant *S. aureus*” is often synonymously used with the term “methicillin-resistant *S. aureus*” (60). The spread of MRSA worldwide became so severe (Figure 5) that currently only a few last-resort antibiotics can be used for the treatment of MRSA infections like linezolid, vancomycin, daptomycin, and clindamycin. However, resistances against these last-resort antibiotics have already been observed, underlining the threat of MRSA infections. In fact, approximately 80,000 patients are infected by MRSA in the USA, resulting in about 11,000 patients deaths annually (59, 61). These numbers again emphasize the urgent need for new anti-staphylococcal therapies.

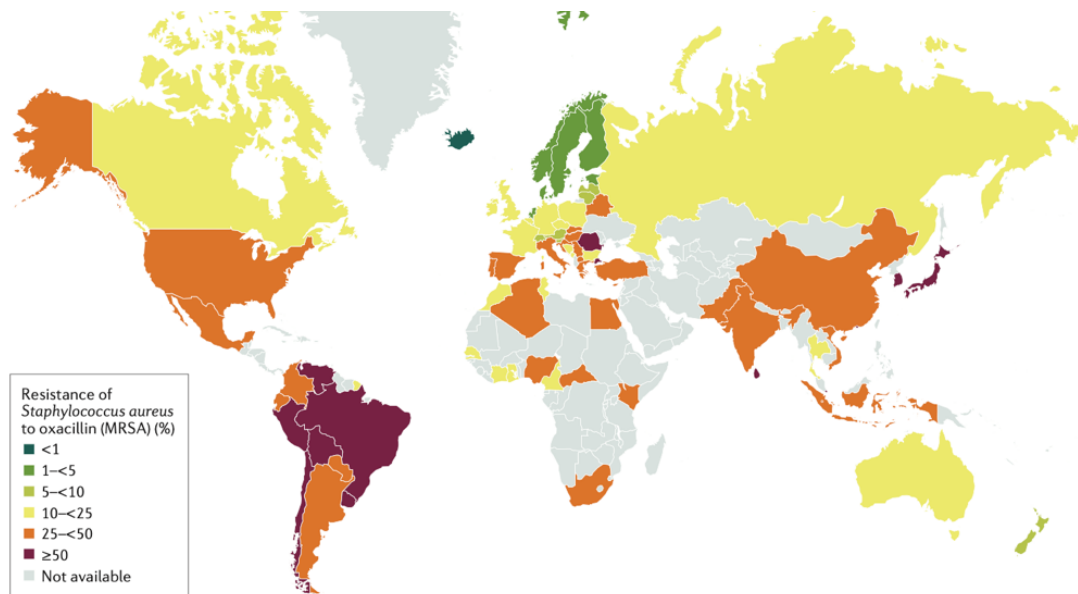


Figure 5: Spread of methicillin-resistant *Staphylococcus aureus* (MRSA) over the world shown by percentages of oxacillin resistances. Taken from Lee *et al.*, 2018 (53)

3.3.3 Virulence Factors of *S. aureus*

S. aureus encodes and exploits a huge arsenal of different virulence factors – both surface-associated and secreted ones – that pave the way to successfully initiate, establish and persist during an infection.

For the first step of infection – the initial attachment to biotic host surfaces like tissues, cells, and extracellular host matrix molecules, or abiotic surfaces like implants - *S. aureus* is equipped with a variety of adhesive factors. Among them are MSCRAMMs, which allow *S. aureus* to attach to fibronectin, fibrinogen, collagen, or plasma clot (55). Prominent MSCRAMMS are the fibronectin-binding proteins A and B (FnbpAB), clumping factor A and B (ClfAB), the serine-aspartic acid repeat proteins SdrCDE, and staphylococcal protein A (SpA) (62-65). Besides their roles in initial attachment, these adhesins do also play a role during biofilm formation. Other adhesive factors, which are important during biofilm formation, are the biofilm-associated protein Bap, teichoic acids, and eDNA (23).

After successful initial attachment and colonization, *S. aureus* secretes several exoproteins in order to hydrolyze host tissues releasing nutrients required for growth. Among these exoproteins secreted by nearly all *S. aureus* strains are nucleases, proteases, lipases, collagenase, and hyaluronidase (62). In addition, there are several exotoxins produced by *S. aureus*, which expose cytolytic activity by forming β -barrels within the membrane of target host cells leading to cytoplasm leakage. Here, cytolytic toxins target human platelets,

erythrocytes, monocytes, and leukocytes, rendering them efficient tools for nutrient acquisition and host immune evasion. The most important cytolytic toxins are α -hemolysin, β -hemolysin, γ -hemolysin, leukocidin, and Pantan-Valentin leukocidin (62). Moreover, another type of cytolytic, amphiphilic, surfactant-like toxins are the Phenol-soluble modulins (PSMs) categorized in four PSM α (approx. 20-25 amino acids long), and two PSM β (approx. 44 amino acids long) proteins. Importantly, besides their cytolytic function, PSMs were also reported to contribute to the formation and spreading of staphylococcal biofilms (66). Another crucial group of *S. aureus* toxins includes the toxic shock syndrome toxin-1 and enterotoxins SEA, SEB, SEC_n, SED, SEE, SEG, SHE, and SEI causing toxic shock syndrome and food-poisoning, respectively (62, 63, 66).

In addition to toxins used for immune evasion, *S. aureus* synthesizes various additional factors to cope with the host immune system. One of the most important immune evasion factors is the staphylococcal protein A (encoded by the *spa* gene). The main function of SpA, which is localized at the cell surface, is impairing immunoglobulin G-mediated opsonization and phagocytosis by binding the antibody Fc domain (63, 66). Interestingly, there is a second protein, designated second immunoglobulin-binding protein Sbi, fulfilling a redundant function (67). *S. aureus* cells also have to cope with oxidative stress imposed i.e., during the oxidative burst of neutrophils. Key proteins during oxidative stress protection include enzymes like superoxide dismutases SodAM, catalase KatA, peroxiredoxin AhpC, as well as a carotenoid pigment staphyloxanthin, which acts as an antioxidant within the cytoplasmic membrane (68, 69). An additional, crucial pathophysiological adaptation, which evolved in *S. aureus* to cope with the host immune system and antimicrobial therapy during infection, is the formation of so-called “small colony variants” (SCVs). SCVs are subpopulations of infecting *S. aureus* cells, which are characterized by reduced metabolic activity, membrane potential and cell wall synthesis. This, in consequence, leads to tolerance against antimicrobial therapy (63, 70). SCVs therewith contribute to biofilm persistence and stability, fueling recurrent infections for years (63, 70).

3.3.4 *S. aureus* Biofilm Formation

As described in section 3.1.2, biofilm development can be categorized into four general phases: primary surface attachment, formation of a monolayer/microcolonies, maturation, and biofilm dispersal (3, 11, 15, 16). Interestingly, for *S. aureus* biofilms Moormeier *et al.* observed that the second phase is characterized by a very intense multiplication leading to a rapid formation of an *S. aureus* monolayer and that a subpopulation prematurely detaches in an additional phase termed “exodus” prior to the designated maturation phase (71).

Historically, early descriptions of *S. aureus* biofilms reported teichoic acids (80%) as well as staphylococcal and host proteins being the most prominent ECM components (72). However, in later studies, the *S. aureus* ECM research focused on a newly discovered polysaccharide, a major component within the *S. aureus* ECM: the polysaccharide intercellular adhesin (PIA, also called poly-N-acetylglucosamine (PNAG)) (72, 73). Importantly, PIA is partially deacetylated, which introduces positive charges at neutral or acidic pH found in biofilms and in natural *S. aureus* habitats like skin. It was proposed that these positive charges render PIA a crucial biofilm stabilizing component due to electrostatic interactions with other biopolymers like negatively charged teichoic acids and eDNA (21). Interestingly, PIA homologs have been identified in various biofilm-forming bacterial pathogens like Pel in *P. aeruginosa*, suggesting that this stabilization mechanism is a widespread concept among biofilm-forming species (21, 23). The genes and gene products responsible for PIA synthesis are encoded on the *ica* locus (N-acetylglucosamine transferase IcaA and IcaD, PIA deacetylase IcaB, a putative PIA exporter IcaC, and a regulator IcaR). These genes are reported to be required for biofilm formation (21) and are upregulated by environmental factors like oxygen limitation, glucose, osmolarity, temperature, ethanol, and antibiotics (72). However, in later studies, it was discovered that the deletion of the *ica* locus not necessarily leads to the inability to form biofilms and that some clinical isolates are able to form PIA/*ica*-independent biofilms. From a clinical point of view it is interesting that the ability to form PIA/*ica*-independent biofilms seems to be strain-specific: strains with mutations/deletions in the *ica* locus belonging to the MRSA group often remain more competent of biofilm-formation, whereas MSSA strains frequently lose their biofilm-forming capability (72, 74). PIA/*ica*-independent biofilms are based on extracellular proteins and eDNA, and a general classification of *S. aureus* in PIA/*ica*-dependent and PIA/*ica*-independent biofilm formers gained scientific acceptance. Accordingly, PIA/*ica*-independent biofilms are susceptible to treatment with proteases, protein-denaturing agents, and nucleases (74). Within PIA/*ica*-independent *S. aureus* biofilms, important roles for biofilm-growth has been described for various proteins like the adhesive fibronectin-binding proteins (FnBPs), clumping factors A and B (ClfAB), *S. aureus* surface proteins C and G (SasCG), Serine-aspartate repeat-containing proteins C, D, and E (SdrCDE), *S. aureus* protein A (Spa), biofilm-associated protein (BAP) as well as α -hemolysin Hla (72, 74). Importantly, proteins involved in cell lysis like the major autolysin Atl and the holing homolog CidA are crucial for stabilizing the ECM by mediating the release of eDNA (72, 74). Moreover, ribosomal proteins, other cytoplasmic proteins as well as secreted virulence factors were reported to have moonlighting functions within the ECM by mediating stability via electrostatic interactions (23, 75). In addition, PSMs play a role in biofilm dissemination due to their surfactant characters but, on the other hand, can also promote biofilm growth by the formation of amyloid fibers stabilizing

the ECM (73). For the modulation of biofilm architecture, proteases play a major role in PIA/*ica*-independent biofilms and are low abundant during biofilm maturation and high abundant during biofilm dispersal (74). Important proteases produced by various *S. aureus* isolates are e.g. the metalloprotease Aur, two cysteine proteases ScpA and ScpB, six serine proteases Spl A-F, and the V8 serine protease SspA (74). Surprisingly, despite its importance in biofilm formation, the overall proteinaceous composition of the *S. aureus* ECM has been barely addressed experimentally so far. Consequently, this research gap is addressed in Article I of this thesis: “Virulence factors of *Staphylococcus aureus* biofilms have a moonlighting function contributing to biofilm integrity”.

3.4 *Candida albicans*

C. albicans is an opportunistic-pathogenic yeast colonizing multiple niches of the human body as a part of the native microbiota in over 50% of healthy individuals. Frequently colonized niches include cutaneous or mucosal surfaces of the digestive, reproductive and urinary systems (76, 77). Importantly, this colonization rate renders *C. albicans* the causative agent of multiple superficial diseases like oral and vaginal infections up to life-threatening systemic infections like sepsis (35), with mortality rates around 40% (77). In fact, *Candida spp.* are considered to be responsible for approximately 15% of all cases of hospital-acquired sepsis (77). *Candida spp.* is of particular concern for immunocompromised patients, who are e.g. suffering from AIDS or are treated with chemo- or other immunocompromising therapies. Moreover, infections by yeast of the genus *Candida* – collectively referred to as candidiasis – are frequently biofilm-associated (76) and develop on abiotic surfaces like indwelling medical devices, as well as on biotic surfaces e.g. found within the oral cavity. Importantly, *Candida* species account for the highest number of fungi recovered from infected medical devices like pacemakers, prosthetic heart valves, joint prostheses, and catheters (77). Moreover, *C. albicans* plays a major role as a foodborne pathogen and spoilage microorganism due to its ability to form biofilms on abiotic surfaces used within the food-processing industry like stainless steel, aluminum, glass, polytetrafluoroethylene, and polyamide (35). Similar to bacterial biofilms, *C. albicans* biofilms show increased antimicrobial tolerance compared to their planktonic counterparts, as well as the presence of persister cells. These characteristics combined with the ability of fungal biofilm-grown cells to detach, reinfect other body sites, and to cause bloodstream infections make *C. albicans* biofilm infections recalcitrant and enormously difficult to treat. Consequently, removal of the infected medical device often remains as the only treatment option (3, 77). *C. albicans* belongs to the fungal species, which are most frequently isolated from mixed-species biofilm infections (76), where it can even

support the biofilm growth of other pathogenic microorganisms. For example, it has been shown, that *C. albicans* enhances the growth of anaerobic bacteria within hypoxic biofilm centers (40). Another well-studied example is *P. aeruginosa*, being frequently found associated with *C. albicans* in CF patients. In CF patients, this type of co-infection is associated with a worse prognosis compared to single *P. aeruginosa* infections (76).

Collectively, *C. albicans* represents one of the most dangerous microbial biofilm-forming pathogens demanding a tremendous need for novel antimicrobial/antibiofilm treatment options. Therefore, a novel treatment strategy – nonthermal atmospheric pressure plasma - against this type of biofilms has been assessed in article III “Nonthermal Plasma Jet Treatment Negatively Affects The Viability and Structure of *Candida albicans* SC5314 Biofilms“ and article IV “Antimicrobial Effects of Microwave-Induced Plasmatorch (MINIMIP) Treatment on *Candida albicans* Biofilms” of this thesis.

3.5 Strategies Combating Microbial Biofilms

3.5.1 Preventing the Initial Step of Biofilm Formation

As outlined in section 3.2.2, microbial biofilms represent an immense burden for both industry and healthcare. Consequently, there has a lot of research been done to prevent and treat/eradicate biofilms resulting in the discovery of a plethora of different strategies and molecules showing antibiofilm properties. However, due to the great genotypically and phenotypically variety of biofilm-forming species, physicochemical and physiological heterogeneities within biofilms, the shielding ECM properties as well as the existence of persister cells within biofilms it is incredibly difficult to fully prevent or eradicate biofilms. Thus, no preventive or eradication strategy so far provides 100% efficiency, entirely avoiding or eliminating microbial biofilms. In general, biofilm prevention and removal strategies can be differentiated into three categories: physical strategies, mechanical strategies, and chemical/enzymatical strategies.

Most intuitively, the best biofilm fighting strategy is the prevention of its development by interfering with the initial attachment of microbes. A common method preventing initial microbial attachment is a physical biofilm control approach by surface modification. This is either achieved directly on the surface or indirectly by a coating (48). Nature-mimicking physical control approaches e.g. include low drag and low adhesion inspired by the lotus leaf and sharkskin and were achieved by the creation of microtextured topographies combined with surface charge manipulation resulting in superhydrophobic or superhydrophilic surfaces (32). However, even though some microbial species show a reduced ability to adhere to these

surfaces, a conditioning film consisting of environmental molecules may form on the surface, facilitating microbial attachment due to altered physicochemical surface properties. Another observed problematic effect is that species failing the initial attachment simply adhere to species, which were still able to attach to the surface resulting in multi-species biofilms on the basis of these early colonizers (11). Another strategy to prevent initial surface colonization is to inhibit the biosynthesis of bacterial adhesins. Examples include pilicides and curlicides, molecules specifically designed to inhibit the assembly of type 1 pili and the polymerization of the major curli subunit protein CsgA in uropathogenic *E. coli* (UPEC), respectively (19, 39). Furthermore, the development of antibiofilm materials pursues the idea of preventing initial attachment by killing approaching planktonic cells with surface-incorporated or -attached antimicrobial agents. This would result in an antimicrobially active microenvironment in direct proximity to the biomaterial surface. An equivalent in nature can be found e.g. in marine seaweeds releasing antibiofilm-active furanones (20). Prominent examples for imitations are bone cements combined with gentamicin, or polymers releasing NO, antibodies, silver ions, or small molecule biofilm inhibitors like phenols, imidazoles, or indole (20, 28, 48). Of note, the kinetics of the release from the surface is key in antibiofilm materials. If the release of antimicrobial compounds is too slow, inhibitory concentrations around the biomaterial surface cannot be achieved, leading to sublethal concentrations, which trigger resistance development and even promote biofilm development in some species. However, if the release kinetics is too quick, the concentration of the antimicrobial compound is too low after the initial burst, which again favors resistance and biofilm development as described above. In other words, the biomaterial might not show the expected long-term effect and durability (20). Another promising approach to prevent initial biofilm formation is the use of protective layers of non-pathogenic microbes preventing attachment of opportunistic pathogens due to increased colonization resistance (39).

3.5.2 Eradicating Established Biofilms

Another concept of fighting microbial biofilms is the removal of already established biofilms rather than preventing their initial formation. This can be achieved physically, mechanically, and/or chemically/enzymatically. Notably, especially in health care settings, it needs to be kept in mind that prevention of biofilm formation should be favored over dispersal, which can lead to the release of cells with the potential to drive secondary-site infections (40). In industrial environments, biofilms are frequently removed mechanically by high-pressure cleaning, brushing, and wiping, resulting in a reasonably big amount of biomass being removed (33). However, in most cases, a thin layer of the biofilm remains on the surface, which regrows to a

potentially even denser and more mechanically resistant biofilm (33). Strategies for physical biofilm control include ultrasound, super-high magnetic fields, and electrical fields. For example, low electrical currents combined with antibiotic treatment effectively controlled biofilm formation in the past (11).

As outlined above, antibiotic treatment alone fails to effectively eradicate microbial biofilms due to the protective ECM and the high intrinsic resistance of persister cells. However, very recent studies show that periodically administered antibiotics (e.g. Oxacillin) – referred to as “pulse dosing” – effectively decreased biofilm populations, including persister cells stating that pausing antibiotic administration can sensitize biofilms towards treatment and reduces the risk of resistance development (61, 62). Furthermore, nanoparticles functionalized with antimicrobials show great potential against *P. aeruginosa* and *S. epidermidis* biofilms due to their high surface-to-volume ratio (19). Another intuitive method to eradicate established biofilms is the breakdown or destabilization of the ECM. Therefore, matrix components contributing to biofilm integrity are targeted by a variety of different chemicals and enzymes. For example, chelators like EDTA, citrate, or iron-binding lactoferrin scavenge metal ions, which stabilize the ECM by electrostatic interactions with other ECM components, thereby destabilizing the entire biofilm (11, 19). Stabilizing ECM components like eDNA and proteins can get degraded by the use of DNase and proteases, respectively – thus, recombinant human DNase is administered to the lung of CF patients degrading biofilm eDNA and reducing mucus viscosity successfully (78).

Given that microbial biofilms go through a live cycle, another very intuitive biofilm combat strategy is the manipulation of physiological processes or pathways being essential for the switch to different biofilm growth stages. Most importantly, there are two approaches: (I) inhibiting the transition from the planktonic to the biofilm lifestyle by interfering with c-di-GMP biosynthesis (by diguanylate cyclase inhibitors) since high c-di-GMP levels are associated with a sessile lifestyle, (II) manipulation or administration of dispersion signal molecules to artificially induce biofilm dispersal (39, 19). Both approaches do not target essential cellular processes, thus reducing the risk of resistance development (20). To be highly effective, these approaches still need to be combined with antimicrobials to kill planktonic, dispersed cells in order to ultimately avoid secondary site infections (48). Additional approaches to induce biofilm dispersal are based on molecules interfering with quorum sensing signaling, NO, surfactants, D-amino acids, and norspermidine, which were reported to interfere with biofilm formation e.g. of *B. subtilis*, *E. coli*, *S. aureus* and *P. aeruginosa*, respectively (43, 20, 39). Another very promising strategy to fight biofilms is phage therapy, either using one specific bacteriophage strain or even a cocktail of different strains. Phages were shown to successfully remove biofilms of *Listeria monocytogenes*, *P. aeruginosa*, *E. coli*, *S. epidermidis* (11, 19, 39). In

essence, phages represent a highly effective, natural, specific, non-toxic alternative to other antibiofilm approaches (11).

Taken together, over the last few years, various new antibiofilm concepts were developed. However, despite these efforts, none of these approaches is able to fully eradicate microbial biofilms in real world industrial and clinical settings. Consequently, the most commonly applied and effective biofilm prevention strategies in clinical environments are still extremely high hygiene standards, well-trained staff, and systemic or local antibiotic prophylaxis during the surgical operation preventing microbial contamination in the first place (39). Of note, hitherto, the most effective option to fight biofilm infections is to surgically remove the affected medical device or area (11), underlining the urgent need for novel, more effective, and less costly antibiofilm strategies. A very promising new approach is the use of nonthermal plasma, which will be discussed in the next section.

3.5.3 Nonthermal Plasma as a new Antibiofilm weapon

Research in nonthermal atmospheric pressure plasmas (NTPs) is a rapidly growing field with great potential to fight microbial biofilms (36, 79). Plasma is an ionized gas, which is considered the fourth state of matter and which can be classified into thermal plasma and nonthermal plasma according to their temperature (79). In order to induce gas ionization to produce a plasma, energy needs to be supplied to the gas, e.g. by electric or electromagnetic fields to induce a nonthermal plasma. This energy accelerates free electrons, ionizes gas atoms and molecules, resulting in the release of more free electrons, which, in turn, ionize more gas atoms and molecules (79). Moreover, electromagnetic radiation in a broad spectrum of wavelengths is emitted when ionized atoms and molecules return into a stable state. Thus, the overall composition of plasma is a mixture of excited reactive particles, namely positively and negatively charged ions, electrons, free radicals like reactive oxygen and nitrogen species (e.g. ozone, hydroxyl radicals, superoxide, singlet oxygen, nitric oxide, or nitrogen dioxide), and UV radiation (79). Importantly, all of these components are able to inhibit a broad spectrum of microorganisms including bacteria and fungi and even spores thereof (79), which renders plasma a potent weapon to combat microbial biofilms.

In fact, a version of nonthermal plasma (nonthermal atmospheric pressure plasmas (NTPs)) is already widely used in microbial decontamination applications in medicine as well as in the dairy and food industry and the fight against biofouling (36). Advantages of the application of NTPs include the nonthermal operation avoiding thermal damage of the treated surfaces and reduced costs compared to thermal plasma sources. So far, no resistance against NTPs has been observed (35), which renders this technique very effective against antibiotic-resistant

strains (35). Indeed, antimicrobial effects of NTPs are reported to exceed more classical UV radiation or peroxide-based approaches.

The evaluation of the antibiofilm potential of two different NTP sources against *C. albicans* biofilms is reported in article III “Nonthermal Plasma Jet Treatment Negatively Affects The Viability and Structure of *Candida albicans* SC5314 Biofilms” and article IV “Antimicrobial Effects of Microwave-Induced Plasmatorch (MINIMIP) Treatment on *Candida albicans* Biofilms” of this thesis.

4 Article I: Virulence Factors Produced by *Staphylococcus aureus* Biofilms have a Moonlighting Function Contributing to Biofilm Integrity

Article I

Virulence Factors Produced by *Staphylococcus aureus* Biofilms have a Moonlighting Function Contributing to Biofilm Integrity

Alexander C. Graf, Anne Leonard, Manuel Schäuble, Lisa M. Rieckmann, Juliane Hoyer, Sandra Maaß, Michael Lalk, Dörte Becher, Jan Pané-Farré , and Katharina Riedel

Molecular and Cellular Proteomics, 2019, 18, 1036–1053

Author contributions:

ACG, JPF and KR designed the experiments, which were performed by ACG, MS, and LMR. AL and ML performed metabolome analyses. ACG, MS, JH, SM, and DB performed proteome analyses. ACG and JPF performed CLSM imaging. ACG analyzed all the data. ACG, JPF, and KR wrote the manuscript, which was critically read and edited by all other co-authors.

Alexander C. Graf

Prof. Dr. Katharina Riedel

Virulence Factors Produced by *Staphylococcus aureus* Biofilms Have a Moonlighting Function Contributing to Biofilm Integrity

Authors

Alexander C. Graf, Anne Leonard, Manuel Schäuble, Lisa M. Rieckmann, Juliane Hoyer, Sandra Maass, Michael Lalk, Dörte Becher, Jan Pané-Farré, and Katharina Riedel

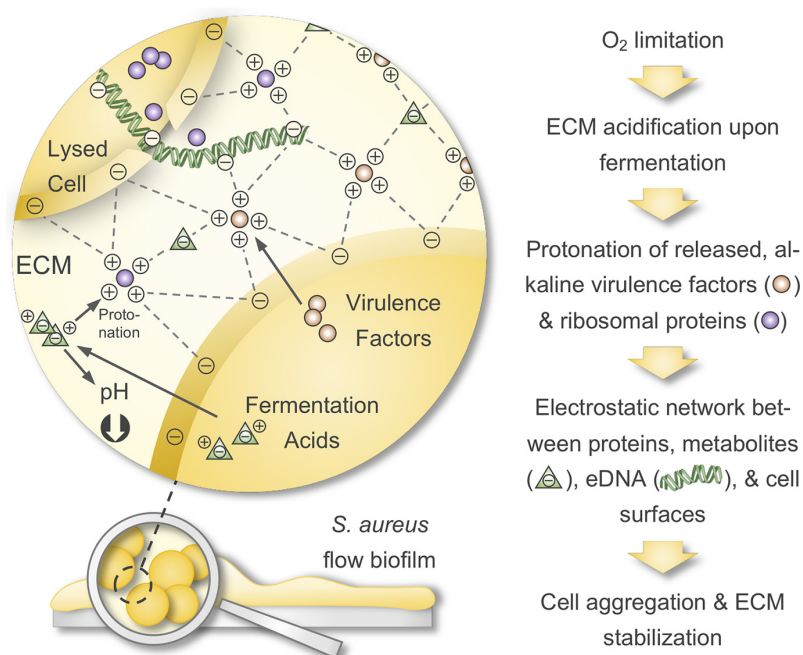
Correspondence

riedela@uni-greifswald.de

In Brief

We comprehensively profiled intracellular and ECM proteomes of *S. aureus* flow biofilms and complemented these data by metabolic footprint analysis and phenotypic assays. We show that moonlighting, secreted virulence factors and ribosomal proteins within the ECM contribute to biofilm stabilization. Mechanistically, we propose that these alkaline proteins get protonated in an acidified ECM (because of the release of acids upon fermentation) mediating electrostatic interactions with anionic cell surface components, eDNA, and metabolites, which leads to cell aggregation and ECM stabilization.

Graphical Abstract



Highlights

- Establishment of a flow system allowing *multi-omics* analysis of *S. aureus* biofilms.
- Biofilm proteome profiling (intracellular and ECM) plus metabolic footprint analysis.
- Virulence factors and ribosomal proteins stabilize the ECM as moonlighting proteins.
- They act as electrostatic bridges between anionic cell surfaces, eDNA and metabolites.



Virulence Factors Produced by *Staphylococcus aureus* Biofilms Have a Moonlighting Function Contributing to Biofilm Integrity*[§]

✉ Alexander C. Graff‡, Anne Leonard§, Manuel Schäuble‡, Lisa M. Rieckmann‡, Juliane Hoyer¶, Sandra Maass¶, Michael Lalk§, Dörte Becher¶, Jan Pané-Farré‡, and Katharina Riedel‡

Staphylococcus aureus is the causative agent of various biofilm-associated infections in humans causing major healthcare problems worldwide. This type of infection is inherently difficult to treat because of a reduced metabolic activity of biofilm-embedded cells and the protective nature of a surrounding extracellular matrix (ECM). However, little is known about *S. aureus* biofilm physiology and the proteinaceous composition of the ECM. Thus, we cultivated *S. aureus* biofilms in a flow system and comprehensively profiled intracellular and extracellular (ECM and flow-through (FT)) biofilm proteomes, as well as the extracellular metabolome compared with planktonic cultures. Our analyses revealed the expression of many pathogenicity factors within *S. aureus* biofilms as indicated by a high abundance of capsule biosynthesis proteins along with various secreted virulence factors, including hemolysins, leukotoxins, and lipases as a part of the ECM. The activity of ECM virulence factors was confirmed in a hemolysis assay and a *Galleria mellonella* pathogenicity model. In addition, we uncovered a so far unacknowledged moonlighting function of secreted virulence factors and ribosomal proteins trapped in the ECM: namely their contribution to biofilm integrity. Mechanistically, it was revealed that this stabilizing effect is mediated by the strong positive charge of alkaline virulence factors and ribosomal proteins in an acidic ECM environment, which is caused by the release of fermentation products like formate, lactate, and acetate because of oxygen limitation in biofilms. The strong positive charge of these proteins most likely mediates electrostatic interactions with anionic cell surface components, eDNA, and anionic metabolites. In consequence, this leads to strong cell aggregation and biofilm stabilization. Collectively, our study identified a new molecular mechanism during *S. aureus* biofilm formation and thus significantly widens the understanding of biofilm-associated *S. aureus* infections - an essential prerequisite for the development of novel antimicrobial therapies. *Molecular & Cellular Proteomics* 18: 1036–1053, 2019. DOI: 10.1074/mcp.RA118.001120.

Bacteria in nature can predominantly be found as surface-attached, multicellular aggregates called biofilms, which are embedded in a self-produced, extracellular matrix (ECM)¹ (1, 2). This matrix mainly contains polymeric substances like polysaccharides, extracellular DNA (eDNA) as well as proteins and varies in its composition depending on environmental conditions and among different bacterial species (3). Compared with planktonically cultivated bacteria, which poorly represent natural conditions, biofilms show an altered growth rate, metabolism, and gene expression profile (2). The reduced metabolic activity of biofilm-embedded cells and the protective nature of the ECM, acting as a barrier against antimicrobial agents and the host immune system, make biofilms inherently difficult to treat thereby causing major healthcare problems (4, 5). Notably, it is estimated that 65 to 80% of all human bacterial infections are biofilm-associated underlining the need for novel therapeutic strategies (6, 7).

The opportunistic pathogen *Staphylococcus aureus* represents a major cause of nosocomial infections and is well known for its capacity to form biofilms on host tissues and implants. This often leads to chronic infections, e.g. in patients suffering from osteomyelitis, endocarditis, cystic fibrosis or during catheterization (8–12). Generally, biofilm development is characterized by three phases: primary surface attachment, maturation, and biofilm dispersal (13). Moormeier and colleagues suggested two more phases during *S. aureus* biofilm development, which can be observed between the attachment and maturation phase and are characterized by intense cellular division (termed “multiplication”) followed by a premature detachment of a biofilm subpopulation (termed “exodus”) (14). Numerous studies mainly focused on elucidating individual molecular factors, which are crucial during these biofilm formation steps of *S. aureus*. Thus, important roles in adhesion to abiotic surfaces and host cells, as well as in biofilm integrity and structuring have been described for proteinaceous and nonproteinaceous factors. This includes mi-

From the ‡Institute of Microbiology, Department of Microbial Physiology and Molecular Biology; §Institute of Biochemistry, Department of Cellular Biochemistry and Metabolomics; ¶Institute of Microbiology, Department of Microbial Proteomics; University of Greifswald, Germany
Received September 28, 2018, and in revised form, February 19, 2019
Published, MCP Papers in Press, March 8, 2019, DOI 10.1074/mcp.RA118.001120

Secreted Virulence Factors Stabilize *S. aureus* Biofilms

crobial surface components recognizing adhesive matrix molecules (MSCRAMMs, e.g. CfiAB, SdrCDE), fibronectin-binding proteins FnBPAB, the autolysin AtlA, protein A, biofilm-associated protein Bap, phenol-soluble modulins (PSMs), proteases, nucleases, teichoic acids, the polysaccharide intercellular adhesin (PIA), and eDNA. A complex regulatory network of specific and global regulators tightly controls the expression and synthesis of these molecular factors during the different stages of biofilm growth. Major regulators involved in biofilm formation are: AgrA and RNAIII, Rot, SigB, SarA, SaeRS, MgrA, IcaR, CodY, CcpA, Spx, CidR, Rbf, LytSR, and TcaR (reviewed and summarized by (4, 15–18).

Global approaches can be particularly useful to unravel the intricate interaction within these regulatory networks and to identify proteins with important roles in biofilm formation. However, so far only a few studies applied different *omics* techniques to analyze *S. aureus* biofilm physiology (18–27). These studies focused either on (1) static biofilm cultivation models, (2) used obsolete *omics* technologies, or (3) lacked a *multi-omics* approach. Most importantly, the composition of the *S. aureus* ECM, particularly at the protein level, and the role of these proteins during biofilm growth are still largely unexplored.

Consequently, the here presented study aims at a comprehensive characterization of the intra- and extracellular (ECM and flow-through (FT)) proteome, as well as the extracellular metabolome of *S. aureus* biofilms cultured in a physiologically highly relevant flow system (28) applying *state-of-the-art omics* technologies. Moreover, we compared these biofilm protein and metabolite profiles to planktonic cells. Our analyses identified a so far nondescribed, molecular mechanism during biofilm formation, which uncovers moonlighting virulence factors and ribosomal proteins in the ECM as key players in mediating biofilm integrity.

EXPERIMENTAL PROCEDURES

Strain and Growth Medium—All experiments were performed using *S. aureus* HG001, which was described by Herbert *et al.*, 2010 (29). For all cultivations, RPMI 1640 medium (R7509, Sigma-Aldrich, St. Louis) was used. The medium was supplemented with 2 mM glutamine, 140 μ M citrate, 7.5 μ M FeCl₃ and trace metals according to Gertz *et al.*, 1999 (30) and Dörries *et al.*, 2013 (31).

Planktonic and Biofilm Cultivation for Omics Analyses—Planktonic overnight cultures were grown in Erlenmeyer flasks filled with 10 ml medium (liquid to air ratio 1:10) with vigorous agitation at 180 rpm and 37 °C for 18 h.

Planktonic main cultures were grown in Erlenmeyer flasks after inoculation of 100 ml prewarmed medium (liquid to air ratio of 1:5) to an OD_{500 nm} of 0.06 using a fresh overnight culture. The cultures were subsequently incubated at 180 rpm and 37 °C for 12 h.

Biofilm cultivation was performed at 37 °C in a continuous flow reactor system adapted from Dohnt *et al.*, 2011 (32) and Brady *et al.*,

2006 (33), which consists of a medium bottle, a multichannel pump, a drop trap, a silicon tube for biofilm growth (4 mm inner diameter, 1 m length, VWR, Darmstadt, Germany) and a waste bottle (supplemental Fig. S1). Before inoculation, the system was filled with growth medium and equilibrated overnight. To inoculate the system, *S. aureus* cells were precultivated for 5 h in a planktonic main culture as described above, diluted in fresh, prewarmed medium to an OD_{500 nm} of 0.1 and injected into the silicon tube using a luer-lock syringe. This precultivation step increased attachment reproducibility compared with inoculation using cells of an overnight culture. After inoculation, the system was left without medium flow for 1 h to allow attachment of the cells. Subsequently, biofilm cultivation was started with a continuous medium flow of 25 ml/h (corresponding to 2 m/h and a retention time of 30 min) for 12 h.

Sample Collection and Protein Extraction—Sample collection for intracellular (planktonic and biofilm) and extracellular (planktonic, biofilm ECM and biofilm flow-through (FT)) proteome analysis of the cultures was carried out after 12 h. All sampling and protein extraction steps were performed on ice.

Planktonic cells were harvested and pelleted by centrifugation at 7000 \times g and 4 °C for 10 min, and the supernatant was collected. The cell pellet was washed twice (resuspended and vortexed for 2 min (34)) using ice-cold high salt Tris-buffer according to Rice *et al.*, 2007 (35) and Bose *et al.*, 2012 (36): 50 mM Tris-HCl, 10 mM EDTA, 500 mM NaCl, pH 8. The resulting supernatants of the washing steps were pooled with the supernatant of the initial centrifugation step and filter-sterilized (0.45 μ m cut off, Sarstedt AG, Nürnberg, Germany). The supernatants and the remaining cell pellets were stored at –70 °C for further analysis.

For biofilm FT samples, the medium eluting from the flow system was collected on ice for 20 min, centrifuged, sterile filtered and stored as described above.

To obtain intracellular and ECM samples of the biofilm, the biofilm tube content was transferred in a centrifugation tube, centrifuged as described above and the supernatant was collected. In a next step, the remaining cell pellet was washed twice with high salt TE-buffer as described for planktonic samples, to effectively separate the ECM from the cells. The cell suspension was centrifuged again and the resulting supernatants containing ECM proteins were pooled with the supernatant of the initial centrifugation step, filter sterilized and stored for further analysis as described above. Applying this method, intracellular protein and metabolite contaminations caused by cell lysis were avoided, which was verified by CFU counting and metabolic footprint analysis comparing samples before and after the separation step (data not shown).

Intracellular protein extracts from the planktonic and biofilm cell pellets were prepared as already described (37, 38) with slight modifications: cells were resuspended in 1 ml TE-buffer followed by mechanical disruption with 500 μ l glass beads (0.1 to 0.11 mm, Sartorius Stedim Biotech, Göttingen, Germany) in 3 homogenization cycles at 6.5 m/s for 30 s using a FastPrep-25 homogenizer (MP Biologicals, Santa Ana, California). Cell debris and glass beads were removed by centrifugation at 20,000 \times g and 4 °C for 10 min. Insoluble and aggregated proteins were removed by an additional centrifugation step at 20,000 \times g and 4 °C for 30 min (37, 38). The resulting intracellular protein extracts were stored at –70 °C for further analysis.

Planktonic extracellular proteins, as well as biofilm ECM and biofilm FT proteins were enriched using StrataClean beads as described by Bonn *et al.*, 2014 (39) with slight modifications. Briefly, 20 μ l aliquots of the beads were washed twice with 500 μ l TE-buffer for StrataClean beads (TE_{SC}, 50 mM Tris-HCl, 10 mM EDTA, pH 8) with intermittent centrifugation at 6000 \times g and room temperature (RT) for 2 min. Subsequently, beads were primed by incubation in 200 μ l HCl at 100 °C for 6 h and washed twice with 1 ml TE_{SC}-buffer. For protein

¹ The abbreviations used are: ECM, extracellular matrix; FT, flow-through; eDNA, extracellular DNA; CLSM, confocal laser scanning microscopy; pl, isoelectric point; LFQ, label-free quantification; (r)IBAQ, (relative) intensity-based absolute quantification.

Secreted Virulence Factors Stabilize *S. aureus* Biofilms

enrichment, beads were incubated with culture supernatants at 4 °C on a rotating tube shaker overnight. Loaded beads were pelleted at 10,000 × *g* and 4 °C for 15 min, washed twice with 500 μl PBS buffer (137 mM NaCl, 0.2 mM KCl, 10 mM Na₂HPO₄, 1.8 mM KH₂PO₄, pH 7.4) and dried in a vacuum centrifuge (Eppendorf AG, Hamburg, Germany) for 20 min.

Sample Preparation for MS/MS Analysis—The concentration of intracellular protein extracts was determined according to Bradford *et al.*, 1967 (40) using Roti@-Nanoquant (Roth, Karlsruhe, Germany) following the manufacturer's instructions. Extracellular/ECM/FT protein amounts loaded on the beads were determined by BCA-assay (ThermoFisher Scientific, Waltham, MA) described by Smith *et al.*, 1985 (41) according to manufacturer's instructions using the standard protocol with additional shaking at 1500 rpm to avoid bead sedimentation. Protein amounts of 25 μg per sample were boiled for 10 min at 95 °C and subsequently separated on a 4–12% SDS-polyacrylamide gradient gel (Criterion, BioRad, Munich, Germany). The gel was fixed for 30 min in fixation solution (10% (v/v) acetic acid, 40% (v/v) ethanol), washed twice for 10 min in water and stained with Colloidal Coomassie Brilliant Blue G-250 as previously described (42, 43). After removing excessive Coomassie stain from the gel using water, gel lanes of intracellular and extracellular/ECM/FT samples were fractionated into 10 and 5 gel pieces, respectively, cut into gel blocks of ~1 mm³ and prepared for MS/MS analysis as follows. Gel blocks were transferred into low binding tubes and washed/destained 5 times with 900 μl gel washing buffer (0.2 M NH₄CO₃ in 30% (v/v) acetonitrile) at 37 °C in a tube shaker (Eppendorf AG) at 1500 rpm for 15 min. Destained gel blocks were dried in a vacuum centrifuge for 30 min, covered with trypsin solution (2 μg/ml, Promega, Madison) and incubated at 37 °C overnight for protein digest. Subsequently, 100 μl water was added, and peptides were eluted by treatment in an ultrasonic bath for 15 min. The supernatant was transferred into a fresh low binding tube, desiccated in a vacuum centrifuge and peptides were stored at –70 °C. Before MS/MS analysis, peptides were resolubilized adding 10 μl of 0.1% (v/v) acetic acid and transferred into glass vials.

MS/MS Analysis—Tryptic peptides were subjected to liquid chromatography (LC) separation and electrospray ionization-based mass spectrometry (MS) measurement applying adjusted injection volumes for each gel fraction of intracellular samples to reach maximum intensities. Injection volumes for extracellular samples were kept constant. Peptides were loaded on a self-made analytical column (Aeris PEPTIDE 3.6 μm XB - C18 (phenomenex), OD 360 μm, ID 100 μm, length 20 cm) and eluted by a binary nonlinear gradient of 5–75% acetonitrile in 0.1% acetic acid over 80 min with a flow rate of 300 nL/min. LC-MS/MS analyses were performed on an LTQ-Orbitrap-Velos mass spectrometer (ThermoFisher Scientific) coupled to an EASY-nLC 1000. For MS analysis, a full scan in the Orbitrap with a resolution of 30,000 and mass deviation of 0.5 Da was followed by CID MS/MS experiments of the 20 most abundant precursor ions acquired in the linear ion trap with a mass tolerance of 20 ppm.

MS Data Analysis—Database search, as well as label-free quantification (LFQ) and intensity-based absolute quantification (iBAQ), was performed using the MaxQuant software suite (version 1.6.0.16, Max Planck Institute of Biochemistry, Martinsried, Germany) running the built-in Andromeda search engine (Max Planck Institute of Biochemistry) (44–47). The database used was downloaded from UniProt on January 24th, 2018 (Proteome ID UP000008816) and contains 2889 protein sequences of *S. aureus* NCTC8325 (representing the parental strain *S. aureus* HG001 was derived from). The entry for protein RsbU was replaced by the corresponding sequence of *S. aureus* Newman because *rsbU* has been repaired in strain HG001 by Herbert and colleagues (29). Common laboratory contaminants and reversed sequences were included by MaxQuant. Database search parameters

were set as follows: Trypsin/P specific digestion (KR) with two allowed missed cleavages, peptide tolerance 20 ppm, fragment ion tolerance 4.5 Da, methionine oxidation (15.99 Da) as a variable modification, peptide spectral match FDR 1% and protein FDR 1%. No fixed modifications were included. LFQ was performed using the following settings: LFQ minimum ratio count 2 considering unique and razor peptides for quantification. Match between runs was enabled with a match time window of 0.7 min and an alignment time window of 20 min.

Results were filtered for proteins identified with 2 or more unique peptides in at least 2 out of 3 biological replicates. LFQ intensities of intracellular and extracellular/ECM/FT proteome data were used to calculate log₂ ratios between biofilm and planktonic samples. No further adjustments for systematic errors were applied. For proteins of intracellular samples, which were identified in 3 out of 3 biological replicates, these log₂ ratios were then visualized in Voronoi treemaps (48, 49) using the Paver software (DECODON GmbH, Greifswald, Germany) based on functional assignment of the SEED database (50) or based on regulon maps (51) created by Moche *et al.*, 2014 (18), respectively. For extracellular/ECM/FT data, treemaps were created based on subcellular localization predicted by PSORTb (52) and theoretical pI values extracted from AureoWiki database (53). Predictions by PSORTb were manually cured based on published localization studies, and LocateP (54) and SignalP (55) predictions. riBAQ values were calculated (47) and used to correlate treemap cell sizes with protein abundance.

Metabolic Footprint Analysis—For metabolic footprint analysis using ¹H-nuclear magnetic resonance (¹H-NMR) spectroscopy, planktonic and biofilm samples were harvested on ice after 12 h of cultivation, sterile filtered (0.45 μm cut off, Sarstedt AG, Nürnberg, Germany) and stored at –20 °C before measurement. For biofilm cultures, ECM samples were collected as described above. Moreover, 1 ml of the FT was collected on ice and prepared as described above. Samples were then thawed at RT, and 400 μl were mixed with 200 μl of sodium hydrogen phosphate buffer (0.2 mol/L, pH 7.0) made up with 50% D₂O, including 1 mM 3-trimethylsilyl-[2,2,3,3-D₄]-1-propanoic acid for ¹H-NMR analysis (31). Samples were analyzed using a Bruker AVANCE-II 600 NMR spectrometer operated by TOPSPIN 3.2 software. Qualitative and quantitative data analyses were carried out using AMIX v3.9.12 software (Bruker Biospin GmbH, Rheinstetten, Germany).

Nitrate concentrations were measured by applying 10 μl cell-free culture supernatant on colorimetric nitrate test stripes (Merck, Darmstadt, Germany). Self-made standards with nitrate concentrations ranging from 0–250 mg/L NO₃[–] served as controls.

Biofilm cultivation for CLSM analysis. To analyze biofilms using confocal laser scanning microscopy (CLSM), flow chambers with three individual growth channels (1 × 4 × 40 mm per channel) were prepared as described by Sternberg and Tolker-Nielsen, 2006 (56). Flow chambers were filled with growth medium overnight to equilibrate the chambers. Each channel of the flow chambers was inoculated with 300 μl of an overnight culture, which was diluted to an OD_{600 nm} of 0.01 using fresh, prewarmed growth medium. For inoculation, a small syringe was used. The flow chambers were left without flow for 1 h to allow bacterial attachment. Subsequent biofilm cultivation was performed with a flow rate of 3 ml/h (0.2 mm/s) for 12 h using a Watson-Marlow 205S peristaltic pump (Watson-Marlow GmbH, Rommerskirchen, Germany). Biofilms were stained with 5 μM Syto9 (prepared in 0.9% NaCl, ThermoFisher Scientific) without flow for 15 min. Subsequently, the biofilms were washed under flow for 15 min.

To elucidate the influence of ECM components on biofilm stability, established biofilms were treated as follows. For enzymatic digestion of ECM proteins, biofilms were incubated with Proteinase K (100

Secreted Virulence Factors Stabilize *S. aureus* Biofilms

$\mu\text{g/ml}$ in growth medium, ThermoFisher Scientific) without flow at 37 °C for 2 h according to Seidl *et al.*, 2008 (57). Treated biofilms were challenged by elevated shear forces applying an increased flow rate (30 ml/h) for 5 min before CLSM analysis. To analyze biofilm stability under alkaline conditions, established biofilms were subjected to an increased flow of growth medium adjusted to pH 12 as described above. For all treatments, fresh growth medium served as controls. CLSM images were acquired after 0, 2 and 5 min of increased flow using a Zeiss LSM 510 CLSM (Carl Zeiss, Jena, Germany) equipped with a water corrected 63 \times /NA1.2 objective and filter and detector settings for monitoring Syto9 fluorescence (excitation at 488 nm using an Ar-laser, emission light selected with a 505–550 nm bandpass filter). Image acquisition was performed using the ZEN 2009 software (Carl Zeiss) with z-stack sections of 0.5 μm . Three-dimensional reconstruction of z-stacks was done using the AMIRA software (version 6.0.1, ThermoFisher Scientific).

To visualize eDNA within the ECM, freshly grown biofilms were stained with the eDNA-specific stain Toto-1 (5 μM) and Syto62 (10 μM) as a counterstain (both prepared in 0.9% NaCl, ThermoFisher Scientific). Biofilm staining and washing was carried out in the dark for 15 min as described above. For biofilm and eDNA visualization, image acquisition was performed as described above with filter and detector settings for monitoring of Syto62 fluorescence (excitation at 633 nm using an HeNe-laser, emission light selected with a 650 nm longpass filter) and Toto-1 fluorescence (excitation at 514 nm with an Ar-laser, emission light selected with a 505–550 nm bandpass filter).

Cell Aggregation Test—The cell aggregation test was performed using biofilm-grown cells, which were cultivated, harvested, and pelleted as described for *omics* analysis. Subsequently, cell pellets were resuspended in the following solutions, which were adjusted to either pH 8 or pH 5.5: (1) planktonic or biofilm culture supernatant containing extracellular/ECM proteins, (2) fresh medium supplemented with bovine serum albumin (BSA, $pI = 4.7$, Sigma-Aldrich) or bovine cytochrome C (CytC, $pI = 10.0$, Sigma-Aldrich), (3) BSA or CytC supplemented growth medium plus DNA (*S. aureus* cDNA). The concentrations of control proteins and DNA used were: proteins = 50 $\mu\text{g/ml}$, DNA = 25 $\mu\text{g/ml}$. Cell suspensions of $OD_{500\text{ nm}} 10$ were prepared and incubated at RT for 1 min. Cells were stained with 5 μM Toto-1 and 10 μM Syto62 (ThermoFisher Scientific) for 15 min in the dark. Four microliters of these cell suspensions were applied on a thin layer of 1.5% agarose in 0.9% NaCl, which was mounted on a microscope slide. Fluorescence microscopy images were acquired and processed using a Zeiss Imager M2 (Carl Zeiss) equipped with a 100 \times /NA 1.3 oil immersion objective and the ZEN 2011 software package (Carl Zeiss).

Test for Osmotic Stress Resistance—Planktonic and biofilm cells were cultivated as described for *omics* analyses and used to test osmotic stress resistance. To this end, Erlenmeyer flasks filled with 10 ml prewarmed RPMI-Medium supplemented with 3 and 4 M NaCl, respectively, were inoculated to an $OD_{500\text{ nm}}$ of 0.05. It was microscopically verified that no cell aggregates were used for inoculation or developed during the experiment ensuring meaningful CFU counting results. Subsequently, cultures were incubated at 37 °C and 180 rpm following counting of surviving CFU every 24 h for 3 days.

pH Determination—Samples were collected as described for *omics* analysis. pH values of the biofilm FT and planktonic cultures were measured using a pH meter (pHenomenal pH1000L, VWR). To be able to determine the pH directly within the ECM, growth medium within silicon tubes was carefully removed by allowing air to enter the tube at a flow rate of 3 ml/h followed by biofilm sampling and centrifugation as described above. The pH of the resulting supernatant was measured using pH-indicator stripes ranging from pH 4.0–7.0 (Merck).

Galleria mellonella Pathogenicity Model—*G. mellonella* experiments were carried out according to Hill *et al.*, 2014 with slight

modifications (58). Larvae weighing ~300–400 mg were disinfected in 70% ethanol for 3 s and allowed to dry. Subsequently, 5 μl of cell-free culture supernatant (corresponding to 40 ng protein) were injected in the last left proleg of 15 larvae per sample using a 10 μl Hamilton syringe. Five microliters growth medium supplemented with 8 $\mu\text{g/ml}$ BSA and noninfected larvae served as controls. The larvae were incubated at 37 °C for 68 h with intermediate counting of surviving animals.

Hemolysis Assay—Hemolysis assays were performed as described by Lauderdale *et al.*, 2009 using samples collected as described above for *omics* analysis (59). Briefly, 0.5 ml rabbit blood (Fiebig Nährstofftechnik, Idstein-Niederauroff, Germany) was pelleted (6000 $\times g$, RT, 5 min) and resuspended in 12.5 ml growth medium. This suspension was mixed 1:1 with biofilm samples followed by an incubation at 37 °C for 10 min. Growth medium and 0.2% SDS prepared in growth medium served as negative and positive controls, respectively. Samples were centrifuged (6000 $\times g$, RT, 5 min), the supernatant was transferred in a 96-well microtiter plate and absorbance was measured at 540 nm in a microtiter plate reader (Synergy MX, BioTek Instruments, Winooski).

Experimental Design and Statistical Rationale—We decided to use an integrated *multi-omics* approach combining *state-of-the-art* proteomics and metabolomics techniques and phenotypic verification experiments to shed light on vital physiological processes in the cytoplasm and the ECM of biofilm forming cells (Fig. 1). Therefore, intra- and extracellular proteome analysis of planktonic cultures and intracellular, ECM and FT proteome analysis of biofilm cultures were performed of three biological replicates resulting in a total of 15 individual samples. All samples were prepared in parallel before LC-MS/MS analysis, which was performed in a randomized order. For metabolic footprint analysis, samples of four biological replicates were measured. Phenotypic experiments, including testing of osmotic stress resistance and hemolytic activity, as well as measurement of OD values and pH values were carried out in three biological replicates. In the *G. mellonella* pathogenicity model, culture supernatants of one biological replicate were used to inject 15 larvae per sample. All microscopy analyses were performed in biological duplicates. Images of 15 randomly selected areas were acquired. Thereof, a representative image of each condition and time point is shown.

Statistical significance was assessed by Student's *t* test and ANOVA using Excel (version 15.32, Microsoft Corporation, Redmond) for normally distributed proteome data by applying *p* values of 0.05. GraphPad PRISM (version 8, GraphPad Software, La Jolla) was used for data analysis of metabolome and phenotypic analyses. *p* values are provided in each figure legend.

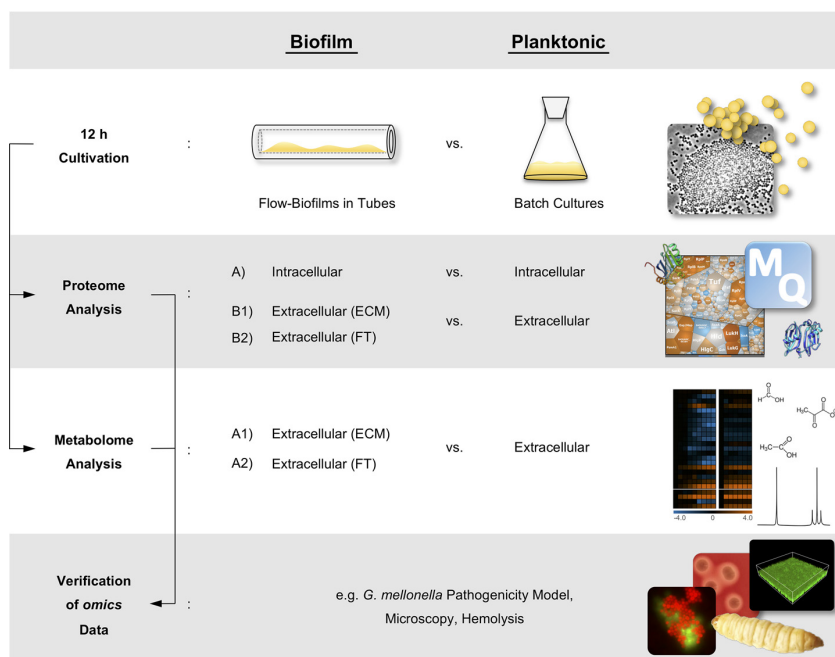
RESULTS AND DISCUSSION

Low metabolic activity of biofilm-embedded cells, as well as the ECM acting as a protective barrier against antimicrobial compounds and the host immune system, make biofilm-associated infections extremely difficult to treat. Although *S. aureus* has been recognized as one of the most frequent causes of biofilm-associated infections, its biofilm physiology and particularly the ECM composition are poorly understood.

Experimental Design—To comprehensively characterize important physiological processes during biofilm formation of *S. aureus*, we used an integrated *multi-omics* approach, which combines *state-of-the-art* proteomics and metabolomics techniques. We compared intracellular and extracellular/ECM/FT protein profiles, as well as ECM and FT metabolite profiles of *S. aureus* biofilms with intracellular and extracellu-

Secreted Virulence Factors Stabilize *S. aureus* Biofilms

FIG. 1. Schematic overview of the experimental design. Intracellular, ECM and FT protein profiles of 12 h biofilm cultures grown under flow conditions were compared with intracellular and extracellular protein profiles of 12 h planktonic batch cultures. These data were complemented by metabolic footprint analysis followed by verification of the *omics* data by different phenotypic analyses *e.g.* including a *G. mellonella* pathogenicity model and microscopy. ECM = Extracellular matrix, FT = Flow-through.



lar protein profiles and extracellular metabolites of their planktonic counterparts. Moreover, we complemented these *omics* data by phenotypic analyses of biofilm and planktonic cells. A workflow summarizing our approach is shown in Fig. 1. All identified intracellular, extracellular/ECM/FT proteins together with detailed information on peptide and protein identification have been deposited to the ProteomeXchange consortium (<http://proteomecentral.proteomexchange.org/cgi/GetDataset>) via the PRIDE partner repository with the data set identifier PXD011157 (see data availability section).

To this end, we established a cultivation system enabling us to investigate *S. aureus* biofilms grown under flow conditions, which reflects the natural environment more accurately compared with static biofilm cultivation models and which allows us to cultivate high amounts of biomass needed for proteome analysis (especially of the ECM).

It is generally believed that the physiology of mature biofilms resembles that of stationary, planktonic batch cultures (60–63), which are therefore an adequate reference for comparative *omics*-analyses of biofilm and planktonic cells. Hence, as a starting point, we were testing after which time period our biofilm and planktonic cultures represented mature biofilms and stationary cells, respectively. In contrast to other studies that analyzed biofilms over a time period of several days (21, 22, 64), we found that our biofilms matured relatively early, *i.e.* after 12 h of growth. This might be because we used, in contrast to the above-mentioned studies, a nutrient-rich medium leading to a quick maturation of *S. aureus* biofilms in our experimental flow setting. Planktonic cultures were harvested 12 h post-inoculation as well, after which they

reached the stationary phase. Interestingly, 36 h old flow cultures revealed a dying biofilm characterized by increased cell lysis as indicated by a high abundance of the major autolysin Atl (20, 90), decreased biofilm mass and a substantially higher amount of intracellular proteins within the ECM (data not shown).

Biofilm Cells Show a Similar but Less Pronounced Nutrient Limitation Response Compared with Planktonic Stationary Cells—To establish our biofilm flow system, we optimized cultivation settings (*e.g.* tube length and flow rate) in preliminary experiments to avoid nutrient depletion and concomitant physiological heterogeneities of the cells along the biofilm tube. According to our metabolome data, this was successfully achieved, because neither glucose nor the amino acids of the growth medium were completely depleted in the biofilm FT (supplemental Fig. S2).

A clear starvation response was observed in planktonic cells, because our metabolome data revealed depletion of glucose and amino acids (supplemental Fig. S2). In agreement with previously published studies (68, 91), this starvation response was indicated by our proteome data showing an increased abundance of proteins belonging to regulons controlled by the carbon catabolite protein A (CcpA), the pleiotropic repressor CodY and CymR, a regulator of sulfur metabolism (65–67) (supplemental Table S1, supplemental Fig. S3). For example, gluconeogenesis (*e.g.* GpmA, PckA, PycA) and TCA cycle enzymes (*e.g.* PdhABC, SucABD, SdhA, FumC), as well as amino acid biosynthesis proteins (*e.g.* LysAC, MetCEFI, LeuABCD, SerA, TrpBCDE), and oligopeptide uptake proteins (*e.g.* Opp-3ABCDF) were strongly up-

Secreted Virulence Factors Stabilize *S. aureus* Biofilms

regulated in stationary planktonic cells compared with biofilm cells. Furthermore, as expected under glucose-limited conditions, glycolysis enzymes were less abundant in planktonic cultures (e.g. Pgi, PfkA, TpiA, GapA, Eno), (supplemental Table S1, Fig. 2). However, differences in abundance of glycolysis/gluconeogenesis and TCA cycle enzymes were rather small. This observation agrees with the hypothesis that deeper layers of the biofilm might also face glucose starvation because of nutrient competition within the biofilm.

Interestingly, iron acquisition proteins of the Fur regulon were found more abundant in planktonic cultures (supplemental Table S1, supplemental Fig. S3), including e.g. iron transporters (SirA, HtsA) and proteins for biosynthesis of the siderophore staphylobactin (SbnEF). Consequently, it can be concluded that iron limitation is more pronounced in planktonic cultures compared with biofilms.

Collectively, these results suggest that the biofilm cells in our setting also experience nutrient limitation albeit to a lesser degree than the stationary planktonic cells. This can intuitively be explained by the nutrient supplying properties of a flow system, which supports the outer cells of the biofilm with enough nutrients during the entire experiment. The deeper layers of the biofilm, however, are likely to suffer from nutrient limitation. Because it was not possible in our experimental setup to analyze outer and inner biofilm cells separately, our proteome data reflect the mean abundance of the detected proteins for a rather heterogeneous population of cells. Nevertheless, dominant physiological effects that are characteristic for the biofilm cells can still be identified. This was particularly obvious for fermentation pathways, which will be explained in the following section.

Oxygen Limitation in Biofilms Leads to ECM Acidification—Biofilms are organized as densely packed communities making it intuitive that nutrient and oxygen availability throughout the biofilm is gradually decreasing and limited in deeper layers because of consumption and diffusion impairment. Especially oxygen limitation has been described for biofilms of various species (18, 21, 24, 68–70). Because of the higher cell densities reached during biofilm growth compared with planktonic growth, we expected to observe oxygen limitation also in our flow biofilms (supplemental Fig. S4).

Indeed, the proteome and metabolome data clearly revealed oxygen limitation in *S. aureus* biofilms indicated by the strong and significant accumulation of enzymes involved in mixed acid and 2,3-butanediol fermentation (e.g. lactate dehydrogenase Ldh1, alcohol dehydrogenase Adh1, pyruvate formate lyase PflB, acetolactate synthase BudB), and fermentation products like formate, lactate, ethanol, and 2,3-butanediol (supplemental Table S1, Fig. 2, supplemental Fig. S5A). In addition to fermentation, *S. aureus* can use nitrate respiration for energy production during oxygen-limited conditions. Our proteome data clearly showed an accumulation of enzymes required for nitrate respiration in biofilms (NarJGH, NasDEK) (supplemental Table S1, Fig. 2). Furthermore, nitrate con-

sumption was observable only in the biofilm but not in planktonic cultures (supplemental Fig. S5B). The fermentation and nitrate respiration proteins are part of the Rex and the NreC regulon, respectively. Both regulators were also found up-regulated in biofilms underlining the importance of these regulons during biofilm growth (supplemental Fig. S3).

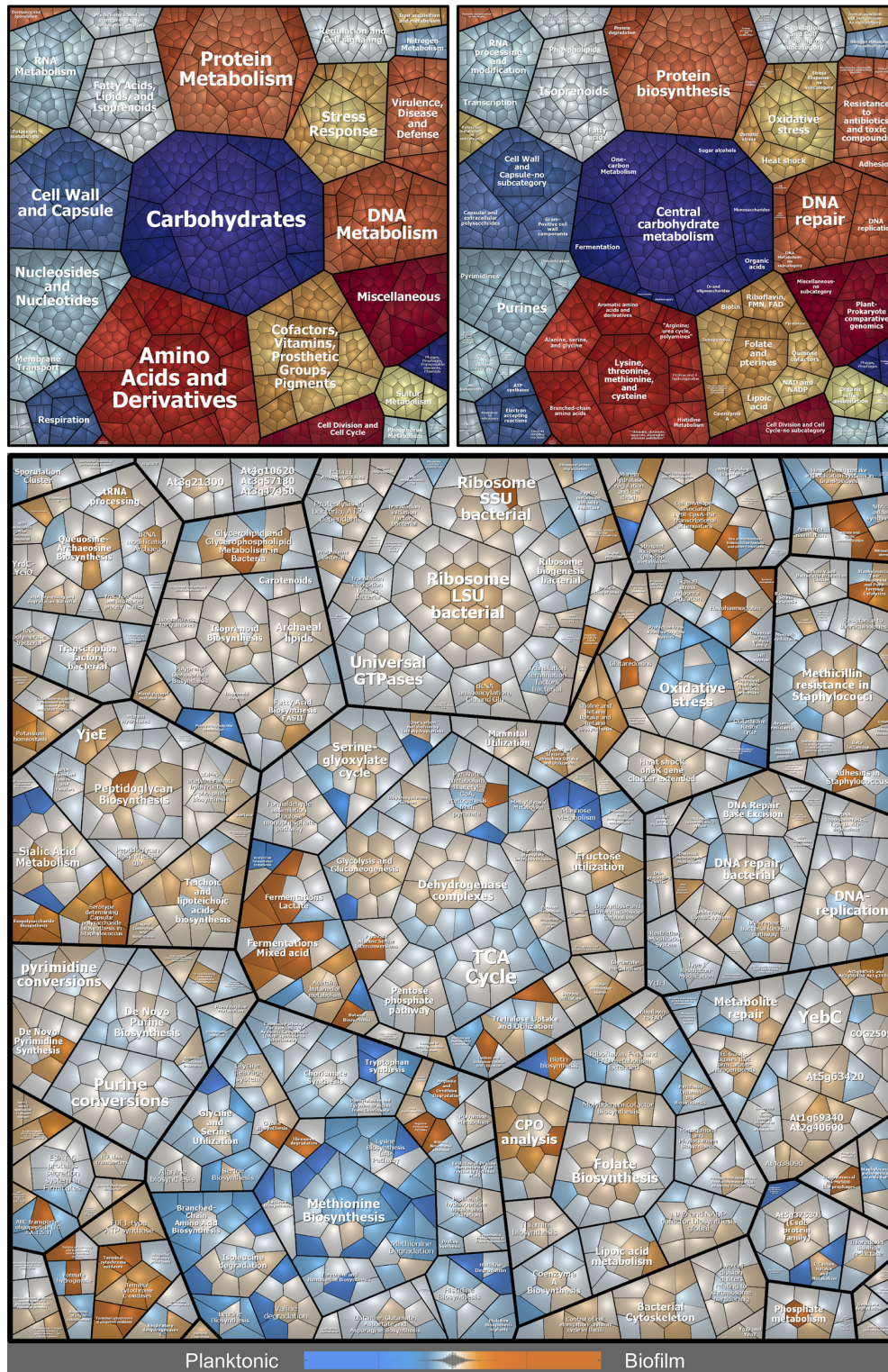
We further observed that the reduced oxygen availability in biofilms impacts proteins of the oxidative stress response, which were found less abundant compared with planktonic cells. This includes superoxide dismutase SodA, catalase KatA, alkyl hydroperoxide reductase AhpC, DNA protection protein Dps, and the glutathione peroxidase BsaA (supplemental Table S1, Fig. 2). Furthermore, proteins of the nitrosative stress response accumulated in biofilm cells (e.g. Hmp, ScdA, SrrAB) probably because of increased reactive nitrogen species production during nitrate respiration (71). As an additional consequence of oxygen limitation and nitrosative stress within biofilms, proteins of the SrrAB regulon involved in electron transport chain maintenance (cytochrome *c* and quinol oxidase assembly, as well as heme biosynthesis: CydAB, QoxABC, and HemBCDEHLQ) were found more abundant in biofilms (supplemental Table S1, Fig. 2). The importance of SrrAB in static *S. aureus* biofilms was also shown by Kinkel *et al.*, 2013 (71).

Most importantly, the accumulation of strong acids upon fermentative metabolism in *S. aureus* biofilms leads to local acidification, which was confirmed by pH measurements revealing a local pH of ~5.5 in the ECM compared with a pH of 7.6 in the FT, 7.5 in planktonic cultures and 8 in fresh growth medium (Fig. 3A). No acidification of the biofilm FT and planktonic cultures can be explained by dilution effects and the buffering properties of the growth medium. Notably, the observed acidification effect within the ECM is perfectly in line with results of other studies investigating *S. aureus* biofilms, where decreased pH values were observed (24, 26, 72–74). Interestingly, we did not observe an upregulation of proteins involved in the arginine deiminase and urease pathway, which were reported to counteract local acidification in *S. aureus* biofilms (supplemental Table S1, Fig. 2) (21, 26, 75, 76). This supports our proposed model of an acidified ECM environment playing a major role in mediating biofilm stability as explained in the following two sections.

***S. aureus* Biofilms Express High Amounts of Virulence Factors**—Next, we were interested in the exact composition of the ECM at the proteome level because it has been frequently reported that proteins are an important component of the ECM of clinical biofilm forming strains (26, 37, 38, 121–125). Moreover, the ECM represents a permeability barrier for many antimicrobial molecules and thus understanding its composition can help to develop novel antimicrobial strategies.

Approximately 30% of the total protein amount we found in the *S. aureus* ECM represented secreted extracellular proteins. However, the most abundant protein class in the ECM were intracellular proteins (~60%), which are primarily repre-

Secreted Virulence Factors Stabilize *S. aureus* Biofilms



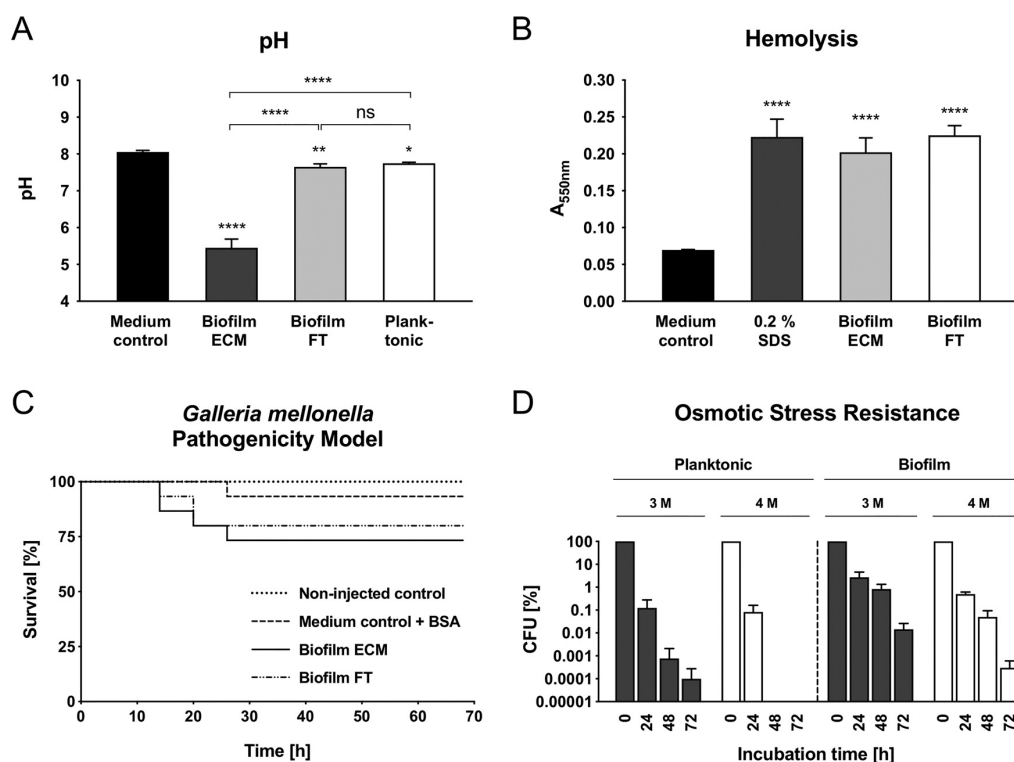
Secreted Virulence Factors Stabilize *S. aureus* Biofilms

FIG. 3. Phenotypic analyses of *S. aureus* cells and culture supernatants derived from flow biofilms and planktonic cultures grown for 12 h. **A**, pH values of a medium control, planktonic, biofilm ECM, and biofilm FT samples are indicated as the mean \pm S.D. of quadruplicate experiments. **B**, Hemolysis assay of a growth medium control, 0.2% SDS as a positive control, cell-free biofilm ECM and FT samples, respectively. Data are displayed as mean values \pm S.D. of triplicate experiments. **C**, *G. mellonella* larvae were injected with 5 μ l of cell-free biofilm ECM or FT samples, respectively. Noninjected larvae and growth medium supplemented with BSA served as controls. The survival of 15 larvae per experiment was monitored for 68 h. **D**, Freshly cultivated biofilm and planktonic cells were used to inoculate fresh growth medium supplemented with 3 M and 4 M NaCl, respectively. CFU were determined after 0, 24, 48, and 72 h. Data are displayed as mean values \pm S.D. of triplicate experiments relative to the CFU (100%) of time point 0 h. * = $p < 0.05$, ** = $p < 0.01$, *** = $p < 0.001$, **** = $p < 0.0001$. ECM = Extracellular matrix, FT = Flow-through.

sented by ribosomal proteins (~42% thereof, which corresponds to 25% of total ECM protein) (Fig. 4, Fig. 5A and supplemental Fig. S6). This can probably be explained by cell lysis within the biofilm or alternatively, as recently suggested, via nonclassical protein export by a yet unknown pathway (77). Interestingly, it has been proposed that intracellular proteins might contribute to pathogenicity by mediating binding to host matrix proteins and host cells (78). Cell lysis in biofilms is a well-reported phenomenon, which is mediated by the major autolysin Atl and the holin/antiholin system CidABC and LrgAB in *S. aureus* (35, 79–81). Interestingly, these proteins were not upregulated in our 12 h biofilms (supplemental Table S1). However, Atl was significantly upregulated in the 36-h

biofilm, which was accompanied by strong lysis and accumulation of intracellular proteins in the ECM (data not shown).

However, proteins with the highest abundance level in the ECM were extracellular proteins, which are primarily represented by virulence factors including e.g. hemolysins (Hla, HlgBC, Hld), a phenol-soluble modulins (Psm α 1), leukotoxins (LukGH), lipases (Geh, Plc), and the extracellular adherence protein (Eap/Map) (supplemental Table S2, Fig. 4, supplemental Fig. S6). Compared with extracellular planktonic samples, most of these virulence factors accumulate at a significantly higher amount in biofilm ECM samples (supplemental Table S2, Fig. 4). All these virulence factors were attributed to fulfill specific functions in *S. aureus* pathogenesis (82–85). Our

FIG. 2. Voronoi treemaps visualizing expression profiles of intracellular proteins in biofilms compared with planktonic cultures. Proteins found in MS analyses are displayed as single cells, which are functionally clustered in three hierarchical levels according to the Seed database: first level = upper left panel, second level = upper right panel, third level = bottom panel. Differences in protein abundance are indicated in the bottom panel by a color code based on LFQ intensities: orange = proteins more abundant in biofilms, blue = proteins more abundant in planktonic cultures, light gray: no difference in protein abundance.

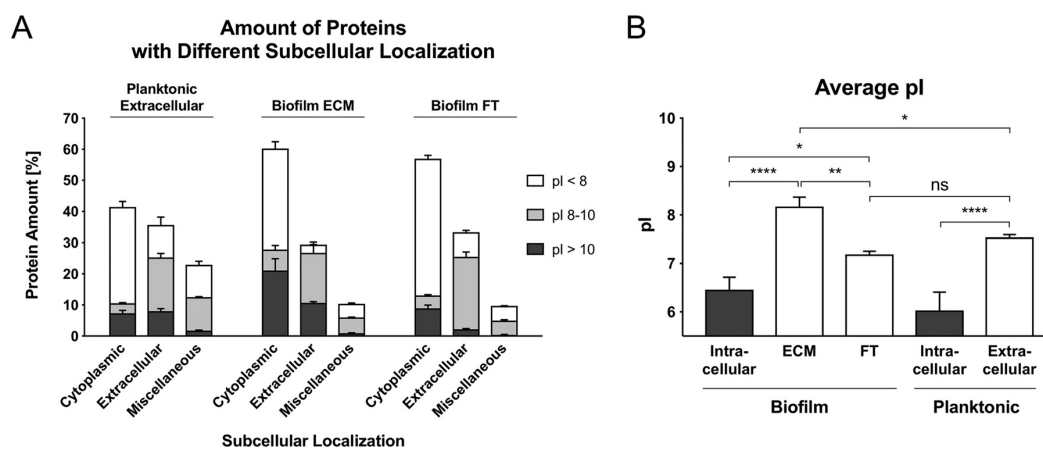
Secreted Virulence Factors Stabilize *S. aureus* Biofilms

FIG. 5. Amount of proteins with different subcellular localizations and differences in the average pI. A, Relative abundance of proteins with different subcellular localizations (predicted by PSORTb and manually cured: Cytoplasmic, Extracellular and Miscellaneous = Cytoplasmic membrane, Cell wall, no significant prediction) and different pI values, which were identified in extracellular planktonic samples, biofilm ECM and biofilm FT samples. The relative protein abundance was calculated based on riBAQ values. B, The average isoelectric point (pI) was calculated and normalized by protein abundance based on riBAQ values. Data are displayed as mean values \pm S.D. of triplicate experiments. pI values were extracted from the AureoWiki database. ns = not significant, * = $p < 0.05$, ** = $p < 0.01$, *** = $p < 0.001$, **** = $p < 0.0001$. ECM = Extracellular matrix, FT = Flow-through.

findings are consistent with other studies, which observed an accumulation of LukAB and Hla in *in vivo* *S. aureus* biofilm models (86–88). In contrast, studies using static biofilm cultivation models often did not identify elevated expression of virulence factors (18, 25, 26, 72), which seems to be an important difference between biofilms cultivated under static and flow conditions, respectively.

Many virulence factors that we found more abundant in biofilms are controlled by the quorum sensing responsive *agr* locus and the transcription factor SarA (18, 64, 89). However, proteins of the *agr* system or SarA were not significantly more abundant in biofilms compared with planktonic cells (supplemental Table S1, supplemental Fig. S3). We speculate that protein expression of the *agr* system reached its maximum in both, biofilm and planktonic cells, so the increased amount of virulence factors in the ECM might be explained by a passive accumulation effect. Alternatively, a local accumulation of the quorum sensing peptide within the ECM compartment could lead to a higher activation of the Agr two component system in biofilm cells as compared with planktonic cells. In addition, other global regulators (SigB, SaeRS, SrrAB, ArlRS, and Rot) known to control virulence gene expression, as well as their corresponding regulons were also more abundant in biofilms identifying these regulators as important players, which might balance virulence gene expression in *S. aureus* biofilms (supplemental Table S1 and S2, supplemental Fig. S3).

To prove that the identified, secreted virulence factors are functional, we tested cell-free supernatant derived from the ECM and the biofilm FT in hemolysis assays and in a *G. mellonella* pathogenicity model. Both samples indeed showed hemolytic activity and killed *G. mellonella* larvae in contrast to medium and BSA controls, respectively, which confirms the pathogenic potential of *S. aureus* biofilms (Fig. 3B and 3C).

Besides the high abundance of secreted virulence factors in the ECM, our intracellular proteome data also revealed that biofilm cells express higher amounts of capsule biosynthesis proteins CapABCDEFGHIJMN compared with planktonic cells (supplemental Table S1, Fig. 2). Interestingly, the same phenomenon was reported by Beenken *et al.*, 2004, who also investigated biofilms grown under constant medium flow (21), but not in other studies comparing planktonic cells and biofilms, which were cultivated as static colony biofilms (18, 25, 26).

Taken together, our findings strongly support the study of Lei *et al.*, 2017 (88), who proposed that *S. aureus* biofilms exhibit a high virulence potential and apply multiple strategies simultaneously to evade the host immune system. These strategies include protection by the ECM, capsule biosynthesis, and secretion of virulence factors like hemolysins, leukotoxins, lipases, and proteases.

S. aureus Virulence Factors and Ribosomal Proteins Exhibit a Moonlighting Function Contributing to Biofilm Integrity—

FIG. 4. Differences in protein profiles of the biofilm ECM and extracellular planktonic samples visualized by Voronoi treemaps. Proteins found in MS analyses are displayed as single cells, which sizes correlate with protein abundance based on riBAQ values of ECM proteins. Proteins are clustered according to their subcellular localization predicted by PSORTb (upper left panel), and isoelectric point (pI) according to AureoWiki (upper right panel). Bottom panel: Differences in protein abundance between biofilm ECM and extracellular planktonic samples are indicated by a color code, which is based on LFQ intensities: orange = proteins more abundant in ECM, blue = proteins more abundant in planktonic cultures, light gray = no difference in protein abundance. ECM = Extracellular matrix.

Secreted Virulence Factors Stabilize *S. aureus* Biofilms

Interestingly, most of the virulence factors we identified in the ECM are characterized by a high isoelectric point (pI) between 8 and 12 (supplemental Table S2, Fig. 4 and 5A). The same accounts for cytoplasmic proteins found within the ECM. In fact, nearly half of these cytoplasmic proteins have an isoelectric point between 8 and 12 and are primarily represented by ribosomal proteins (Fig. 4 and 5A). Moreover, the average pI of ECM samples is significantly higher compared with planktonic cultures and to the FT (Fig. 4 and 5B, supplemental Fig. S7).

We suspected that these alkaline virulence factors and ribosomal proteins will carry a strong positive charge in an acidic ECM environment created by formate, lactate, acetate, and pyruvate produced during glucose fermentation under oxygen-limited conditions (Fig. 3A, supplemental Fig. S5A).

As a consequence, these cationic proteins in the ECM might interact with anionic cell surfaces (90) and eDNA and thereby act as electrostatic bridges between cells providing physical strength to the biofilm, similarly as was proposed by Foulston *et al.*, 2014 and Dengler *et al.*, 2015 for intracellular proteins (72, 73). To further test this hypothesis, we used freshly cultivated biofilm cells, which were harvested, washed, pelleted and resuspended in either planktonic or biofilm ECM supernatant of pH 8 and pH 5.5, respectively, and investigated cell aggregation using fluorescence microscopy after staining with the eDNA stain Toto-1 and Syto62 as a counterstain. Strikingly, biofilm supernatant indeed induced the formation of cell aggregates under low pH conditions, which could not be observed for planktonic supernatant or a medium control at pH 5.5. At pH 8, no cell aggregates could be observed at all (Fig. 6A).

To verify that cationic proteins induce cell aggregation, we repeated the experiment using fresh medium supplemented with either cytochrome C (CytC, pI = 10.0) or BSA (pI = 4.7) as a negative control. We observed that only CytC and not BSA induced cell aggregation at pH 5.5 (Fig. 6A). These findings indicate, that cell aggregation in *S. aureus* biofilms is mediated by cationic proteins and is eDNA independent, because no eDNA was present in this experiment. However, because our CLSM analysis revealed high amounts of eDNA within the ECM (Fig. 6C), we tested if eDNA supplementation enhances the cell aggregation effect and repeated the experiment with planktonic and ECM supernatant in the presence of cDNA isolated from *S. aureus* to mimic eDNA. Although we observed binding of cDNA to cell aggregates, we did not observe an enhanced cell aggregation effect after addition of cDNA (Fig 6A). A possible explanation for this observation could be that the protein concentration used in our assay was in a range masking an enhancing aggregation eDNA effect besides the fact that ECM protein concentration used in this experiment corresponded to the concentration as determined for our biofilm ECM fraction.

Interestingly, we observed that other anionic metabolites, namely glutamate, aspartate and pyruvate, tend to accumu-

late within the ECM because they were found in higher concentrations in the ECM compared with the biofilm FT (supplemental Fig. S5A). This accumulation effect was not observed for acetate and lactate, because we measured high concentrations in the ECM, but even higher concentrations in the biofilm FT. This might be because of a saturation effect, because acetate and lactate represent the most abundant negatively charged metabolites within the ECM (supplemental Fig. S5A). We hypothesize that these anionic metabolites located in the ECM act as electrostatic counterparts to cationic proteins and thereby functionally act like eDNA.

To further characterize the role of cationic proteins in biofilm integrity, we treated established flow biofilms with Proteinase K according to Seidl *et al.*, 2008 (57), or alkaline medium adjusted to pH 12 to eliminate positive protein charges, followed by challenging the biofilms with elevated shear forces. The effects on biofilm integrity were visualized using CLSM. Strikingly, Proteinase K-treated and alkalized biofilms clearly showed impaired integrity because it was possible to almost completely eradicate the biofilm within 5 min of elevated shear stress (Fig. 6B). Importantly, alkaline growth medium with pH 12 does not kill *S. aureus* within 5 min, which was verified by CFU counting (data not shown). Supporting our findings, inhibiting effects of alkaline pH against Staphylococcal biofilm maturation were already reported, without significant inhibition of planktonic growth (91). Of note, DNase treatment of *S. aureus* biofilms did not impair integrity, which might be because of proteins protecting eDNA within the ECM from digestion (data not shown). In summary, these results strongly support the idea that cationic proteins play a major role in biofilm integrity under the tested conditions.

At present, *S. aureus* ECM stability is mainly attributed to PIA, an N-acetylglucosamine-based exopolysaccharide found in biofilms of numerous *S. aureus* strains. PIA is partly de-acetylated, which introduces positive charges at neutral and acidic pH suggesting that PIA mediates cell aggregation via electrostatic interactions with anionic cell surfaces and possibly eDNA (4). A similar concept was also shown in *P. aeruginosa* biofilms, where Pel, an abundant positively charged exopolysaccharide, interacts with eDNA (92). However, we were not able to identify any of the PIA biosynthesis proteins IcaABCD in our proteome data and the regulator IcaR was slightly less abundant in biofilms compared with planktonic cells, which points to a PIA-independent biofilm (supplemental Table S1). Interestingly, more recent studies reported an increasing number of *S. aureus* isolates including community- and hospital-acquired MRSA strains, which form PIA-independent, Proteinase K-sensitive biofilms (59, 64, 93–98). Biofilms of these strains were stated to be protein-dependent, which was attributed to adhesive surface proteins (59, 97, 99) and intracellular proteins (72, 73). More precisely, Foulston *et al.*, 2014 showed that cationic, intracellular proteins derived from *S. aureus* biofilms reversibly bind to cell

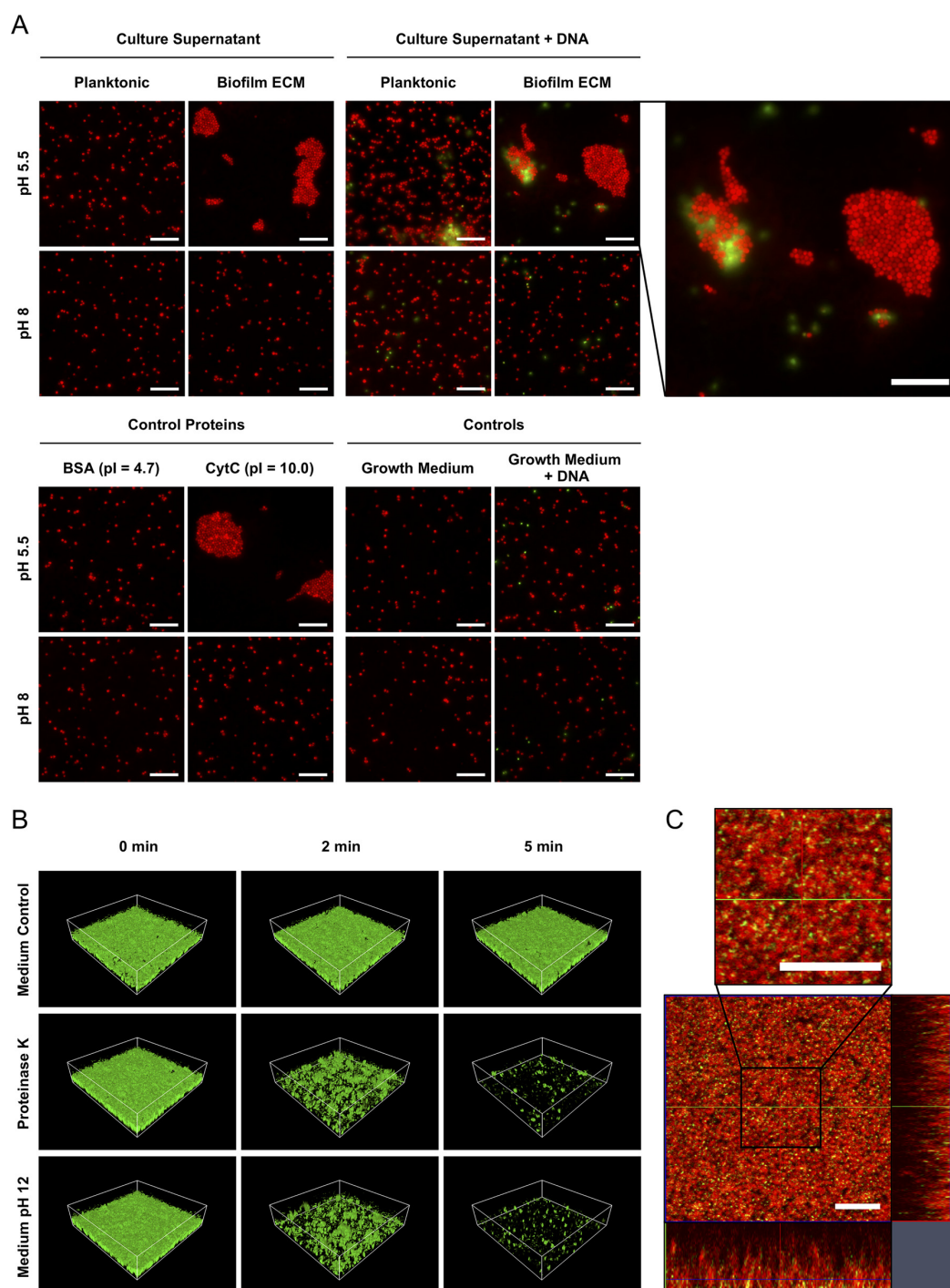
Secreted Virulence Factors Stabilize *S. aureus* Biofilms

FIG. 6. Microscopic analyses of the impact of cationic proteins and eDNA on *S. aureus* cell aggregation and biofilm stability. A, Freshly cultivated biofilm cells were harvested, washed, pelleted, and resuspended in the following solutions, which were adjusted to either pH 5.5 or pH 8, and investigated by fluorescence microscopy after staining with the eDNA stain Toto-1 and Syto62 as a counterstain: planktonic or biofilm ECM supernatant, fresh growth medium supplemented with BSA or CytC as control proteins, planktonic or biofilm ECM supernatant supplemented with cDNA isolated from *S. aureus*, medium control, medium control plus cDNA. Representative images of 15 randomly selected areas of duplicate experiments are shown. The scale bar indicates 10 μm . B, Biofilms were cultivated in flow cells for

Secreted Virulence Factors Stabilize *S. aureus* Biofilms

surfaces upon drop in pH, which contributes to multicellular behavior (72). Moreover, Dengler *et al.*, 2015 speculated that the function of cationic PIA within biofilms could be replaced by cationic proteins, which interact with anionic cell surfaces and eDNA. Thereby, they emphasized the crucial role of eDNA as an electrostatic bridge (73). Both studies suggested local acidification within biofilms following the release of fermentation products, which is perfectly in line with our proteome, metabolome and pH data. In agreement, we also identified a large proportion of cytosolic proteins within the ECM. Importantly, we were able to provide a more detailed view on the proteinaceous composition of the *S. aureus* ECM, thereby identifying specific proteins dominating the ECM (Fig. 4). Furthermore, we demonstrated that eDNA is a highly abundant component of the ECM (Fig. 6C), which is in line with numerous studies showing an important role of eDNA during both early and later stages of biofilm development (14, 35, 79, 100). However, compared with Dengler *et al.*, 2015 we were not able to observe enhanced cell aggregation after the addition of cDNA to cells mixed with ECM proteins, suggesting that the stability of our biofilm grown under flow-through conditions is predominantly depending on the proteins within the ECM (Fig. 6A). Interestingly, the negative cell surface charge, which seems to be key for cell aggregation, was previously suggested to be caused by teichoic acids in the *S. aureus* cell wall (4, 101). Supporting this idea, we found a slight but consistent upregulation of many proteins for teichoic acid biosynthesis in biofilms compared with planktonic cells (supplemental Table S1, Fig. 2).

It remains debatable if *S. aureus* actively increases secretion of alkaline virulence factors as an evolutionary favorable mechanism to stabilize biofilm structures, or if the high abundance of virulence factors within the ECM is caused by a passive accumulation because of the described electrostatic interactions (supplemental Table S1, Fig. 2).

Accumulation of Cationic Proteins and Anionic Metabolites Within the ECM Causes Osmotic Stress in Biofilm-embedded Cells—According to our model of ECM architecture, cells are electrostatically linked in the ECM environment by highly abundant proteins, eDNA and metabolites (Fig. 7). Because each of these molecules is osmotically active and theoretically elevates osmotic pressure, we hypothesized that biofilm-embedded *S. aureus* cells experience osmotic stress. Supportively, we found several proteins associated with osmotic stress resistance more abundant in biofilm cells. This includes proteins for the uptake and biosynthesis of osmoprotectants like OpuBCD and BetAB (supplemental Table S1, Fig. 2). In

addition, we found elevated levels of both cardiolipin synthases Cls1 and Cls2 in biofilms. Cardiolipin was shown to be important for *S. aureus* during long-term survival under osmotic stress conditions (102). Furthermore, we found the two-component system KdpDE and one protein of a potassium uptake system, KtrA, more abundant in biofilm cells, which mediate osmotic stress resistance (supplemental Table S1) (103, 104). This is in line with results of Price-Whelan *et al.*, 2013, who identified elevated transcript levels of *kdpDE* and a protective role of the Ktr potassium uptake system under osmotic stress conditions (104). Consequently, biofilm cells might be more osmotolerant than their planktonic counterparts.

To test this hypothesis, fresh medium supplemented with elevated NaCl concentrations (3 M and 4 M, respectively) was inoculated with cell suspensions derived from either planktonic or biofilm cultivations and subsequently analyzed for survival using CFU counting. We used cell suspensions instead of intact biofilms in this assay to separate effects of increased cell resistance from potential interference of a protective ECM. Strikingly, biofilm-grown cells show an increased survival rate compared with planktonic cells under both tested NaCl concentrations. Biofilm derived cells even survived in 4 M NaCl medium for 72 h, whereas planktonic cells already died after 48 h (Fig. 3D). Importantly, cells did not aggregate during the experiment (usually caused by the chaotropic properties of high salt concentrations) as we assessed by phase contrast microscopy, which ensured reliable CFU counting results (data not shown) (105).

To our knowledge, high osmotic pressure in *S. aureus* biofilms has not been reported yet, although it has been described that high osmolarity has a positive effect on biofilm formation, which is mediated by the alternative sigma factor B (106). Furthermore, others have also described an induction of osmotic stress protection systems in *S. aureus* biofilms. For example, Resch *et al.*, 2015 and Moche *et al.*, 2015 found genes and proteins induced in colony biofilms, which are associated with osmoprotectant uptake, but did not find elevated expression of the *kdp* system or *cls* (18, 25). Beenken and colleagues reported elevated transcript levels of *kdpDE* and *kdpABC*, as well as *cls* in flow biofilms, but not of genes associated with osmoprotectant uptake (21). In addition, a transposon mutant library screening by Boles *et al.*, 2010 revealed that a defect in genes involved in osmoregulation results in impaired biofilm formation (98). Contrary to these studies, metabolic profiling of Junka *et al.*, 2013 revealed an accumulation of osmoprotectants in planktonic cells but not in static biofilms (24).

12 h followed by a treatment with a growth medium control, Proteinase K, and alkalized growth medium of pH 12, respectively. Biofilms were subsequently challenged by elevated shear forces to test biofilm stability and analyzed by confocal laser scanning microscopy (CLSM). For each biofilm, 3 CLSM images of randomly selected areas (spanning 100 $\mu\text{m} \times 100 \mu\text{m}$) were acquired after 0, 2, and 5 min of elevated shear stress in duplicate experiments. A representative image of each treatment and time point is shown. C, Biofilms were cultivated in flow cells for 12 h, stained with the eDNA stain Toto-1 (green) and Syto62 (red) as a counterstain, washed and analyzed by CLSM. A representative image of 5 randomly selected areas of duplicate experiments is shown. The scale bar indicates 10 μm .

Cell Aggregation and ECM Stabilization

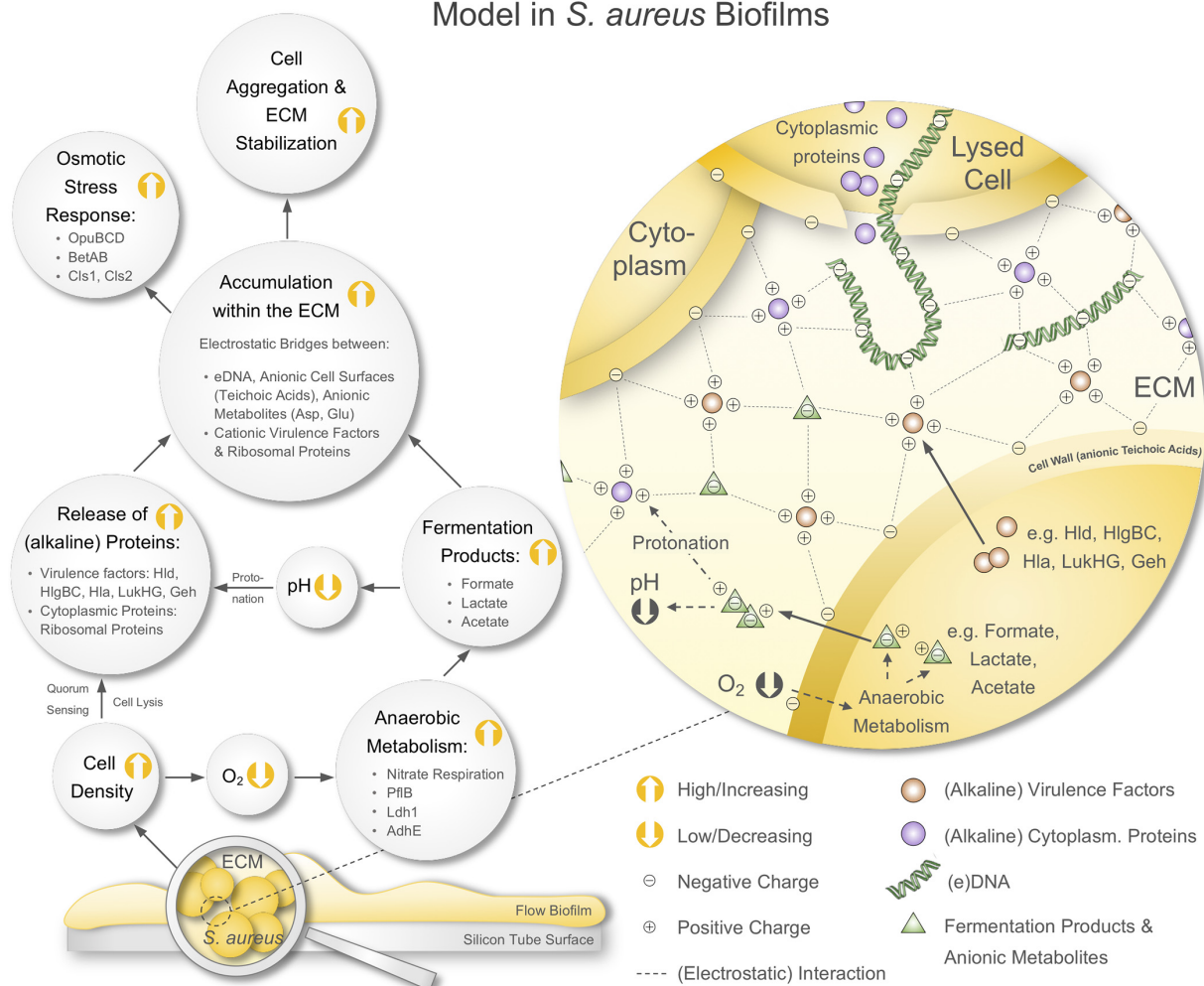
Model in *S. aureus* Biofilms

FIG. 7. Proposed model of cell aggregation and ECM stabilization mediated by moonlighting virulence factors and ribosomal proteins in *S. aureus* biofilms. Biofilms cultivated in a continuous flow system on a silicon tube surface grow to high cell densities, which leads to oxygen limitation. Consequently, biofilm-embedded cells are driven toward anaerobic metabolism and secrete high amounts of fermentation products lowering the local pH within the ECM. Furthermore, *S. aureus* biofilm cells release high amounts of eDNA, virulence factors and ribosomal proteins (besides other cytoplasmic proteins). These proteins get protonated in the acidic ECM environment because of their alkaline character. The accumulation of these cationic proteins, eDNA and anionic fermentation products along with other anionic metabolites (I) creates an electrostatic network involving eDNA and anionic cell surfaces (harboring anionic teichoic acids), which leads to cell aggregation and ECM stabilization and (II) leads to an osmotic stress response in biofilm-embedded cells. ECM = Extracellular matrix.

Interestingly, studies on *Bacillus subtilis* and *Vibrio cholera* biofilms proposed that ECM components generate osmotic pressure thereby helping biofilm-embedded cells to spread over the growth substratum (107, 108). If a comparable mechanism also exists in *S. aureus* biofilms and which specific ECM components might contribute to elevated osmotic pressure remains elusive. However, there are reports suggesting a connection of K^+ /osmolarity sensing by the KdpDE two-com-

ponent system and regulation of virulence factor expression, which includes positive regulation of capsule biosynthesis genes *cap*, and negative regulation of invasion factors like lipase Geh, the proteinase Aur and the hemolysins Hla and HlgB (109–111). Notably, in our experiment all of these proteins were found to be more abundant in *S. aureus* biofilms compared with their planktonic counterparts (supplemental Table S1, S2, Fig. 2 and 4). Because expression of these

Secreted Virulence Factors Stabilize *S. aureus* Biofilms

virulence factors is primarily controlled by other major regulators including *e.g.* Agr/RNAlII, Rot, CodY, SarA, SaeRS, SrrAB, and ArlRS (64, 89, 112–119), it could be speculated that the KdpDE system has a fine-tuning function for virulence gene expression in *S. aureus* biofilms.

CONCLUSIONS

Establishing a flow system for highly reproducible cultivation of *S. aureus* biofilms enabled us to grow biofilms under conditions, which are relevant for different clinical scenarios, *i.e.* endocarditis or catheter-associated infections, thereby complementing studies employing static biofilm cultivation models. This flow system allowed the cultivation of high amounts of biofilm biomass, which was a prerequisite to apply a *multi-omics* approach investigating intracellular and ECM proteome profiles in combination with extracellular metabolome profiles.

Using this *multi-omics* approach, we showed that *S. aureus* biofilms secrete high amounts of functional virulence factors like hemolysins, leukotoxins, and lipases, which are part of the ECM but can also be found in the biofilm FT. Applying a *G. mellonella* pathogenicity model and a hemolysis assay, we demonstrated that these virulence factors are active. Furthermore, we show that the *S. aureus* biofilm ECM consists to a large extent of ribosomal proteins. We demonstrate that secreted virulence factors and ribosomal proteins play a so far unacknowledged role as moonlighting proteins, which contribute to biofilm integrity. This stabilizing effect is mediated by an acidic ECM environment caused by the release of fermentation products like formate, lactate, and acetate. Positive charges on alkaline proteins introduced by the acidic environment promote the interaction of proteins with negatively charged cell surfaces, eDNA and anionic metabolites.

Moreover, we suggest that the proteins and metabolites, which are accumulating within the ECM cause osmotic stress in biofilm-embedded cells. Our proposed model is summarized in Fig. 7. Taken together, our study provides a comprehensive map of the intracellular and ECM proteome of *S. aureus* flow biofilms.

Acknowledgments—We thank Anica Graf, Susanne Sievers, Daniela Zühlke, and Jörg Bernhardt for fruitful discussions. Moreover, we thank Silvia Dittmann for excellent technical assistance as well as Claudia Hirschfeld and Pierre Mücke for help with MS analysis. Furthermore, we are grateful to Rabea Schlüter and Stefan Bock (Imaging Center of the Faculty of Biology, University of Greifswald) for providing the Amira software and help with 3D biofilm image reconstruction.

DATA AVAILABILITY

MS raw data, MaxQuant output files and the used database were deposited to the ProteomeXchange consortium (<http://proteomecentral.proteomexchange.org/cgi/GetDataset>) via the PRIDE partner repository (120) with the data set identifier PXD011157.

* This work was funded by the German Research Foundation (Collaborative Research Center Transregio 34, subprojects A3, A8, and Z4, and the Research Training Group 1870).

☐ This article contains supplemental Figures and Tables. We have declared no conflict of interest.

|| To whom correspondence should be addressed. Tel.: +49 38344205900; E-mail: riedela@uni-greifswald.de.

Author contributions: A.C.G., J.P.-F., and K.R. designed research; A.C.G., A.L., M.S., L.M.R., J.H., S.M., M.L., D.B., and J.P.-F. performed research; A.C.G. analyzed data; A.C.G., J.P.-F., and K.R. wrote the paper.

REFERENCES

- Costerton, J. W., Geesey, G. G., and Cheng, K. J. (1978) How bacteria stick. *Sci. Am.* **238**, 2–11
- Donlan, R. M. (2002) Biofilms: microbial life on surfaces. *Emerg. Infect. Dis.* **8**, 881–890
- Flemming, H. C., and Wingender, J. (2010) The biofilm matrix. *Nat. Rev. Microbiol.* **8**, 1–11
- Otto, M. (2008) Staphylococcal biofilms. *Curr. Top. Microbiol. Immunol.* **322**, 207–228
- Stewart, P. S., and William Costerton, J. (2001) Antibiotic resistance of bacteria in biofilms. *Lancet* **358**, 135–138
- Joo, H. S., and Otto, M. (2012) Molecular basis of in vivo biofilm formation by bacterial pathogens. *Chem. Biol.* **19**, 1503–1513
- Römling, U., and Balsalobre, C. (2012) Biofilm infections, their resilience to therapy and innovative treatment strategies. *J. Int. Med.* **272**, 541–561
- Lister, J. L., and Horswill, A. R. (2014) Staphylococcus aureus biofilms: recent developments in biofilm dispersal. *Front Cell Infect Microbiol.* **4**, 1–9
- Chatterjee, S., Maiti, P., Dey, R., Kundu, A., and Dey, R. (2014) Biofilms on indwelling urologic devices: microbes and antimicrobial management prospect. *Ann. Med. Health Sci. Res.* **4**, 100–104
- Kiedrowski, M. R., and Horswill, A. R. (2011) New approaches for treating staphylococcal biofilm infections. *Ann. N.Y. Acad. Sci.* **1241**, 104–121
- Barrett, L., and Atkins, B. (2014) The clinical presentation of prosthetic joint infection. *J. Antimicrob. Chemother.* **69**, i25–i27
- Parsek, M. R., and Singh, P. K. (2003) Bacterial biofilms: an emerging link to disease pathogenesis. *Annu. Rev. Microbiol.* **57**, 677–701
- O'Toole, G. A., Kaplan, H. B., and Kolter, R. (2000) Biofilm formation as microbial development. *Annu. Rev. Microbiol.* **54**, 1–37
- Moormeier, D. E., Bose, J. L., Horswill, A. R., and Bayles, K. W. (2014) Temporal and stochastic control of Staphylococcus aureus biofilm development **5**, e01341-14
- Speziale, P., Pietrocola, G., Foster, T. J., and Geoghegan, J. A. (2014) Protein-based biofilm matrices in Staphylococci. *Front Cell Infect Microbiol.* **4**, 1–10
- Payne, D. E., and Boles, B. R. (2016) Emerging interactions between matrix components during biofilm development. *Curr. Genet.* **62**, 137–141
- Paharik, A. E., and Horswill, A. R. (2016) The Staphylococcal biofilm: adhesins, regulation, and host response. *Microbiol. Spectr.* **4**, 1–48
- Moche, M., Schlüter, R., Bernhardt, J., Plate, K., Riedel, K., Hecker, M., and Becher, D. (2015) Time-resolved analysis of cytosolic and surface-associated proteins of Staphylococcus aureus HG001 under planktonic and biofilm conditions. *J. Proteome Res.* **14**, 3804–3822
- Ammons, M. C. B., Tripet, B. P., Carlson, R. P., Kirker, K. R., Gross, M. A., Stanisich, J. J., and Copié, V. (2014) Quantitative NMR Metabolite Profiling of Methicillin-Resistant and Methicillin-Susceptible Staphylococcus aureus Discriminates between Biofilm and Planktonic Phenotypes. *J. Proteome Res.* **13**, 2973–2985
- Atshan, S. S., Shamsudin, M. N., Sekawi, Z., Thian Lung, L. T., Barantalab, F., Liew, Y. K., Alreshidi, M. A., Abduljaleel, S. A., and Hamat, R. A. (2015) Comparative proteomic analysis of extracellular proteins expressed by various clonal types of Staphylococcus aureus and during planktonic growth and biofilm development. *Front. Microbiol.* **6**, 1081–1089
- Beenken, K. E., Dunman, P. M., McAleese, F., Macapagal, D., Murphy, E., Projan, S. J., Blevins, J. S., Smeltzer, M. S. (2004) Global gene expression in Staphylococcus aureus biofilms. *J. Bacteriol.* **186**, 4665–4684

Secreted Virulence Factors Stabilize *S. aureus* Biofilms

22. Bénard, L., Litzler, P. Y., Cosette, P., Lemeland, J. F., Jouenne, T., and Junter, G. A. (2009) Proteomic analysis of *Staphylococcus aureus* biofilms grown in vitro on mechanical heart valve leaflets. *J. Biomed. Mater. Res.* **88**, 1069–1078
23. Islam, N., Ross, J. M., and Marten, M. R. (2015) Proteome analyses of *Staphylococcus aureus* biofilm at elevated levels of NaCl. *Clin. Microbiol.* **4**, 1–15
24. Junka, A. F., Deja, S., Smutnicka, D., Szymczyk, P., Ziolkowski, G., Bartoszewicz, M., and Młynarz, P. (2013) Differences in metabolic profiles of planktonic and biofilm cells in *Staphylococcus aureus* - (1)H Nuclear Magnetic Resonance search for candidate biomarkers. *Acta Biochim. Pol.* **60**, 701–706
25. Resch, A., Leicht, S., Saric, M., Pásztor, L., Jakob, A., Götz, F., Nordheim, A. (2006) Comparative proteome analysis of *S. aureus* biofilm and planktonic cells and correlation with transcriptome profiling. *Proteomics* **6**, 1867–1877
26. Resch, A., Rosenstein, R., Nerz, C., and Götz, F. (2005) Differential gene expression profiling of *Staphylococcus aureus* cultivated under biofilm and planktonic conditions. *Appl. Environ. Microbiol.* **71**, 2663–2676
27. Tan, X., Qin, N., Wu, C., Sheng, J., Yang, R., Zheng, B., Ma, Z., Liu, L., Peng, X., and Jia, A. (2015) Transcriptome analysis of the biofilm formed by methicillin-susceptible *Staphylococcus aureus*. *Sci. Rep.* **5**, 1–12
28. Seper, A., Pressler, K., Kariisa, A., Haid, A. G., Roier, S., Leitner, D. R., Reidl, J., Tamayo, R., and Schild, S. (2014) Identification of genes induced in *Vibrio cholerae* in a dynamic biofilm system. *Int. J. Med. Microbiol.* **304**, 749–763
29. Herbert, S., Ziebandt, A. K., Ohlsen, K., Schäfer, T., Hecker, M., Albrecht, D., Novick, R., and Götz, F. (2010) Repair of global regulators in *Staphylococcus aureus* 8325 and comparative analysis with other clinical isolates. *Infection Immunity* **78**, 2877–2889
30. Gertz, S., Engelmann, S., Schmid, R., Ohlsen, K., Hacker, J., and Hecker, M. (1999) Regulation of SigmaB-dependent transcription of sigB and asp23 in two different *S. aureus* strains. *Mol. Gen. Genet.* **61**, 558–566
31. Dörries, K., and Lalk, M. (2013) Metabolic footprint analysis uncovers strain specific overflow metabolism and D-isoleucine production of *Staphylococcus aureus* COL and HG001. *PLOS ONE* **8**, e81500-9
32. Dohnt, K., Sauer, M., Müller, M., Atallah, K., Weidemann, M., Gronemeyer, P., Rasch, D., Tiele, P., and Krull, R. (2011) An in vitro urinary tract catheter system to investigate biofilm development in catheter-associated urinary tract infections. *J. Microbiol. Methods* **87**, 302–308
33. Brady, R. A., Leid, J. G., Camper, A. K., Costerton, J. W., and Shirliff, M. E. (2006) Identification of *Staphylococcus aureus* proteins recognized by the antibody-mediated immune response to a biofilm infection. *Infection Immunity* **74**, 3415–3426
34. Toyofuku, M., Roschitzki, B., Riedel, K., and Eberl, L. (2012) Identification of proteins associated with the *Pseudomonas aeruginosa* biofilm extracellular matrix. *J. Proteome Res.* **11**, 4906–4915
35. Rice, K. C., Mann, E. E., Endres, J. L., Weiss, E. C., Cassat, J. E., Smeltzer, M. S., and Bayles, K. W. (2007) The cidA murein hydrolase regulator contributes to DNA release and biofilm development in *Staphylococcus aureus*. *Proc. Natl. Acad. Sci. U.S.A.* **104**, 8113–8118
36. Bose, J. L., Lehman, M. K., Fey, P. D., and Bayles, K. W. (2012) Contribution of the *Staphylococcus aureus* Atl AM and GL murein hydrolase activities in cell division, autolysis, and biofilm formation. *PLOS ONE* **7**, e42244-11
37. Becher, D., Hempel, K., Sievers, S., Zühlke, D., Pané-Farré, J., Otto, A., Fuchs, S., Albrecht, D., Bernhardt, J., Engelmann, S., Völker, U., van Dijk, J. M., and Hecker, M. (2009) A proteomic view of an important human pathogen - towards the quantification of the entire *Staphylococcus aureus* proteome. *PLOS ONE* **4**, e8176-12
38. Zühlke, D., Dörries, K., Bernhardt, J., Maaß, S., Muntel, J., Liebscher, V., Pané-Farré, J., Riedel, K., Lalk, M., Völker, U., Engelmann, S., Becher, D., Fuchs, S., and Hecker, M. (2016) Costs of life - Dynamics of the protein inventory of *Staphylococcus aureus* during anaerobiosis. *Sci. Rep.* **6**, 1–13
39. Bonn, F., Bartel, J., Büttner, K., Hecker, M., Otto, A., and Becher, D. (2014) Picking vanished proteins from the void: how to collect and ship/share extremely dilute proteins in a reproducible and highly efficient manner. *Anal. Chem.* **86**, 7421–7427
40. Bradford, M. M. (1976) A rapid and sensitive method for the quantitation of microgram quantities of protein utilizing the principle of protein-dye binding. *Anal. Biochem.* **72**, 248–254
41. Smith, P. K., Krohn, R. I., Hermanson, G. T., and Mallia, A. K. (1985) Measurement of protein using bicinchoninic acid. *Anal. Biochem.* **150**, 76–85
42. Laemmli, U. K. (1970) Cleavage of structural proteins during the assembly of the head of bacteriophage T4. *Nature* **227**, 680–685
43. Neuhoff, V., Arold, N., Taube, D., and Ehrhardt, W. (1988) Improved staining of proteins in polyacrylamide gels including isoelectric focusing gels with clear background at nanogram sensitivity using Coomassie Brilliant Blue G-250 and R-250. *Electrophoresis* **9**, 255–262
44. Cox, J., and Mann, M. (2008) MaxQuant enables high peptide identification rates, individualized p.p.b.-range mass accuracies and proteome-wide protein quantification. *Nat. Biotechnol.* **26**, 1367–1372
45. Cox, J., Neuhauser, N., Michalski, A., Scheltema, R. A., Olsen, J. V., and Mann, M. (2011) Andromeda: a peptide search engine integrated into the MaxQuant environment. *J. Proteome Res.* **10**, 1794–1805
46. Cox, J., Hein, M.Y., Lubner, C.A., Paron, I., Nagaraj, N., and Mann, M. (2014) Accurate proteome-wide label-free quantification by delayed normalization and maximal peptide ratio extraction, termed MaxLFQ. *Mol. Cell. Proteomics* **13**, 2513–2526
47. Tyanova, S., Temu, T., and Cox, J. (2016) The MaxQuant computational platform for mass spectrometry-based shotgun proteomics. *Nat. Protocols* **11**, 2301–2319
48. Bernhardt, J., Funke, S., Hecker, M., and Siebourg, J. Visualizing gene expression data via Voronoi treemaps. *2009 Sixth International Symposium on Voronoi Diagrams*, pp. 233–241, Copenhagen
49. Liebermeister, W., Noor, E., Flamholz, A., Davidi, D., Bernhardt, J., and Milo, R. (2014) Visual account of protein investment in cellular functions. *Proc. Natl. Acad. Sci. U.S.A.* **111**, 8488–8493
50. Overbeek, R. (2005) The subsystems approach to genome annotation and its use in the project to annotate 1000 genomes. *Nucleic Acids Res.* **33**, 5691–5702
51. Otto, A., Bernhardt, J. O. R., Meyer, H., Schaffer, M., Herbst, F. A., Siebourg, J., Mader, U., Lalk, M., Hecker, M., and Becher, D. 2010. Systems-wide temporal proteomic profiling in glucose-starved *Bacillus subtilis*. *Nat. Communications* **1**, 137–139
52. Yu, N. Y., Wagner, J. R., Laird, M. R., Melli, G., Rey, S., Lo, R., Dao, P., Sahinalp, S. C., Ester, M., Foster, L. J., Brinkman, F. S. L. (2010) PSORTb 3.0: improved protein subcellular localization prediction with refined localization subcategories and predictive capabilities for all prokaryotes. *Bioinformatics* **26**, 1608–1615
53. Fuchs, S., Mehlan, H., Bernhardt, J., Hennig, A., Michalik, S., Surmann, K., Pané-Farré, J., Giese, A., Weiss, S., Backert, L., Herbig, A., Nieselt, K., Hecker, M., Völker, U., and Mäder, U. (2017) AureoWiki - The repository of the *Staphylococcus aureus* research and annotation community. *Int. J. Med. Microbiol.* **308**, 558–568
54. Zhou, M., Boekhorst, J., Francke, C., and Siezen, R. J. (2008) LocateP: Genome-scale subcellular-location predictor for bacterial proteins. *BMC Bioinformatics* **9**, 173–117
55. Petersen, T. N., Brunak, S., Heijne von, G., and Nielsen, H. (2011) SignalP 4.0: discriminating signal peptides from transmembrane regions. *Nat. Rev. Microbiol.* **8**, 785–786
56. Sternberg, C., and Tolker-Nielsen, T. (2006) Growing and analyzing biofilms in flow cells. *Curr. Protoc. Microbiol.* Chapter 1:Unit 1B.2-1B.2.15
57. Seidl, K., Goerke, C., Wolz, C., Mack, D., Berger-Bachi, B., and Bischoff, M. (2008) *Staphylococcus aureus* CcpA affects biofilm formation, infection and immunity. *Infect. Immun.* **76**, 2044–2050
58. Hill, L., Veli, N., and Coote, P.J. (2014) Evaluation of *Galleria mellonella* larvae for measuring the efficacy and pharmacokinetics of antibiotic therapies against *Pseudomonas aeruginosa* infection. *Int. J. Antimicrobial Agents* **43**, 254–261
59. Lauderdale, K. J., Boles, B. R., Cheung, A. L., and Horswill, A. R. (2009) Interconnections between Sigma B, agr, and proteolytic activity in *Staphylococcus aureus* biofilm maturation. *Infection Immunity* **77**, 1623–1635
60. Stoodley, P., Sauer, K., Davies, D. G., and Costerton, J. W. (2002) Biofilms as complex differentiated communities. *Annu. Rev. Microbiol.* **56**, 187–209

Secreted Virulence Factors Stabilize *S. aureus* Biofilms

61. Spoering, A. L., and Lewis, K. (2001) Biofilms and planktonic cells of *Pseudomonas aeruginosa* have similar resistance to killing by antimicrobials. *J. Bacteriol.* **183**, 6746–6751
62. Waite, R. D., Papakonstantinou, A., Littler, E., and Curtis, M. A. (2005) Transcriptome analysis of *Pseudomonas aeruginosa* growth: comparison of gene expression in planktonic cultures and developing and mature biofilms. *J. Bacteriol.* **187**, 6571–6576
63. Folsom, J. P., Richards, L., Pitts, B., Roe, F., Ehrlich, G. D., Parker, A., Mazurie, A., and Stewart, P. S. (2010) Physiology of *Pseudomonas aeruginosa* in biofilms as revealed by transcriptome analysis. *BMC Microbiol.* **10**, 294
64. Boles, B. R., and Horswill, A. R. (2008) agr-mediated dispersal of *Staphylococcus aureus* biofilms. *PLoS Pathog.* **4**, e1000052-13
65. Egeter, O., and Bruckner, R. (1996) Catabolite repression mediated by the catabolite control protein CcpA in *Staphylococcus xylosum*. *Mol. Microbiol.* **21**, 739–749
66. Geiger, T., and Wolz, C. (2014) Intersection of the stringent response and the CodY regulon in low GC Gram-positive bacteria. *Int. J. Med. Microbiol.* **304**, 150–155
67. Soutourina, O., Poupel, O., Coppée, J. Y., Danchin, A., Msadek, T., and Martin-Verstraete, I. (2009) CymR, the master regulator of cysteine metabolism in *Staphylococcus aureus*, controls host sulphur source utilization and plays a role in biofilm formation. *Mol. Microbiol.* **73**, 194–211
68. Prigent-Combaret, C., Vidal, O., Dorel, C., and Lejeune, P. (1999) Abiotic surface sensing and biofilm-dependent regulation of gene expression in *Escherichia coli*. *J. Bacteriol.* **181**, 5993–6002
69. Borriello, G., Werner, E., Roe, F., Kim, A. M., Ehrlich, G. D., and Stewart, P. S. (2004) Oxygen limitation contributes to antibiotic tolerance of *Pseudomonas aeruginosa* in biofilms. *Antimicrobial Agents Chemother.* **48**, 2659–2664
70. Sønderholm, M., Bjarsholt, T., Alhede, M., Kolpen, M., Jensen, P., Kühl, M., and Kragh, K. (2017) The consequences of being in an infectious biofilm: microenvironmental conditions governing antibiotic tolerance. *IJMS* **18**, 2688–2614
71. Kinkel, T. L., Roux, C. M., Dunman, P. M., and Fang, F. C. (2013) The *Staphylococcus aureus* SrrAB two-component system promotes resistance to nitrosative stress and hypoxia. *mBio* **4**, e00696-13
72. Foulston, L., Elsholz, A. K. W., DeFrancesco, A. S., and Losick, R. (2014) The extracellular matrix of *Staphylococcus aureus* biofilms comprises cytoplasmic proteins that associate with the cell surface in response to decreasing pH. *Mbio* **5**, e01667-14
73. Dengler, V., Foulston, L., DeFrancesco, A. S., and Losick, R. (2015) An electrostatic net model for the role of extracellular DNA in biofilm formation by *Staphylococcus aureus*. *J. Bacteriol.* **197**, 3779–3787
74. Xu, Y., Maltesen, R. G., Larsen, L. H., Schonheyder, H. C., Le, V. Q., Nielsen, J. L., Nielsen, P. H., Thomsen, T. R., and Nielsen, K. L. (2016) In vivo gene expression in a *Staphylococcus aureus* prosthetic joint infection characterized by RNA sequencing and metabolomics: a pilot study. *BMC Microbiol.* **16**, 1–12
75. Li, Y. H., Chen, Y. Y. M., and Burne, R. A. (2000) Regulation of urease gene expression by *Streptococcus salivarius* growing in biofilms. *Environmental Microbiol.* **2**, 169–177
76. Lassek, C., Burghartz, M., Chaves-Moreno, D., Otto, A., Hentschker, C., Fuchs, S., Bernhardt, J., Jauregui, R., Neubauer, R., Becher, D., Pieper, D. H., Jahn, M., Jahn, D., and Riedel, K. (2015) A metaproteomics approach to elucidate host and pathogen protein expression during catheter-associated urinary tract infections (CAUTIs). *Mol. Cell. Proteomics* **14**, 989–1008
77. Ebner, P., Prax, M., Nega, M., Koch, I., Dube, L., Yu, W., Rinker, J., Popella, P., Flötenmeyer, M., and Götz, F. (2015) Excretion of cytoplasmic proteins (ECP) in *Staphylococcus aureus*. *Mol. Microbiol.* **97**, 775–789
78. Ebner, P., Rinker, J., Nguyen, M. T., Popella, P., Nega, M., Luqman, A., Schitteck, B., Di Marco, M., Stevanovic, S., and Götz, F. (2016) Excreted cytoplasmic proteins contribute to pathogenicity in *Staphylococcus aureus*. *Infection Immunity* **84**, 1672–1681
79. Houston, P., Rowe, S. E., Pozzi, C., Waters, E. M., and O’Gara, J.P. (2011) Essential role for the major autolysin in the fibronectin-binding protein-mediated *Staphylococcus aureus* biofilm phenotype. *Infection Immunity* **79**, 1153–1165
80. Mashruwala, A.A., van de Guchte, A., and Boyd, J.M. (2017) Impaired respiration elicits SrrAB-dependent programmed cell lysis and biofilm formation in *Staphylococcus aureus*. *eLife* **6**, e23845
81. Pásztor, L., Ziebandt, A. K., Nega, M., Schlag, M., Haase, S., Franz-Wachtel, M., Madlung, J., Nordheim, A., Heinrichs, D. E., and Götz, F. (2010) Staphylococcal major autolysin (Atl) is involved in excretion of cytoplasmic proteins. *J. Biol. Chem.* **285**, 36794–36803
82. Dinges, M. M., Orwin, P. M., and Schlievert, P. M. (2000) Exotoxins of *Staphylococcus aureus*. *Clin. Microbiol. Rev.* **13**, 16–34
83. Peschel, A., and Otto, M. (2013) Phenol-soluble modulins and staphylococcal infection. *Nat. Rev. Microbiol.* **11**, 667–673
84. Alonzo, F., and Torres, V. J. (2014) The bicomponent pore-forming leukocidins of *Staphylococcus aureus*. *Microbiol. Mol. Biol. Rev.* **78**, 199–230
85. Nguyen, M. T., Luqman, A., Bitschar, K., Hertlein, T., Dick, J., Ohlsen, K., Bröker, B., Schitteck, B., and Götz, F. (2017) Staphylococcal (phospho)lipases promote biofilm formation and host cell invasion. *Int. J. Med. Microbiol.* **308**, 1–11
86. Scherr, T. D., Hanke, M. L., Huang, O., James, D. B. A., Horswill, A. R., Bayles, K. W., Fey, P. D., Torres, V. J., and Kielian, T. (2015) *Staphylococcus aureus* biofilms induce macrophage dysfunction through leukocidin AB and alpha-toxin. *mBio* **6**, e01021-15-13
87. Reijer den, P. M., Haisma, E. M., Lemmens-den Toom, N. A., Willemsse, J., Koning, R. A., Demmers, J. A. A., Dekkers, D. H. W., Rijkers, E., Ghalbzouri, E., Nibbering, P. H., and van Wamel, W. (2016) Detection of alpha-toxin and other virulence factors in biofilms of *Staphylococcus aureus* on polystyrene and a human epidermal model. *PLOS ONE* **11**, e0152544
88. Lei, M. G., Gupta, R. K., and Lee, C. Y. (2017) Proteomics of *Staphylococcus aureus* biofilm matrix in a rat model of orthopedic implant-associated infection. *PLOS ONE* **12**, e0187981
89. Bayer, M. G., Heinrichs, J. H., and Cheung, A. L. (1996) The molecular architecture of the sar locus in *Staphylococcus aureus*. *J. Bacteriol.* **178**, 4563–4570
90. Sonohara, R., Muramatsu, N., Ohshima, H., and Kondo, T. (1995) Difference in surface-properties between *Escherichia coli* and *Staphylococcus aureus* as revealed by electrophoretic mobility measurements. *Biophys. Chem.* **55**, 273–277
91. Nostro, A., Cellini, L., Di Giulio, M., D’Arrigo, M., Marino, A., Blanco, A. R., Favalaro, A., Cutroneo, G., and Bisignano, G. (2012) Effect of alkaline pH on staphylococcal biofilm formation. *APMIS* **120**, 733–742
92. Jennings, L. K., Storek, K. M., Ledvina, H. E., Coulon, C., Marmont, L. S., Sadovskaya, I., Secor, P. R., Tseng, B. S., Scian, M., Filloux, A., Wozniak, D. J., Howell, P. L., and Parsek, M. R. (2015) Pel is a cationic exopolysaccharide that cross-links extracellular DNA in the *Pseudomonas aeruginosa* biofilm matrix. *Proc. Natl. Acad. Sci. U.S.A.* **112**, 11353–11358
93. Beenken, K. E., Blevins, J. S., and Smeltzer, M. S. (2003) Mutation of sarA in *Staphylococcus aureus* limits biofilm formation. *Infection and Immunity* **71**, 4206–4211
94. O’Neill, E., Pozzi, C., Houston, P., Smyth, D., Humphreys, H., Robinson, D. A., and O’Gara, J. P. 2007. Association between methicillin susceptibility and biofilm regulation in *Staphylococcus aureus* isolates from device-related infections. *J. Clin. Microbiol.* **45**, 1379–1388
95. Lauderdale, K. J., Malone, C. L., Boles, B. R., Morcuende, J., and Horswill, A. R. (2009) Biofilm dispersal of community-associated methicillin-resistant *Staphylococcus aureus* on orthopedic implant material. *J. Orthop. Res.* **81**, 55–61
96. Tsang, L. H., Cassat, J. E., Shaw, L. N., Beenken, K. E., and Smeltzer, M. S. (2008) Factors Contributing to the Biofilm-Deficient Phenotype of *Staphylococcus aureus* sarA Mutants. *PLOS ONE* **3**, e3361
97. O’Neill, E., Pozzi, C., Houston, P., Humphreys, H., Robinson, D. A., Loughman, A., Foster, T. J., and O’Gara, J. P. (2008) A novel *Staphylococcus aureus* biofilm phenotype mediated by the fibronectin-binding proteins, FnBPA and FnBPB. *J. Bacteriol.* **190**, 3835–3850
98. Boles, B. R., Thoendel, M., Roth, A. J., Horswill, A. R. (2010) Identification of genes involved in polysaccharide-independent *Staphylococcus aureus* biofilm formation. *PLOS ONE* **5**, e10146

Secreted Virulence Factors Stabilize *S. aureus* Biofilms

99. Foster, T.J., Geoghegan, J.A., Ganesh, V.K., and Höök, M. (2014) Adhesion, invasion and evasion: the many functions of the surface proteins of *Staphylococcus aureus*. *Nat. Rev. Microbiol.* **12**, 49–62
100. Mann, E. E., Rice, K. C., Boles, B. R., Endres, J. L., Ranjit, D., Chandramohan, L., Tsang, L. H., Smeltzer, M. S., Horswill, A. R., and Bayles, K. W. (2009) Modulation of eDNA release and degradation affects *Staphylococcus aureus* biofilm maturation. *PLOS ONE* **4**, e5822
101. Peschel, A., Otto, M., Jack, R. W., Kalbacher, H., Jung, G., and Götz, F. (1999) Inactivation of the *dlt* operon in *Staphylococcus aureus* confers sensitivity to defensins, protegrins, and other antimicrobial peptides. *J. Biol. Chem.* **274**, 8405–8410
102. Tsai, M., Ohniwa, R. L., Kato, Y., Takeshita, S. L., Ohta, T., Saito, S., Hayashi, H., and Morikawa, K. (2011) *Staphylococcus aureus* requires cardiolipin for survival under conditions of high salinity. *BMC Microbiol.* **11**, 13
103. Gries, C. M., Bose, J. L., Nuxoll, A. S., Fey, P. D., and Bayles, K. W. (2013) The Ktr potassium transport system in *Staphylococcus aureus* and its role in cell physiology, antimicrobial resistance and pathogenesis. *Mol. Microbiol.* **89**, 760–773
104. Price-Whelan, A., Poon, C. K., Benson, M. A., Eidem, T. T., Roux, C. M., Boyd, J. M., Dunman, P. M., Torres, V. J., and Krulwich, T. A. (2013) Transcriptional profiling of *Staphylococcus aureus* during growth in 2 M NaCl leads to clarification of physiological roles for Kdp and Ktr K⁺ uptake systems. *MBio* **4**, e00407
105. Jonsson, P., and Wadström, T. (1984) Cell-surface hydrophobicity of *Staphylococcus aureus* measured by the salt aggregation test (Sat). *Curr. Microbiol.* **10**, 203–209
106. Rachid, S., Ohlsen, K., Wallner, U., Hacker, J., Hecker, M., and Ziebuhr, W. (2000) Alternative transcription factor sigma(B) is involved in regulation of biofilm expression in a *Staphylococcus aureus* mucosal isolate. *J. Bacteriol.* **182**, 6824–6826
107. Seminara, A., Angelini, T. E., Wilking, J. N., Vlamakis, H., Ebrahim, S., Kolter, R., Weitz, D. A., and Brenner, M. P. 2012. Osmotic spreading of *Bacillus subtilis* biofilms driven by an extracellular matrix. *Proc. Natl. Acad. Sci. U.S.A.* **109**, 1116–1121
108. Yan, J., Nadell, C. D., Stone, H. A., Wingreen, N. S., and Bassler, B. L. (2017) Extracellular-matrix-mediated osmotic pressure drives *Vibrio cholerae* biofilm expansion and cheater exclusion. *Nat. Commun.* **8**, 1–11
109. Freeman, Z. N., Dorus, S., and Waterfield, N. R. (2013) The KdpD/KdpE two-component system: integrating K⁺ homeostasis and virulence. *PLoS Pathog.* **9**, e1003201
110. Xue, T., You, Y., Hong, D., Sun, H., and Sun, B. (2011) The *Staphylococcus aureus* KdpDE two-component system couples extracellular K⁺ sensing and Agr signaling to infection programming. *Infection Immunity* **79**, 2154–2167
111. Zhao, L., Xue, T., Shang, F., Sun, H., and Sun, B. (2010) *Staphylococcus aureus* AI-2 quorum sensing associates with the KdpDE two-component system to regulate capsular polysaccharide synthesis and virulence. *Infection Immunity* **78**, 3506–3515
112. Coelho, L. R., Souza, R. R., Ferreira, F. A., Guimaraes, M. A., Ferreira-Carvalho, B. T., and Figueiredo, A. M. S. (2008) agr RNAIII divergently regulates glucose-induced biofilm formation in clinical isolates of *Staphylococcus aureus*. *Microbiology* **154**, 3480–3490
113. Queck, S. Y., Jameson-Lee, M., Villaruz, A. E., Bach, T. H. L., Khan, B. A., Sturdevant, D. E., Ricklefs, S. M., Li, M., and Otto, M. (2008) RNAIII-independent target gene control by the agr quorum-sensing system: insight into the evolution of virulence regulation in *Staphylococcus aureus*. *Mol. Cell* **32**, 150–158
114. Said-Salim, B., Dunman, P. M., McAleese, F. M., Macapagal, D., Murphy, E., McNamara, P. J., Arvidson, S., Foster, T. J., Projan, S. J., and Kreiswirth, B. N. (2003) Global regulation of *Staphylococcus aureus* genes by Rot. *J. Bacteriol.* **185**, 610–619
115. Majerczyk, C. D., Sadykov, M. R., Luong, T. T., Lee, C., Somerville, G. A., and Sonenshein, A. L. (2008) *Staphylococcus aureus* CodY negatively regulates virulence gene expression. *J. Bacteriol.* **190**, 2257–2265
116. Mrak, L. N., Zielinska, A. K., Beenken, K. E., Mrak, I. N., Atwood, D. N., Griffin, L. M., Lee, C. Y., and Smeltzer, M. S. (2012) *saeRS* and *sarA* act synergistically to repress protease production and promote biofilm formation in *Staphylococcus aureus*. *PLOS ONE* **7**, e38453
117. Rogasch, K., Ruhmling, V., Pané-Farré, J., Hoper, D., Weinberg, C., Fuchs, S., Schmutte, M., Broker, B.M., Wolz, C., Hecker, M., and Engemann, S. (2006) Influence of the two-component system *SaeRS* on global gene expression in two different *Staphylococcus aureus* strains. *J. Bacteriol.* **188**, 7742–7758
118. Pragman, A. A., Yarwood, J. M., Tripp, T. J., and Schlievert, P. M. (2004) Characterization of virulence factor regulation by *SrrAB*, a two-component system in *Staphylococcus aureus*. *J. Bacteriol.* **186**, 2430–2438
119. Fournier, B., and Hooper, D. C. (2000) A new two-component regulatory system involved in adhesion, autolysis, and extracellular proteolytic activity of *Staphylococcus aureus*. *J. Bacteriol.* **182**, 3955–3964
120. Vizcaino, A., Côté, R.G., Csordas, A., Dianes, J.A., Fabregat, A., Foster, J.M., Griss, J., Alpi, E., Birim, M., Contell, J., O’Kelly, G., Schoenegger, A., Ovelheiro, D., Pérez-Riverol, Y., Reisinger, F., Ríos, D., Wang, R., and Hermjakob, H. (2012) The proteomics identifications (PRIDE) database and associated tools: status in 2013. *Nucleic Acids Res.* **41**, D1063–D1069

- 5 Article II: An innovative protocol for metaproteomic analyses of microbial pathogens in cystic fibrosis sputum

Article II

An innovative protocol for metaproteomic analyses of microbial pathogens in cystic fibrosis sputum

Alexander C. Graf, Johanna Striesow, Jan Pané-Farré, Thomas Sura, Martina Wurster, Michael Lalk, Dietmar H. Pieper, Dörte Becher, Barbara C. Kahl, and Katharina Riedel

Frontiers in Cellular and Infection Microbiology, 2021, 11

Author contributions:

ACG, JPF, and KR were responsible for the study conceptualization. BCK carried out the prospective study including CF sputum sampling, collection of clinical data and microbiological work-up of sputum specimens. ACG and JS performed the experiments to develop the sputum processing protocol. Metagenome analyses were performed by DHP. ACG, TS and DB performed metaproteome analyses and ML and MW were responsible for metabolome analyses. DHP analyzed metagenome data, while ACG analyzed metaproteome and metabolome data. ACG, JPF and KR wrote the manuscript, which was critically edited by all other co-authors.

Alexander C. Graf

Prof. Dr. Katharina Riedel



An Innovative Protocol for Metaproteomic Analyses of Microbial Pathogens in Cystic Fibrosis Sputum

Alexander C. Graf^{1*}, Johanna Striesow², Jan Pané-Farré³, Thomas Sura⁴, Martina Wurster⁵, Michael Lalk⁵, Dietmar H. Pieper⁶, Dörte Becher⁴, Barbara C. Kahl⁷ and Katharina Riedel¹

¹ Institute of Microbiology, Department of Microbial Physiology & Molecular Biology, University of Greifswald, Greifswald, Germany, ² Research Group ZIK Plasmatis, Leibniz Institute for Plasma Science and Technology, Greifswald, Germany, ³ Center for Synthetic Microbiology, Department of Chemistry, Philipps-University Marburg, Marburg, Germany, ⁴ Institute of Microbiology, Department of Microbial Proteomics, University of Greifswald, Greifswald, Germany, ⁵ Institute of Biochemistry, Department of Cellular Biochemistry & Metabolomics, University of Greifswald, Greifswald, Germany, ⁶ Research Group Microbial Interactions and Processes, Helmholtz Centre for Infection Research, Braunschweig, Germany, ⁷ Institute of Medical Microbiology, University Hospital Münster, Münster, Germany

OPEN ACCESS

Edited by:

Chelsie Armbruster,
University at Buffalo, United States

Reviewed by:

Megan R. Kiedrowski,
University of Alabama at Birmingham,
United States
Lucia Grenga,
Commissariat à l'Energie Atomique et
aux Energies Alternatives (CEA),
France

*Correspondence:

Alexander C. Graf
grafa@uni-greifswald.de

Specialty section:

This article was submitted to
Molecular Bacterial Pathogenesis,
a section of the journal
Frontiers in Cellular and
Infection Microbiology

Received: 13 June 2021

Accepted: 11 August 2021

Published: 27 August 2021

Citation:

Graf AC, Striesow J, Pané-Farré J, Sura T, Wurster M, Lalk M, Pieper DH, Becher D, Kahl BC and Riedel K (2021) An Innovative Protocol for Metaproteomic Analyses of Microbial Pathogens in Cystic Fibrosis Sputum. *Front. Cell. Infect. Microbiol.* 11:724569. doi: 10.3389/fcimb.2021.724569

Hallmarks of cystic fibrosis (CF) are increased viscosity of mucus and impaired mucociliary clearance within the airways due to mutations of the cystic fibrosis conductance regulator gene. This facilitates the colonization of the lung by microbial pathogens and the concomitant establishment of chronic infections leading to tissue damage, reduced lung function, and decreased life expectancy. Although the interplay between key CF pathogens plays a major role during disease progression, the pathophysiology of the microbial community in CF lungs remains poorly understood. Particular challenges in the analysis of the microbial population present in CF sputum is (I) the inhomogeneous, viscous, and slimy consistence of CF sputum, and (II) the high number of human proteins masking comparably low abundant microbial proteins. To address these challenges, we used 21 CF sputum samples to develop a reliable, reproducible and widely applicable protocol for sputum processing, microbial enrichment, cell disruption, protein extraction and subsequent metaproteomic analyses. As a proof of concept, we selected three sputum samples for detailed metaproteome analyses and complemented and validated metaproteome data by 16S sequencing, metabolomic as well as microscopic analyses. Applying our protocol, the number of bacterial proteins/protein groups increased from 199-425 to 392-868 in enriched samples compared to nonenriched controls. These early microbial metaproteome data suggest that the arginine deiminase pathway and multiple proteases and peptidases identified from various bacterial genera could so far be underappreciated in their contribution to the CF pathophysiology. By providing a standardized and effective protocol for sputum processing and microbial enrichment, our study represents an important basis for future studies investigating the physiology of microbial pathogens in CF *in vivo* – an important prerequisite for the development of novel antimicrobial therapies to combat chronic recurrent airway infection in CF.

Keywords: cystic fibrosis, sputum, microbial community, microbiome, 16S sequencing, metaproteomics, metabolomics, *in vivo*

INTRODUCTION

Cystic fibrosis is the most common inherited monogenic disorder in Caucasian populations with an incidence of approx. one in 3,000 births (O'Sullivan and Freedman, 2009). The disease is caused by mutations in the cystic fibrosis transmembrane conductance regulator (CFTR) gene, encoding an anion channel localized in epithelial cells e.g. of the respiratory and gastrointestinal tract (Chmiel and Davis, 2003). More than 1,500 mutations of the CFTR gene are described, which all lead to the CF phenotype. Most importantly, the CF phenotype is characterized by an impaired ion homeostasis, which, in consequence, leads to a sticky, dehydrated mucus within the respiratory tract and an impaired mucociliary clearance (Ratjen, 2009). Ultimately, these hallmarks of CF pave the way for the colonization by opportunistic microbial pathogens establishing chronic infections, which starts already early after birth, and is considered to be the main reason for mortality (Rogers et al., 2014). Typically, *Staphylococcus aureus* and *Haemophilus influenzae* represent early colonizers, which are followed by other bacterial pathogens including e.g. *Pseudomonas aeruginosa*, *Burkholderia cepacia* complex and *Stenotrophomonas maltophilia* but also fungal pathogens like *Aspergillus fumigatus* and *Candida albicans*, and viruses (e.g. influenza and respiratory syncytial virus) (Filkins and O'Toole, 2015). The polymicrobial communities within the CF lung are highly dynamic and differ greatly from patient to patient. In the past few years, culture independent diagnostic methods revealed even larger diversity of core genera, which are abundant in the majority of adult patients including *Streptococcus* and *Neisseria*, as well as obligate anaerobes like *Prevotella*, *Veillonella*, and *Catonella* (Rogers et al., 2014; Filkins et al., 2015).

Of note, CF airways are characterized by an inflammatory milieu, which can be attributed to the microbial colonization/infection eliciting a host immune response characterized by the dysregulation of epithelial innate immunity and airway leukocytes. Proteolytic and oxidative products derived from an exuberant immune response in combination with microbial virulence factors are the main reasons for lung tissue damage, which ultimately lead to respiratory failure and death (Cohen and Prince, 2012; Eiserich et al., 2012; Kamath et al., 2015). Thus, deeper insights into these complex polymicrobial infections, focusing on the (patho-)physiology of the microbial CF lung community as well as host-microbe interactions are of essential importance for a better understanding of the disease progression and the development of novel treatment strategies.

In the past, (meta-)proteomics approaches were used as a powerful tool to investigate the physiological alterations of lung tissues and body fluids (e.g. bronchoalveolar lavage, blood, feces, and sputum) in CF patients as well as CFTR post-translational modifications and CF biomarkers (Eiserich et al., 2012; Kamath et al., 2015; Debyser et al., 2016; Liessi et al., 2020). However, most of these studies were limited by focusing on the host perspective while overlooking the microbial side of infection. Studies characterizing the bacterial and fungal pathogens of CF lungs were typically performed *in vitro*, using lung isolates grown under lung-mimicking conditions (Kamath et al., 2015). Consequently, novel

approaches for the *in vivo* analyses of the microbial pathophysiology directly at the site of infection are urgently needed. Here, we present the first *in vivo* microbial metaproteome analysis, complemented by 16S sequencing, metabolomics, and microscopic analyses to study microbial communities and facultative microbial pathogens within CF sputum. To this end, we established an innovative sputum processing protocol, which overcomes major technical and analytical challenges of CF sputum including (I) limited sample volume, (II) challenging processability of CF sputum due to its viscous and slimy character, (III) extraction of nucleic acids, proteins and metabolites out of a single sputum sample, (IV) enormous dominance of human proteins (e.g. mucins, albumins, immunoglobulins) over microbial proteins of interest, and (V) high abundance of (neutrophil-derived) proteases unspecifically digesting microbial proteins of interest (Kamath et al., 2015). In this protocol, a combination of differential centrifugation and filtration is used as key elements for the enrichment of bacterial cells significantly increasing bacterial protein identification coverage.

Our study represents a fundamental basis for follow-up studies investigating the microbial metaproteome and bacterial pathophysiology in CF sputum, which is an essential prerequisite for the development of innovative antimicrobial treatment approaches.

EXPERIMENTAL PROCEDURES

Study Cohort, Ethics Statement, and Sputum Sampling

In total, 24 sputum samples derived from 20 different patients were collected. The study was approved by the institutional ethics review board Münster, Germany (2010-155-f-S). Of the 24 sputum samples, 21 were used as test samples to establish a reliable, reproducible and widely applicable protocol suitable for sputum processing, nucleic acid extraction, microbial enrichment and subsequent protein and metabolite extraction. As a proof of concept, three samples, which were derived from three individual patients (designated Patient A, Patient B, and Patient C, respectively) were selected for detailed 16S sequencing, metaproteome and metabolome analyses. Clinical data of these three patients are summarized in **Table 1**. Patient B carried the homozygous Phe508del CFTR genotype, while Patients A and C carried other CFTR-mutations. Importantly, antibiotic therapy of all three patients finished before the time point of sputum sample collection, reducing the risk of false functional analysis due to lysed and/or dead microbial cells. The three Patients A, B, and C were selected based on their differences in age, lung function, antibiotic therapy, disease progression, and microbial lung community structure in order to show the applicability of our sputum processing protocol over preferably diverse samples.

The freshly expectorated sputum samples were immediately chilled on ice and transported to the laboratory for further processing. Next, samples were transferred into 5 mL reaction tubes, three ceramic beads (diameter approx. 2 mm) were added and the samples were homogenized using a Retsch mill at 15 Hz for 120 s (Stokell et al., 2014). Aliquots of the homogenized sputum samples were stained according to the Gram procedure

TABLE 1 | Clinical Data of the three CF patients A, B, and C included in metaproteome and metabolome analyses.

	Patient A	Patient B	Patient C
Age	19	24	38
Sex	male	male	male
Exacerbation acc. to Fuchs ^a	0	0	1
FEV1% predicted ^b	81%	52%	28%
Antibiotic therapy	Cefaclor	Cefuroxim	Amoxicillin/Clavulanic acid, Meropenem
CFU/mL <i>S. aureus</i>	1.4 × 10 ⁷	3.6 × 10 ⁶	3.2 × 10 ⁷
CFU/mL <i>P. aeruginosa</i>	–	–	1.5 × 10 ⁸
Quantification Neutrophils ^c	3	2	2
Quantification Epithelial Cells ^c	1	2	2

^a0 = no exacerbation; 1 = a minimum of 4 criteria acc. to Fuchs pertain (Fuchs et al., 1994).

^bFEV = forced expiratory volume at 1 s.

^c1 = 1 cell/field of view, 2 = up to 10 cells/field of view, 3 = up to 100 cells/field of view.

and numbers of neutrophils, epithelial cells and bacteria were semi-quantitatively evaluated according to standard diagnostic procedures for CF specimens (Gilligan, 2014). Samples were aliquoted and diluted using 250 μ L of homogenized samples and 250 μ L ice-cold 0.9% NaCl. Glycerol was added to a final concentration of 10% and samples were subsequently stored at -80 $^{\circ}$ C for further analyses.

Community Composition Analysis by 16S Sequencing

Samples were gently mixed with an equivalent volume of Sputolysin (10%) and incubated for 30 min at 37 $^{\circ}$ C on a ThermoMixer. RNA was extracted using the RNeasy kit (Qiagen, Hilden, Germany) following the manufacturer's instructions, but including a mechanical lysis step (Schulz et al., 2018). After DNA digestion, first-strand complementary DNA was synthesized using the Superscript IV First-Strand Synthesis System (Invitrogen, Carlsbad, CA) and random primers, following the manufacturer's instructions. DNA was extracted from the samples using the FastDNA Spin Kit for Soil (MP Biomedicals, Solon, OH, USA) following the manufacturer's instructions (Camarinha-Silva et al., 2014). Amplicon libraries covering the V1-V2 region of the 16S rRNA gene were amplified in a two-step PCR as previously described (Rath et al., 2017) and sequenced on a MiSeq (2X250 bp, Illumina, Hayward, California, USA). Bioinformatic processing was performed as previously described. Raw reads were merged with the Ribosomal Database Project (RDP) assembler (Cole et al., 2013). Sequences were aligned within MOTHUR (gotoh algorithm using the SILVA reference database) and subjected to preclustering (diffs=2) (Schloss et al., 2009) yielding so-called phylotypes that were filtered for an average abundance of $\geq 0.001\%$ and a sequence length ≥ 250 bp before analysis. Phylotypes were assigned to a taxonomic affiliation based on the naive Bayesian classification (Wang et al., 2007) with a pseudo-bootstrap threshold of 80%. Phylotypes were then manually analyzed against the RDP database using the Seqmatch function. A species name was assigned to a phylotype when only 16S rRNA gene fragments of previously described isolates of that species showed a seqmatch score >0.95 .

Sputum Sample Processing and Microbial Enrichment

All sputum processing steps were carried out at 4 $^{\circ}$ C in order to minimize changes of the *in vivo* sputum metaproteome and the metabolome, respectively. The entire workflow is summarized in **Figure 1**. Homogenization of 500 μ L sputum samples (250 μ L Retsch mill treated sputum plus 250 μ L 0.9% NaCl) was performed by adding 3 mL ice-cold PBS_{EDTA/PIC} (137 mM NaCl, 0.2 mM KCl, 10 mM Na₂HPO₄, 1.8 mM KH₂PO₄, pH 7.4, plus 10 mM EDTA, and 1 tablet protease inhibitor cocktail (PIC, cOplete, Mini, Sigma-Aldrich) per 10 mL), which was additionally supplemented with DNase I (10 U/mL, ThermoFisher) to break down eDNA-based aggregates (Shak et al., 1990). The samples were subsequently incubated on a rotation shaker (Stuart, Cole-Parmer) at 20 rpm for 15 min. Success of the further homogenization and breakdown of eDNA-based aggregates was microscopically verified (see below). The homogenized sputum suspensions (3.5 mL) were split into a first sub-sample (3 mL) for further enrichment of microbial cells and a second sub-sample (500 μ L) to obtain a non-enriched control.

For enrichment of microbial cells, the first sub-sample was subjected to differential centrifugation as the first enrichment step of microbial cells. Here, the samples were centrifuged at 500 g for 5 min (keeping cell lysis as low as possible) and the pellet containing human cells and bigger aggregates was discarded. The supernatant, which contained microbial cells, was subsequently centrifuged at 8,000 g for 5 min. The resulting supernatant was filter-sterilized (0.45 μ m cut-off, Sarstedt) and used for metabolome analyses (see below). The pellet was resuspended in 500 μ L PBS_{EDTA/PIC}, which was additionally supplemented with DTT (10 mM, Sigma-Aldrich) and incubated at 4 $^{\circ}$ C for 10 min on a rotation shaker (Stuart, Cole-Parmer) to further homogenize and liquify the sample. As the second enrichment step for microbial cells, the cell suspension was subsequently filtered (10 μ m cut-off, Merck) to remove remaining human cells/aggregates, the filter was washed with 1 mL ice-cold PBS_{EDTA/PIC} and the filtrate was collected. The filtrate containing enriched microbial cells was then centrifuged (8,000 g, 5 min), and the pellet was washed twice using ice-cold TE_{PIC}-buffer (10 mM Tris-HCl, 1 mM EDTA, pH 8, containing 1 tablet protease inhibitor cocktail (PIC, cOplete, Mini, Sigma-Aldrich) per 10 mL) to further reduce contamination by human proteins. The washed pellet was resuspended in 200 μ L TE_{PIC} and subjected to protein extraction for MS-analyses as described below.

In order to keep preparation protocols of the enriched sample and the non-enriched control as similar as possible, the non-enriched control sample was also subjected to differential centrifugation as described above (500 g, 5 min followed by 8,000 g, 5 min), pooled again and also subjected to liquefaction using 500 μ L PBS_{EDTA/PIC} with DTT (10 mM, Sigma-Aldrich). The suspension was incubated and again centrifuged as described above. The pellets were resuspended using 200 μ L TE_{PIC}, pooled again, and subjected to protein extraction for MS-analyses as described below.

Protein Extraction

Suspensions of enriched microbial cells and the non-enriched control were subjected to mechanical cell disruption as

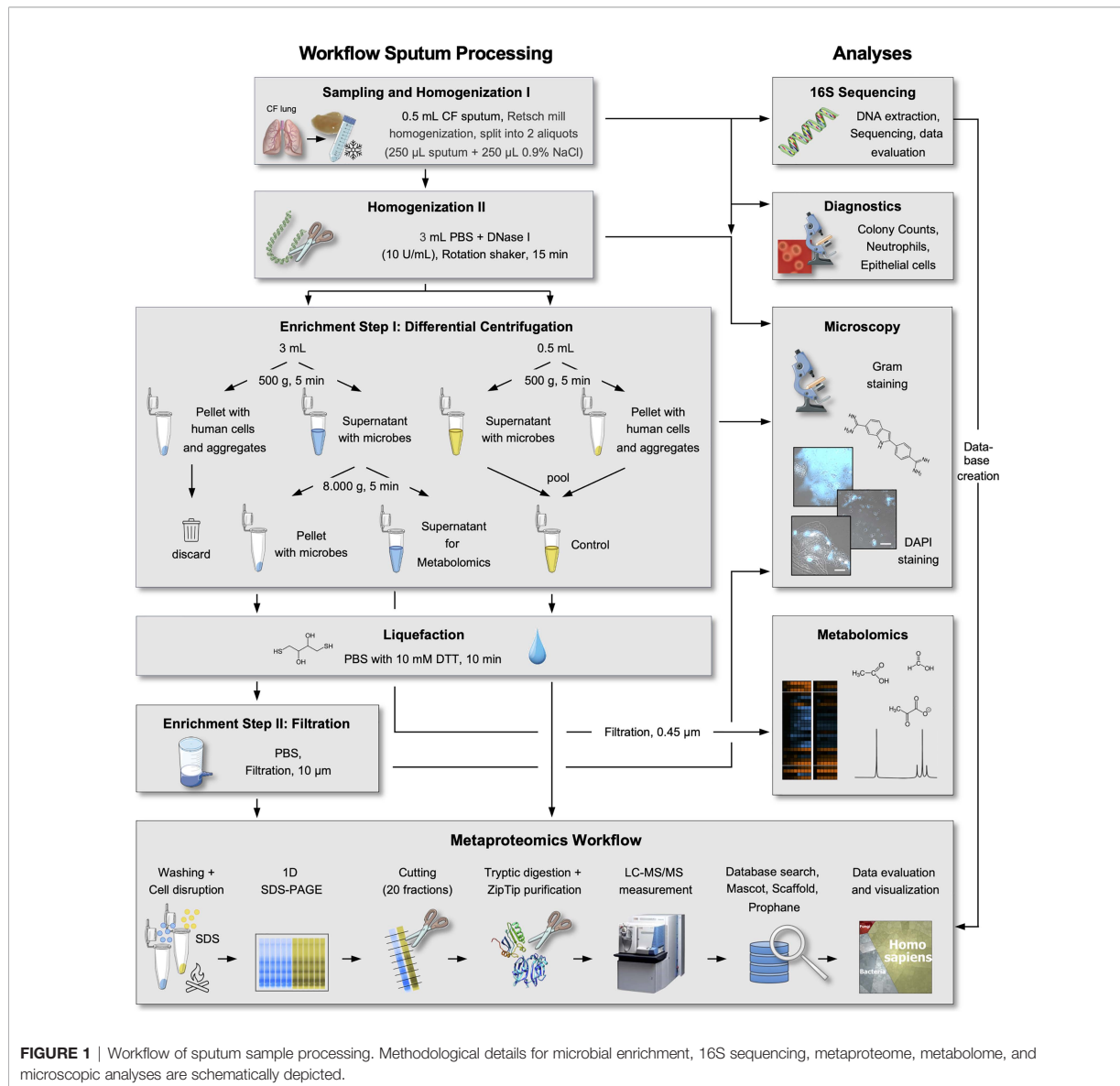


FIGURE 1 | Workflow of sputum sample processing. Methodological details for microbial enrichment, 16S sequencing, metaproteome, metabolome, and microscopic analyses are schematically depicted.

previously described (Becher et al., 2009; Zühlke et al., 2016) since this method was shown to effectively disrupt one of the most robust cell types we expected in our samples – the gram-positive, spherical cocci of *S. aureus*. Due to limited sputum-sample volume and the concomitant small number of microbial cells in the enriched sample, the cell disruption described by (Becher et al., 2009; Zühlke et al., 2016) was downscaled using 200 µL of the respective suspensions and 150 mg glass beads (0.1 to 0.11 mm, Sartorius Stedim Biotech) in 0.5 mL cryotubes (Sarstedt) followed by 3 homogenization cycles at 6.5 m/s for 30 s with intermittent cooling on ice for 1 min in a FastPrep-24™ classic bead beating grinder and lysis system (MP Biomedicals). Subsequently, the samples were centrifuged (15,000 g, 4°C,

5 min) and the tube content (including glass beads and cell debris) was transferred into a fresh 1.5 mL reaction tube. 200 µL 2x extraction buffer (100 mM Tris-HCl, 0.3 M NaCl, 2 mM EDTA, 4% SDS, pH 8.5, adapted from (Chourey et al., 2010)) were added and the suspension was boiled at 95°C and 1,200 rpm for 10 min in a thermo-shaker (Eppendorf). Glass beads and cell debris were pelleted by centrifugation at 15,000 g at 4°C for 5 min and the supernatant, representing the protein extract, was collected. Proteins were concentrated (approx. 4-fold) in a vacuum centrifuge (Eppendorf AG) for 1 h followed by determination of the protein concentration using the BCA-assay microplate procedure (ThermoFisher) according to the manufacturer's instructions.

MS Sample Preparation

40 µg protein per sample were mixed 3:1 with an SDS-sample buffer (15% glycerol, 5% 2-mercaptoethanol, 2.4% SDS, 0.8% Tris, 0.005% bromophenol blue), boiled for 10 min at 95°C and subsequently separated on a 4-12 % SDS-polyacrylamide gradient gel (Criterion, BioRad). The gel was fixed, washed and stained using Colloidal Coomassie Brilliant Blue G-250 as previously described (Laemmli, 1970; Neuhoff et al., 1988). After the staining procedure, excessive Coomassie stain was removed from the gel using water. Subsequently, gel lanes were fractionated into 20 gel pieces, cut into gel blocks of approx. 1 mm³ and prepared for MS/MS analysis as described by (Lassek et al., 2015). Obtained peptides were resolved in 0.1% acetic acid and desalted using ZipTips (C18, Merck Millipore). The desalted peptide mixtures were again vacuum-dried and stored at -80°C until MS/MS analysis.

MS/MS Analysis

Purified peptides were reconstituted with 0.1% acetic acid and analyzed by reversed phase liquid chromatography (LC) electrospray ionization (ESI) MS/MS using an Orbitrap Elite mass spectrometer (Thermo Fisher Scientific, Waltham, USA). Nano-reversed-phase-LC columns (20 cm length x 100 µm diameter) packed with 3.0 µm C18 particles (Dr. Maisch GmbH, Ammerbuch-Entringen, Germany) and heated to 45°C were used to separate the purified peptides with an EASY-nLC 1200 system (Thermo Fisher Scientific, Waltham, USA). The peptides were loaded with solvent A [0.1% acetic acid (v/v)] and subsequently eluted by a non-linear gradient from 2% to 99% solvent B (0.1% acetic acid (v/v), 95% acetonitrile) at a flow rate of 300 nl*min⁻¹ over 91 min. A full scan was recorded in the Orbitrap with a resolution of 60,000 at m/z 400. The twenty most abundant precursor ions were consecutively isolated and fragmented *via* collision-induced dissociation (CID) with a normalized collision energy of 35. Singly charged ions and ions with unassigned charge state were rejected and lock mass correction as well as dynamic exclusion (fragmented precursors were excluded from fragmentation for 30 s) were enabled. Each sample was measured twice, creating two technical replicates per sample.

Metaproteomics Data Base Assembly and Search

Three patient-specific databases were constructed based on the phylogenetic information derived from community composition analysis by 16S sequencing. In order to keep the databases and concomitant computational costs as small as possible, genera with a relative abundance of less than 0.1% according to sequencing results were not considered (Table S1). The following protein sequences were added: *Homo sapiens*, the most common (pathogenic) fungal genera in CF (*Aspergillus*, *Blumeria*, *Candida*, *Cladosporium*, *Cryptococcus*, *Exophiala*, *Rasamsonia*, *Rhodotorula*, *Saccharomyces*, *Scedosporium*, and *Sporobolomyces* according to (Chotirmall and McElvaney, 2014; Williams et al., 2016), common laboratory contaminants, and DNase I. For this purpose, FASTA protein sequences were downloaded from

UniProt on September 18, 2018 and redundant entries were removed using the Linux-implemented FASTA tool kit resulting in three patient-specific protein databases, which contained 5.546.037 (Patient A), 4.024.158 (Patient B), and 3.331.936 (Patient C) entries, respectively. Database search was performed using the Mascot software (version 2.6.2, Matrix Science, Boston, MA, USA) with the following settings: peptide tolerance of 10 ppm, MS/MS tolerance of 0.8 Da, up to two missed cleavages allowed, methionine oxidation set as a variable modification, and carbamidomethylation set as a fixed modification. A second database search was performed using Scaffold (version 4.8.7, Proteome Software, Portland, OR, USA) and the built-in X! Tandem search engine with the same settings as described above, as well as the following settings: protein probability = 95%, peptide probability = 99%, single peptide identifications allowed. Here, Mascot and Scaffold used the given databases (containing bacterial, fungal, and human protein sequences) for an *in silico* digestion calculating theoretical peptide sequences and creating theoretical spectra thereof. These theoretical spectra were then matched with experimentally achieved MS/MS spectra for protein identification (Schiebenhoefer et al., 2020). Protein quantification was based on normalized spectral abundance factors (NSAF) as previously described (Zybailov et al., 2006; Zhu et al., 2010). Taxonomic and functional assignment of identified protein groups was performed using ProPhane (Schiebenhoefer et al., 2020) (version 3.1.4) with the settings stated in Table S2. Here, ProPhane provides an automated bioinformatic platform enabling the taxonomic and functional annotation of metaproteome data by integrating various databases (e.g. NCBI, EggNog, Pfams) and algorithms (e.g. diamond blastp, Hmmer) (Schiebenhoefer et al., 2020).

Metaproteomics Data Analyses and Visualization

ProPhane output files were used to calculate the mean NSAF of both technical replicates and to create Voronoi treemaps (Bernhardt et al., 2009; Liebermeister et al., 2014) using the Paver software (version 2.1, DECODON GmbH, Greifswald, Germany). Here, Voronoi treemaps visualize taxonomic and functional diversity of sputum samples, respectively, according to relative NSAF-based abundances of different taxonomic genera. To this end, mean NSAF values of all protein/protein group were used, which were identified in at least one out of two technical replicates. Moreover, mean values of both technical replicates were used to visualize protein abundances in bar graphs according to NSAF-based relative abundance as well as absolute number of protein groups for each patient. The protein abundances of each patient were used to calculate mean values and to assess statistically significant differences of protein abundances between enriched and control samples by multiple unpaired t-tests. Enrichment factors of bacterial proteins/protein groups were calculated using three complementary approaches: (i) sum of all NSAFs in the enriched sample divided by the sum of all NSAFs in the control, (ii) absolute number of proteins/protein groups identified in the enriched sample divided by absolute number of proteins/protein groups identified in the control, (iii) percentage of proteins/protein groups identified in

the enriched sample divided by absolute number of proteins/protein groups identified in the control.

Metabolome Analyses

Samples were lyophilized overnight (Christ, Germany). Dried samples were derivatized for 90 min at 37°C in 40 µl Methoxyamine hydrochloride (MeOX) (20 mg/ml in pyridine) and afterwards for 30 min with 80 µl of N-methyl-N-(trimethylsilyl) trifluoroacetamide (MSTFA) at 37°C. Analytical GC-MS system consisted of an Agilent Technologies 7890B gas chromatograph and a mass selective detector (5977B Inert Plus Turbo MSD, Agilent Technologies). Injection was done with SSL (split/splitless) injector (G4513A, Agilent Technologies) (split 1:25 at 250°C, 1.0 µl; carrier gas: Helium with a flow of 1.0 ml/min). The MS operated in the electron impact mode with an ionization energy of 70 eV. The oven program started with 1 min at 70°C, was increased up to 76°C with 1.5°C/min followed by heating up to 220°C with 5°C/min and heating up to 325°C with 20°C/min. The final temperature of 325°C was hold for 8 min. Mass spectra were acquired in scan mode from 50-500 m/z at a rate of 2.74 scans/s and with a solvent delay of 6.0 minutes. Chromatography was performed using a 30 m HP-5 column (Agilent Technologies) with 0.25 mm i.d. and 0.25 µm film thickness. The detected compounds were identified by processing of the raw GC-MS data with MassHunter software Qual B.08.00 and comparing with NIST 2017 and Fiehn mass spectral databases and with retention times and mass spectra of standard compounds (inhouse database). The supplemented list contains compounds with scores to libraries of 70 or more (Table S6). Metabolites were relatively quantified among the three patient samples and depicted as circles, which areas correlate with metabolite abundance.

Microscopic Analyses

25 µL of the samples derived from different sputum processing steps as indicated in Figure 1 (after homogenization, after the first differential centrifugation step, after filtration) were transferred into a 96-well microtiter plate and diluted to an OD of 5 using PBS. OD was measured at 500 nm in a microtiter plate reader (Synergy MX, BioTek Instruments, Winooski, USA). Samples were stained in the dark at room temperature for 15 min using DAPI (2 µg/mL final concentration, Merck Millipore). 4 µL of these samples were applied on a thin layer of 1.5 % agarose in 0.9 % NaCl, which was mounted on a microscope slide. Phase contrast and fluorescence microscopy images were acquired and processed using a Zeiss Imager M2 (Carl Zeiss, Jena, Germany) equipped with a 100x/NA 1.3 oil immersion objective, a filter for monitoring DAPI fluorescence (excitation at 358 nm, emission at 461 nm), and the ZEN 2011 software package (Carl Zeiss, Jena, Germany). The number of human cells, particles/aggregates of different sizes, and microbial cells were counted in 50 randomly selected fields-of-view per sample. The results were averaged among Patient A, B, and C, and statistically significant differences were assessed by multiple unpaired t-tests.

RESULTS AND DISCUSSION

It is well described that microbial pathogens frequently establish infections in the airways of CF patients during infancy, which

may become chronic, cause severe tissue damage and ultimately lead to death due to respiratory failure (Lyczak et al., 2002) - the leading cause of CF mortality (Rogers et al., 2014). However, the molecular mechanisms underlying co-infection, microbial interplay, and disease progression are still poorly understood.

In order to address these critical open questions, we developed an *in vivo* approach with a specific focus on the metaproteomic analyses of the CF microbiome, driven by 16S sequencing community composition analyses. We complemented these results by metatranscriptomic data acquired by metabolic footprint analyses, and microscopic data. Since major technical challenges, related to sputum consistency and processability, have so far precluded such analyses, we first established a reliable, reproducible and widely applicable protocol for sputum sample processing and subsequent metaproteomic and metabolomic analyses with a focus on microbial pathogens.

A Metaproteomic and Metabolomic Analyses Protocol Overcoming Major Technical Challenges Related to CF Sputum Processing

We established a straight-forward workflow allowing nucleic acid extraction, metabolome footprint analyses and microbial protein enrichment and analyses from a single CF sputum sample. The major technical challenges and the different steps of our protocol addressing these technical challenges (Figure 1) are presented and discussed in the following paragraphs:

Limited Sample Volume

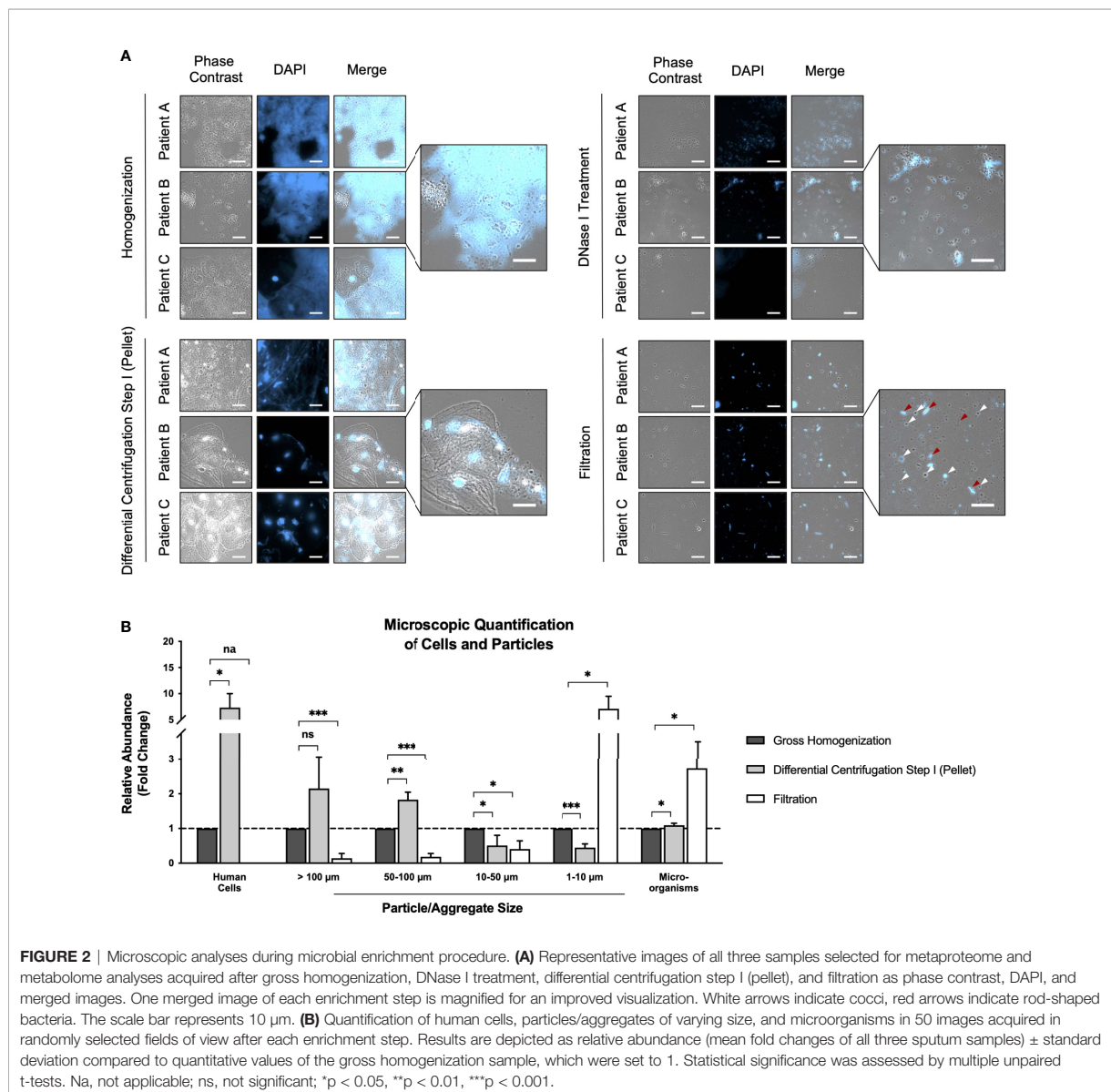
The amount of CF sputum sampled varies from patient to patient and rarely exceeds volumes of a few milliliters, which limits the biomass available for simultaneous nucleic acid, protein, and metabolite extraction. For this study, we collected 24 sputum samples derived from 20 different patients with a sample volume ranging from 0.3 ml to 2 ml (average = 0.7 ml, median = 0.6 ml). In order to establish a protocol, which is applicable to a great variety of different CF patients, we used a sputum volume of 0.5 ml as starting material. This amount was sufficient for simultaneous analyses of nucleic acids, proteins, and metabolites from a single sample.

Homogenization and Digestion of eDNA-Based Aggregates

CF sputum represents a very viscous and slimy matrix due to macromolecules like eDNA and heavily glycosylated mucins (Stokell et al., 2014; Kamath et al., 2015), which complicates and prolongs downstream processing. Indeed, our microscopic analyses clearly showed massive cell clusters embedded in “clouds” of eDNA, which partially exceeded sizes of 500 µm. A common source of this eDNA are NETs (neutrophil extracellular traps): networks of primarily neutrophil-derived eDNA loaded with proteins, which show antimicrobial activity and simultaneously protect the eDNA from degradation (Herzog et al., 2019). To make cells trapped in these eDNA “clouds” accessible, they needed to be broken down prior to further processing (Figure 2A). Available techniques for sputum homogenization and liquefaction include mechanical,

chemical or enzymatic treatment at room temperature, or 37 °C (Palmer et al., 2007; Son et al., 2007; Fu et al., 2012; Yang et al., 2012; Wu et al., 2019). However, for metaproteome and metabolome analyses sputum processing needs to be carried out quickly and at 4 °C in order to avoid changes in the composition of the metaproteome and metabolome. Consequently, all sample processing steps were performed at 4 °C. We started our microbial enrichment protocol by homogenizing the sputum samples using a Retsch mill followed by the addition of ice-cold PBS including DNase I and subsequent incubation on a rotary shaker at 4°C. This combination of mechanical and enzymatic treatment resulted in a very efficient homogenization of the sputum

samples. Following this treatment, samples can be pipetted easily and appear homogeneous with the naked eye. Fluorescence microscopy demonstrated that the aforementioned “clouds” of eDNA were successfully digested (**Figure 2A**). Importantly, DNase-treatment not only reduces viscosity of sputum samples (Shak et al., 1990), but also releases microbes trapped within eDNA “clouds” as we confirmed microscopically (**Figure 2A**). Furthermore, DNA digest also releases microbes from biofilms, which are frequently formed by microbial pathogens within the CF lung and contain eDNA as one of the major stabilizing components (Otto, 2008; Goerke and Wolz, 2010; Schwartzbeck et al., 2016; Kovach et al., 2017). Thus, DNase-treatment at 4°C critically



improves microbial enrichment and protein identification coverage of CF sputum samples.

Since sputum processing time needs to be kept as short as possible in order to preserve the metaproteome and the metabolome, we used sputum test samples to gradually reduce DNase I incubation time from 30 min to 10 min, without observing a decrease in DNA digestion efficiency (**Figure S1**), resulting in a total sputum processing time of approx. 60 min.

Avoiding Liquefaction and Homogenization Strategies Interfering With Metaproteome and Metabolome Analyses

Other methods for mechanical homogenization and eDNA breakdown like vortexing, intense shaking, and sonification, respectively, were intentionally avoided in order to keep human and microbial cells as much intact as possible, which is a prerequisite for unbiased metaproteome and metabolome quantification. Moreover, another commonly used method for sputum homogenization and liquefaction - the digestion of the sputum samples using proteases (Son et al., 2007; Wu et al., 2019) - was also avoided, because it would interfere with metaproteome analysis and would significantly decrease protein coverage. To further reduce unwanted protein degradation due to the high abundance of serine- and metalloproteases in CF sputum samples, a protease inhibitor cocktail was added to all processing steps for metaproteome preservation (Sloane et al., 2005; Kamath et al., 2015).

A further frequently applied strategy for sputum homogenization and liquefaction is the use of chemicals, primarily DTT (commercially available as Sputasol, Sputolysin, or Cleland's reagent) (Stokell et al., 2014). Stokell et al. even considered DTT treatment mandatory, since it is not possible to pipette sputum samples due to their high viscosity without DTT treatment (Stokell et al., 2014). However, we avoided DTT treatment in early steps of our protocol, since high amounts of DTT inhibit DNase I activity and also interfere with metabolome analyses by masking other analytes. Therefore, DTT was only added at a late step of our protocol (after DNase-treatment and sampling aliquots for metabolome analysis) for liquefying the remaining pellet allowing filtration (**Figure 1**). However, depending on the viscosity of the remaining pellet, it should be carefully assessed, if DTT should be used or not since DTT can assist bacterial cell lysis and therefore might have a negative impact on microbial cell recovery (Liu et al., 2018).

Enrichment of Microbial Proteins Overcoming the Outnumbering Human Protein Abundance

The enormous abundance of human proteins (e.g. mucins, serine and metalloproteases, immunoglobulins, serum albumin) (Kamath et al., 2015) masks comparably low abundant microbial proteins during MS/MS analyses. Confirming this, we found high amounts of human proteins in the non-enriched controls (**Tables S3–S5**). In order not to increase this problem, we kept the first steps of sputum processing as mild as possible, to minimize lysis of human cells and a concomitant contamination of the microbial metaproteome (and metabolic footprint, see above). Thus, to further increase the amount of

microbial proteins compared to human proteins, microbial cells were enriched, while human cells were depleted, prior to MS/MS analyses. Several approaches were tested using the sputum test samples to reduce sample complexity and enrich microbial cells: differential centrifugation (Tanca et al., 2014; Tanca et al., 2017), filtration (Xiong et al., 2015; Schultz et al., 2020), as well as density gradient centrifugation (Hevia et al., 2016). Each procedure was investigated for the enrichment success microscopically (**Figure S2**). Since *S. aureus* is one of the most prevalent and important CF pathogens, we additionally tested an enrichment protocol combining *S. aureus* specific antibodies and magnetic beads adapted from (Bicart-See et al., 2016; Wei et al., 2016) (**Figure S2**). However, neither density gradient centrifugation, nor antibody/magnetic bead enrichment resulted in a reproducible and sufficient enrichment. However, differential centrifugation as well as filtration did result in reproducible but only small enrichment of microbial cells as observed microscopically (data not shown). Therefore, differential centrifugation and filtration were combined resulting in a successful enrichment of microbial cells and an efficient depletion of human cells, respectively (**Figure 2**).

Although our enrichment strategy markedly increased the concentration of recovered microbial cells, a significant amount of biomass was lost during this two-step enrichment procedure. This reasons the necessity to use a higher starting volume of the homogenized sputum for microbial enrichment (3 mL) than for the non-enriched control (0.5 mL) ensuring that the protein yield after enrichment is still sufficiently high. Equal protein amounts (40 µg) of both the enriched samples and the non-enriched controls were used for metaproteome analyses to account for the different input volumes.

Increasing Protein Yield by Optimizing Cell Disruption and Protein Extraction

Moreover, it has been reported that the cell disruption method critically impacts the extraction efficiency and true species representation in various environmental samples (Starke et al., 2019). Therefore, the subsequent cell disruption and protein extraction process was optimized to increase protein yield. To this end, we used the sputum samples for protocol development and evaluated multiple cell disruption and protein extraction procedures. These included sonification, freeze and thaw cycles, boiling, bead beating, enzymatic treatment, harsh extraction buffers and different combinations of these procedures. Cell disruption and protein extraction efficiency was evaluated by measuring extracted protein concentrations and total protein amounts, respectively (data not shown). Based on these results, we decided to use a combination of downscaled beat-beating adapted from (Becher et al., 2009; Zühlke et al., 2016), which was shown to most effectively disrupt the enormously robust cells of the spheric, Gram-positive CF key pathogen *S. aureus* followed by subsequent boiling of the samples in an harsh SDS-based extraction buffer with a final SDS concentration of 1% adapted from (Chourey et al., 2010). Using this method, we were able to extract the highest protein amounts out of the enriched microbial fraction ranging from approximately 40 to 110 µg, which is sufficient for subsequent metaproteome analysis.

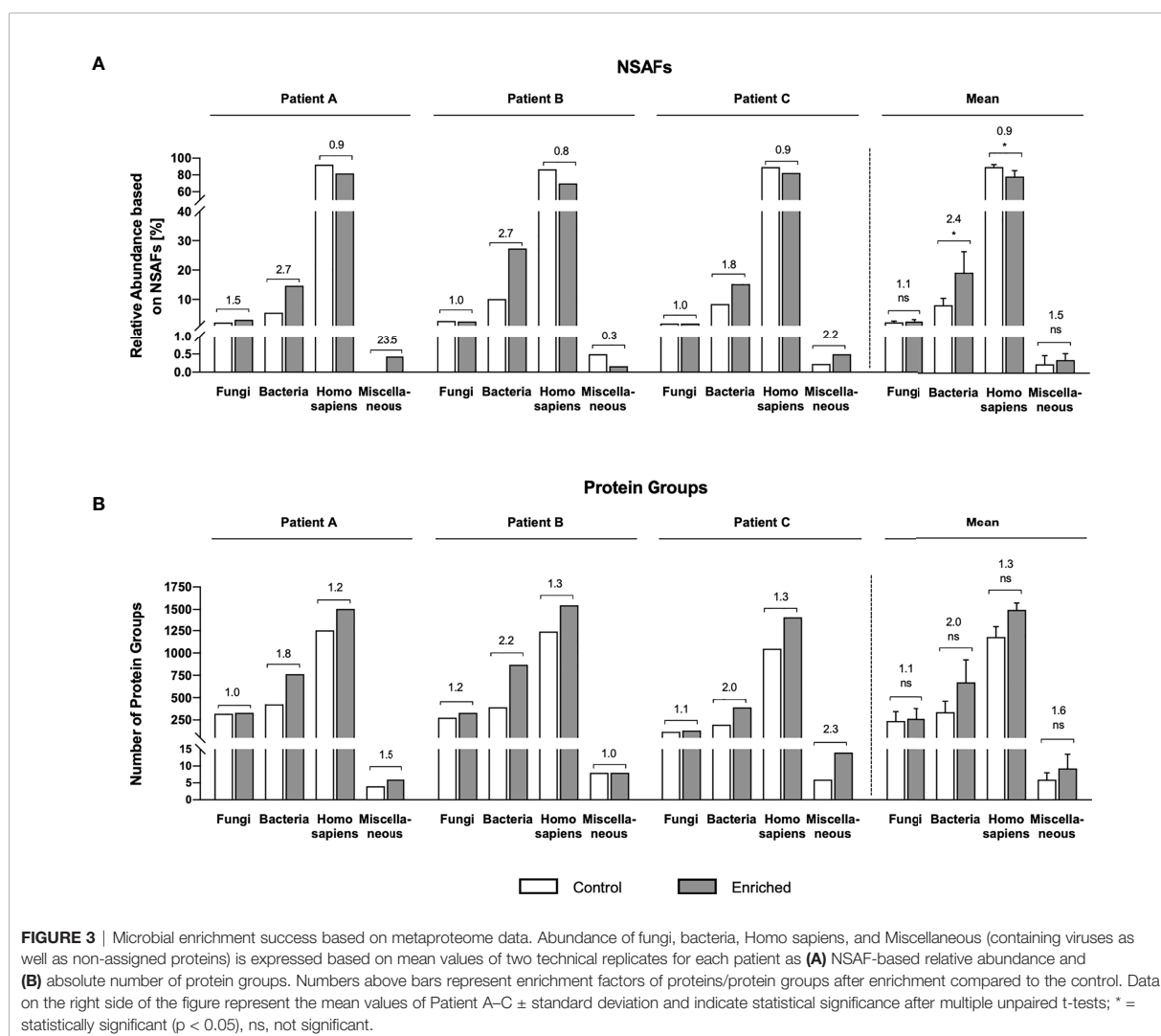
Taken together, we established and optimized a sputum-processing protocol for microbial enrichment characterized by the following major steps (i) mechanical and enzymatic homogenization, (ii) differential centrifugation as the first microbial enrichment step, (iii) liquefaction with DTT, (iv) filtration as the second microbial enrichment step, (v) optimized cell disruption and protein extraction by a combination of beat beating and boiling in SDS extraction buffer.

Microbial Proteins Were Enriched by a Maximum Factor of 2.7

After we established a protocol for microbial enrichment, we selected three different patients, designated Patient A, Patient B, and Patient C, for detailed metaproteome analyses as a proof of concept. In order to assess the enrichment efficiency of these three sputum samples, we compared a non-enriched control and the enriched sample using a state-of-the-art metaproteomics workflow (Figure 1) and monitored

microbial cell count microscopically (Figure 2). For metaproteome analyses, we measured two technical replicates of each sample in LC-MS/MS experiments showing decent reproducibility (Figure S3). However, the overall percentage of assigned spectra is rather low compared to other metaproteomics datasets (Hinze et al., 2019), which most likely might be attributed to the typically high proteolysis rates within CF sputum caused by neutrophil-derived proteases (Sloane et al., 2005; Folkesson et al., 2012).

Two different complementary read-outs were used to evaluate microbial protein enrichment efficiency: relative protein abundance based on NSAFs, and the number of identified proteins/protein groups (= group of proteins sharing the same identified peptide(s)) (Figure 3). Briefly, NSAF-based quantification of proteomic data refers to a label-free quantification method relying on a spectral counting approach. More precisely, quantification of proteins is carried out by comparing the number of identified MS/MS spectra



of a specific protein over several LC-MS/MS experiments, since protein abundance correlates with the number of proteolytic peptides and thus with the number of total MS/MS spectra (spectral counts). Considering that large proteins naturally contribute a higher number of peptides/spectra compared to small proteins, spectral counts undergo normalization to create the NSAF. Therefore, the number of spectral counts (SC) of a specific protein is divided by the protein's length (L), divided by the sum of all SC/L values from the given experiment (Zhu et al., 2010) allowing relative quantification of proteins throughout samples.

Both, the NSAF as well as the protein group-based evaluation showed a clear trend of successful enrichment of bacterial proteins and depletion of human proteins in all three samples (Figure 3). In fact, the 250 most prominent human proteins (e.g. including mucins, albumins, immunoglobulins), which contribute to the total proteome mass by approx. 40%, were depleted by a mean factor of 1.6 fold (Tables S3–S5). Regarding the enrichment of bacterial proteins, NSAF-based enrichment factors range from 1.8-fold (Patient C) to 2.7-fold (Patient A and Patient B) (Figure 3A). Notably, these enrichment factors are also well reflected by our microscopic analyses. 50 randomly selected fields of view were acquired for the different steps of the protocol. Both qualitatively (Figure 2A) as well as quantitatively (Figure 2B) we observed a clear reduction of human (epithelial) cells and particles bigger than 50 μm in our samples after the first step of differential centrifugation (Figure 1). Particles smaller than 10 μm as well as microbial cells were obviously enriched after filtration (Figure 2). Notably, the mean enrichment factor of bacterial cells calculated from microscopic analyses of 2.7-fold is very close to the bacterial enrichment factors calculated from NSAFs.

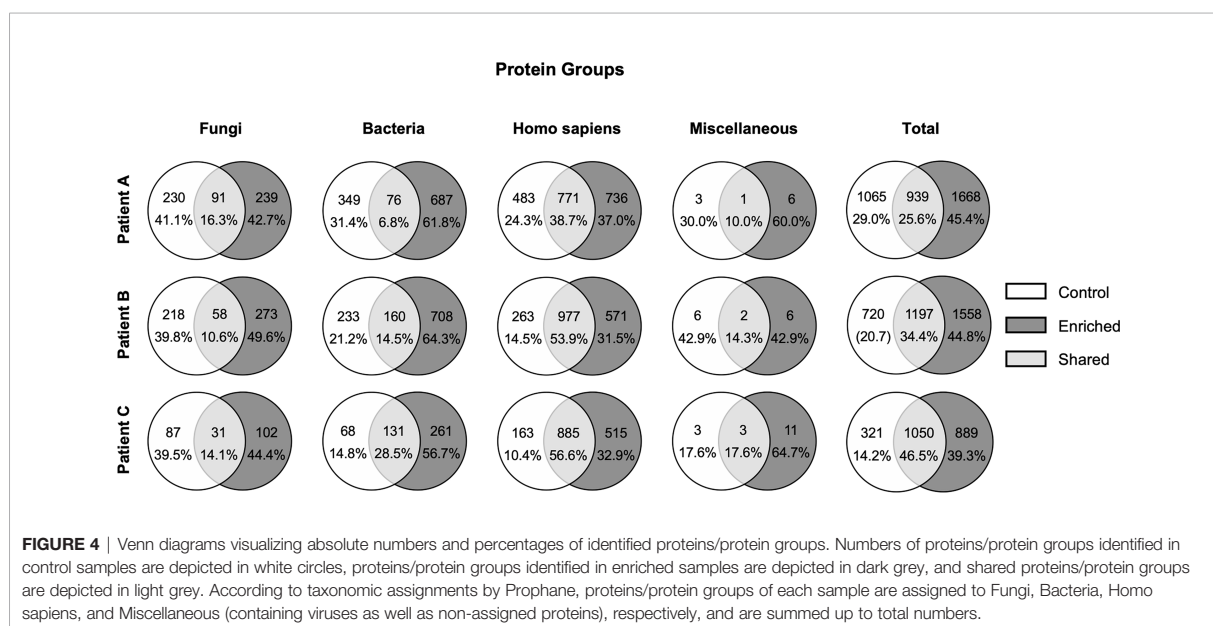
Protein group-based enrichment factors for bacterial proteins range from 1.8-fold (Patient A: 425 total protein groups in control, 763 after enrichment), to 2.0 fold (Patient C: 199 total

protein groups in control, 392 after enrichment), and 2.2-fold (Patient B: 393 total protein groups in control, 868 after enrichment) (Figures 3B, 4). However, considering that the total number of identified proteins/protein groups is overall higher after enrichment compared to the control, the enrichment factors need to be normalized accordingly. Doing so, normalized protein group-based enrichment factors range from 1.4-fold (Patient A and C) to 1.5-fold (Patient B).

Total numbers of protein groups depicted in Figure 4 indicate a rather small overlap between proteins/protein groups found in the control and the enriched fraction, respectively. This overlap ranges from 6.8% (Patient A), to 14.5% (Patient B) and 28.5% (Patient C). One explanation for this might be that a high proportion of bacterial proteins was lost during the enrichment process. Surprisingly, these potentially lost proteins are only partially annotated as extracellular proteins (e.g. nucleases and toxins, Tables S3–S5), which indicates that a great number of proteins in the extracellular sputum milieu are derived from cell lysis (e.g. proteins belonging to energy metabolism or DNA replication, ribosomal proteins, stress response proteins, Tables S3–S5).

Evaluation of the Bias Introduced by Microbial Enrichment

In general, every enrichment process introduces a bias. E.g. the composition of microbial proteins in stool changes in the ratio of Firmicutes- and Bacteroidetes-derived proteins after differential centrifugation and in the proportion of extracellular and host proteins (Tanca et al., 2015). This emphasizes the relevance of the chosen processing protocol influencing metaproteome data acquisition. Here, we cannot exclude that we lost big multicellular aggregates/biofilms during the enrichment. To address this problem, it might be useful to analyze different fractions during sputum processing in order to increase bacterial protein



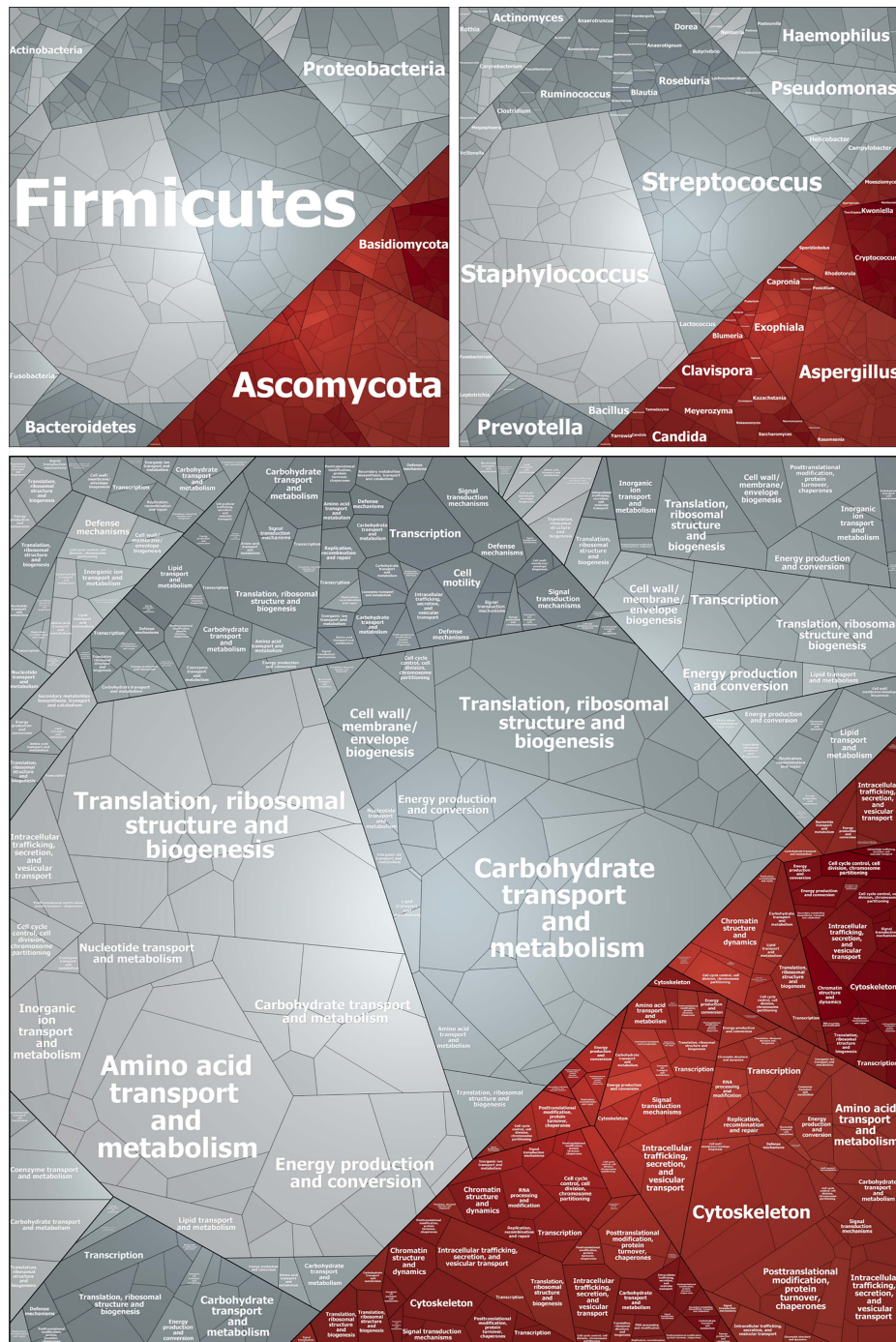


FIGURE 5 | Voronoi treemap visualizing the taxonomic and functional affiliation of bacterial (grey) and fungal (red) protein/protein groups identified after enrichment in Patient A. Each cell represents a single protein/protein group, which size correlates with NSAF-based protein abundance. Proteins/protein groups are clustered according to Prophane results based on their taxonomic assignment on class level (upper left), genus level (upper right), and based on their functional assignment (lower panel). Proteins of unknown function are excluded from this visualization.

identification coverage. For instance, extracellular proteins can easily be enriched and extracted using Strata-Clean beads as described by (Bonn et al., 2014; Graf et al., 2019) (data not shown) and subsequently analyzed by metaproteomics. However, to exclude that a systematic error is inherent with our enrichment protocol and the abundancies of bacterial proteins are not excessively over- or underrepresenting any bacterial species, we compared the NSAF-based protein abundances of different species with CFU counts revealing a reasonable relation (Table 1, Figure 5 and Figures S4, S5).

Interestingly, according to our metaproteome data, fungal cells/proteins were not enriched (Figure 3). This might be explained by the varying cells size of different fungal species in yeast or hyphae form e.g. ranging from 4 to 12 µm in diameter for yeast cells, 1 to 3 µm in diameter and several 100 µm in length for hyphae, and 1 to 5 µm for spores and conidia (Hickey and Read, 2009; Chotirmall and McElvaney, 2014; Thomson et al., 2016; Williams et al., 2016). This means, that small fungal cells would be enriched during our first enrichment step by differential centrifugation, but bigger fungal cells will be depleted during our second enrichment step by filtration (cut off 10 µm). However, those fungal genera, which are most frequently identified in CF in the literature, match the genera we identified as the most abundant by metaproteomics: namely, *Aspergillus* (prevalence up to 57%), *Candida*, *Blumeria*, *Exophiala*, *Clavisporea*, and *Cryptococcus* (Figure 5 and Figures S4, S5) (Chotirmall and McElvaney, 2014; Williams et al., 2016; Tracy and Moss, 2018). The genus *Scedosporium* (prevalence ranging from 3.1% to 10.6% (Williams et al., 2016), however, plays a minor role according to our data (Figure 5 and Figures S4 1, S5).

Important Bacterial (Patho-)Physiological Pathways Revealed by Metaproteome and Metabolome Analyses

The total number of identified proteins/protein groups after enrichment differs from patient to patient. In more detail, we identified 2607 proteins/protein groups for Patient A, 2755 for Patient B and the lowest number of 1939 for Patient C (Figure 4) – the patient whose microbial lung community is dominated by *P. aeruginosa* and who shows the lowest lung function (Table 1 and Table S1, Figure S4). Interestingly, these results are in line with the literature stating an exacerbation/reduced lung function due to *P. aeruginosa* infection, which is caused by the extensive recruitment of neutrophils and concomitant proteolytic digestion of lung tissue and proteins of bacterial pathogens (Sloane et al., 2005; Folkesson et al., 2012). This neutrophil-derived proteolytic digestion in consequence likely leads to a reduced protein identification coverage (and reduced percentage of assigned spectra) as observed in Patient C (Figure 4 and Figure S3).

The number of protein/protein groups assigned to the most prominent bacterial genera in CF like *Pseudomonas* (166 in Patient C), *Staphylococcus* (185 in Patient A), *Burkholderia* (408 in Patient B), *Haemophilus* (127 in Patient B), and *Streptococcus* (128 in Patient A) give a first insight into the physiology of these pathogens during CF infection. This means that there is still room for improvement of our enrichment protocol to ultimately increase bacterial protein identification coverage. Notably, the majority of

protein groups assigned to the aforementioned dominant bacterial pathogens are poorly or even uncharacterized, indicating that important host-adaptation strategies of the identified pathogens have so far not been addressed and uncovered experimentally. Protein groups of known function identify various physiological pathways and virulence factors, which are key for bacterial pathogens to establish chronic infections: host immune evasion, anaerobic metabolism, and virulence/antibiotic resistance (Folkesson et al., 2012). We would like to emphasize that out of the 69 proteins/protein groups related to the above mentioned traits (Figure 6) 46 proteins/protein groups were exclusively identified in the enriched samples. Only 4 proteins/protein groups were exclusively identified in the control samples, while 19 proteins/protein groups were shared by control and enriched samples. Out of those 19 proteins/protein groups two were slightly less abundant in the enriched samples. Together this underlines the value of our enrichment protocol.

Oxidative Stress

During host immune response, large numbers of neutrophils are recruited, which fight pathogens by the production of reactive oxygen species (Folkesson et al., 2012; Kamath et al., 2015). Consistently, in Patient A we detected an alkyl hydroperoxide reductase (*Staphylococcus* sp.), a Glutathione S-transferase (*Haemophilus* sp.), an iron-sulfur-cluster repair protein (*Staphylococcus* sp.), glutathione-disulfide reductase (*Streptococcus* sp.), and the molecular chaperones DnaK (*Staphylococcus* sp.) and GroL (various species) as well as the protease ClpP (*Streptococcus* sp.), which all are involved in protein protection, repair, or degradation of proteins and inducible after various stress conditions like oxidative stress (Michta et al., 2014; Ezraty et al., 2017). Moreover, in Patient B *Burkholderia* sp. express the chaperone GroL, the protease ClpB and ClpX as well as catalase/peroxidase. In this sample, we additionally identified thioredoxin, glutathione disulfide reductase, peroxiredoxin, and iron/manganese superoxide dismutase expressed by *Burkholderia* sp., *Haemophilus* sp., *Streptococcus* sp., and *Staphylococcus* sp., respectively. In Patient C, we identified the following (oxidative) stress proteins: thioredoxin, peroxiredoxin, thioredoxin-disulfide reductase, DnaK, and ClpB expressed by *Pseudomonas* sp. and *Staphylococcus* sp. (Tables S3–S5). Collectively, these data suggest that the most important CF pathogens within our samples might cope with oxidative stress during CF infection, which is in line with the literature (Treffon et al., 2018).

Oxygen Limitation and pH Homeostasis

The lung environment and especially the CF lung is not considered to be entirely aerobic, due to the viscous character of mucus, oxygen consumption by colonizing microbes, and phagocytes. Rather, oxygen gradients ranging from hypoxic to even anoxic/anaerobic microenvironments characterize the CF-lung (Worlitzsch et al., 2002). Thus, even strict anaerobic bacteria are able to thrive in lungs of CF patients (Filkins and O'Toole, 2015). Consistent with hypoxic and anaerobic conditions, we identified marker-proteins of fermentative metabolism from *Staphylococcus* sp. including lactate

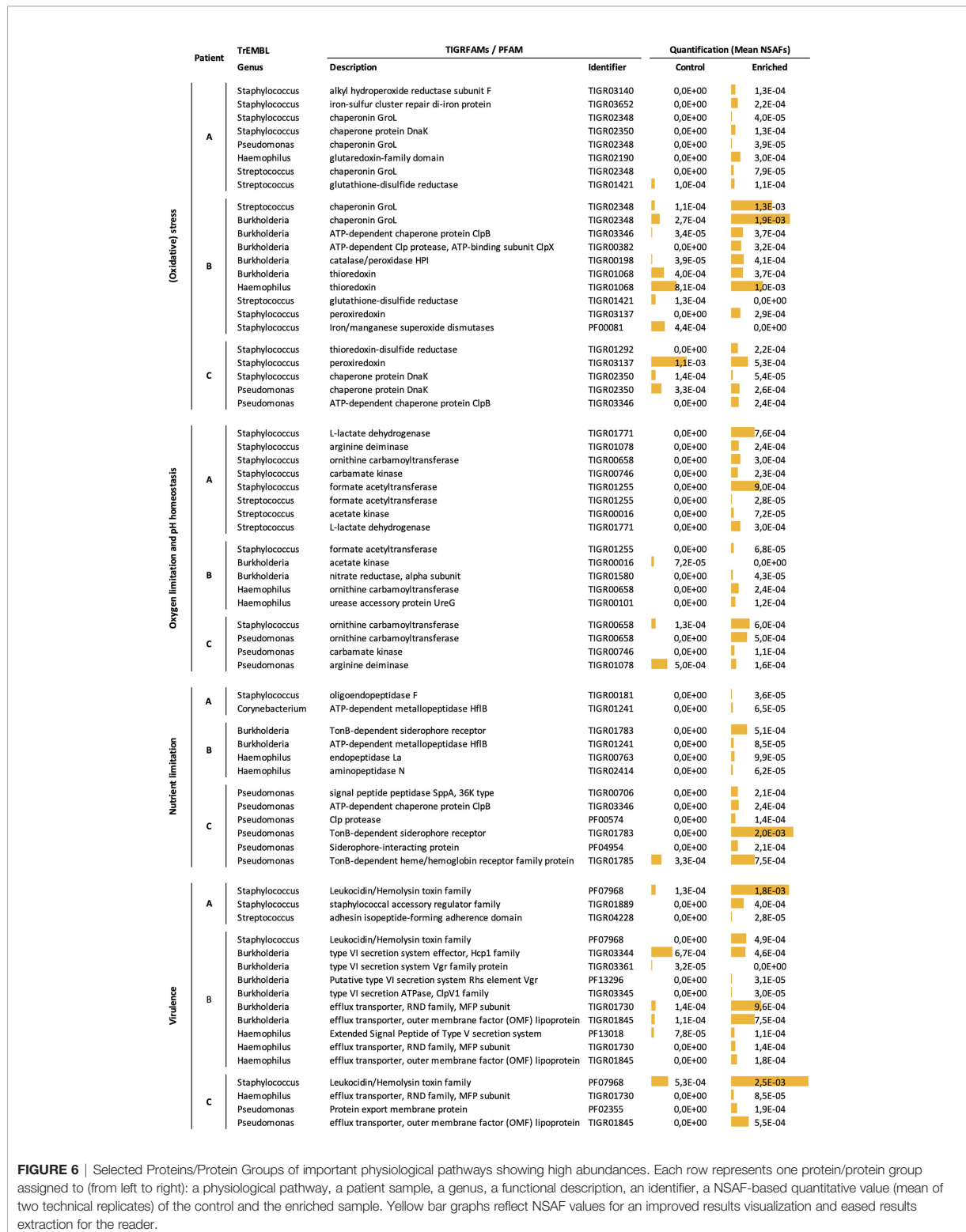


FIGURE 6 | Selected Proteins/Protein Groups of important physiological pathways showing high abundances. Each row represents one protein/protein group assigned to (from left to right): a physiological pathway, a patient sample, a genus, a functional description, an identifier, a NSAF-based quantitative value (mean of two technical replicates) of the control and the enriched sample. Yellow bar graphs reflect NSAF values for an improved results visualization and eased results extraction for the reader.

dehydrogenase, formate acetyltransferase and acetate kinase in all three samples. In the samples of Patient A and Patient B we further identified formate acetyltransferase, L-lactate dehydrogenase and acetate kinase, assigned to the genera *Streptococcus*, *Staphylococcus*, and *Burkholderia*, respectively (Figure 6 and Tables S3–S5). A further metabolic strategy to overcome oxygen limitation conserved in many pathogens is the fermentation of arginine via the arginine deiminase pathway (Lindgren et al., 2014). According to our metaproteome data, arginine deiminase, ornithine carbamoyltransferase, and carbamate kinase, are highly abundant and identified in multiple genera: *Staphylococcus* in Patient A and Patient C, *Haemophilus* in Patient B, and *Pseudomonas* in Patient C (Figure 6 and Tables S3–S5). In support of our metaproteome data, we identified ornithine (Patient A-C) and citrulline (Patient B), key metabolites of the arginine deiminase pathway, by metabolic footprint analysis (Figure S6) (Lindgren et al., 2014). Clear induction of the arginine deiminase pathway suggests that not only ATP production, but also raise in pH due to production of ammonia is important for the pathogen to counteract acidification upon fermentation and likely upon phagocytosis by immune cells (Li et al., 2000; Beenken et al., 2004; Resch et al., 2005; Filkins and O'Toole, 2015). As evidence for anaerobic metabolism and acidification, we identified lactic acid as a fermentation product in all three samples (Figure S6). Moreover, we identified the urease accessory protein UreG from *Haemophilus* sp. in Patient B, which is a protein of the urease pathway and similarly to the arginine pathway is involved in pH homeostasis (Figure 6 and Table S4) (Li et al., 2000). Notably, urea as the substrate of the urease pathway was also detected in Patient A and Patient B (Figure S6). Finally, we identified the alpha subunit of the nitrate reductase from *Burkholderia* sp. in Patient B as part of the nitrate respiration pathway (Figure 6 and Table S4) (Filkins and O'Toole, 2015) utilizing nitrate as an alternative terminal electron acceptor.

Nutrient Limitation

The competition for nutrients within the CF airways is an important selective pressure influencing the composition of the CF community. For example *Pseudomonads* and *Streptococci* are able to efficiently utilize amino acids, organic acids and alcohols (partly produced by other community members) leading to high growth rates within the lung (Yang et al., 2008; Henson et al., 2019; La Rosa and Molin, 2019). Notably, our metabolome data revealed various amino acids (and organic acids) within all three sputum samples (Figure S6), which supports that amino acids are the major carbon- and nitrogen source in CF sputum (Palmer et al., 2005; La Rosa and Molin, 2019). Moreover, we found evidence that these amino acids could result from the hydrolytic activity of a variety of different proteases and peptidases (Kamath et al., 2015; Quinn et al., 2019). Currently, proteases of human origin are believed to be the key players responsible for proteolytic digestion in the CF airways. Specifically, human neutrophil-derived elastase and cathepsins are considered to be the most abundant and potent proteases (Voynow et al., 2008). Although we identified these human proteases among the most abundant in our proteome

data, we additionally found a great number of proteases and peptidases of bacterial origin. For example, we identified a staphylococcal oligopeptidase in Patient A, the metallopeptidase HflB, peptidase Do, and protease HslVU from *Burkholderia* sp. and *Streptococcus* sp. as well as endopeptidase La, and aminopeptidase N from *Haemophilus* sp. in Patient B, and multiple Clp protease proteins in Patient C (Figure 6 and Table S3–S5). In fact, by using NSAFs to calculate the contribution of all human and all bacterial proteases and peptidases to the total proteome mass, we found that the human proteases/peptidases in the non-enriched control accounts for 2.15% of the total proteome mass and bacterial proteases/peptidases in the enriched sample for 0.84% (Figure 6 and Tables S3–S5). This suggests that the role of bacterial proteases and peptidases in the CF pathophysiology is larger than previously acknowledged (Kamath et al., 2015).

Another vital nutrient during CF infection is iron, which is needed by bacteria as a cofactor in essential metabolic enzymes (Reid et al., 2009). Although the iron concentration within the CF airway is relatively high compared to other human body sites, pathogens within the CF lung fight for iron by sequestering iron chelating siderophores and proteases degrading transferrin, lactoferrin, and heme-containing proteins like hemoglobin and myoglobin (Reid et al., 2009; Runyen-Janecky, 2013; Treffon et al., 2018). This fight for iron is well reflected by our metaproteome data, e.g. revealing multiple TonB-dependent siderophore receptors and TonB-dependent heme/hemoglobin receptor family proteins of *Burkholderia* sp. and *Pseudomonas* sp. in Patient B and Patient C, respectively (Figure 6 and Tables S3–S5).

Virulence Factors

Among the identified microbial proteins many important virulence factors were detected. For instance, staphylococcal leukocidin, an immune evasion protein that mediates lysis of leukocytes (Scherr et al., 2015) was very abundant in all three samples, underlining the ongoing battle between the host immune system and the pathogen within the CF-lung (Figure 6 and Tables S3–S5). However, our proteomic data did not provide support for presence of microbial biofilms in the samples, which is considered a major microbial phenotype during infection (Folkesson et al., 2012; Filkins and O'Toole, 2015; Kovach et al., 2017). Only a streptococcal adhesin (Patient A), one adhesin of *Pseudomonas* sp. (Patient C), and the aforementioned staphylococcal leukocidins (Patient A-C), which have the potential to moonlight as a stabilizing extracellular matrix component under acidic conditions, were detected (Figure 6 and Tables S3–S5) (Graf et al., 2019). We cannot entirely exclude that the lack of biofilm-related proteins in our sample is related to the enrichment procedure, as large cellular clusters were cleared from the sample during the first centrifugation and/or the filtration step.

Another well described concept of bacterial virulence are secretion systems, which transport effectors or DNA across membranes to manipulate the physiology of host cells or competing bacteria (Voth et al., 2012). Indeed, we identified

multiple proteins of a Type VI secretion system of *Burkholderia* sp. in Patient B. Furthermore, we found an Extended Signal Peptide of Type V secretion system protein in *Haemophilus* sp. (Patient B) (Figure 6 and Tables S3–S5). This emphasizes the importance of secretion systems, especially for *Burkholderia* sp., during successful CF infection. Finally, we found multiple efflux transporter mediating antibiotic resistance (Li and Nikaido, 2009) in *Burkholderia* sp., *Haemophilus* sp., *Pseudomonas* sp. (Patient B and Patient C), which likely reflect a response towards the antimicrobial therapy that the three investigated patients underwent (Figure 6, Table 1 and Tables S4, S5).

Limitations of Our Study

The detailed analysis of three sputum samples provided novel insights into the microbial pathophysiology within the CF lung and revealed high expression of the arginine deiminase pathway and multiple proteases, demonstrating the applicability of our protocol. We are aware that larger sample numbers will be required to validate the significance of these findings. Future studies should not only include larger sample numbers but should also consider specific mutations of the CFTR gene and the individual patient treatment regimens to account for the high in-between variability of CF patients (Tanca et al., 2014). Additionally, larger numbers of biological and technical replicates will also increase protein coverage. Including a proteomic analysis of the supernatant of the differential centrifugation step II could provide further insight into the microbial secretome (Bonn et al., 2014; Graf et al., 2019) (Figure 1). An additional question that deserves further investigation is the small overlap of protein groups between enriched and non-enriched samples (Figure 4) (Starr et al., 2017). Moreover, to increase the coverage of our metabolome analysis (La Rosa and Molin, 2019), in addition to PBS-buffer based metabolite extraction combined with GC-MS analyses resulting in the identification of 52 metabolites, further metabolite extraction and analysis methods e.g. according to (Yang et al., 2012; Quinn et al., 2015) could be beneficial. Finally, measuring absolute metabolite concentrations will improve the comparison of metabolite levels between different studies.

CONCLUSIONS

We established an innovative, reliable, and easy-to-handle sputum processing protocol for *in vivo* metaproteome analyses. With this protocol in hand, we provide the first *in vivo* study of microbial CF sputum communities combining metaproteomic and metabolomic analyses supported by 16S sequencing and microscopic data as a proof of concept. Our metaproteome data show that we were able to enrich bacterial proteins by a maximum factor of 2.7, thereby increasing protein identification coverage to a level, which provides novel valuable insights into bacterial CF-lung pathophysiology. Our early data, which are derived from just 3 sputum samples proof the applicability of our protocol but do lack statistical power. However, they still indicate that the infecting bacteria might be coping with oxygen and nutrient limitation as well as

oxidative stress and the human immune system, respectively. Our early data also provide evidence that the arginine deiminase pathway as well as bacterial proteases play an underappreciated role in CF pathophysiology.

DATA AVAILABILITY STATEMENT

The original contributions presented in the study are publicly available in NCBI (using accession number PRJNA741386 for 16S sequencing data) and within the ProteomeXchange consortium via the PRIDE partner repository (using dataset identifier PXD025134 for metaproteome data).

ETHICS STATEMENT

The studies involving human participants were reviewed and approved by Institutional ethics review board Münster, Germany (2010-155-f-S). The patients/participants provided their written informed consent to participate in this study.

AUTHOR CONTRIBUTIONS

AG, JP-F, and KR were responsible for the study conceptualization. BK carried out the prospective study including CF sputum sampling, collection of clinical data and microbiological work-up of sputum specimens. AG and JS performed the experiments to develop the sputum processing protocol. 16S sequencing analyses were performed by DP. AG, TS, and DB performed metaproteome analyses and ML and MW were responsible for metabolome analyses. DP analyzed 16S sequencing data, while AG analyzed metaproteome and metabolome data. AG, JP-F and KR wrote the manuscript, which was critically edited by all other co-authors. All authors contributed to the article and approved the submitted version.

FUNDING

This work was funded by the German research foundation (<https://www.dfg.de/en/>) Collaborative Research Center Transregio 34, subprojects A3 to KR, A8 to JP-F, C7 to BK, Z2 to DB, and Z4 to ML. The funders had no role in study design, data collection and analysis, decision to publish, or preparation of the manuscript.

ACKNOWLEDGMENTS

We are very grateful to Tobias Kroniger, Stephan Fuchs, Daniela Zühlke, and Dirk Albrecht for help with the MS analyses and database search, respectively.

SUPPLEMENTARY MATERIAL

The Supplementary Material for this article can be found online at: <https://www.frontiersin.org/articles/10.3389/fcimb.2021.724569/full#supplementary-material>

REFERENCES

- Becher, D., Hempel, K., Sievers, S., Zühlke, D., Pané-Farré, J., Otto, A., et al. (2009). A Proteomic View of an Important Human Pathogen – Towards the Quantification of the Entire Staphylococcus Aureus Proteome. *PLoS One* 4, e8176–e8112. doi: 10.1371/journal.pone.0008176
- Beenken, K. E., Dunman, P. M., McAleese, F., Macapagal, D., Murphy, E., Projan, S. J., et al. (2004). Global Gene Expression in Staphylococcus Aureus Biofilms. *J. Bacteriol.* 186, 4665–4684. doi: 10.1128/JB.186.14.4665-4684.2004
- Bernhardt, J., Funke, S., Hecker, M., and Siebourg, J. (2009). *Visualizing Gene Expression Data via Voronoi Treemaps*. 233–241.
- Bicart-See, A., Rottman, M., Cartwright, M., Seiler, B., Gamini, N., Rodas, M., et al. (2016). Rapid Isolation of Staphylococcus Aureus Pathogens From Infected Clinical Samples Using Magnetic Beads Coated With Fc-Mannose Binding Lectin. *PLoS One* 11, e0156287–12. doi: 10.1371/journal.pone.0156287
- Bonn, F., Bartel, J., Büttner, K., Hecker, M., Otto, A., and Becher, D. (2014). Picking Vanished Proteins From the Void: How to Collect and Ship/Share Extremely Dilute Proteins in a Reproducible and Highly Efficient Manner. *Anal. Chem.* 86, 7421–7427. doi: 10.1021/ac501189j
- Camarinha-Silva, A., Jauregui, R., Chaves-Moreno, D., Oxley, A. P. A., Schaumburg, F., Becker, K., et al. (2014). Comparing the Anterior Nare Bacterial Community of Two Discrete Human Populations Using Illumina Amplicon Sequencing. *Environ. Microbiol.* 16, 2939–2952. doi: 10.1111/1462-2920.12362
- Chmiel, J. F., and Davis, P. B. (2003). State of the Art: Why do the Lungs of Patients With Cystic Fibrosis Become Infected and Why Can't They Clear the Infection? *Respir. Res.* 4, 8. doi: 10.1186/1465-9921-4-8
- Chotirmall, S. H., and McElvaney, N. G. (2014). Fungi in the Cystic Fibrosis Lung: Bystanders or Pathogens? *Int. J. Biochem. Cell Biol.* 52, 161–173. doi: 10.1016/j.biocel.2014.03.001
- Chourey, K., Jansson, J., VerBerkmoes, N., Shah, M., Chavarria, K. L., Tom, L. M., et al. (2010). Direct Cellular Lysis/Protein Extraction Protocol for Soil Metaproteomics. *J. Proteome Res.* 9, 6615–6622. doi: 10.1021/pr100787q
- Cohen, T. S., and Prince, A. (2012). Cystic Fibrosis: A Mucosal Immunodeficiency Syndrome. *Nat. Med.* 18, 509–519. doi: 10.1038/nm.2715
- Cole, J. R., Wang, Q., Fish, J. A., Chai, B., McGarrell, D. M., Sun, Y., et al. (2013). Ribosomal Database Project: Data and Tools for High Throughput rRNA Analysis. *Nucleic Acids Res.* 42, D633–D642. doi: 10.1093/nar/gkt1244
- Debyser, G., Mesuere, B., Clement, L., Van de Weygaert, J., Van Hecke, P., Duytschaever, G., et al. (2016). Faecal Proteomics: A Tool to Investigate Dysbiosis and Inflammation in Patients With Cystic Fibrosis. *J. Cyst. Fibros.* 15, 242–250. doi: 10.1016/j.jcf.2015.08.003
- Eiserich, J. P., Yang, J., Morrissey, B. M., Hammock, B. D., and Cross, C. E. (2012). Omics Approaches in Cystic Fibrosis Research: A Focus on Oxylipin Profiling in Airway Secretions. *Ann. N. Y. Acad. Sci.* 1259, 1–9. doi: 10.1111/j.1749-6632.2012.06580.x
- Ezraty, B., Gennaris, A., Barras, F., and Collet, J.-F. (2017). Oxidative Stress, Protein Damage and Repair in Bacteria. *Nat. Rev. Microbiol.* 15, 1–12. doi: 10.1038/nrmicro.2017.26
- Filkins, L. M., Graber, J. A., Olson, D. G., Dolben, E. L., Lynd, L. R., Bhujju, S., et al. (2015). Coculture of Staphylococcus Aureus With Pseudomonas Aeruginosa Drives S. Aureus Towards Fermentative Metabolism and Reduced Viability in a Cystic Fibrosis Model. *J. Bacteriol.* 197, 2252–2264. doi: 10.1128/JB.00059-15
- Filkins, L. M., and O'Toole, G. A. (2015). Cystic Fibrosis Lung Infections: Polymicrobial, Complex, and Hard to Treat. *PLoS Pathog.* 11, e1005258–8. doi: 10.1371/journal.ppat.1005258
- Folkesson, A., Jelsbak, L., Yang, L., Johansen, H. K., Ciofu, O., and Molin, S. (2012). Adaptation of Pseudomonas Aeruginosa to the Cystic Fibrosis Airway: An Evolutionary Perspective. *Nat. Rev. Microbiol.* 10, 841–851. doi: 10.1038/nrmicro2907
- Fuchs, H. J., Borowitz, D. S., Christiansen, D. H., Morris, E. M., Nash, M. L., Ramsey, B. W., et al. (1994). Effect of Aerosolized Recombinant Human DNase on Exacerbations of Respiratory Symptoms and on Pulmonary Function in Patients With Cystic Fibrosis. The Pulmozyme Study Group. *N. Engl. J. Med.* 331, 637–642. doi: 10.1056/NEJM199409083311003
- Fu, Y. R., Yi, Z. J., Guan, S. Z., Zhang, S. Y., and Li, M. (2012). Proteomic Analysis of Sputum in Patients With Active Pulmonary Tuberculosis. *Clin. Microbiol. Infect.* 18, 1241–1247. doi: 10.1111/j.1469-0691.2012.03824.x
- Gilligan, P. H. (2014). Infections in Patients With Cystic Fibrosis. *Clin. Lab. Med.* 34, 197–217. doi: 10.1016/j.clm.2014.02.001
- Goerke, C., and Wolz, C. (2010). Adaptation of Staphylococcus Aureus to the Cystic Fibrosis Lung. *Int. J. Med. Microbiol.* 300, 520–525. doi: 10.1016/j.ijmm.2010.08.003
- Graf, A. C., Leonard, A., Schäuble, M., Rieckmann, L. M., Hoyer, J., Maaß, S., et al. (2019). Virulence Factors Produced by Staphylococcus Aureus Biofilms Have a Moonlighting Function Contributing to Biofilm Integrity. *Mol. Cell Proteomics* 18, 1036–1053. doi: 10.1074/mcp.RA118.001120
- Henson, M. A., Orazi, G., Phalak, P., and O'Toole, G. (2019). Metabolic Modeling of Cystic Fibrosis Airway Communities Predicts Mechanisms of Pathogen Dominance: Supplemental Tables 1–43. *mSystems* 4. doi: 10.1101/520619
- Herzog, S., Dach, F., de Buhr, N., Niemann, S., Schlagowski, J., Chaves-Moreno, D., et al. (2019). High Nuclease Activity of Long Persisting Staphylococcus Aureus Isolates Within the Airways of Cystic Fibrosis Patients Protects Against NET-Mediated Killing. *Front. Immunol.* 10, 2552. doi: 10.3389/fimmu.2019.02552
- Hevia, A., Delgado, S., Margolles, A., and Sánchez, B. (2016). Application of Density Gradient for the Isolation of the Fecal Microbial Stool Component and the Potential Use Thereof. *Sci. Rep.* 5, 16807–9. doi: 10.1038/srep16807
- Hickey, P. C., and Read, N. D. (2009). Imaging Living Cells of Aspergillus *In Vitro*. *Med. Mycol.* 47, S110–S119. doi: 10.1080/13693780802546541
- Hinzke, T., Kouris, A., Hughes, R.-A., Strous, M., and Kleiner, M. (2019). More Is Not Always Better: Evaluation of 1D and 2D-LC-MS/MS Methods for Metaproteomics. *Front. Microbiol.* 10, 238. doi: 10.3389/fmicb.2019.00238
- Kamath, K. S., Kumar, S. S., Kaur, J., Venkatakrishnan, V., Paulsen, I. T., Nevalainen, H., et al. (2015). Proteomics of Hosts and Pathogens in Cystic Fibrosis. *Prot. Clin. Appl.* 9, 134–146. doi: 10.1002/prca.201400122
- Kovach, K., Davis-Fields, M., Irie, Y., Jain, K., Doorwar, S., Vuong, K., et al. (2017). Evolutionary Adaptations of Biofilms Infecting Cystic Fibrosis Lungs Promote Mechanical Toughness by Adjusting Polysaccharide Production. *NPJ Biofilms Microbiomes*, 3, 1. doi: 10.1038/s41522-016-0007-9
- Laemmli, U. K. (1970). Cleavage of Structural Proteins During the Assembly of the Head of Bacteriophage T4. *Nature* 227, 680–685. doi: 10.1038/227680a0
- La Rosa, J., and Molin, (2019). Adapting to the Airways: Metabolic Requirements of Pseudomonas Aeruginosa During the Infection of Cystic Fibrosis Patients. *Metabolites* 9, 234–215. doi: 10.3390/metabo9100234
- Lassek, C., Burghartz, M., Chaves-Moreno, D., Otto, A., Hentschker, C., Fuchs, S., et al. (2015). A Metaproteomics Approach to Elucidate Host and Pathogen Protein Expression During Catheter-Associated Urinary Tract Infections (CAUTIs). *Mol. Cell Proteomics* 14, 989–1008. doi: 10.1074/mcp.M114.043463
- Li, Y. H., Chen, Y. Y. M., and Burne, R. A. (2000). Regulation of Urease Gene Expression by Streptococcus Salivarius Growing in Biofilms. *Environ. Microbiol.* 2, 169–177. doi: 10.1046/j.1462-2920.2000.00088.x
- Liebermeister, W., Noor, E., Flamholz, A., Davidi, D., Bernhardt, J., and Milo, R. (2014). Visual Account of Protein Investment in Cellular Functions. *PNAS* 111, 8488–8493. doi: 10.1073/pnas.1314810111
- Liessi, N., Pedemonte, N., Armirotti, A., and Braccia, C. (2020). Proteomics and Metabolomics for Cystic Fibrosis Research. *IJMS* 21, 5439. doi: 10.3390/ijms21155439
- Lindgren, J. K., Thomas, V. C., Olson, M. E., Chaudhari, S. S., Nuxoll, A. S., Schaeffer, C. R., et al. (2014). Arginine Deiminase in Staphylococcus Epidermidis Functions to Augment Biofilm Maturation Through pH Homeostasis. *J. Bacteriol.* 196, 2277–2289. doi: 10.1128/JB.00051-14
- Li, X.-Z., and Nikaido, H. (2009). Efflux-Mediated Drug Resistance in Bacteria. *Drugs* 69, 1555–1623. doi: 10.2165/11317030-000000000-00000
- Liu, Y., Schulze-Makuch, D., de Vera, J.-P., Cockell, C., Leya, T., Baqué, M., et al. (2018). The Development of an Effective Bacterial Single-Cell Lysis Method Suitable for Whole Genome Amplification in Microfluidic Platforms. *Micromachines (Basel)* 9, 367. doi: 10.3390/mi9080367
- Lyczak, J. B., Cannon, C. L., and Pier, G. B. (2002). Lung Infections Associated With Cystic Fibrosis. *Clin. Microbiol. Rev.* 15, 194–222. doi: 10.1128/CMR.15.2.194-222.2002
- Michta, E., Ding, W., Zhu, S., Blin, K., Ruan, H., Wang, R., et al. (2014). Proteomic Approach to Reveal the Regulatory Function of Aconitase AconA in Oxidative Stress Response in the Antibiotic Producer Streptomyces Viridochromogenes Tü494. *PLoS One* 9, e87905–e87910. doi: 10.1371/journal.pone.0087905
- Neuhoff, V., Arold, N., Taube, D., and Ehrhardt, W. (1988). Improved Staining of Proteins in Polyacrylamide Gels Including Isoelectric Focusing Gels With Clear Background at Nanogram Sensitivity Using Coomassie Brilliant Blue G-250 and R-250. *Electrophoresis* 9, 255–262. doi: 10.1002/elps.1150090603
- O'Sullivan, B. P., and Freedman, S. D. (2009). Cystic Fibrosis. *Lancet* 373, 1891–1904. doi: 10.1016/S0140-6736(09)60327-5

- Otto, M. (2008). Staphylococcal Biofilms. *Curr. Top. Microbiol. Immunol.* 322, 207–228. doi: 10.1007/978-3-540-75418-3_10
- Palmer, K. L., Aye, L. M., and Whiteley, M. (2007). Nutritional Cues Control *Pseudomonas Aeruginosa* Multicellular Behavior in Cystic Fibrosis Sputum. *J. Bacteriol.* 189, 8079–8087. doi: 10.1128/JB.01138-07
- Palmer, K. L., Mashburn, L. M., Singh, P. K., and Whiteley, M. (2005). Cystic Fibrosis Sputum Supports Growth and Cues Key Aspects of *Pseudomonas Aeruginosa* Physiology. *J. Bacteriol.* 187, 5267–5277. doi: 10.1128/JB.187.15.5267-5277.2005
- Quinn, R. A., Adem, S., Mills, R. H., Comstock, W., Goldasich, L. D., Humphrey, G., et al. (2019). Neutrophilic Proteolysis in the Cystic Fibrosis Lung Correlates With a Pathogenic Microbiome 1–13. *Microbiome* 7, 23. doi: 10.1186/s40168-019-0636-3
- Quinn, R. A., Phelan, V. V., Whiteson, K. L., Garg, N., Bailey, B. A., Lim, Y. W., et al. (2015). Microbial, Host and Xenobiotic Diversity in the Cystic Fibrosis Sputum Metabolome. *ISME J.* 10, 1–16. doi: 10.1038/ismej.2015.207
- Rath, S., Heidrich, B., Pieper, D. H., and Vital, M. (2017). Uncovering the Trimethylamine-Producing Bacteria of the Human Gut Microbiota *Microbiome* 5, 54–14. doi: 10.1186/s40168-017-0271-9
- Ratjen, F. A. (2009). Cystic Fibrosis: Pathogenesis and Future Treatment Strategies. *Respir. Care* 54, 595–605. doi: 10.4187/aarc0427
- Reid, D. W., Anderson, G. J., and Lamont, I. L. (2009). Role of Lung Iron in Determining the Bacterial and Host Struggle in Cystic Fibrosis. *Am. J. Physiol. Lung Cell. Mol. Physiol.* 297, L795–L802. doi: 10.1152/ajplung.00132.2009
- Resch, A., Rosenstein, R., Nerz, C., and Götz, F. (2005). Differential Gene Expression Profiling of *Staphylococcus Aureus* Cultivated Under Biofilm and Planktonic Conditions. *Appl. Environ. Microbiol.* 71, 2663–2676. doi: 10.1128/AEM.71.5.2663-2676.2005
- Rogers, G. B., Carroll, M., Hoffman, L., Walker, A., Fine, D., and Bruce, K. (2014). Comparing the Microbiota of the Cystic Fibrosis Lung and Human Gut. *Gut Microbes* 1, 85–93. doi: 10.4161/gmic.1.2.11350
- Runyen-Janecky, L. J. (2013). Role and Regulation of Heme Iron Acquisition in Gram-Negative Pathogens. *Front Cell Infect Microbiol* 3, 55. doi: 10.3389/fcimb.2013.00055/abstract
- Scherr, T. D., Hanke, M. L., Huang, O., James, D. B. A., Horswill, A. R., Bayles, K. W., et al. (2015). *Staphylococcus Aureus* Biofilms Induce Macrophage Dysfunction Through Leukocidin AB and Alpha-Toxin. *mBio* 6, e01021–15–13. doi: 10.1128/mBio.01021-15
- Schiebenhoefer, H., Schallert, K., Renard, B. Y., Trappe, K., Schmid, E., Benndorf, D., et al. (2020). A Complete and Flexible Workflow for Metaproteomics Data Analysis Based on MetaProteomeAnalyzer and Prophan. *Nat. Protoc.*, 15, 3212–3239. doi: 10.1038/s41596-020-0368-7
- Schloss, P. D., Westcott, S. L., Ryabin, T., Hall, J. R., Hartmann, M., Hollister, E. B., et al. (2009). Introducing Mothur: Open-Source, Platform-Independent, Community-Supported Software for Describing and Comparing Microbial Communities. *Appl. Environ. Microbiol.* 75, 7537–7541. doi: 10.1128/AEM.01541-09
- Schultz, D., Zühlke, D., Bernhardt, J., Francis, T. B., Albrecht, D., Hirschfeld, C., et al. (2020). An Optimized Metaproteomics Protocol for a Holistic Taxonomic and Functional Characterization of Microbial Communities From Marine Particles. *Environ. Microbiol. Rep.* 13, 290210. doi: 10.1111/1758-2229.12842
- Schulz, C., Schütte, K., Koch, N., Vilchez-Vargas, R., Wos-Oxley, M. L., Oxley, A. P. A., et al. (2018). The Active Bacterial Assemblages of the Upper GI Tract in Individuals With and Without Helicobacter Infection. *Gut* 67, 216–225. doi: 10.1136/gutjnl-2016-312904
- Schwartzbeck, B., Birtel, J., Treffon, J., Langhanki, L., Mellmann, A., Kale, D., et al. (2016). Dynamic *In Vivo* Mutations Within the *Ica* Operon During Persistence of *Staphylococcus Aureus* in the Airways of Cystic Fibrosis Patients. *PLoS Pathog.* 12, e1006024. doi: 10.1371/journal.ppat.1006024
- Shak, S., Capon, D. J., Hellmiss, R., Marsters, S. A., and Baker, C. L. (1990). Recombinant Human DNase I Reduces the Viscosity of Cystic Fibrosis Sputum. *PNAS* 87, 9188–9192. doi: 10.1073/pnas.87.23.9188
- Sloane, A. J., Lindner, R. A., Prasad, S. S., Sebastian, L. T., Pedersen, S. K., Robinson, M., et al. (2005). Proteomic Analysis of Sputum From Adults and Children With Cystic Fibrosis and From Control Subjects. *Am. J. Respir. Crit. Care Med.* 172, 1416–1426. doi: 10.1164/rccm.200409-1215OC
- Son, M. S., Matthews, W. J., Kang, Y., Nguyen, D. T., and Hoang, T. T. (2007). *In Vivo* Evidence of *Pseudomonas Aeruginosa* Nutrient Acquisition and Pathogenesis in the Lungs of Cystic Fibrosis Patients. *Infect. Immun.* 75, 5313–5324. doi: 10.1128/IAI.01807-06
- Starke, R., Jehmlich, N., Alfaro, T., Dohnalkova, A., Capek, P., Bell, S. L., et al. (2019). Incomplete Cell Disruption of Resistant Microbes. *Sci. Rep.*, 9, 5618–5. doi: 10.1038/s41598-019-42188-9
- Starr, A. E., Deeke, S. A., Li, L., Zhang, X., Daoud, R., Ryan, J., et al. (2017). Proteomic and Metaproteomic Approaches to Understand Host–Microbe Interactions. *Anal. Chem.* 90, 86–109. doi: 10.1021/acs.analchem.7b04340
- Stokell, J. R., Khan, A., and Steck, T. R. (2014). Mechanical Homogenization Increases Bacterial Homogeneity in Sputum. *J. Clin. Microbiol.* 52, 2340–2345. doi: 10.1128/JCM.00487-14
- Tanca, A., Fraumene, C., Manghina, V., Palomba, A., Abbondio, M., Deligios, M., et al. (2017). Diversity and Functions of the Sheep Faecal Microbiota: A Multi-Omic Characterization. *Microb. Biotechnol.* 10, 541–554. doi: 10.1111/1751-7915.12462
- Tanca, A., Palomba, A., Pisanu, S., Addis, M. F., and Uzzau, S. (2015). Enrichment or Depletion? The Impact of Stool Pretreatment on Metaproteomic Characterization of the Human Gut Microbiota. *Proteomics* 15, 3474–3485. doi: 10.1002/pmic.201400573
- Tanca, A., Palomba, A., Pisanu, S., Deligios, M., Fraumene, C., Manghina, V., et al. (2014). A Straightforward and Efficient Analytical Pipeline for Metaproteome Characterization. *Microbiome* 2, 1–16. doi: 10.1186/s40168-014-0049-2
- Thomson, D. D., Berman, J., and Brand, A. C. (2016). High Frame-Rate Resolution of Cell Division During *Candida Albicans* Filamentation. *Fungal Genet. Biol.* 88, 54–58. doi: 10.1016/j.fgb.2016.02.001
- Tracy, M. C., and Moss, R. B. (2018). The Myriad Challenges of Respiratory Fungal Infection in Cystic Fibrosis. *Pediatr. Pulmonol.* 53, S75–S85. doi: 10.1002/ppul.24126
- Treffon, J., Block, D., Moche, M., Reiß, S., Fuchs, S., Engelmann, S., et al. (2018). Adaptation of *Staphylococcus Aureus* to Airway Environments in Patients With Cystic Fibrosis by Upregulation of Superoxide Dismutase M and Iron-Scavenging Proteins. *J. Infect. Dis.* 217, 1453–1461. doi: 10.1093/infdis/jiy012
- Voth, D. E., Broderdorf, L. J., and Graham, J. G. (2012). Bacterial Type IV Secretion Systems: Versatile Virulence Machines. *Future Microbiol.* 7, 241–257. doi: 10.2217/fmb.11.150
- Voynow, J., Fischer, B., and Zheng, S. (2008). Proteases and Cystic Fibrosis. *Int. J. Biochem. Cell Biol.* 40, 1238–1245. doi: 10.1016/j.biocel.2008.03.003
- Wang, Q., Garrity, G. M., Tiedje, J. M., and Cole, J. R. (2007). Naïve Bayesian Classifier for Rapid Assignment of rRNA Sequences Into the New Bacterial Taxonomy. *Appl. Environ. Microbiol.* 73, 5261–5267. doi: 10.1128/AEM.00062-07
- Wei, S., Park, B.-J., Seo, K.-H., and Oh, D.-H. (2016). Highly Efficient and Specific Separation of *Staphylococcus Aureus* From Lettuce and Milk Using Dynabeads Protein G Conjugates. *Food Sci. Biotechnol.* 25, 1501–1505. doi: 10.1007/s10068-016-0233-1
- Williams, C., Ranjendran, R., and Ramage, G. (2016). Pathogenesis of Fungal Infections in Cystic Fibrosis. *Curr. Fungal Infect. Rep.*, 10, 163–169. doi: 10.1007/s12281-016-0268-z
- Worlitzsch, D., Tarran, R., Ulrich, M., Schwab, U., Cekici, A., Meyer, K. C., et al. (2002). Effects of Reduced Mucus Oxygen Concentration in Airway *Pseudomonas* Infections of Cystic Fibrosis Patients. *J. Clin. Invest.* 109, 317–325. doi: 10.1172/JCI13870
- Wu, X., Siehnel, R. J., Garudathri, J., Staudinger, B. J., Hisert, K. B., Ozer, E. A., et al. (2019). *In Vivo* Proteome of *Pseudomonas Aeruginosa* in Airways of Cystic Fibrosis Patients. *J. Proteome Res.* 18, 2601–2612. doi: 10.1021/acs.jproteome.9b00122
- Xiong, W., Giannone, R. J., Morowitz, M. J., Banfield, J. F., and Hettich, R. L. (2015). Development of an Enhanced Metaproteomic Approach for Deepening the Microbiome Characterization of the Human Infant Gut. *J. Proteome Res.* 14, 133–141. doi: 10.1021/pr500936p
- Yang, J., Eiserich, J. P., Cross, C. E., Morrissey, B. M., and Hammock, B. D. (2012). Metabolomic Profiling of Regulatory Lipid Mediators in Sputum From Adult Cystic Fibrosis Patients. *Free Radical Biol. Med.* 53, 160–171. doi: 10.1016/j.freeradbiomed.2012.05.001
- Yang, L., Haagensen, J. A. J., Jelsbak, L., Johansen, H. K., Sternberg, C., and Molin, S. (2008). *In Situ* Growth Rates and Biofilm Development of *Pseudomonas Aeruginosa* Populations in Chronic Lung Infections. *J. Bacteriol.* 190, 2767–2776. doi: 10.1128/JB.01581-07
- Zhu, W., Smith, J. W., and Huang, C.-M. (2010). Mass Spectrometry-Based Label-Free Quantitative Proteomics. *J. BioMed. Biotechnol.* 2010, 840518. doi: 10.1155/2010/840518
- Zühlke, D., Dörries, K., Bernhardt, J., Maaf, S., Muntel, J., Liebscher, V., et al. (2016). Costs of Life - Dynamics of the Protein Inventory of *Staphylococcus Aureus* During Anaerobiosis. *Sci. Rep.* 6, 1–13. doi: 10.1038/srep28172

Zybailov, B, Mosley, AL, Sardi, ME, Coleman, MK, Florens, L, and Washburn, MP. (2006). Statistical Analysis of Membrane Proteome Expression Changes in *Saccharomyces Cerevisiae*. *J Proteome Res* 5, 2339–2347.

Conflict of Interest: The authors declare that the research was conducted in the absence of any commercial or financial relationships that could be construed as a potential conflict of interest.

Publisher's Note: All claims expressed in this article are solely those of the authors and do not necessarily represent those of their affiliated organizations, or those of

the publisher, the editors and the reviewers. Any product that may be evaluated in this article, or claim that may be made by its manufacturer, is not guaranteed or endorsed by the publisher.

Copyright © 2021 Graf, Striesow, Pané-Farré, Sura, Wurster, Lalk, Pieper, Becher, Kahl and Riedel. This is an open-access article distributed under the terms of the Creative Commons Attribution License (CC BY). The use, distribution or reproduction in other forums is permitted, provided the original author(s) and the copyright owner(s) are credited and that the original publication in this journal is cited, in accordance with accepted academic practice. No use, distribution or reproduction is permitted which does not comply with these terms.

6 Article III: Nonthermal Plasma Jet Treatment Negatively Affects The Viability and Structure of *Candida albicans* SC5314 Biofilms

Article III

Nonthermal Plasma Jet Treatment Negatively Affects the Viability and Structure of
Candida albicans SC5314 Biofilms

Oliver Handorf, Thomas Weihe, Sander Bekeschus, Alexander C. Graf, Uta Schnabel, Katharina Riedel, Jörg Ehlbeck

Applied and Environmental Microbiology, 2018, 84:1054–15

Author contributions:

As a co-author, ACG performed CLSM image acquisition, CLSM figure preparation and contributed to manuscript writing and editing.

Alexander C. Graf

Prof. Dr. Katharina Riedel



Nonthermal Plasma Jet Treatment Negatively Affects the Viability and Structure of *Candida albicans* SC5314 Biofilms

O. Handorf,^a T. Weihe,^a S. Bekeschus,^a A. C. Graf,^b U. Schnabel,^a K. Riedel,^b J. Ehlbeck^a

^aLeibniz Institute for Plasma Science and Technology (INP), Greifswald, Germany

^bErnst Moritz Arndt University, Microbial Physiology and Molecular Biology, Greifswald, Germany

ABSTRACT Microorganisms are predominantly organized in biofilms, where cells live in dense communities and are more resistant to external stresses than are their planktonic counterparts. With *in vitro* experiments, the susceptibility of *Candida albicans* biofilms to a nonthermal plasma treatment (plasma source, kINPen09) in terms of growth, survival, and cell viability was investigated. *C. albicans* strain SC5314 (ATCC MYA-2876) was plasma treated for different time periods (30 s, 60 s, 120 s, 180 s, 300 s). The results of the experiments, encompassing CFU, fluorescence Live/Dead, and 2,3-bis-(2-methoxy-4-nitro-5-sulphophenyl)-2H-tetrazolium-5-carboxanilide salt (XTT) assays, revealed a negative influence of the plasma treatment on the proliferation ability, vitality, and metabolism of *C. albicans* biofilms, respectively. Morphological analysis of plasma-treated biofilms using atomic force microscopy supported the indications for lethal plasma effects concomitant with membrane disruptions and the loss of intracellular fluid. Yielding controversial results compared to those of other publications, fluorescence and confocal laser scanning microscopic inspection of plasma-treated biofilms indicated that an inactivation of cells appeared mainly on the bottom of the biofilms. If this inactivation leads to a detachment of the biofilms from the overgrown surface, it might offer completely new approaches in the plasma treatment of biofilms. Because of plasma's biochemical-mechanical mode of action, resistance of microbial cells against plasma is unknown at this state of research.

IMPORTANCE Microbial communities are an increasing problem in medicine but also in industry. Thus, an efficient and rapid removal of biofilms is becoming increasingly important. With the aid of the kINPen09, a radiofrequency plasma jet (RFPJ) instrument, decisive new findings on the effects of plasma on *C. albicans* biofilms were obtained. This work showed that the inactivation of biofilms takes place mainly on the bottom, which in turn offers new possibilities for the removal of biofilms by other strategies, e.g., mechanical treatment. This result demonstrated that nonthermal atmospheric pressure plasma is well suited for biofilm decontamination.

KEYWORDS antimicrobial, atomic force microscopy, biological decontamination, confocal laser scanning microscopy, fluorescence microscopy, inactivation, viability, cell viability

Candida albicans is one of the most common pathogens causing mycosis worldwide. It is the eponym of the *Candida* group, which is a yeast genus that can cause fungal infections in humans and animals. *C. albicans* is an imperfect fungus that multiplies by budding (1). Typically, *C. albicans* cells bind to biogenic or abiotic surfaces and grow as three-dimensional (3D) structures, also designated biofilms (2). Especially foodborne pathogens and spoilage microorganisms like *C. albicans* prefer biofilm formation on stainless steel, aluminum, glass, polytetrafluoroethylene (PTFE) seals and polyamide (PA) materials, which are typically found in food-processing environments (3–5). The fungus can form mono- or multispecies biofilms, which can be considered densely

Received 15 May 2018 Accepted 15 August 2018

Accepted manuscript posted online 24 August 2018

Citation Handorf O, Weihe T, Bekeschus S, Graf AC, Schnabel U, Riedel K, Ehlbeck J. 2018.

Nonthermal plasma jet treatment negatively affects the viability and structure of *Candida albicans* SC5314 biofilms. *Appl Environ Microbiol* 84:e01163-18. <https://doi.org/10.1128/AEM.01163-18>.

Editor Janet L. Schottel, University of Minnesota

Copyright © 2018 American Society for Microbiology. All Rights Reserved.

Address correspondence to O. Handorf, oliver.handorf@inp-greifswald.de.

packed cellular communities embedded in an extracellular matrix (6). These biofilm communities are known to be more resistant to physical and chemical stresses than planktonic cells and can cause major economic loss within industrial sectors (7). Moreover, more than 4 million people in Germany suffer from chronic wounds, which are often caused by resistant biofilm-forming pathogens (8). The treatment costs for these patients amount to up to 4 billion euros per year in Germany alone (9). Catheter-related bloodstream infections (CRBSI), caused by biofilms and their direct access to the bloodstream, are a big problem in the United States. Several studies counted 80,000 CRBSI each year in the United States, leading to costs between \$4,888 and \$11,591 for each CRBSI event. These facts demonstrate the need for successful treatment of biofilms in medicine.

Candida sp. is responsible for two types of infections: superficial infections like oral and vaginal candidiasis and systemic infections (10, 11). In about 75% of the world's population, *C. albicans* appears in the oral cavity and is the fourth most common cause of hospital-acquired systemic infections in the United States, with up to 50% mortality (12–15). Due to the increased life span of today's population, there is also an increase in the number of patients who wear dental prostheses, which leads to a concomitant increase in *Candida* stomatitis (16–18). Dental diseases like periodontitis, gingivitis, caries, oral candidiasis, or periimplantitis are relevant diseases for people of all ages. Depending on the oral food intake, the oral cavity is constantly exposed to a high level of microbial contamination induced by the assimilated food (19). Thus, the germ load of the oral cavity is much higher than for other parts of the human body. Lesions in the oral cavity often lead to diseases such as oral submucous fibrosis or stomatitis (20) and therefore play an important role as a symptom for immunodeficiency. During the infection process, colonization factors such as adhesins, invasins, and hyphae and their thigmotropic properties are of major importance (21). Together with *Staphylococcus aureus*, *C. albicans* has a much higher incidence of 11 to 65% for a stomatitis than in a monospecies biofilm (22). At present, the conventional treatment method for biofilms consists of antibiotics. Biofilms have a higher resistance to antimicrobial agents and a higher physicochemical tolerance than do planktonic cells (23, 24). These resistances are mainly due to complex interactions of the cells in the biofilm and the surrounding extracellular matrix (6, 25–27).

In 243 episodes of candidemia, 45 (19%) had reduced susceptibility and 27 of them were fully resistant to fluconazole, the main antifungal agent for candidemia treatment. Despite 8% of *C. albicans*, 4% of *C. tropicalis*, and 4% of *C. parapsilosis* isolates having reduced susceptibility to fluconazole, these species embrace 36% of the reduced-susceptibility group and 48% of the fully resistant group (28). Thus, there is a much higher probability for fully resistant *C. albicans* strains than for strains with reduced susceptibility. Antimicrobial resistance will be of increasing interest to society, as it is associated with rising mortality rates and higher medical costs (29). Therefore, alternatives to conventional antibiotic therapies are urgently needed.

An innovative technology addressing these problems is nonthermal atmospheric pressure plasma (NTP). With moderate temperatures, NTPs avoid thermal host tissue damage but have in fact much higher antimicrobial effects than, e.g., UV or hydrogen peroxide treatments (30, 31). In addition, NTPs are very effective against antibiotic-resistant pathogens and there are no antimicrobial resistance mechanisms against plasma known to date (32–34). Therefore, NTPs could be used for the decontamination of dental cavities and a wide range of other applications and devices in industry and medicine (35).

A basic understanding of the mechanistic effects of plasma on prokaryotic and eukaryotic biofilms is a prerequisite for its application. Consequently, this work investigated the inactivation effects of plasma on *C. albicans* biofilms. For this purpose, biofilm viability, vitality, and metabolism were examined after plasma treatment. The impact of plasma treatment on the three-dimensional biofilm structures was examined by employing epifluorescence and confocal laser scanning microscopy (CLSM); moreover, cell morphological changes were detected with atomic force microscopy (AFM).

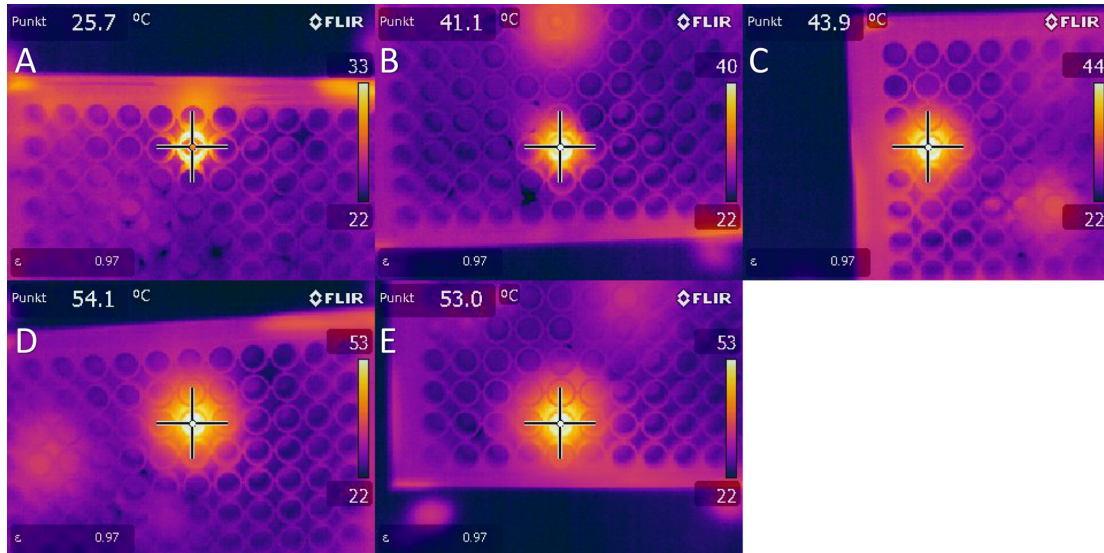


FIG 1 Thermal image measurements of biofilms taken directly after plasma treatment. Images were taken at a distance of 20 cm with an FLIR thermal imaging camera at plasma treatment times of 30 s (A), 60 s (B), 120 s (C), 180 s (D), and 300 s (E).

RESULTS

The antimicrobial effect of plasma components on biofilm cells might be caused by different mechanisms. To unravel the exact mode of action of the plasma treatment, its effect on *C. albicans* biofilms was monitored using CFU counting to investigate the proliferation of the surviving cells (36), vitality assays with fluorescence Live/Dead staining, and a metabolism assay using the 2,3-bis-(2-methoxy-4-nitro-5-sulphophenyl)-2H-tetrazolium-5-carboxanilide salt (XTT) assay. In order to exclude negative effects on the biofilms due to increased temperature, thermal imaging measurements were carried out.

Effects of temperature generated by plasma treatment on biofilm cells. Five different treatment times were measured directly after plasma treatment with regard to the temperatures reached in the biofilm. Temperatures in the range of 25 to 55°C were measured for the selected plasma treatment times (Fig. 1). Because the temperatures were above 37°C, we further analyzed the effect of temperature on the biofilm cells. For this, a 96-well plate with *C. albicans* biofilms was heated on a plate heater for 60 s at 130°C. A temperature of 74.2°C was reached after this treatment (Fig. 2). We used these biofilms for further analysis with the aid of CFU, fluorescence, and XTT assays to exclude temperature effects in a broader spectrum than we were able to measure at the radiofrequency plasma jet (RFPJ) treatment. The results of the CFU, fluorescence, and XTT measurements of the untreated biofilms were compared with those of the heated biofilms (Fig. 3). We detected a decrease in the RF of 0.5 in the median (Fig. 3A) and a reduction of the absorption of 0.7, which represented a reduction of 24% compared to the untreated biofilms (Fig. 3C). In the Live/Dead assay, no influence of the temperature was detected (Fig. 3B). In addition, fluorescence microscopic images of the heated biofilms were taken to exclude effects of temperature on the biofilms (Fig. 4).

Effects of plasma treatment on the proliferation ability of biofilm cells. Five different treatment times between 30 and 300 s were selected, which should demonstrate the dynamic range of the plasma effect. Six biofilms were treated with plasma for the respective times in 4-fold repetitions (Fig. 5). The effect of plasma treatment on the biofilm CFU is displayed as reduction factor (RF). After 60 s of plasma treatment time,

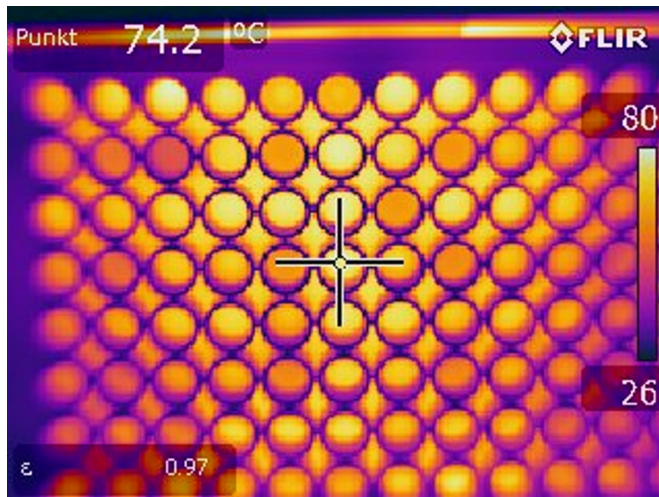


FIG 2 Thermal image measurements of biofilms taken directly after heating. Images were taken at a distance of 20 cm with an FLIR thermal imaging camera. Biofilms were heated 1 min at 130°C on a plate heater.

a significant increase in the RF was detected. The RF reached a maximum of 2.0 after 300 s of plasma treatment. The orange line in Fig. 5 represents the detection limit in the range of which we could detect the CFU.

Effects of plasma treatment on the biofilm vitality. The Live/Dead BacLight assay kit (Thermo Scientific, Waltham, MA, USA) contains the DNA intercalating dyes SYTO9, staining living cells of the biofilm, and propidium iodide, which is membrane impermeable and reduces SYTO9 in cells with damaged cell membranes. After 30 s of plasma treatment, a decrease in the green fluorescence intensity to red fluorescence intensity ratio (G/R) of 0.97 was detected, which corresponded to a 39% reduction compared to the untreated reference biofilms (Fig. 6). After 60 s of plasma treatment, a maximum decrease of 1.78 in G/R was observed, which corresponded to a 71.08% reduction. There was no significant change in the G/R ratio after longer treatment times (Fig. 6). Thus, significant changes in the vitality of the biofilm took place only in the first 60 s of plasma treatment.

Effect of plasma treatment on the metabolism of the cells. Due to the fact that the CFU and the Live/Dead fluorescence showed antimicrobial effects after plasma treatment, the metabolism of cells was investigated as a third indicator of inactivation. For this, the XTT assay was used. The metabolic activity based on XTT quantification assay was reduced by 41% at 30 s and by 89% at 60 s (Fig. 7). Longer treatment time did not further reduce cell metabolic activity.

Confirmation of plasma treatment effects by fluorescence microscopy. The Live/Dead BacLight staining was also used for an epifluorescent inspection of plasma-treated *C. albicans* biofilms cultivated in 96-well plates. Bottom view images of the biofilms revealed that 30 s of treatment affected mainly the area of the biofilm that was in the direct range of the plasma effluent (Fig. 8B). This area showed orange/yellow staining, representing dead cells, which was not observed in the untreated control biofilms. With increasing treatment time, the effect could be observed throughout the well (Fig. 8C to F). After 120 s of treatment time, living cells were visible in the center of the biofilm (Fig. 8D). More living cells became visible with longer treatment times. However, this effect did not occur after every plasma treatment, but it was included for a complete display of the results.

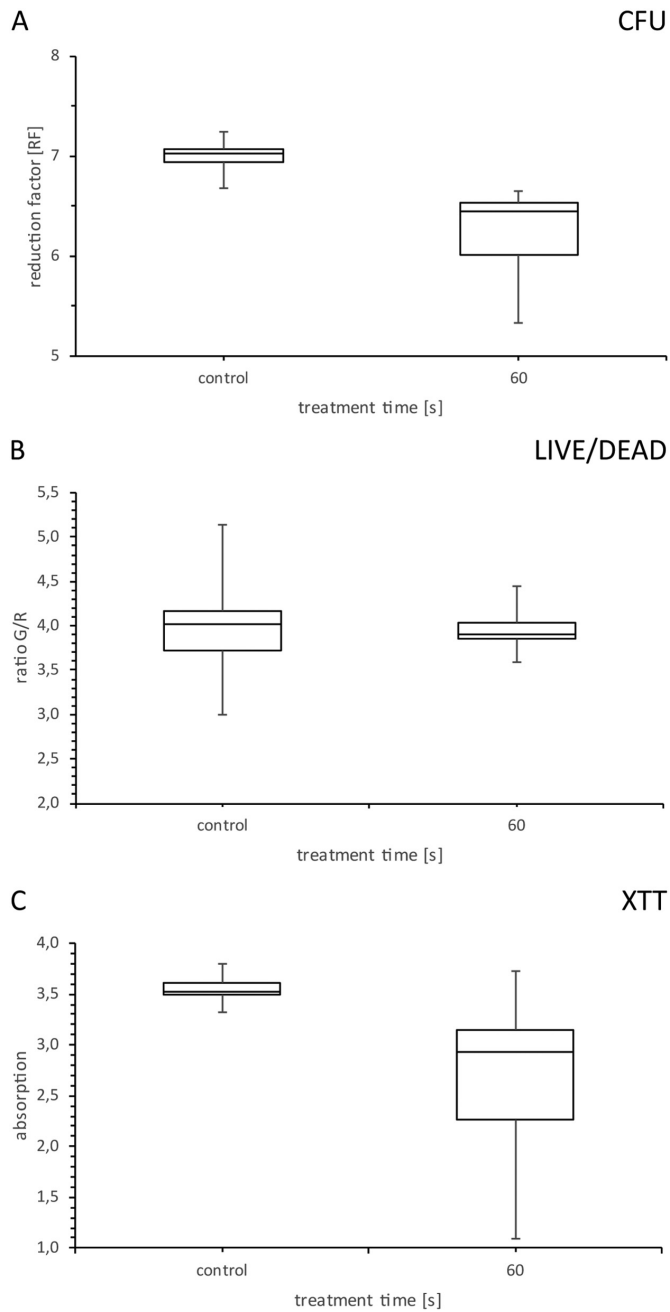


FIG 3 Box and whisker plots of CFU, fluorescence, and XTT measurements of biofilms heated on a plate heater. *Candida albicans* biofilms were heated 1 min at 130°C on a plate heater and used for CFU (A), fluorescence (B), and XTT (C) assays. Biofilms were compared to untreated control biofilms. $n = 15$.

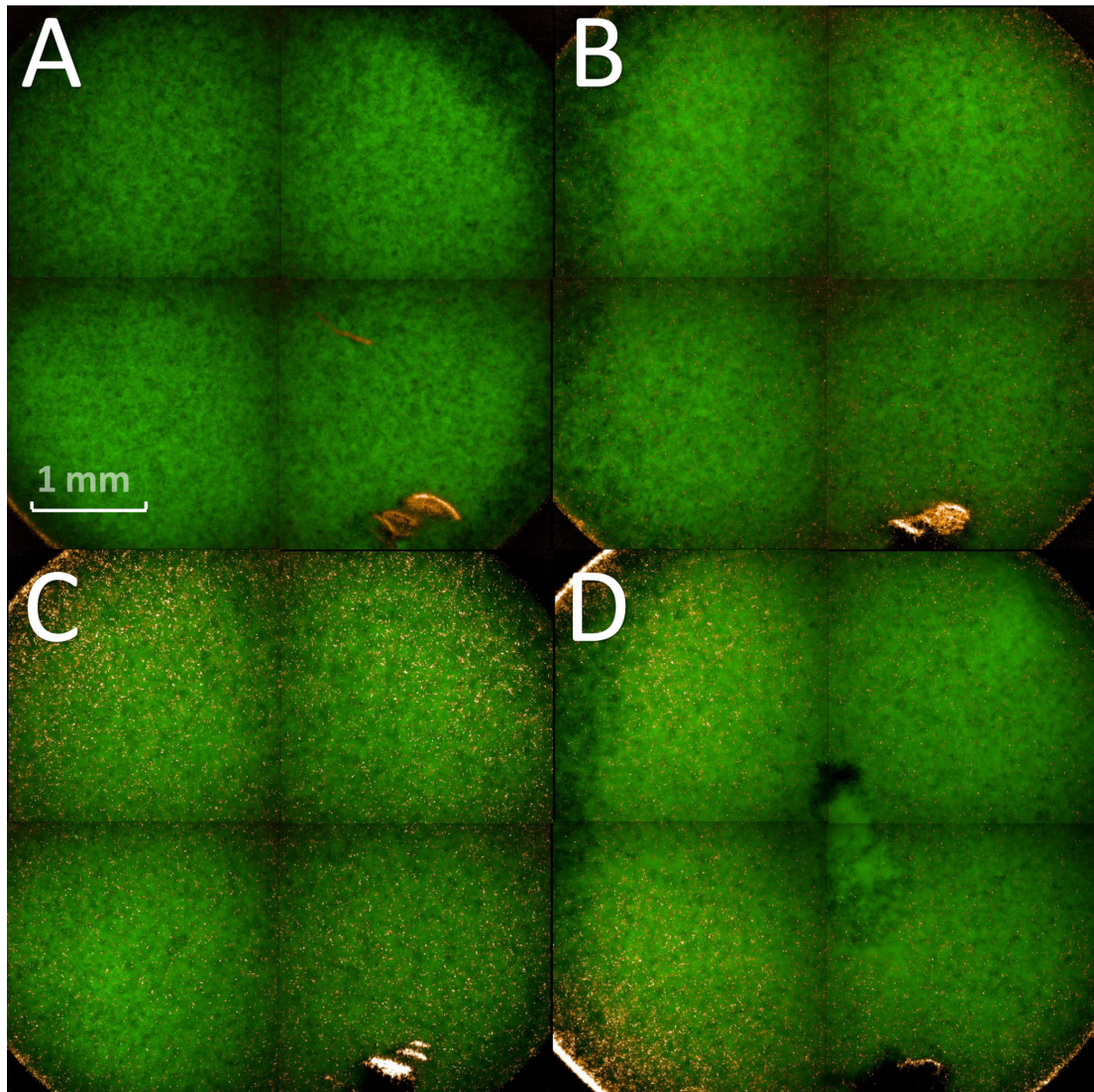


FIG 4 Fluorescence microscopy of *Candida albicans* biofilms after heating on a plate heater. Biofilms were heated 1 min at 130°C on a plate heater. Shown are four different biofilms from different locations of the 96-well plate after heating on a plate heater. Green, living cells; red (orange), dead cells.

CLSM confirmed cell inactivation being most dominant on the bottom of the biofilms. Using CLSM, 5.5- μm sections of the treated biofilms were acquired and displayed in orthogonal and 3D views (Fig. 9). All plasma treatments caused an enhanced propidium iodide staining indicating cell death compared to the reference (Fig. 9, orthogonal view). After 30 s, plasma treatment affected mostly the cells located at the bottom of the biofilm, indicated by a strong propidium iodide staining, whereas the top of the biofilm appeared to be less affected (Fig. 9, 3D view).

AFM confirmed alterations in the cell morphology of the biofilm after plasma treatment. AFM is often used to investigate cell morphological alterations in the micrometer range. The AFM images of an untreated biofilm and plasma-treated bio-

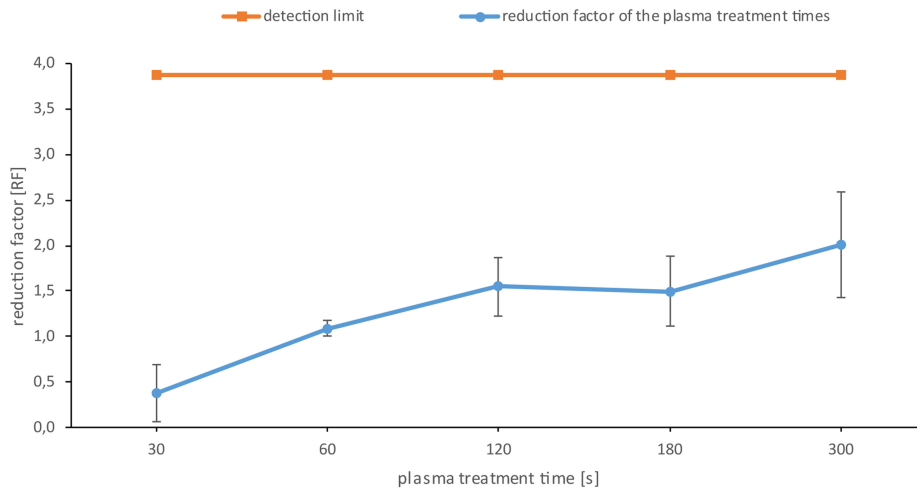


FIG 5 CFU assay of the *Candida albicans* biofilms after plasma treatment. The orange line represents the detection limit up to which representative values could be counted. The blue line shows the reduction factor (RF) of the different plasma treatment times. The error bars were calculated using the propagation of error and weighted error for the controls and the weighted mean value for the samples. The data points are the weighted mean values for the total population of the quadruple repetition. $n = 6$ for each repetition. $P < 0.05$.

films for different time periods are shown in Fig. 10. Each image was taken as a topographic image on the left and as an error signal image on the right. In order to detect the alterations caused by the plasma treatment clearly, the average treatment time and the maximum treatment time were examined and recorded. They indicate major changes in the cell morphology even after 120 s of treatment time (Fig. 10). Membrane disruptions and the loss of intracellular fluid could be detected. In contrast, the cells of the untreated biofilm appeared to be vital and without visible damage.

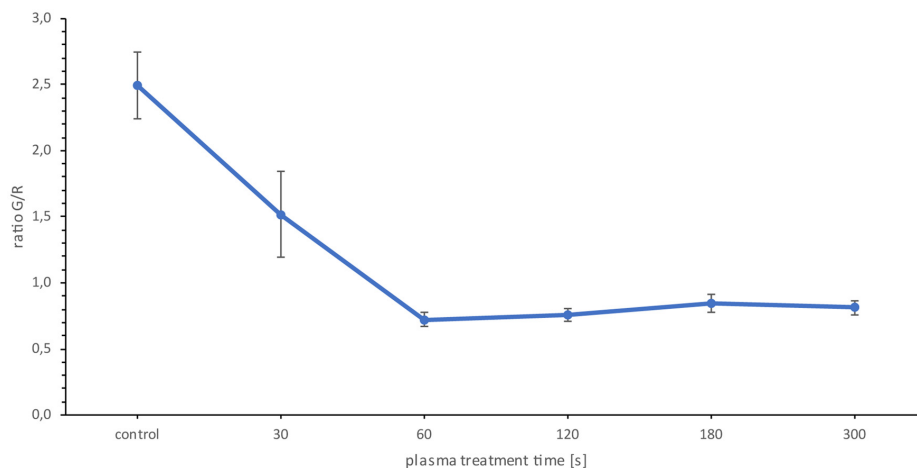


FIG 6 Fluorescence assay of *Candida albicans* biofilms. The G/R ratio is the quotient of green fluorescence intensity and red fluorescence intensity. The data points are the mean values for the total population of the quadruple repetition. $n = 6$ for each repetition. $P < 0.05$.

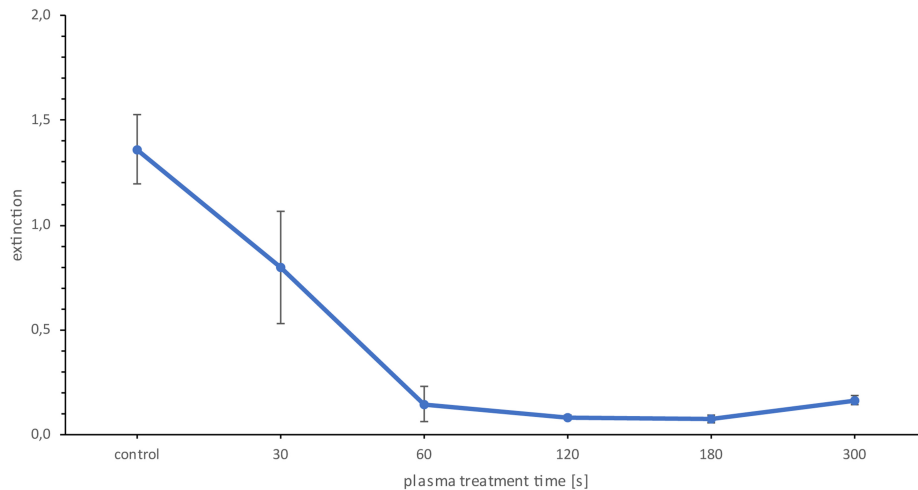


FIG 7 XTT assay of *Candida albicans* biofilms. The data points are the mean values for the total population of the quadruple repetition. $n = 6$ for each repetition. $P < 0.05$.

DISCUSSION

Since the invention of nonthermal plasma sources operating at atmospheric pressure, a large number of studies dealing with the effects of plasma itself (direct mode) and its effluents (indirect mode) on pathogens or living tissue have been published (37–41). However, much less is known about the treatment of living biofilms with nonthermal plasma sources. Koban et al. treated 48-h-old *C. albicans* biofilms on titanium discs with different plasma sources and were able to detect an RF of 0.5 after 300 s of treatment with the RFPJ at a distance of 0.7 mm with an argon gas flow of 5

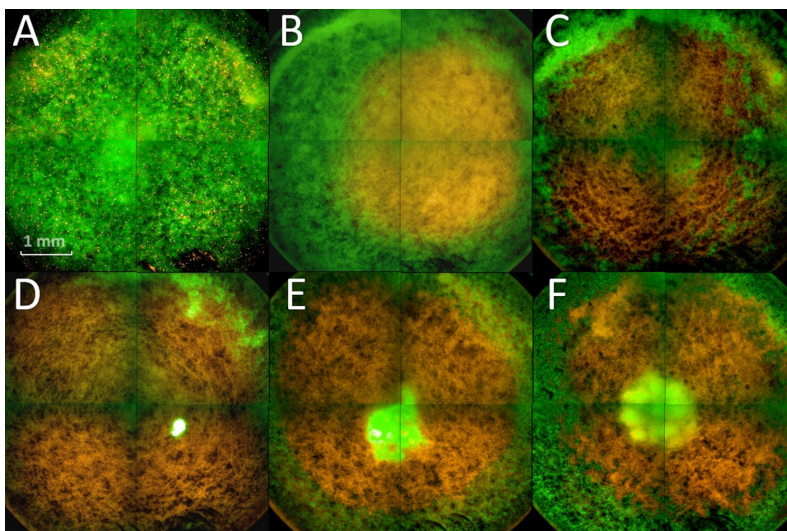


FIG 8 Fluorescence microscopy of plasma-treated biofilms. (A) Control; (B to F) plasma treatment for 30 s (B), 60 s (C), 120 s (D), 180 s (E), and 300 s (F). The biofilms were stained with SYTO9, showing green fluorescence (living cells), and propidium iodide, showing red fluorescence (dead cells).

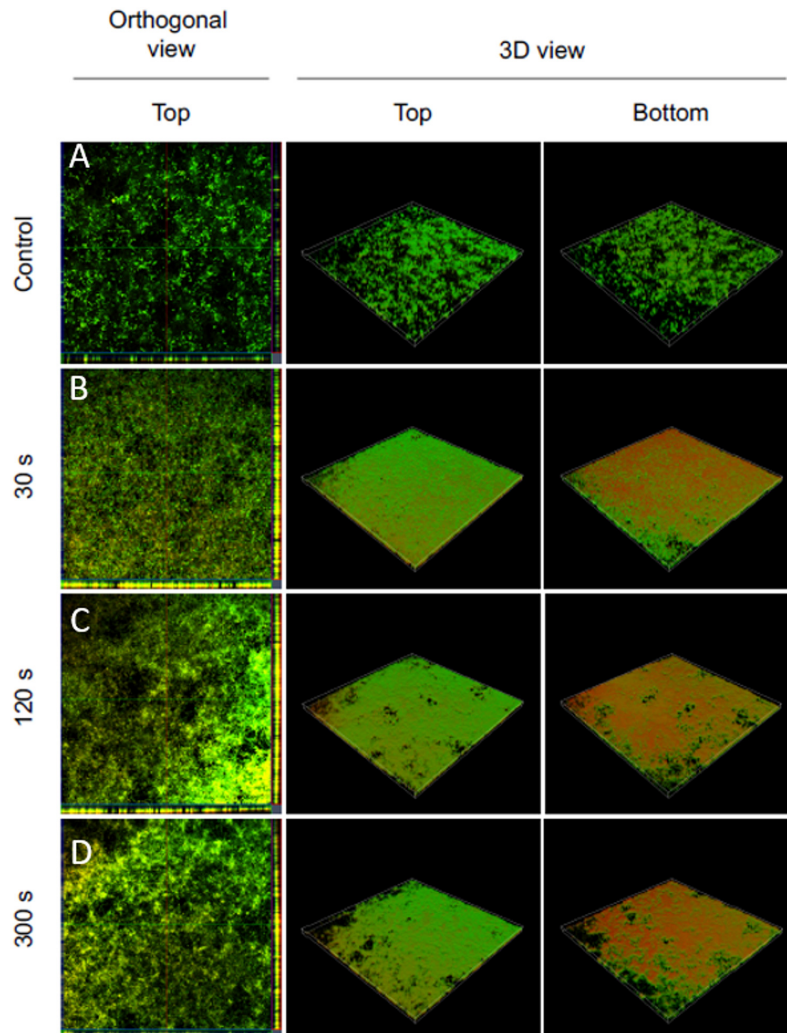


FIG 9 Confocal laser scanning microscopy of Live/Dead-stained *Candida albicans* biofilms after plasma treatment. Left panels show an orthogonal view of the top biofilm layer (horizontal optical sections in the center and vertical optical sections in the flanking pictures). Central and right panels show 3D images with top and bottom views of the biofilms. For each biofilm, an area of $1,272.2 \mu\text{m}$ by $1,272.2 \mu\text{m}$ was visualized.

standard liters per minute (slm) (42). Gorynia et al. used the same experimental setup at a distance of 10 mm for 72-h-grown *Streptococcus sanguinis* biofilms on titanium discs and could also demonstrate an RF of 0.58 after 180 s of plasma treatment (43). In contrast to these results, we obtained an RF of 1.1 after just 60 s of plasma treatment. Although the same plasma source was used, the experimental setups were different. It is therefore difficult to compare our values with those from the studies previously mentioned. In our study, e.g., no titanium discs were used for cultivation, but *C. albicans* was grown directly on coated 96-well plates. Furthermore, a distance of 18 mm from the nozzle to the biofilm was selected. Despite the greater distance, we were able to detect a temperature of 54°C directly in the biofilm after 180 s of plasma treatment with the RFPJ in the same experimental setup. However, our results indicated that the

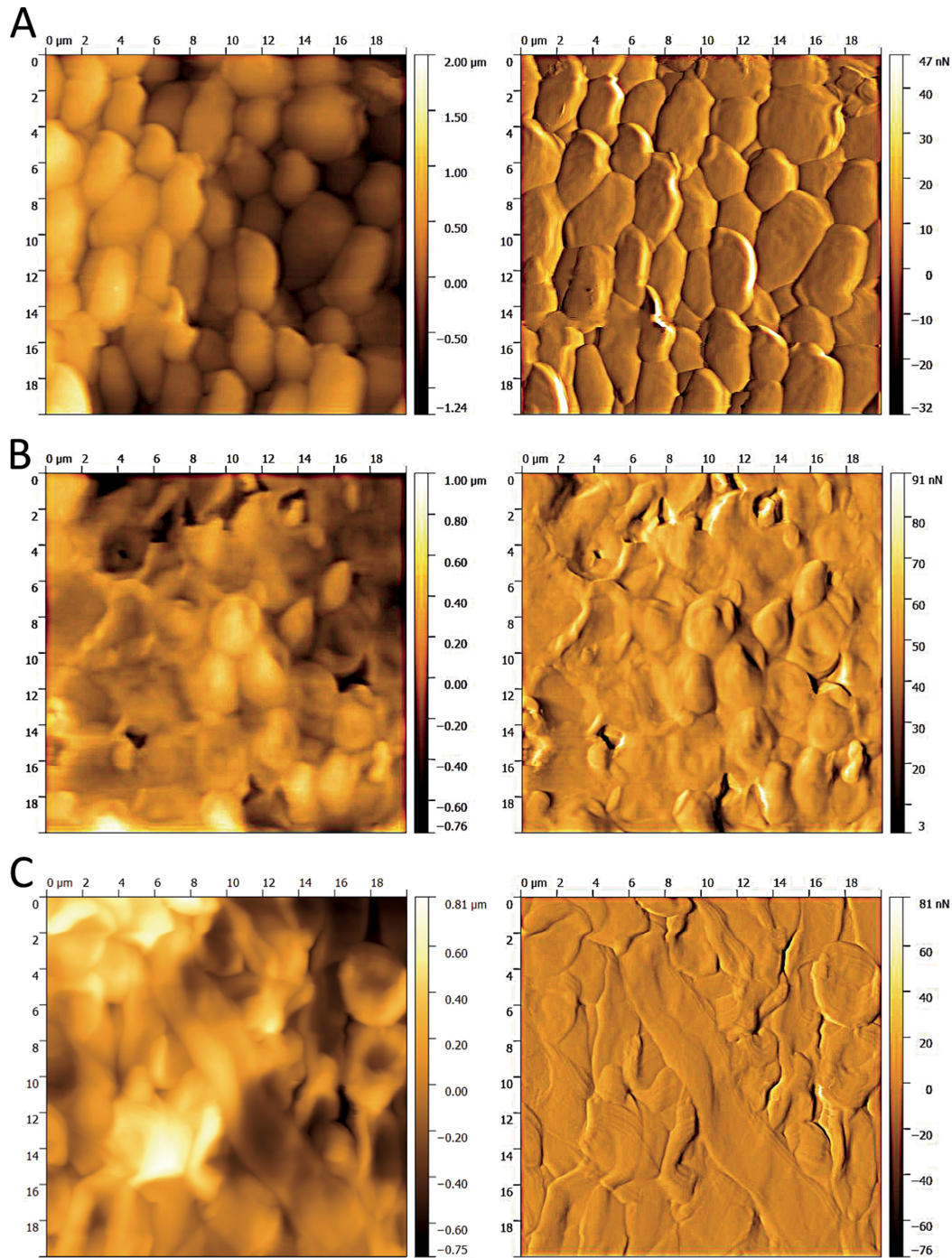


FIG 10 Atomic-force microscopy images of the plasma-treated biofilms. The left panels show topographical images from the top of the biofilm layer, and the right panels show error signal images of the same section. (A) Control; (B and C) plasma treatment times of 120 s (B) and 300 s (C). The images were taken in contact mode with a cantilever spring constant (k) of 0.1 to 0.6 N/m² and a frequency of 0.4 Hz, the set point at 8 N/m², and an area of 20 μm².

increased temperature has no significant influence on the biofilms (Fig. 3 and 4). Moravsky et al. treated *C. albicans* with a radiofrequency plasma jet and were able to achieve a reduction of 65.2% after 30 s of plasma treatment and up to 99.6% after 60 s of plasma treatment using the XTT assay (44). These results show that the efficiency of our plasma treatment of eukaryotic pathogens is comparable to those reported in other publications. The inactivation of the cells after plasma treatment was proven by different experimental approaches. Counting of CFUs was used to test the proliferation ability of treated cells, fluorescence Live/Dead assay was employed to monitor the vitality of the cells, and an XTT assay was used to investigate the plasma effect on cellular metabolism. Using these three complementary methods ensured that the inactivation of the biofilms by the plasma treatment was indeed reliable (45).

Recent studies dealing with the treatment of *C. albicans* biofilms with RFPJ demonstrated an inactivation of cells exclusively in the area of plasma effluents. However, most of these studies did not investigate the three-dimensional inactivation effects within the biofilm. Pei et al. reported the inactivation of a 25.5- μm -thick biofilm of *Enterococcus faecalis* after treatment with a handheld air plasma jet (46). Here, the authors demonstrated a complete inactivation of the whole biofilm after 300 s of treatment. Delben et al. also showed an influence of plasma treatment with an atmospheric pressure plasma jet (APPJ) on three-dimensional biofilms of *C. albicans* (47). However, both of these studies used a different plasma source and a generally different experimental setup. It is well known that the biofilm thickness, the microorganism, the treatment conditions, and the gas used play a predominant role in microbial inactivation.

Even though a whole series of publications reported the ability to microscopically detect the inactivation of biofilms using plasma treatments, we are not aware of any work that has shown that primarily the bottom of the biofilm was affected by the plasma treatment. This new insight naturally raises the question of how this kind of inactivation was done.

Wilking et al. were able to detect water channels in *Bacillus subtilis* biofilms for the transport of fluids in biofilms (48). For this, they used an aqueous solution containing a mixture of fluorescent beads to visualize the connectivity of the channels. Interestingly, they were able to detect a dense network of channels in the center of the biofilm, which reached to the surface of the biofilm, extended downwards, and spread over the entire biofilm. Another important aspect of their work was the microscopic proof of the water channel structure. These channels use the surface to which the cells of the biofilm have adhered to form their bottom structure. There is a range of other studies that also detected such water channels in bacterial biofilms (49–51). If such water channels exist in *C. albicans* biofilms, this could explain the results obtained in our work. Due to these structures and the expulsion rates of the gases through the plasma effluent, it can be assumed that the reactive oxygen species (ROS) will accumulate in the lower part of the biofilm. In addition, deposits of the liquids contained in the lower part of the biofilm are more likely to occur, in which the reactive species dissolve and then have a permanent effect on the cells of the lower part of the biofilm. Because the reactive species react very quickly, the short reaction times with the upper cell layers of the biofilm are probably sufficient to trigger visible inactivation effects.

Pure argon gas (Linde, Pullach, Germany) has a purity of 99.9%. Nevertheless, secondary components of ≤ 5 mol fractions N_2 and ≤ 2 mol fractions O_2 are present in the gas. However, the most important components were the species of ambient air that reacts with the components of the effluent. The energy generated by the RFPJ breaks up the oxygen bonds mainly, in contrast to the triple bonds of the nitrogen components. Shield gas experiments have shown that ambient air can account for up to 15% of the active species of plasma treatment (52). Stewart determined diffusion times of different gases in biofilms (53). Based on those results, a diffusion time of 4.47 s for nitrogen, representing all light gases, could be calculated for the *C. albicans* biofilms investigated here. These results offered plausible explanations for the effects that were observed in fluorescence microscopy. Another effect that became apparent in fluorescence micros-

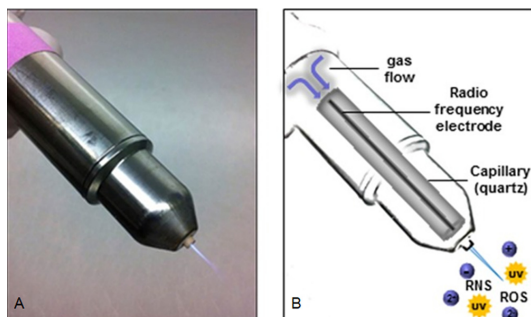


FIG 11 Radiofrequency plasma jet (RFPJ) instrument kINPen09 (Neoplas GmbH; Greifswald, Germany). (A) Photograph of RFPJ; (B) schematic structure of the RFPJ and composition of the physical plasma. (Reprinted from reference 58 with permission.)

copy was a central spot of living cells, which were visible in the 120-s plasma-treated biofilms. Desiccation effects, caused by the plasma, might cause this phenomenon. Reduced layer thicknesses of the biofilm in the direct treatment area of the plasma effluent were excluded by the 3D models of the CLSM for this phenomenon. Dead cells on the bottom of the biofilm have disrupted membranes (Fig. 10). As the intracellular fluid escapes, cells might have lost their integrity and detached from the biofilm structure. Due to the dehydration, disruptions and dissolutions in the actin filament may occur (54). As a result, the biofilm structure partially dispersed and the next layer of living cells became visible. This occurred primarily in the center of the biofilm, since the plasma nozzle was placed directly over the center of the biofilm during treatment. However, this observation was not made for every plasma treatment, but it was added for the completeness of the results.

Conclusion. Microbial biofilms are an important and costly problem, not only in medicine, but also in industrial applications. Thus, an efficient and rapid removal of biofilms is becoming increasingly important. This work provides new insights into the successful inactivation of *C. albicans* biofilms by plasma using kINPen09 (see Materials and Methods). Notably, this study provides evidences that the employed plasma treatment caused a primary inactivation of cells located at the basement of the biofilm, which at the same time facilitates the removal of biofilms by other strategies, e.g., mechanical treatment. This novel insight into plasma inactivation of biofilms indicates that plasma is well suited to fight biofilms growing on various surfaces, since surface detachment of biofilms is an important prerequisite for an effective removal of biofilms, especially in industrial settings.

MATERIALS AND METHODS

Fungal strain and growth conditions. A fungus strain with primarily vertical biofilm growth named *Candida albicans* SC5314 (ATCC MYA-2876) was used. The fungus was grown on Sabouraud agar and incubated 24 h at 37°C. A suspension of the fungus in phosphate-buffered saline (PBS; pH 7.2, according to Sørensen) was adjusted to an optical density (OD) at 520 nm of 0.375. One milliliter of this suspension was added to 9 ml RPMI medium (without bicarbonate; Merck, Darmstadt, Germany), which served as an inoculum for biofilm cultivation in microtiter plates. For plasma treatment, a coated Polystyrol 96-well plate (Sarstedt, Nümbrecht, Germany) was used. As an exception, a 12-well plate was used for the AFM. Two hundred microliters of the suspension was pipetted per well and incubated 90 min at 37°C and 80 rpm on a rotary shaker to allow cell attachment. After incubation, the medium was removed, the well was washed with 200 μ l PBS (pH 7.2 according to Sørensen), and 200 μ l RPMI medium was added. The plate was incubated 24 h at 37°C and 80 rpm on a rotary shaker, resulting in well-established *C. albicans* biofilms for further analysis. This protocol was kindly provided by the research group of Christiane Yumi Koga-Ito, Institute of Science and Technology—UNESP, Department of Oral Sciences and Diagnosis.

Plasma source. kINPen09 (neoplas GmbH; Greifswald, Germany), a commercial APPJ, was used for plasma treatment. Using a direct current (DC) power supply (system energy, 8 W at 220 V, 50/60 Hz) and 99.999% argon gas connection (Linde, Pullach, Germany) with 5 slm, plasma was generated under atmospheric pressure. The inside of the APPJ handpiece consists of a 1.6-mm-diameter quartz capillary with an embedded electrode of 1-mm diameter (Fig. 11). When the APPJ was in operation, a high-

frequency voltage of 1.1 MHz, 2 to 6 kVpp, was applied to the electrode. This generated the plasma at the tip of the electrode and expelled it into the surrounding medium, forming an effluent (55).

Plasma treatment of *C. albicans* SC5314 biofilms. Established biofilms were washed with PBS (pH 7.2 according to Sørensen), followed by complete removal of the liquid. Five different time intervals were used at a distance of 18 mm from the plasma effluent tip to the biofilm surface using a computer-controlled XYZ table (CNC Maschinenbau; Geldern, Germany), to which the plasma source was attached. Only one sample group was treated per time point to avoid dehydration effects of the biofilms. For CFU counting, fluorescence Live/Dead assays, and XTT assays, 200 μ l PBS (pH 7.2 according to Sørensen) was added per well, the biofilms were mechanically disrupted, and the resulting cell suspension was collected. This step was repeated three times, until the complete biofilm was transferred.

Analytical determinations. First, the effect of temperature on the biofilms was investigated. Therefore, biofilms were plasma treated and thermal images were taken directly after the treatment with a FLIR thermal imaging camera (FLIR Systems; Frankfurt am Main, Germany) at a distance of 20 cm. To determine the influence of the temperatures reached in the biofilms, they were grown in 96-well plates and incubated for 60 s at 130°C on a heating plate until the desired temperature could be detected at a distance of 20 cm using the FLIR thermal imaging camera. The biofilms were then examined by fluorescence microscopy using the Operetta CLS and further analyzed using CFU, fluorescence, and XTT assays. The CFU assay was used to determine the proliferation rate of the *C. albicans* biofilms after plasma treatment. Serial dilution of the samples was done by diluting the sample solution after plasma treatment 1:10 with maximum recovery diluent (MRD; 0.85% NaCl, 1% Trypton). The references were finally diluted 1:10,000 and the samples 1:1,000. Each dilution step was plated on Sabouraud agar by pipetting 10 μ l per dilution onto the plate, and by means of the tilting technique, the sample was spread out. The plates were then incubated for 24 h at 37°C. The colonies for the respective dilution levels were counted, and the CFU per milliliter values were calculated as follows:

$$\text{CFU/ml} = \frac{10^x}{v} \times \frac{\sum c_y + \sum c_{y+1}}{n_y + 0.1n_{y+1}}$$

where 10^x is the dilution factor for the lowest dilution, v is the volume of diluted cell suspension per plate in milliliters, $\sum c_y$ is the total number of colonies on all (n_y) plates of the lowest evaluated dilution level, 10^{-x} , and $\sum c_{y+1}$ is the total number of colonies on all (n_{y+1}) plates of the next-highest dilution level evaluated, $10^{-(x+1)}$ (56). After calculating the CFU per milliliter, the reduction factor (RF) was determined using the equation $\text{RF} = \text{MV}_{\log_{10}} - \text{MV}_{\log_{10}}$, where $\text{MV}_{\log_{10}}$ represents the mean value of the CFU per milliliter of the reference group and $\text{MV}_{\log_{10}}$ is the mean value of the CFU per milliliter of the treated samples. For the final illustration, the weighted mean value of the total population was used. The propagation of error of the different experimental days was calculated, and the weighted error was calculated from the sum of the propagation of errors and is displayed as error bars in the illustrations (57).

Fluorescence Live/Dead assay. The Live/Dead BacLight bacterial viability kit was prepared by mixing reagents A and B at a ratio of 1:1. After the mixing step, 0.9 μ l of this solution was pipetted to 300 μ l of the sample solution after plasma treatment for each well, followed by incubation for 20 min at room temperature with 80 rpm on a rotary shaker in the dark. In the next step, the 96-well plate was scanned with an excitation wavelength of 470 nm and emission wavelength of 530 nm for green fluorescence and 630 nm for red fluorescence with the Varioskan-Flash device (Thermo Scientific, Waltham, MA, USA). Finally, the G/R ratio was calculated by dividing the fluorescence intensity of the red fluorescence from the fluorescence intensity of the green fluorescence. The experiments were repeated 4 times ($n = 6$).

XTT assay. For the XTT assays, the XTT cell proliferation assay kit (Applichem, St. Louis, MO, USA) was used. The activation solution and the XTT solution were mixed 1:50, and 50 μ l of the mixture was transferred in a 96-well plate containing 100 μ l sample solution after plasma treatment per well. The 96-well plate was incubated for 2 h at 37°C and 80 rpm in the dark. After the incubation time, 96-well plates were scanned at a wavelength of 470 nm using a Varioskan-Flash device. The obtained values were blank corrected. The experiments were repeated 4 times ($n = 6$).

Fluorescence microscopy. Biofilms were cultivated as previously described, using a black 96-well plate with a glass bottom (PerkinElmer, Hamburg, Germany). Plasma-treated biofilms were resuspended in 300 μ l of 0.85% NaCl after treatment to avoid dehydration of the biofilms. The Live/Dead BacLight bacterial viability kit was prepared by mixing reagents A and B in a ratio of 1:1. Next, 0.9 μ l of the fluorescence solution was added to each well and the 96-well plate was incubated at room temperature for 20 min and 80 rpm in the dark. After incubation, the supernatants were removed, and the samples were washed again three times with 0.85% NaCl. Epifluorescence images were acquired using the Operetta CLS high-content imager (PerkinElmer, Hamburg, Germany) with the following objectives (Zeiss, Oberkochen, Germany): 1.25 \times (air, numerical aperture [NA] = 0.03), 5 \times (air, NA = 0.16), 20 \times (air, NA = 0.4), 40 \times (washing, NA = 1.1). Depending on the experiment, several fields of view were recorded and combined in the software. SYTO9 was excited by 475-nm (110-mW) light-emitting diode (LED), and the fluorescence was collected with a 525- \pm 25-nm band pass filter. Propidium iodide was excited by a 550-nm (170-mW) LED, and fluorescence was collected with a 610- \pm 40-nm band pass filter. A laser autofocus (785 nm) was available for all measurements. The images were displayed using Harmony 4.6 software.

CLSM. Biofilms were cultivated, plasma treated, and Live/Dead stained as described above. After the staining and washing procedure, the supernatants were removed and the biofilms were analyzed using a Zeiss LSM 510 microscope (Carl Zeiss, Jena, Germany) equipped with a 10 \times objective (air, NA = 0.1). Filter and detector settings for monitoring SYTO9 and propidium iodide fluorescence (excitation at 488

nm using an argon laser, emission light of SYTO9 selected with a 505- to 530-nm bandpass filter, emission light of propidium iodide selected with a 650-nm longpass filter). Three-dimensional images were acquired using the ZEN 2009 software (Carl Zeiss, Jena, Germany) with an area of 1,272.2 μm by 1,272.2 μm and z-stack sections of 5.5 μm .

Atomic force microscopy. For better adhesion of the coverslips (13 mm; Sarstedt, Nümbrecht, Germany) to the surface of the well plates and to avoid growth of the fungus at the bottom of the coverslips, 50 ml Gelrite (Duchefa, Haarlem, Netherlands) was autoclaved and directly used after the autoclaving process due to a rapid thermal curing process. A volume of 200 μl liquid Gelrite was pipetted to each well of a 12-well plate. The coverslips were placed at the surface of the liquid Gelrite and were thermally cured. The biofilms were cultivated as described above, and 1 ml of the RPMI medium was pipetted to each well until the coverslips were topped with the medium. Twelve-well plates were incubated at 37°C and 80 rpm for 1 h. After the incubation time, additional washing steps with 1 ml of 0.85% NaCl in each well were performed. Twenty-four hours later, the cultivation medium was removed and the biofilm-overgrown coverslips were washed with 1 ml 0.85% NaCl again. After washing, samples were treated for 120 s and 300 s by the RFPJ plasma effluent. Dehydration of the coverslips before AFM analysis was avoided by using a humidity chamber. The AFM measurements were carried out on a DI CP II SPM (Veeco, Plainview, NY, USA), which was mounted on a vibration-free object table (TS-150; Table Stable, Zwillikon, Switzerland). The setup was standing on an optical bench encased by an additional acoustic protection. The AFM was equipped with a linearized piezo scanner, on which the coverslips were mounted on a metal sample holder with leading tabs. The samples were measured using cantilevers with nominal spring constants ($k = 0.1$ to 0.6 N m^{-2}) in contact mode. The pictures were taken by a scanning speed of 0.4 Hz by a picture size of $20 \mu\text{m}^2$ and a set point of 8 N m^{-2} . Pictures were edited with Gwyddion (Czech Metrology Institute, Brno, Czech Republic).

ACKNOWLEDGMENTS

This work was supported by the Leibniz Institute for Plasma Science and Technology, INP, in Greifswald, Germany, and the DFG-TRR34 (A3 subproject granted to Katharina Riedel). Fluorescence microscopy was supported by the group of Sander Bekeschus within the project "Zentrum für Innovationskompetenz plasmatis, Nachwuchsgruppe: Plasma-Redox-Effekte," which was financially supported by the German Federal Ministry of Education and Research (BMBF).

REFERENCES

- Nguyen Q, Tudisco F, Gautier A, Hein M. 2017. An efficient multilinear optimization framework for hypergraph matching. *IEEE Trans Pattern Analysis Machine Intelligence* 39:1054–1075. <https://doi.org/10.1109/TPAMI.2016.2574706>.
- Serra E, Hidalgo-Bastida LA, Verran J, Williams D, Malic S. 2017. Antifungal activity of commercial essential oils and biocides against *Candida albicans*. *Pathogens* 7:15. <https://doi.org/10.3390/pathogens7010015>.
- Herald PJ, Zottola EA. 1988. Attachment of *Listeria monocytogenes* to stainless-steel surfaces at various temperatures and pH values. *J Food Sci* 53:1549–1562. <https://doi.org/10.1111/j.1365-2621.1988.tb09321.x>.
- Mafu AA, Roy D, Goulet J, Magny P. 1990. Attachment of *Listeria monocytogenes* to stainless-steel, glass, polypropylene, and rubber surfaces after short contact times. *J Food Prot* 53:742–746. <https://doi.org/10.4315/0362-028X-53.9.742>.
- Notermans S, Dormans JAMA, Mead GC. 1991. Contribution of surface attachment to the establishment of micro-organisms in food processing plants: a review. *J Bioadhesion Biofilm Res* 5:21–36. <https://doi.org/10.1080/08927019109378226>.
- Steenackers HP, Parijs I, Foster KR, Vanderleyden J. 2016. Experimental evolution in biofilm populations. *FEMS Microbiol Rev* 40:373–397. <https://doi.org/10.1093/femsre/fuw002>.
- Davies D. 2003. Understanding biofilm resistance to antibacterial agents. *Nat Rev Drug Discov* 2:114–122. <https://doi.org/10.1038/nrd1008>.
- Debus ES, Winkler MS, Larena-Avellaneda A, Bültemann A, Daum H, Lingenfelder M, Schulenburg B, Gross-Fengels W. 2003. Medizinische und ökonomische Aspekte der Zentrumsbildung in der Wundbehandlung. *Gefäßchirurgie* 8:259–268.
- Lauterbach S. 2006. Chronische Wunden - Ulcus cruris, diabetisches Fußsyndrom, Dekubitus, Verbrennungen. *PZ Prisma* 2:239.
- Calderone RA, Clancy C. 2012. *Candida and candidiasis*, 2nd ed. ASM Press, Washington, DC.
- Mayer FL, Wilson D, Hube B. 2013. *Candida albicans* pathogenicity mechanisms. *Virulence* 4:119–128. <https://doi.org/10.4161/viru.22913>.
- Pfaller MA, Diekema DJ. 2007. Epidemiology of invasive candidiasis: a persistent public health problem. *Clin Microbiol Rev* 20:133–163. <https://doi.org/10.1128/CMR.00029-06>.
- Pfaller MA, Diekema DJ. 2010. Epidemiology of invasive mycoses in North America. *Crit Rev Microbiol* 36:1–53. <https://doi.org/10.3109/10408410903241444>.
- Ruhnke M. 2006. Epidemiology of *Candida albicans* infections and role of non-*Candida albicans* yeasts. *Curr Drug Targets* 7:495–504. <https://doi.org/10.2174/138945006776359421>.
- Calderone RA. 2002. *Candida and candidiasis*. ASM Press, Washington, DC.
- Gleizmys A, Zdanaviciene E, Zilinskas J. 2015. *Candida albicans* importance to denture wearers. A literature review. *Stomatologija* 17:54–66.
- Yasui M, Ryu M, Sakurai K, Ishihara K. 2012. Colonisation of the oral cavity by periodontopathic bacteria in complete denture wearers. *Gerodontology* 29:e494–e502. <https://doi.org/10.1111/j.1741-2358.2011.00506.x>.
- Douglass CW, Shih A, Ostry L. 2002. Will there be a need for complete dentures in the United States in 2020? *Prosthet Dent* 87:5–8. <https://doi.org/10.1067/mp.2002.121203>.
- Li XJ, Kolltveit KM, Tronstad L, Olsen I. 2000. Systemic diseases caused by oral infection. *Clin Microbiol Rev* 13:547–558. <https://doi.org/10.1128/CMR.13.4.547-558.2000>.
- Sankari SL, Gayathri K, Balachander N, Malathi L. 2015. *Candida* in potentially malignant oral disorders. *J Pharm Bioallied Sci* 7:162–164. <https://doi.org/10.4103/0975-7406.155902>.
- Alalwan H, Rajendran R, Lappin DF, Combet E, Shahzad M, Robertson D, Nile CJ, Williams C, Ramage G. 2017. The anti-adhesive effect of curcumin on *Candida albicans* biofilms on denture materials. *Front Microbiol* 8:659. <https://doi.org/10.3389/fmicb.2017.00659>.
- Dias KD, Barbugli PA, de Patta F, Lordello VB, Penteado LD, Medeiros AI, Vergani CE. 2017. Soluble factors from biofilm of *Candida albicans* and *Staphylococcus aureus* promote cell death and inflammatory response. *BMC Microbiol* 17:146. <https://doi.org/10.1186/s12866-017-1031-5>.
- Steenackers HP, Parijs I, Dubey A, Foster KR, Vanderleyden J. 2016. Experimental evolution in biofilm populations. *FEMS Microbiol Rev* 40:980–980. <https://doi.org/10.1093/femsre/fuw030>.
- Hall CW, Mah TF. 2017. Molecular mechanisms of biofilm-based antibi-

- otic resistance and tolerance in pathogenic bacteria. *FEMS Microbiol Rev* 41:276–301. <https://doi.org/10.1093/femsre/fux010>.
25. Costerton JW. 1995. Overview of microbial biofilms. *J Ind Microbiol* 15:137–140. <https://doi.org/10.1007/BF01569816>.
 26. Hornemann JA, Lysova AA, Codd SL, Seymour JD, Busse SC, Stewart PS, Brown JR. 2008. Biopolymer and water dynamics in microbial biofilm extracellular polymeric substance. *Biomacromolecules* 9:2322–2328. <https://doi.org/10.1021/bm800269h>.
 27. Nadell CD, Xavier JB, Foster KR. 2009. The sociobiology of biofilms. *FEMS Microbiol Rev* 33:206–224. <https://doi.org/10.1111/j.1574-6976.2008.00150.x>.
 28. Oxman DA, Chow JK, Frenzl G, Hadley S, Hershkovitz S, Ireland P, McDermott LA, Tsai K, Marty FM, Kontoyiannis DP, Golan Y. 2010. Candidaemia associated with decreased in vitro fluconazole susceptibility: is Candida speciation predictive of the susceptibility pattern? *J Antimicrob Chemother* 65:1460–1465. <https://doi.org/10.1093/jac/dkq136>.
 29. Cosgrove SE, Carmeli Y. 2003. The impact of antimicrobial resistance on health and economic outcomes. *Clin Infect Dis* 36:1433–1437. <https://doi.org/10.1086/375081>.
 30. Ranjan R, Krishnamraju PV, Shankar T, Gowd S. 2017. Nonthermal plasma in dentistry: an update. *J Int Soc Prev Community Dent* 7:71–75. https://doi.org/10.4103/jispcd.JISPCD_512_16.
 31. Öngel C, Keleş M, Acar E, Bırcer Ö. 2015. Atmospheric pressure plasma jet treatment of human hair fibers. *J Bio-Tribo-Corrosion* 1:7. <https://doi.org/10.1007/s40735-015-0007-y>.
 32. Flynn PB, Higginbotham S, Alshraideh NH, Gorman SP, Graham WG, Gilmore BF. 2015. Bactericidal efficacy of atmospheric pressure non-thermal plasma (APNTP) against the ESKAPE pathogens. *Int J Antimicrobial Agents* 46:101–107. <https://doi.org/10.1016/j.ijantimicag.2015.02.026>.
 33. Ermolaeva SA, Varfolomeev AF, Chernukha MY, Yurov DS, Vasilev MM, Kaminskaya AA, Moisenovich MM, Romanova JM, Murashev AN, Selezneva II, Shimizu T, Sysolyatina EV, Shaginyan IA, Petrov OF, Mayevsky EI, Fortov VE, Morfill GE, Naroditsky BS, Gintsburg AL. 2011. Bactericidal effects of non-thermal argon plasma in vitro, in biofilms and in the animal model of infected wounds. *J Med Microbiol* 60:75–83. <https://doi.org/10.1099/jmm.0.020263-0>.
 34. Pannong K, Lee SH, Park DH, Sim GB, Kim YH, Uhm HS, Park G, Choi EH. 2014. Non-thermal plasma treatment diminishes fungal viability and up-regulates resistance genes in a plant host. *PLoS One* 9:e99300. <https://doi.org/10.1371/journal.pone.0099300>.
 35. Laroussi M. 2005. Low temperature plasma-based sterilization: overview and state-of-the-art. *Plasma Processes Polymers* 2:391–400. <https://doi.org/10.1002/ppap.200400078>.
 36. Todar K. 2004. The good, the bad, and the deadly. *Science* 304:1421.
 37. Guo L, Xu R, Zhao Y, Liu D, Liu Z, Wang X, Chen H, Kong MG. 2018. Gas plasma pre-treatment increases antibiotic sensitivity and persisters eradication in methicillin-resistant *Staphylococcus aureus*. *Front Microbiol* 9:537. <https://doi.org/10.3389/fmicb.2018.00537>.
 38. Vieugels M, Shama G, Deng XT, Greenacre E, Brocklehurst T, Kong MG. 2005. Atmospheric plasma inactivation of biofilm-forming bacteria for food safety control. *IEEE Trans Plasma Sci* 33:824–828. <https://doi.org/10.1109/TPS.2005.844524>.
 39. Goree J, Liu B, Drake D, Stoffels E. 2006. Killing of S-mutans bacteria using a plasma needle at atmospheric pressure. *IEEE Trans Plasma Sci* 34:1317–1324. <https://doi.org/10.1109/TPS.2006.878431>.
 40. Dobrynin D, Fridman G, Friedman G, Fridman A. 2009. Physical and biological mechanisms of direct plasma interaction with living tissue. *New J Phys* 11:e115020. <https://doi.org/10.1088/1367-2630/11/11/115020>.
 41. Shashurin A, Keidar M, Bronnikov S, Jurjus RA, Stepp MA. 2008. Living tissue under treatment of cold plasma atmospheric jet. *Appl Phys Lett* 93:e181501. <https://doi.org/10.1063/1.3020223>.
 42. Koban I, Matthes R, Hubner NO, Welk A, Meisel P, Holtfreter B, Sietmann R, Kindel E, Weltmann KD, Kramer A, Kocher T. 2010. Treatment of *Candida albicans* biofilms with low-temperature plasma induced by dielectric barrier discharge and atmospheric pressure plasma jet. *New J Phys* 12:e073039. <https://doi.org/10.1088/1367-2630/12/7/073039>.
 43. Gorynia S, Koban I, Matthes R, Welk A, Gorynia S, Hubner NO, Kocher T, Kramer A. 2013. In vitro efficacy of cold atmospheric pressure plasma on *S. sanguinis* biofilms in comparison of two test models. *GMS Hyg Infect Control* 8:Doc01. <https://doi.org/10.3205/dgkh000201>.
 44. Moravsky L, Klas M, Machova E, Pisklova K, Matejcek S. 2015. Influence of a plasma jet on the viability of *Candida albicans*. *Open Chem* 13:257–262.
 45. Pantanella P, Valenti P, Natalizi T, Passeri D. 2013. Analytical techniques to study microbial biofilm on abiotic surfaces: pros and cons of the main techniques currently in use. *Ann Ig* 25:31–42.
 46. Pei X, Lu X, Liu J, Liu D, Yang Y, Ostrikov K, Chu PK, Pan Y. 2012. Inactivation of a 25.5 μm *Enterococcus faecalis* biofilm by a room-temperature, battery-operated, handheld air plasma jet. *J Phys D Appl Phys* 45:e165205. <https://doi.org/10.1088/0022-3727/45/16/165205>.
 47. Delben JA, Zago CE, Tyhovych N, Duarte S, Vergani CE. 2016. Effect of atmospheric-pressure cold plasma on pathogenic oral biofilms and in vitro reconstituted oral epithelium. *PLoS One* 11:e0155427. <https://doi.org/10.1371/journal.pone.0155427>.
 48. Wilking JN, Zaburdaev V, De Volder M, Losick R, Brenner MP, Weitz DA. 2013. Liquid transport facilitated by channels in *Bacillus subtilis* biofilms. *Proc Natl Acad Sci U S A* 110:848–852. <https://doi.org/10.1073/pnas.1216376110>.
 49. Cai WL, De La Fuente L, Arias CR. 2013. Biofilm formation by the fish pathogen *Flavobacterium columnare*: development and parameters affecting surface attachment. *Appl Environ Microbiol* 79:5633–5642. <https://doi.org/10.1128/AEM.01192-13>.
 50. O'Toole G, Kaplan HB, Kolter R. 2000. Biofilm formation as microbial development. *Annu Rev Microbiol* 54:49–79. <https://doi.org/10.1146/annurev.micro.54.1.49>.
 51. Dunne NJW. 2002. Bacterial adhesion: seen any good biofilms lately? *Clin Microbiol Rev* 15:155–166. <https://doi.org/10.1128/CMR.15.2.155-166.2002>.
 52. Reuter S, Winter J, Schmidt-Bleker A, Tresp H, Hammer MU, Weltmann KD. 2012. Controlling the ambient air affected reactive species composition in the effluent of an argon plasma jet. *IEEE Trans Plasma Sci* 40:2788–2794. <https://doi.org/10.1109/TPS.2012.2204280>.
 53. Stewart PS. 2003. Diffusion in biofilms. *J Bacteriol* 185:1485–1491. <https://doi.org/10.1128/JB.185.5.1485-1491.2003>.
 54. Small JV. 1981. Organization of actin in the leading-edge of cultured-cells—influence of osmium-tetroxide and dehydration on the ultrastructure of actin meshworks. *J Cell Biol* 91:695–705. <https://doi.org/10.1083/jcb.91.3.695>.
 55. Weltmann KD, Kindel E, Brandenburg R, Meyer C, Bussiahn R, Wilke C, von Woedtke T. 2009. Atmospheric pressure plasma jet for medical therapy: plasma parameters and risk estimation. *Contrib Plasma Phys* 49:631–640. <https://doi.org/10.1002/ctpp.200910067>.
 56. Bast E. 2001. *Mikrobiologische Methoden: eine Einführung in grundlegende Arbeitstechniken*, vol 2, p 429. Elsevier, Amsterdam, Netherlands.
 57. Gränicher WHH. 1994. Messung beendet—was nun?, 2section 6.2.2./S6-4-6-9. Hochschulverlag AG, Zurich, Switzerland.
 58. Weiss M, Gumbel D, Hanschmann EM, Mandelkow R, Gelbrich N, Zimmermann U, Walther R, Ekkernkamp A, Sckell A, Kramer A, Burchardt M, Lillig CH, Stope MB. 2015. Cold atmospheric plasma treatment induces anti-proliferative effects in prostate cancer cells by redox and apoptotic signaling pathways. *PLoS One* 10:e0130350. <https://doi.org/10.1371/journal.pone.0130350>.

7 Article IV: Antimicrobial Effects of Microwave-Induced Plasmatorch (MINIMIP) Treatment on *Candida albicans* Biofilms

Article IV

Antimicrobial effects of microwave-induced plasma torch (MiniMIP) treatment on
Candida albicans biofilms

Oliver Handorf, Uta Schnabel, André Bösel, Thomas Weihe, Sander Bekeschus,
Alexander C. Graf, Katharina Riedel, Jörg Ehlbeck

Microbial Biotechnology, 2019, 12:1034–1048.

Author contributions:

As a co-author, ACG performed CLSM image acquisition, CLSM figure preparation and contributed to manuscript writing and editing.

Alexander C. Graf







Prof. Dr. Katharina Riedel



microbial biotechnology

Open Access

Antimicrobial effects of microwave-induced plasma torch (MiniMIP) treatment on *Candida albicans* biofilms

Oliver Handorf^{1*}  Uta Schnabel,^{1,2}  André Bösel,¹ Thomas Weihe,¹  Sander Bekeschus,¹  Alexander Christian Graf,³  Katharina Riedel³ and Jörg Ehlbeck¹ 

¹Leibniz Institute for Plasma Science and Technology (INP), Felix-Hausdorff-Str. 2, 17489 Greifswald, Germany.

²School of Food Science and Environmental Health, College of Sciences and Health, Technological University, Dublin, Cathal Brugha Street D01 HV58, Dublin, Ireland.

³Institute of Microbial Physiology and Molecular Biology, University of Greifswald, Felix-Hausdorff-Str. 8, 17489, Greifswald, Germany.

Summary

The susceptibility of *Candida albicans* biofilms to a non-thermal plasma treatment has been investigated in terms of growth, survival and cell viability by a series of *in vitro* experiments. For different time periods, the *C. albicans* strain SC5314 was treated with a microwave-induced plasma torch (MiniMIP). The MiniMIP treatment had a strong effect (reduction factor (RF) = 2.97 after 50 s treatment) at a distance of 3 cm between the nozzle and the superior regions of the biofilms. In addition, a viability reduction of 77% after a 20 s plasma treatment and a metabolism reduction of 90% after a 40 s plasma treatment time were observed for *C. albicans*. After such a treatment, the biofilms revealed an altered morphology of their cells by atomic force microscopy (AFM). Additionally, fluorescence microscopy and confocal laser scanning microscopy (CLSM) analyses of plasma-treated biofilms showed that an inactivation of cells mainly appeared on the bottom side of the biofilms. Thus, the plasma inactivation of the overgrown surface reveals a new possibility to combat biofilms.

Received 12 March, 2019; revised 5 June, 2019; accepted 17 June, 2019.

*For correspondence. E-mail oliver.handorf@inp-greifswald.de; Tel. +49 3834 554 3825; Fax +49 3834 554 301.

Microbial Biotechnology, (2019) 12(5), 1034–1048
doi:10.1111/1751-7915.13459

Funding information

Bundesministerium für Bildung und Forschung (Grant/Award Number: '03Z22Dn11'); Deutsche Forschungsgemeinschaft (Grant/Award Number: 'CRC-TRR34, subproject A3').

Introduction

Non-thermal plasmas (NTPs) are also known as non-equilibrium plasmas, honouring the fact that the cooling of ions and uncharged particles is more effective than an energy transfer of energetically excited electrons to the latter particles. Thus, the gaseous environment is not heated up, which is contrary to thermal plasmas (Friedman, Friedman *et al.*, 2008). Today, NTPs play an increasingly important role in both medicine and industry. They combine the advantage of non-thermal operation and high antimicrobial activity (Surowsky, Schlüter *et al.*, 2015). Hence, NTPs are used in today's medicine for many different applications such as wound healing (Shekhter, Serezhenkov *et al.*, 2005; Ghaffari, Jalili *et al.*, 2007), cell detachment as well as reattachment (Kieft, Darios *et al.*, 2005; Kieft, Kurdi *et al.*, 2006) and biological decontamination (Laroussi, Alexeff *et al.*, 2000; Laroussi, Mendis *et al.*, 2003). Due to their capability of biological decontamination, NTPs have gained interest in many industries. In the dairy and food industry, biofouling caused by microbial biofilms is a serious problem, which leads to a considerable loss of resources. This is caused not only by the microbial contamination of end-products such as meat, fruits and vegetables (Kumar and Anand, 1998), but also by increased corrosion rates at processing surfaces and increased fluid frictional resistance and heat flow across the surface (Criado, Suarez *et al.*, 1994).

The predominant microbial life cycle implies attachment to solid surfaces and the formation of three-dimensional, multicellular aggregates called biofilms, which are embedded in a self-produced, extracellular matrix (ECM; Steenackers, Parijs *et al.*, 2016; Serra, Hidalgo-Bastida *et al.*, 2017). Especially, food-borne pathogens and spoilage microorganisms like *Candida albicans* prefer biofilm formation on stainless steel, aluminium, glass, polytetrafluoroethylene (PTFE) seals and polyamide (PA) material, which are typically found in food-processing environments (Herald and Zottola, 1988; Mafu, Roy *et al.*, 1990; Notermans, Dormans *et al.*, 1991). *Candida* spp., for example, can often be isolated from conveyor tracks of the food and beverage industry (Loureiro and Malfeito-Ferreira, 2003; Brugnoni, Lozano *et al.*, 2007).

Economic losses in the food and healthcare sector as well as a more sensitive public awareness put food safety

© 2019 The Authors. *Microbial Biotechnology* published by John Wiley & Sons Ltd and Society for Applied Microbiology.

This is an open access article under the terms of the Creative Commons Attribution License, which permits use, distribution and reproduction in any medium, provided the original work is properly cited.

into the spotlight. Consequently, European countries implemented the Good Manufacturing Practice (GMP) and Hazard Analysis Critical Control Point (HACCP) for food industries. As a consequence, in 2016 the European Food Safety Authority was able to identify 49,950 food-borne outbreaks resulting in illness, 3869 hospitalizations and 20 deaths (European Centre for Disease Prevention and Control & European Food Safety Authority, 2017). Notably, 99,392 outbreaks resulting in illness were reported in the United States, leading to 2625 hospitalizations and 115 deaths (Centers for Disease Control and Prevention, 2016). Conventional methods like the mechanical removal of biofilms by high-pressure cleaners or brushing and wiping indeed lead to a loss of biomass, but not to an efficient extent. Due to intense and brief-acting shear forces, the majority of the biomass is removed but a thin biofilm most likely remains which further grows much denser with an increased resistance (Liu and Tay, 2002). Additionally, in older mature biofilms, significant components of the biofilm often remain, causing the biofilm to grow again (Jang, Rusconi *et al.*, 2017). The treatment of biofilms with biocides is just as problematic as the biofilms show increased resistance to these biocides compared to their planktonic counterparts. This is mainly due to the extracellular matrix which prevents deep penetration of the biofilm with the biocides (Bridier, Dubois-Brissonnet *et al.*, 2011). This leads to low concentrations in the deeper layers of the biofilm, which in turn leads to increased horizontal gene transfer of resistance genes (Jutkina, Marathe *et al.*, 2018). Thus, there is a strong need for novel strategies combating biofilms in the food industry. These range from the treatment of biofilms with special oils (Kerekes, Vidács *et al.*, 2015) and enzymes (Meireles, Borges *et al.*, 2016) to bacteriophages. The treatment of microorganisms with NTPs is a constantly growing field in which new insights into the effects are constantly being gained (Sladek, Filoche *et al.*, 2007; Koban, Holtfreter *et al.*, 2011; Xu, Tu *et al.*, 2011; Alkawa-reek, Algwari *et al.*, 2012; Ermolaeva, Sysolyatina *et al.*, 2015; Flynn, Higginbotham *et al.*, 2015). Results obtained in the here presented study suggest that the microwave-induced plasma torch (MiniMIP) is a powerful tool for microbial decontamination. In order to meet the industrial requirements, it is of particular importance to find standardized parameters for the plasma source. Despite antimicrobial effects of a different plasma source on *C. albicans* having been shown (Handorf, Weihe *et al.*, 2018), no studies exist, which investigated the effects of the MiniMIP on *C. albicans* biofilms up to this date.

Results

The path of the development from a new plasma source concept to its effective use in a specific application also

Microwave plasma treatment on *C. albicans* biofilms 1035

includes the investigation of a potential antimicrobial impact on surface-bound biofilms and their basic physical adaptations to it. Consequently, the presented work summarizes test series to determine the antimicrobial effect of the MiniMIP plasma source on eukaryotic biofilms. Due to its ubiquitous presence in medical and food sectors, *C. albicans* has been chosen as a model microbe, because its biofilm formation has been intensely studied and it is contaminant of medical as well as industrial importance (Kabir, Hussain *et al.*, 2012; Morata and Loira, 2017). In particular, *C. albicans* strain SC5314 is known for its rapid vertical growth and could be compared with *Saccharomyces cerevisiae*, a yeast of great importance in the food and beverage industry because of its high sugar consumption and the fermentation of juices into alcoholic end-products (Battey, Duffy *et al.*, 2002; Walker and Stewart, 2016; Lorenzini, Simonato *et al.*, 2019). This study investigated the viability of the cells [revealed via the fluorescence assay (2.5)] and cellular metabolism [XTT assay (2.6)] and was complemented by the determination of the post-treatment viability (CFU 2.4). Additionally, we used fluorescence microscopy (2.7), CLSM (2.8) and AFM (2.9) to obtain optical evidence of the plasma influence on the cells. Finally, OES (2.10) was used to give a general overview of the chemical composition of the plasma gas.

Effects of plasma treatment on the proliferation of the cells

A reduction factor (RF) was calculated as the difference between the \log_{10} (CFU) of an untreated control and the \log_{10} found for the samples after the treatment. The controls hosted in average 10^6 cells. The RFs quantify the inhibitory effect of the plasma treatment. The treatment with the MiniMIP revealed a RF of 2.97 after a 50 s treatment (Fig. 1A). The RF for the 10 s treatment with the MiniMIP shown to intersect the x-axis was not statistically significant. A continuous increase in RF could be detected up to a 40 s plasma treatment. Longer plasma treatment times did not lead to a significant increase in RF.

Effects of plasma treatment on the viability of the cells

The fluorescence LIVE/DEAD assay, which was used to detect the viability of the cells after the plasma treatment, showed a declined G/R ratio from 2.6 to 0.58 after a 20 s MiniMIP plasma treatment (Fig. 1B), which corresponds to a 77% reduction of the G/R ratio. The maximum reduction observed for a MiniMIP treatment was reached after 20 s. Longer treatment times revealed no further changes in the viability.

1036 O. Handorf et al.

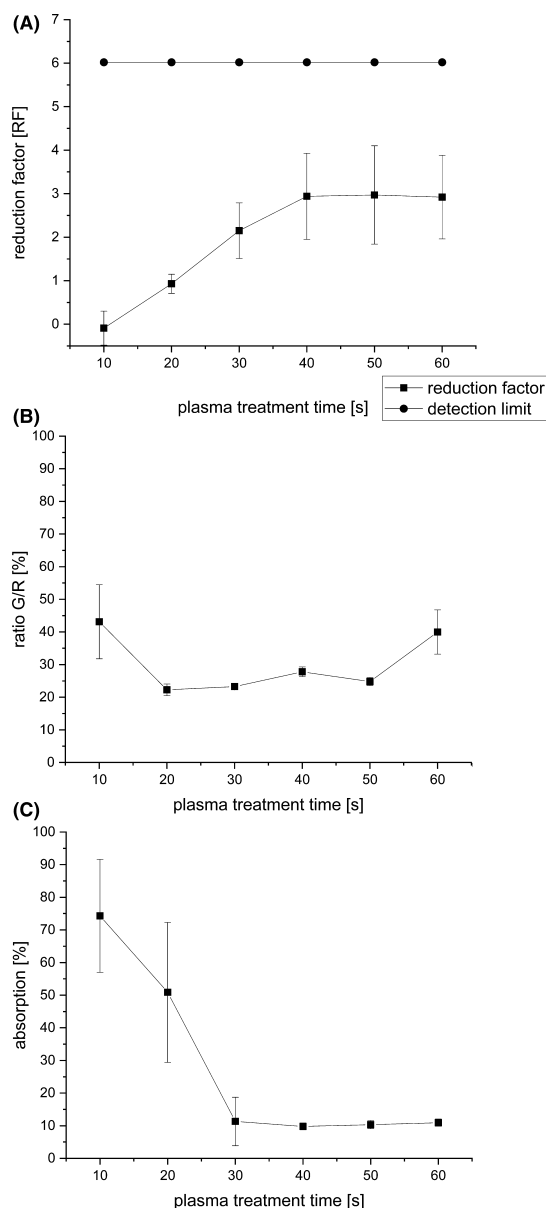


Fig. 1. CFU, fluorescence and XTT assay of *C. albicans* biofilms after treatment with the MiniMIP. (A) CFU measurements of the MiniMIP-treated *C. albicans* biofilms. The line with ● represents the detection limit. The line with ■ shows the reduction factor (RF) of the different plasma treatment times. The error bars were calculated using the propagation of error and the weighted error. The RF for the 10 s treatment with the MiniMIP shown to intersect the x-axis was not statistically significant. (B) Fluorescence LIVE/DEAD assay of the MiniMIP-treated *C. albicans* biofilms. The ratio G/R is defined as the division of the emission of green fluorescence by the emission of red fluorescence. (C) XTT measurements of the MiniMIP-treated *C. albicans* biofilms. The data points of all measurements represent the weighted mean value of the total population of the treatment time from the quadruple repetition $n = 6$.

Effect of plasma treatment on the metabolism of the cells

The XTT assay, which was used to determine the metabolic activity of the cells after plasma treatment, showed a reduction in the absorption from 2.09 to 0.20 after a 40 s MiniMIP plasma treatment (Fig. 1C). It represented a reduction of 90%. No further decrease in the cell metabolism could be measured for longer treatment times.

Fluorescence microscopic confirmation of plasma treatment effects

Fluorescence microscopy indicated a massive impact of the plasma treatment on cells which were located on the bottom of the biofilms already after a 20–30 s treatment (Fig. 2C,D). The biofilm degenerated from its exterior, and the inactivation of cells amplified into the centre of the biofilm with increasing treatment times (Fig. 2E–G). After 60 s treatment time, almost the entire biofilm was affected by the treatment (Fig. 2G).

CLSM confirmed cell inactivation processes predominantly on the bottom of the biofilms

The influence of a plasma treatment on the three-dimensional structure of a *C. albicans* biofilm was studied by CLSM (Fig. 3). The right side of the figure shows an inferior view of the 3D biofilm structure, which reveals highly influenced regions already after a 10 s treatment. Although the propagation of inactivated cells in the biofilm was more pronounced in the inferior regions, an inactivation was already noticeable in more peripheral layers of the biofilm, which became obvious in a 3D-model (Fig. 3) as well as in orthogonal views of the top layers. With increasing plasma treatment time, almost the entire bottom of the biofilm was inactivated and clear effects were visible on the top layers of the biofilms. Furthermore, increasing separations and holes in the biofilm could be detected with longer treatment times.

AFM confirmed alterations in the cell morphology of the biofilm after plasma treatment

With the aid of AFM, more profound insights in the cell morphological alteration of the biofilm after plasma treatment have been obtained. Due to the method of cantilever visualization, AFM can only visualize the morphological changes of the cells on the surface of the biofilm. The control cells appeared vital and commonly shaped (Fig. 4A). In contrast, cells treated with plasma for 60 s appeared more spherical and partially ruptured with distinct sites fractures. In addition, they were smaller than the control cells (Fig. 4C).

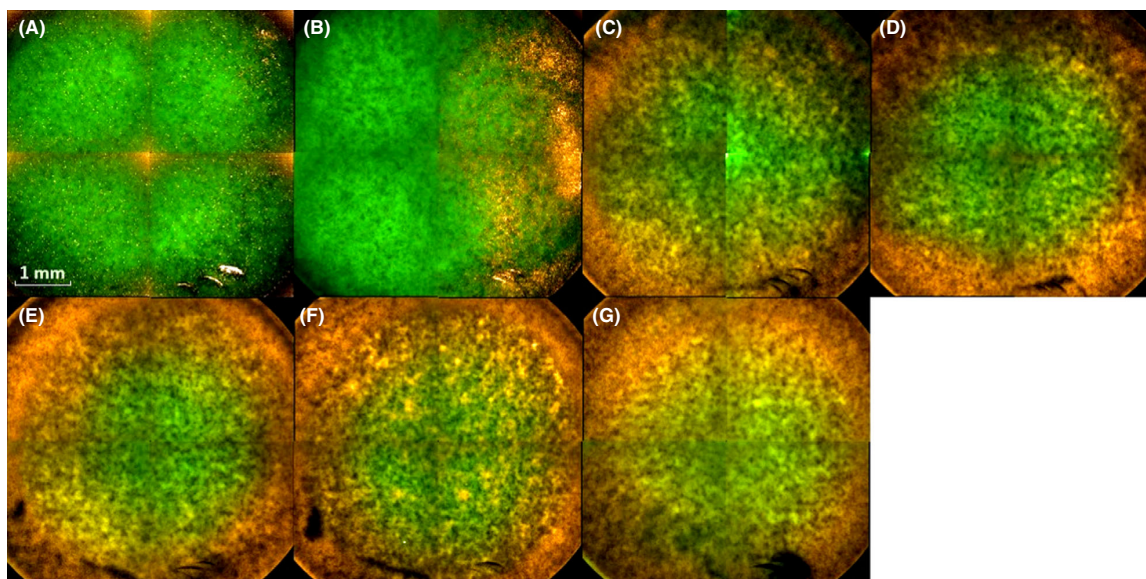


Fig. 2. Overview with the Operetta CLS fluorescence microscope of MiniMIP-treated biofilms. (A) Control; (B) 10 s plasma treatment time; (C) 20 s plasma treatment time; (D) 30 s plasma treatment time; (E) 40 s plasma treatment time; (F) 50 s plasma treatment time; (G) 60 s plasma treatment time. The biofilms were stained with SYTO 9 (green fluorescence for all cells) and propidium iodide (red fluorescence of dead cells). The pictures show inverse images. The scale bar indicates 1 mm.

OES demonstrated the chemical composition of the plasma gas

OES detects molecular and atomic emission bands of electromagnetic radiation, which provide information about the plasma composition. Unfortunately, differences in the peak height do not simultaneously indicate differences in the quantity of the molecules. Nevertheless, qualitative statements could be made based on the molecule spectra. Molecular absorption bands for nitrogen and hydroxyl groups were obtained, as well as spectral lines of atomic oxygen and argon in the measurements of the plasma gas. However, additional bands in the range of 520–620 nm were visible in the effluent of the MiniMIP compared to the kINPen09, a well-studied plasma device with regard to its plasma gas composition (Fig. 5).

Discussion

Currently, the road in NTP research and development points to an increasing importance for application-oriented plasma sources because of their differences in design, performance and application, depending on the respective task. The number of different NTP sources including plasma needles (Stoffels, Flikweert *et al.*, 2002; Bora, Aguilera *et al.*, 2018; Mohammed and Abas, 2018), plasma jets (Fricke, Koban *et al.*, 2012; Xu, Shen *et al.*, 2015; Xu, Shen *et al.*, 2017), dielectric barrier

discharge (DBD; Pietsch, 2001, de Souza, Neto *et al.*, 2016, Offerhaus, Lackmann *et al.*, 2017) or microwave-induced plasmas (Jovicevic, Ivkovic *et al.*, 2000; Baeva, Bösel *et al.*, 2012) is constantly growing.

Each of these plasma sources have specific application areas for which they are suited best. Plasma needles, for example, have already been used in dentistry for root canal treatments (Sladek, Stoffels *et al.*, 2004; Goree, Liu *et al.*, 2006). Radiofrequency plasma jet (RFPJ) like the kINPen09 or the new version kINPen MED has already been used for chronic wound healing in medicine (Lademann, Ulrich *et al.*, 2013; Bekeschus, Schmidt *et al.*, 2016). DBD is a promising tool for the microbial decontamination of water (Baroch and Saito, 2011) and has already been applied for the treatment of surfaces (Oehmigen, Hähnel *et al.*, 2010; Baroch and Saito, 2011; Banaschik, Lukeš *et al.*, 2015), for example textiles (Müller, Zahn *et al.*, 2010; Simor, Creyghton *et al.*, 2010). In comparison, the decontamination of biofilms with cold atmospheric pressure plasmas is an emerging field of research with a series of promising results (Machala, Chladekova *et al.*, 2010; Ehlbeck, Schnabel *et al.*, 2011; Misra, Tiwari *et al.*, 2011; Scholtz, Pazlarova *et al.*, 2015; Liguori, Cochis *et al.*, 2017).

So far, microwave-induced plasmas (MIPs) are mainly used in spectroscopy for the analysis of gas components (Broekaert and Engel, 2006), surface modifications (Jia, Kuraseko *et al.*, 2008) or the processing of biogas (Tip-payawong, Chaiya *et al.*, 2015). Not much is known

1038 O. Handorf et al.

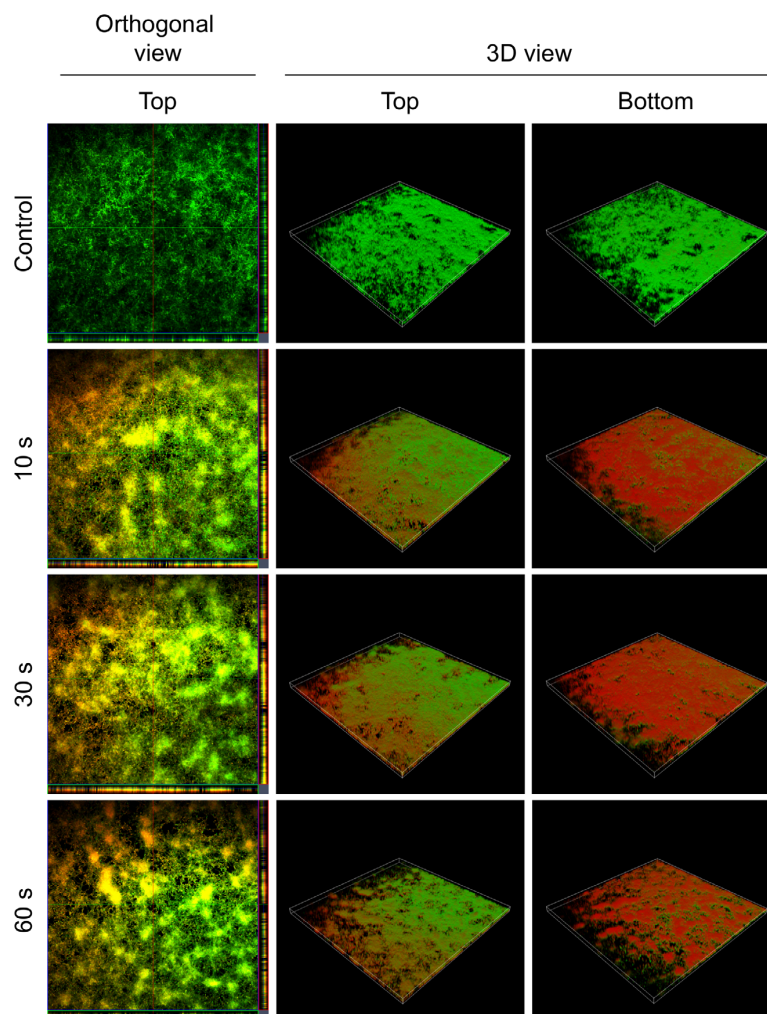


Fig. 3. Confocal laser scanning microscopy (CLSM) images of LIVE/DEAD-stained *C. albicans* biofilms after plasma treatment with the Mini-MIP. Left panels show an orthogonal view of the top biofilm layer (horizontal optical sections in the centre and vertical optical sections in the flanking pictures). Central and right panels show 3D images with a top and a bottom view of the biofilms. For each biofilm, an area of $1272.2 \mu\text{m} \times 1272.2 \mu\text{m}$ was visualized.

about microwave plasmas which are already used in medical technology apart from SteriPlas (Adtec, Hounslow, UK). The latter technology is based on the microwave plasma technology of the Max Planck Institute for extraterrestrial Physics in Germany. During an 8 year period, chronic wounds of 379 patients were treated with this plasma source and significant reductions in the bacterial count were detected (Isbary, Morfill *et al.*, 2010). Based on the RFs obtained in our experiments, the Mini-MIP shown in this study appeared as a versatile tool to combat microbial biofilms in the food and beverage industry.

In general, a distinction has to be made between the type of treatment and the type of plasma generation/

ignition (Niemira, 2012). In this work, we used a microwave-driven plasma source (type of plasma generation) and an indirect treatment of the biofilms (type of treatment). For a comparison, the most reasonable way is to work with plasma sources with a comparable power output and the same working gas. If two plasma sources have to be compared in their antimicrobial effects, they should be used in a standardized assay (Mann, Schnabel *et al.*, 2015; Sarangapani, Patange *et al.*, 2018). For instance, Ehlbeck *et al.* (2008) showed the treatment of contaminated PET bottles with microwave-induced plasma. In this case, the type of treatment and the type of plasma generation were the same and they reached reduction factors of up to 7. Contrary, comparison of the

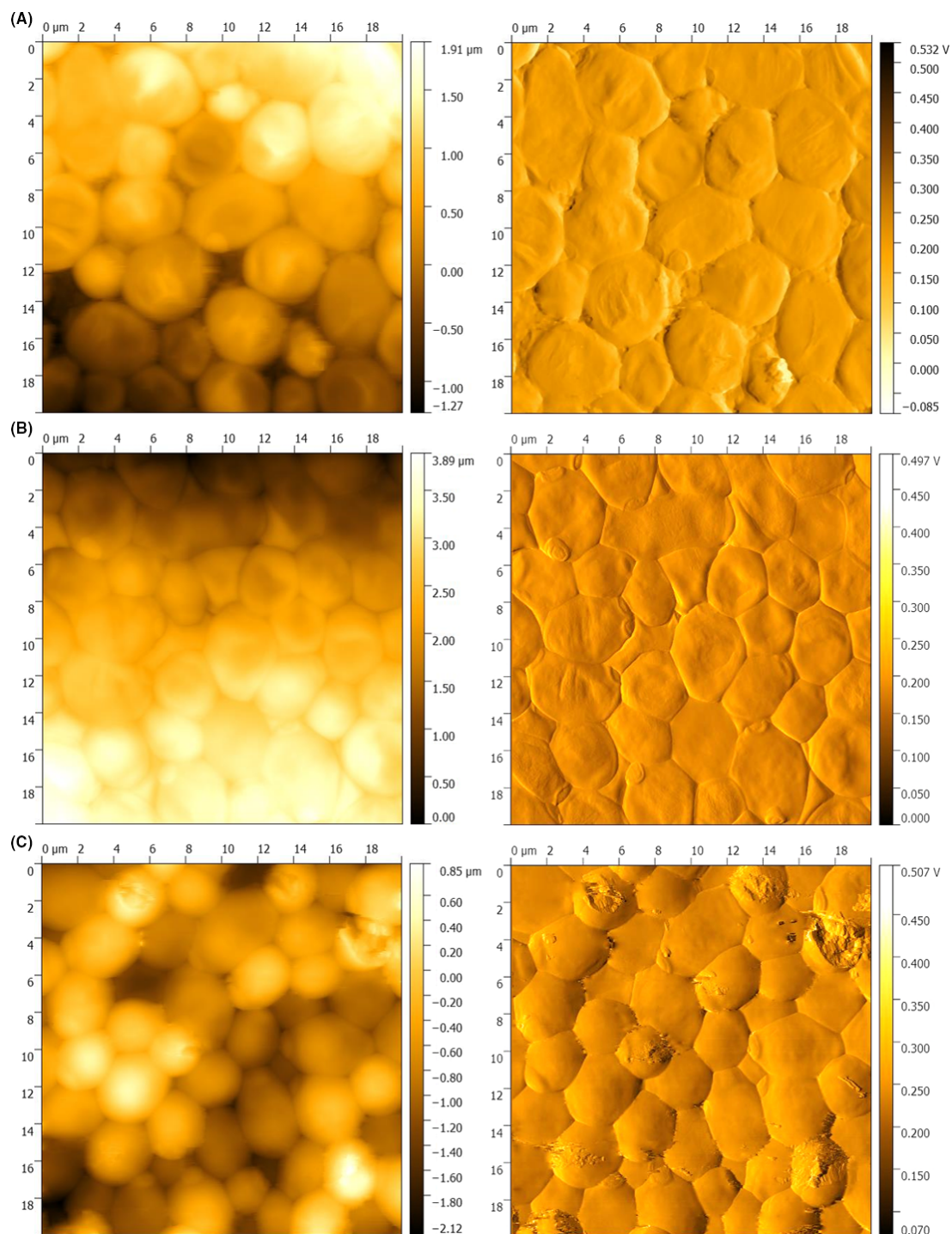


Fig. 4. Atomic force microscopy (AFM) images of the MiniMIP-treated biofilms and untreated controls. The left side shows the topographic image and the right side the error-signal image of the same spot. (A) Untreated control; (B) 30 s plasma treatment time; (C) 60 s plasma treatment time. The images were acquired in contact mode with a cantilever spring constant of $k = 0.1\text{--}0.6\text{ N/m}^2$ and a frequency of 0.4 Hz, the set point at 8 N/m^2 and an area of $20\ \mu\text{m}^2$.

1040 O. Handorf et al.

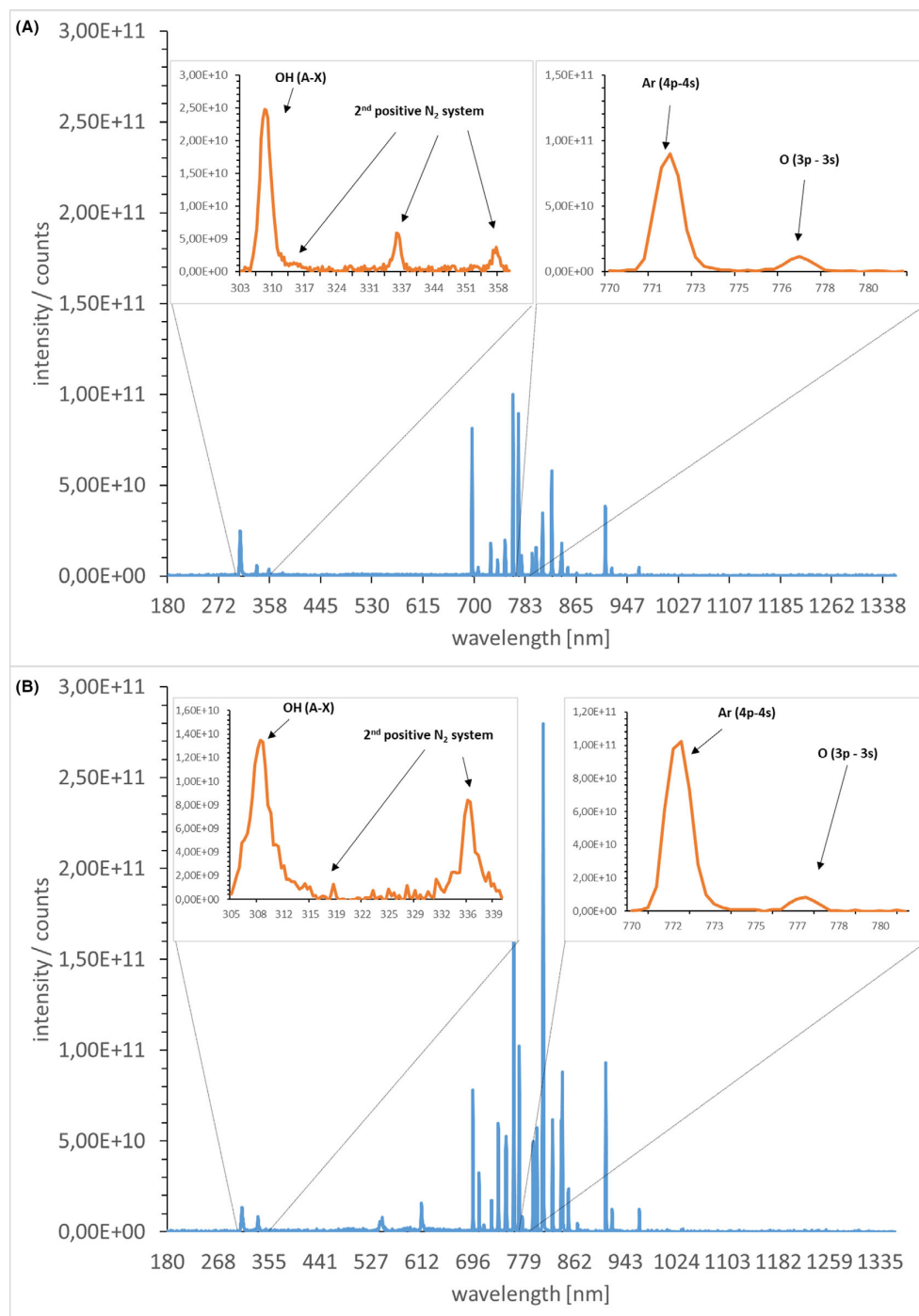


Fig. 5. Optical emission spectroscopy (OES) of the radiofrequency plasma jet kINPen09 and the microwave-induced plasma torch MiniMIP. (A) Emission spectra of the radiofrequency plasma jet kINPen09. (B) Emission spectra of the MiniMIP. The inset boxes represent the respective wavelength region at higher resolution. The emission spectra represent the respective molecules. The measurement results were obtained with LabVIEW and evaluated with MATLAB.

reduction factors is difficult, as the plasma used in that work had a much higher power and was operated with compressed air instead of argon gas.

The trend for microwave plasmas in microbial decontamination tends more in the direction of plasma-processed air (PPA) or plasma-treated water (PTW) which subsequently affect the microorganisms (Schnabel, Andrasch *et al.*, 2014; Thirumdas, Kothakota *et al.*, 2018; Schnabel, Handorf *et al.*, 2019). Especially in terms of industrial manufacturing, PPA and PTW offer advantages over a conventional plasma treatment. For instance, not all areas which need to be treated are easily accessible for plasma devices. In this context, washing and flushing processes with PTW or PPA can offer a decisive advantage.

Indirect treatment of microorganisms where the effluent has been brought into a short distance over the biofilms is published for plasma jets or DBDs (Maisch, Shimizu *et al.*, 2012; Khan, Lee *et al.*, 2016; Handorf, Weihe *et al.*, 2018). If only the achieved reduction factors are considered for the same treatment time regardless of the type of plasma generation and type of application, RFs of 0.6 for the kINPen09, 2.9 for the hollow electrode dielectric discharge (HDBD) and 2.3 for the volume dielectric discharge (VDBD) were obtained after 1 min treatment time (Koban, Matthes *et al.*, 2010). In relation to these results, the MiniMIP showed the strongest inactivation with a reduction factor of 2.92 after 1 min treatment time (Fig. 1A).

In the present study, three different methods (CFU, fluorescence and XTT assay) were used to investigate the viability of *C. albicans* cells organized in a biofilm, after a plasma treatment. However, these methods do not reveal the same effects on the cells. The CFU shows the ability of the cells to proliferate after treatment. The fluorescence assay indicates membrane damage of the cells, and the XTT assay monitors the metabolic activity of the cells after treatment. The results of the methods cannot be directly compared. Not only based on the current study, the increasing importance of viable but non-culturable (VBNC) cells becomes more and more obvious but should be discussed more nuanced, and it is essential that the results of several different methods are considered together. Concretely, together they give a comprehensive overview which makes it possible to exclude a VBNC status as far as possible (Ramamurthy, Ghosh *et al.*, 2014; Saprykina, Bolgova *et al.*, 2016; Bolgova, Saprykina *et al.*, 2017). The results (Fig. 1) showed that already 20 s after treatment the cells had significant membrane damages and their metabolic activity was strongly reduced. Their ability to proliferate was also severely restricted.

In terms of three-dimensional effects, RFPJ treatments showed centralized spots of dead cells while the majority

of biofilm cells were not affected by plasma treatment (Handorf, Weihe *et al.*, 2018). This occurred mainly due to the relatively fine and centralized effluent of plasma jets. In contrast, a very broad effect has been demonstrated in the treatment of biofilms with the MiniMIP, which rather spreads from the marginal areas to the centre and affected the complete biofilm already after 20–40 s (Fig. 2C–E). Most publications showed that the biofilm structures with increasing treatment times were either inactivated on their surfaces or completely inactivated during the course of the treatment (Pei, Lu *et al.*, 2012; Traba and Liang, 2015; Delben, Zago *et al.*, 2016). This could have been a result of the higher power of the plasma sources or the longer treatment times.

It is very likely that the applied plasma treatment times of 10–60 s mirror the dynamic range. In the indirect treatments, the formed reactive oxygen species (ROS) and reactive nitrogen species (RNS) played a major role in inactivation (Klampfl, Isbary *et al.*, 2012; Xu, Shen *et al.*, 2015; Ziuzina, Boehm *et al.*, 2015). There may have been an increase in the concentration of ROS/RNS in the liquid residues of the biofilm that have accumulated on the bottom of the biofilm. In combination with water, RNS such as nitrates and nitrites are to be expected when treating with the MiniMIP. Consequently, PTW was generated at the bottom layers of the biofilm and predominantly led to an inactivation in that area. This was also indicated in treatments with the kINPen09 in the same experimental set-up (Handorf, Weihe *et al.*, 2018).

The AFM images revealed differences in the cell morphology between a treatment with the MiniMIP or the kINPen09 (Handorf, Weihe *et al.*, 2018). It is most likely caused by the device-dependent reaction pathways, which lead to ROS/RNS (Yusupov, Neyts *et al.*, 2012; Gilmore, Flynn *et al.*, 2018). However, more in-depth investigations of the MiniMIP plasma gas constituents have not yet been completed. The PLexc microwave plasma comes closest to the gas physics of the MiniMIP (Pipa, Andrasch *et al.*, 2012). Investigations of the gas physics of this plasma source have shown that RNS is mainly produced during the latter process (Schnabel, Handorf *et al.*, 2019). This knowledge was additionally supported by the temperature-dependent dissociation rates of the different gas molecules (Drost, 1980). Investigations have already shown that the temperature in the plasma discharge area within the MiniMIP is above 2000°C, where ROS were already dissociated and mainly RNS still exist (Baeva, Bösel *et al.*, 2012). Therefore, the OES spectra in this paper serve as an overview of the gas molecules.

Notably, plasma treatment could overcome various limitations of conventional antimycotic drugs. For instance, it is well-known that reactive species of plasma

1042 O. Handorf et al.

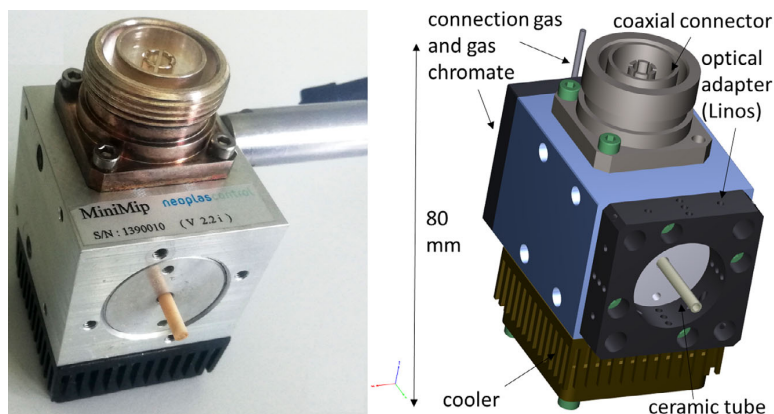


Fig. 6. Structure of the microwave-driven plasma torch MiniMIP. The ceramic tube leads completely into the inside of the housing, where it is encased by an aluminium tube. The ignition of the plasma takes place at the front edge of the aluminium tube, and plasma propagation is driven by the surrounding microwave field and the gas flow along the longitudinal axis of the ceramic tube leading to a small plasma plume of about 10 mm in length and 3 mm in diameter outside the device. Left: microwave-driven plasma torch MiniMIP; right: schematic structure of the MiniMIP.

gases are able to overcome the barrier of the ECM and inhibit cells in the biofilm or even completely degrade the ECM (Delben, Zago *et al.*, 2016; Modic, McLeod *et al.*, 2017; Gilmore, Flynn *et al.*, 2018). *C. albicans* exploits a range of resistance mechanisms to conventional antimicrobial treatment strategies. Its resistance is primarily due to the activity of efflux pumps, the production of an ECM and the presence of recalcitrant persister cells during biofilm growth (Nobile and Johnson, 2015). The efflux pumps of *C. albicans* comprise two major classes: the ATP-binding cassette transporter superfamily and the major facilitator class (Anderson, 2005; Cowen, 2008). The ECM represents a mechanical barrier to drugs and thus leads to higher drug resistance of *C. albicans* cells embedded in biofilms (Baillie and Douglas, 2000; Al-Fattani and Douglas, 2006). Persister cells are a small subset of metabolically dormant yeast cells in biofilms that are extremely resistant to antimycotics (LaFleur, Kumamoto *et al.*, 2006). Comparative studies between plasma treatment of *C. albicans* biofilms and treatment with antimycotics or chemical disinfectants showed a stronger reduction in the CFU during plasma treatment and indicated no correlation between plasma effects and efflux pumps of the pathogen (Koban, Matthes *et al.*, 2010). Furthermore, it could be shown that pre-treatment with plasma even significantly increases the effect of antimycotics on the pathogens (Sun, Yu *et al.*, 2012).

The results of our work offer new promising fields of application for MIPs. The results of the MiniMIP compared to already well-investigated plasma sources showed a stronger reduction of *C. albicans* biofilms in a shorter treatment time despite a larger distance of the plasma source to the surface of the biofilm (Handorf,

Weihe *et al.*, 2018). The MiniMIP is therefore a promising new tool in the field of plasma-based antimicrobial decontamination of biofilms. Although the investigation of the effect of MiniMIP on prokaryotic and eukaryotic biofilms is still in its infancy, the results shown here are highly motivating and represent a solid basis for further investigations and applications of this innovative plasma source.

Conclusion

Our results show the influence of plasma treatment of *C. albicans* biofilms with the microwave-induced plasma source MiniMIP for the first time. A stronger influence of the MiniMIP on the biofilms could be shown within a shorter plasma treatment time and greater distance compared to already commercially available and well-studied plasma sources, for example the RFPJ kINPen09. The composition of the plasma gases can be of decisive importance for the different results shown in the CFU, the fluorescence and the XTT assay. Furthermore, an influence mainly on the bottom side of the biofilms could be shown with the aid of fluorescence microscopy and CLSM. Diffusion processes, water channels and plasma flow dynamics might be crucial for this phenomenon. Based on the highly reproducible and new findings, which are generated by the selection of the plasma source and its settings to a certain problem, it would be a decisive step for the industrial use of MIPs in several value chains. For instance, the removal of biofilms from an overgrown surface is of great interest in the food industry. If the inactivation of the bottom side of the biofilms shown in this work also led to its surface detachment, it could be a crucial advantage for the application in the industry.

Experimental procedures

Fungal strain and growth conditions

Because of its primarily vertical growth, *C. albicans* SC5314, which is a commonly used strain in laboratory experiments, was grown on Sabouraud agar 4% glucose (Roth, Karlsruhe, Germany) for 24 h at 37°C. Grown colonies were suspended in 10 ml phosphate-buffered saline (PBS; pH 7.2, according to Sørensen) to an OD₆₀₀ of 0.375–0.385. Afterwards, 1 ml of the suspension was pipetted in 9 ml RPMI medium without bicarbonate (Merck, Darmstadt, Germany). From this inoculum, 200 µl was pipetted into each well of a 96-well plate and subsequently incubated at 37°C and 80 rpm on a rotary shaker for 90 min to achieve homogeneous oxygen distribution in the biofilm resulting in improved biofilm growth compared to a static grown biofilm. Subsequently, the medium was removed and each well was washed with 200 µl PBS and refilled with 200 µl RPMI medium to remove non-adhered cells. The plate was incubated at 37°C and 80 rpm on a rotary shaker for 24 h. 96-well coated polystyrol plates (Sarstedt, Nümbrecht, Germany) were used for biofilm cultivation. For scanning probe measurements (SPM), 12-well plates with 12 mm coverslips (Sarstedt, Nümbrecht, German) were used. This protocol was kindly provided by the research group of Christiane Yumi Koga-Ito, Institute of Science and Technology – UNESP, Department of Oral Sciences and Diagnosis (Borges, Lima *et al.*, 2018).

Plasma source

The MiniMIP worked at a frequency of 2.45 GHz at atmospheric pressure with a forward power in the range of 20–200 W. The microwave discharge was induced in a ceramic tube, which has an inner radius of 0.75 mm and an outer radius of 1.5 mm. The length of the ceramic tube is approximately 31 mm (Fig. 6). The ceramic tube leads completely into the inside of the housing, where it is encased by an aluminium tube. The ignition of the plasma takes place at the front edge of the aluminium tube, and plasma propagation is driven by the surrounding microwave field and the gas flow along the longitudinal axis of the ceramic tube leading to a small plasma plume of about 10 mm in length and 3 mm in diameter outside the device (Baeva, Bösel *et al.*, 2012). In this work, the MiniMIP was operated with a forward power of 40 W and a reverse power of 20 W at a gas flow of 5 slm pure argon gas.

Plasma treatment of *C. albicans* SC5314 biofilms

After the incubation, mature biofilms (2.1) were washed with PBS (pH 7.2 according to Sørensen) followed by a

complete removal of the liquid. Throughout the treatment, the plasma source was attached to a xyz table, holding a constant distance between the source and the biofilm surface. For the treatment, the MiniMIP was horizontally guided into the centre of the biofilm during the treatment and then brought into the desired distance to the biofilm via the computer control software. During the horizontal movement between the treatments of individual well, the plasma source was vertically positioned at the distance of approximately 30 cm (10 times of the treatment distance). A distance of 3 cm was chosen from the beginning of the outer part of the ceramic tube to the surface of the biofilms during the treatment. Each biofilm underwent one of six different treatment times. To avoid dehydration effects, all sample groups were treated in a row. For the colony-forming units (CFU), the fluorescence LIVE/DEAD assays and the XTT assays, 200 µl PBS (pH 7.2 according to Sørensen) per well was added. Subsequently, the biofilms were mechanically removed from the overgrown surface by repeated pipetting of 200 µl PBS and the resulting cell suspensions were collected. To ensure the transfer of the entire biofilm, this step was repeated three times in total which resulted in a final suspension volume of 600 µl.

Analytical determinations

First, the influence of the temperature on a biofilm was determined. For temperature measurements, thermal images of the biofilms were acquired directly after plasma treatment with a FLIR thermal imaging camera (FLIR Systems, Frankfurt am Main, Germany) at distance of 20 cm. The temperature had no significant influence on the biofilms (data not shown). The viability of a *C. albicans* biofilm after a plasma treatment was analysed by counting the viable number of microorganisms via the CFU method. Therefore, a 1:10 serial dilution of the samples with maximum recovery diluent (MRD, 0.85% NaCl, 1% tryptone) was performed. Controls and the samples were diluted 1:10 000 and 1:1000 respectively. Each dilution step was plated on Sabouraud agar by pipetting 10 µl per dilution onto the plate and spread out using the tilting technique. Subsequently, the plates were incubated at 37°C for 24 h. The colonies of the dilution levels were counted, and the CFU/ml was calculated as follows:

$$\text{CFU/ml} = \frac{10^x}{v} \times \frac{\sum c_y + \sum c_{y+1}}{n_y + 0,1n_{y+1}} \quad (1)$$

10^x = the dilution factor for the lowest dilution; v = the volume of diluted cell suspension per plate in ml; $\sum c_y$ = the total number of colonies on all (n_y) plates of the lowest evaluated dilution level 10^{-x}; $\sum c_{y+1}$ = the total

1044 O. Handorf et al.

number of colonies on all ($n_y + 1$) plates of the next highest dilution level evaluated $10^{-(x+1)}$ (Bast, 2001).

After the calculation (1), the reduction factor (RF) was determined as follows:

$$RF = MV_k \log_{10} - MV_p \log_{10} \quad (2)$$

$MV_k \log_{10}$ = the mean value of the CFU/ml of the reference group. $MV_p \log_{10}$ = the mean value of the CFU/ml of the treated specimens.

For the final illustration of the data points, the weighted mean value of the total population was used with the formula:

$$\bar{x} = \frac{\sum_{i=1}^n p_i x_i}{\sum_i p_i} = \frac{[p x]}{[p]}$$

The weight p_i is calculated according to the following formula:

$$p_i = k \times \frac{1}{\sigma_i^2}$$

where k = arbitrary constant. This ensures that the weight of the mean values is not included in the calculation as values. The weighted mean value has the advantage compared to the arithmetic mean value that it is more resistant to aberrations (Gränicher, 1994).

The propagation of error was calculated for each treatment group. This finally resulted in four different error propagations for each treatment time from which the weighted error was calculated and used as error bars in the illustration (Gränicher, 1994). The experiments were repeated fourfold with $n = 6$.

Fluorescence LIVE/DEAD assay

The LIVE/DEAD BacLight™ Bacterial Viability Kit (Thermo Scientific, Waltham, USA) was prepared according to product instructions. Subsequently, 0.9 μ l of the mixture was added to 300 μ l of the sample solution (2.3) followed by an incubation on a rotary shaker in the dark at room temperature for 20 min. A fluorescence microplate reader (Varioskan Flash®, Thermo Scientific, Waltham, USA) was used to determine the fluorescence of each well of a 96-well plate with an excitation wavelength of 470 nm and an emission wavelength of 530 nm (G, green) or 630 nm (R, red). Conclusively, a ratio G/R was calculated by dividing the fluorescence intensity value of green fluorescence by the value of red fluorescence.

XTT assay

A colorimetric assay was used to determine the cell viability after plasma treatment (XTT Cell Proliferation

Assay Kit; AppliChem, St. Louis, MO, USA). Therefore, XTT was applied to reveal the cell viability as a function of redox potential, which arises from a trans-plasma membrane electron transport (Scudiero, Shoemaker *et al.*, 1988). The sterile activation solution, which contains N-methyl dibenzopyrazine methyl sulphate (PMS) as an intermediate electron carrier, and the XTT solution were mixed 1:50. For each well, these mixtures were added at a ratio of 1:3 to the sample solution (2.3). The 96-well plate was incubated at 37°C with continuous horizontal shaking (80 rpm) in the dark for 2 h. After the incubation time, 96-well plates were scanned at a wavelength of 470 nm using the Varioskan Flash® device. The obtained values were blank-corrected using XTT and activation solution mix without sample. The experiments were repeated fourfold with $n = 6$.

Fluorescence microscopy

Black 96-well plates with a glass bottom (PerkinElmer, Hamburg, Germany) were used for fluorescence microscopy. To avoid dehydration of the biofilms, plasma-treated biofilms were resuspended in 300 μ l of 0.85% NaCl after treatment. The LIVE/DEAD BacLight™ Bacterial Viability Kit was used as previously described (2.5). Epifluorescence images were acquired using Operetta CLS High-Content Imager (PerkinElmer, Hamburg, Germany) using a 5 \times objective (air, NA = 0.16, Zeiss, Oberkochen, Germany). Depending on the experiment, several fields of view were recorded and combined in the software. SYTO™ 9 was excited by a 475 nm (110 mW) LED, and the fluorescence was collected with a 525 \pm 25 nm band-pass filter. Propidium iodide was excited by a 550 nm (170 mW) LED, and the emission light was collected with a 610 \pm 40 nm band-pass filter. A laser autofocus (785 nm) was available for all measurements. The images were displayed using Harmony 4.6 software.

Confocal laser scanning microscopy (CLSM)

Biofilms were cultivated (2.1), plasma-treated (2.3) and LIVE/DEAD (2.5)-stained as previously described. The supernatant was removed after the staining and the washing procedure. Subsequently, the biofilms were analysed using a Zeiss LSM 510 microscope (Carl Zeiss, Jena, Germany) equipped with a 10 \times objective (air, NA = 0.1). The filter and detector settings were adapted to the fluorescent dyes SYTO™ 9 and propidium iodide. The dyes were excited by an argon laser at 488 nm and the emission was collected at 505–530 nm (band-pass filter) and 650 nm (long-pass filter) respectively. Three-dimensional images were acquired using the ZEN 2009 software (Carl Zeiss) with an area of

1272.2 μm \times 1272.2 μm and z-stack sections of 5.5 μm .

Atomic force microscopy

For topographic atomic force microscopy (AFM), coverslips were placed on a gel-like mass Gelrite™ (Duchefa, Haarlem, Netherlands), which avoids unwanted adherence on the bottom side of the coverslip. Because of its rapid curing process, 50 ml Gelrite was autoclaved and directly used hereafter. For the preparation of the liquid mass, a 12-well plate was used, which was filled with 200 μl per well. While it cooled down, coverslips were placed at the surface of the hardening mass. The biofilms were cultivated as described above (2.1), except that 1 ml of the *C. albicans*–RPMI mix was pipetted to each well until the coverslips were completely topped with the mix. Subsequently, the 12-well plates were incubated at 37°C and 80 rpm on a rotary shaker for 90 min. Hereafter, the biofilms underwent additional washing steps with 0.85% NaCl. The biofilms were stored overnight in 37°C to ensure the growth of enough biofilm mass. The cultivation medium was removed, and the biofilm-overgrown coverslips were repeatedly washed with 1 ml 0.85% NaCl the following day.

For the experiments, samples were treated 30 s and 60 s with the MiniMIP. Dehydration of the coverslips before AFM analysis was avoided by using a humidity chamber. The AFM measurements were carried out on a DI CP II SPM (Veeco, Plainview, USA), which was mounted on a vibration-free object table (TS-150, Table Stable, Zwillikon, Switzerland). The set-up was mounted on an optical bench encased by an additional acoustic protection. The AFM was equipped with a linearized piezo scanner, on which the coverslips were mounted with a metal sample holder with leading tabs. The samples were measured using cantilevers with nominal spring constant of $k = 0.1\text{--}0.6 \text{ N} \times \text{m}^2$ in contact mode, a frequency of 0.4 Hz and set point = 8 N/m^2 with a picture size of 20 μm^2 . Pictures were edited with Gwyddion (Czech Metrology Institute, Brno, Czech Republic).

Optical emission spectroscopy (OES)

For stable OES measurements, the plasma device was left in operation for 30 min until condensation water escaped from the gas pipes and the effluent was optimally adjusted. An optical fibre with an internal diameter of 400 μm was connected to the USB compact spectrometer AvaSpec 2048 (Apeldoorn, Netherlands), which was connected to a laptop. For better focusing, the optical fibre was clamped within a holding bracket. For

Microwave plasma treatment on *C. albicans* biofilms 1045

measurement correction, a black cap was placed on the tip of the fibre optic cable and the dark current was determined. Afterwards, the cap was removed, the fibre optic cable was placed in front of the effluent, and the spectra were measured. The measurement was done for the MiniMIP and the kINPen09, an already commercially used radiofrequency plasma source, for comparison of the OES. The data were read out using MATLAB® (MathWorks®, Natick, MA, USA) and evaluated and displayed visually as diagrams using Excel.

Acknowledgements

This work was supported by the Leibniz Institute for Plasma Science and Technology, INP, in Greifswald, Germany. Katharina Riedel received funding from the German Research Foundation (DFG; CRC-TRR34, sub-project A3). Sander Bekeschus is funded by the German Federal Ministry of Education and Research (BMBF), grant number 03Z22DN11.

Conflict of interest

None declared.

References

- Al-Fattani, M.A., and Douglas, L.J. (2006) Biofilm matrix of *Candida albicans* and *Candida tropicalis*: chemical composition and role in drug resistance. *J Med Microbiol* **55**: 999–1008.
- Alkawareek, M.Y., Algwari, Q.T., Laverty, G., Gorman, S.P., Graham, W.G., O'Connell, D., and Gilmore, B.F. (2012) Eradication of *Pseudomonas aeruginosa* biofilms by atmospheric pressure non-thermal plasma. *PLoS ONE* **7**: e44289.
- Anderson, J.B. (2005) Evolution of antifungal-drug resistance: mechanisms and pathogen fitness. *Nat Rev Microbiol* **3**: 547–556.
- Baeva, M., Bösel, A., Ehlbeck, J., and Loffhagen, D. (2012) Modeling of microwave-induced plasma in argon at atmospheric pressure. *Phys Rev E* **85**: 056404.
- Baillie, G.S., and Douglas, L.J. (2000) Matrix polymers of *Candida* biofilms and their possible role in biofilm resistance to antifungal agents. *J Antimicrob Chemother* **46**: 397–403.
- Banaschik, R., Lukeš, P., Jablonowski, H., Hammer, M.U., Weltmann, K.D., and Kolb, J.F. (2015) Potential of pulsed corona discharges generated in water for the degradation of persistent pharmaceutical residues. *Water Res* **84**: 127–135.
- Baroch, P., and Saito, N. (2011) Dielectric barrier discharge system with catalytically active porous segment for improvement of water treatment.
- Bast, E. (2001) *Mikrobiologische Methoden*, 2nd edn. Munich, Germany: Elsevier, p. 429.
- Batley, A.S., Duffy, S., and Schaffner, D.W. (2002) Modeling yeast spoilage in cold-filled ready-to-drink beverages with

1046 O. Handorf et al.

- Saccharomyces cerevisiae*, *Zygosaccharomyces bailii*, and *Candida lipolytica*. *Appl Environ Microbiol* **68**: 1901–1906.
- Bekeschus, S., Schmidt, A., Weltmann, K.D., and Woedtke, T. (2016) The plasma jet kINPen – a powerful tool for wound healing. *Clinical Plasma Medicine* **4**: 19–28.
- Bolgova, E.S., Saprykina, M.N., and Goncharuk, V.V. (2017) Optimal recultivation conditions of *Candida albicans* staying in non-culturable state. *J Water Chem Technol* **39**: 305–309.
- Bora, B., Aguilera, A., Jain, J., Avaria, G., Moreno, J., Gupta, S.B., and Soto, L. (2018) Development, characterizations, and applications of a hand touchable DC plasma needle for biomedical investigation. *IEEE Trans Plasma Sci* **46**: 1768–1774.
- Borges, A.C., Lima, G.D.G., Nishime, T.M.C., Gontijo, A.V.L., Kostov, K.G., and Koga-Ito, C.Y. (2018) Amplitude-modulated cold atmospheric pressure plasma jet for treatment of oral candidiasis: in vivo study. *PLoS ONE* **13**: e0199832.
- Bridier, A., Dubois-Brissonnet, F., Greub, G., Thomas, V., and Briandet, R. (2011) Dynamics of the action of biocides in *Pseudomonas aeruginosa* biofilms. *Antimicrob Agents Chemother* **55**: 2648–2654.
- Broekaert, J.A.C., and Engel, U. (2006) Microwave-induced plasma systems in atomic spectroscopy. *Encyclopedia of Analytical Chemistry* **1**: 1–81.
- Brugnoni, L.I., Lozano, J.E., and Cubitto, M.A. (2007) Potential of yeast isolated from apple juice to adhere to stainless steel surfaces in the apple juice processing industry. *Food Res Int* **40**: 332–340.
- Centers for Disease Control and Prevention (2016) National Outbreak Reporting System (NORS).
- Cowen, L.E. (2008) The evolution of fungal drug resistance: modulating the trajectory from genotype to phenotype. *Nat Rev Microbiol* **6**: 187–198.
- Criado, M.T., Suarez, B., and Ferreiros, C.M. (1994) The importance of bacterial adhesion in the dairy industry. *Food Technology* **48**: 123–126.
- Delben, J.A., Zago, C.E., Tyhovych, N., Duarte, S., and Vergani, C.E. (2016) Effect of atmospheric-pressure cold plasma on pathogenic oral biofilms and in vitro reconstituted oral epithelium. *PLoS ONE* **11**: e0155427.
- Drost, H. (1980) Plasmachemie. Prozesse der chemischen Stoffwandlung unter Plasma-Bedingungen. *Zeitschrift für Chemie* **20**: 420.
- Ehlbeck, J., Brandenburg, R., von Woedtke, T., Krohmann, U., Stieber, M., and Weltmann, K. D. (2008) PLASMOSE – antimicrobial effects of modular atmospheric plasma sources. *GMS Krankenhhyg Interdiszip* **3**: Doc14.
- Ehlbeck, J., Schnabel, U., Polak, M., Winter, J., von Woedtke, T., Brandenburg, R., et al. (2011) Low temperature atmospheric pressure plasma sources for microbial decontamination. *J Phys D Appl Phys* **44**: 013002.
- Ermolaeva, S.A., Sysolyatina, E.V., and Gintsburg, A.L. (2015) Atmospheric pressure nonthermal plasmas for bacterial biofilm prevention and eradication. *Biointerphases* **10**: 029404.
- European Centre for Disease Prevention and Control, and European Food Safety Authority (2017) The European Union summary report on trends and sources of zoonoses, zoonotic agents and food-borne outbreaks in 2016. *EFSA J* **15**: 228.
- Flynn, P.B., Higginbotham, S., Alshraideh, N.H., Gorman, S.P., Graham, W.G., and Gilmore, B.F. (2015) Bactericidal efficacy of atmospheric pressure non-thermal plasma (APNTP) against the ESKAPE pathogens. *Int J Antimicrob Agents* **46**: 101–107.
- Fricke, K., Koban, I., Tresp, H., Jablonowski, L., Schroder, K., Kramer, A., et al. (2012) Atmospheric pressure plasma: a high-performance tool for the efficient removal of biofilms. *PLoS ONE* **7**: e42539.
- Fridman, G., Friedman, G., Gutsol, A., Shekhter, A.B., Vasilets, V.N., and Fridman, A. (2008) Applied plasma medicine. *Plasma Processes Polym* **5**: 503–533.
- Ghaffari, A., Jalili, R., Ghaffari, M., Miller, C., and Ghahary, A. (2007) Efficacy of gaseous nitric oxide in the treatment of skin and soft tissue infections. *Wound Repair Regen* **15**: 368–377.
- Gilmore, B.F., Flynn, P.B., O'Brien, S., Hickok, N., Freeman, T., and Bourke, P. (2018) Cold plasmas for biofilm control: opportunities and challenges. *Trends Biotechnol* **36**: 627–638.
- Goree, J., Liu, B., Drake, D., and Stoffels, E. (2006) Killing of S-mutans bacteria using a plasma needle at atmospheric pressure. *IEEE Trans Plasma Sci* **34**: 1317–1324.
- Gränicher, W.H.H. (1994) Messung beendet – was nun? *Hochschulverlag AG der ETH Zürich* 6-4-6-9.
- Handorf, O., Weihe, T., Bekeschus, S., Graf, A.C., Schnabel, U., Riedel, K., and Ehlbeck, J. (2018) Non-thermal plasma jet treatment negatively affects viability and structure of *C. albicans* SC5314 biofilms. *Appl Environ Microbiol*. **84**: e01163-18.
- Herald, P.J., and Zottola, E.A. (1988) Attachment of listeria-monoxytogenes to stainless-steel surfaces at various temperatures and pH values. *J Food Sci* **53**: 1549.
- Isbary, G., Morfill, G., Schmidt, H.U., Georgi, M., Ramrath, K., Heinlin, J., et al. (2010) A first prospective randomized controlled trial to decrease bacterial load using cold atmospheric argon plasma on chronic wounds in patients. *Br J Dermatol* **163**: 78–82.
- Jang, H.C., Rusconi, R., and Stocker, R. (2017) Biofilm disruption by an air bubble reveals heterogeneous age-dependent detachment patterns dictated by initial extracellular matrix distribution. *NPJ Biofilms Microbiomes* **3**: 6.
- Jia, H.J., Kuraseko, H., and Kondo, M. (2008) A microwave-induced plasma source: characterization and application for the fast deposition of crystalline silicon films. *J Appl Phys* **103**: 024904.
- Jovicevic, S., Ivkovic, M., Pavlovic, Z., and Konjevic, N. (2000) Parametric study of an atmospheric pressure microwave-induced plasma of the mini MIP torch – I. Two-dimensional spatially resolved electron-number density measurements. *Spectrochim Acta B Atomic Spectroscopy* **55**: 1879–1893.
- Jutkina, J., Marathe, N.P., Flach, C.F., and Larsson, D.G.J. (2018) Antibiotics and common antibacterial biocides stimulate horizontal transfer of resistance at low concentrations. *Sci Total Environ* **616**: 172–178.
- Kabir, M.A., Hussain, M.A., and Ahmad, Z. (2012) *Candida albicans*: a model organism for studying fungal pathogens. *ISRN Microbiol* **2012**: 538694.

- Kerekes, E.B., Vidács, A., Jenei, J.T., Gömöri, C., Takó, M., Muthusamy, C., *et al.* (2015) Essential oils against bacterial biofilm formation and quorum sensing of food-borne pathogens and spoilage microorganisms. The Battle Against Microbial Pathogens: Basic Science, Technological Advances and Educational Programs 1.
- Khan, M.S.I., Lee, E.J., and Kim, Y.J. (2016) A submerged dielectric barrier discharge plasma inactivation mechanism of biofilms produced by *Escherichia coli* O157: H7, *Cronobacter sakazakii*, and *Staphylococcus aureus*. *Sci Rep* **6**: 37072.
- Kieft, I.E., Darios, D., Roks, A.J.M., and Stoffels, E. (2005) Plasma treatment of mammalian vascular cells: a quantitative description. *IEEE Trans Plasma Sci* **33**: 771–775.
- Kieft, I.E., Kurdi, M., and Stoffels, E. (2006) Reattachment and apoptosis after plasma-needle treatment of cultured cells. *IEEE Trans Plasma Sci* **34**: 1331–1336.
- Klampfl, T.G., Isbary, G., Shimizu, T., Li, Y.F., Zimmermann, J.L., Stolz, W., *et al.* (2012) Cold atmospheric air plasma sterilization against spores and other microorganisms of clinical interest. *Appl Environ Microbiol* **78**: 5077–5082.
- Koban, I., Matthes, R., Hubner, N.O., Welk, A., Meisel, P., Holtfreter, B., *et al.* (2010) Treatment of *Candida albicans* biofilms with low-temperature plasma induced by dielectric barrier discharge and atmospheric pressure plasma jet. *New J Phys* **12**: 073039.
- Koban, I., Holtfreter, B., Hubner, N.O., Matthes, R., Sietmann, R., Kindel, E., *et al.* (2011) Antimicrobial efficacy of non-thermal plasma in comparison to chlorhexidine against dental biofilms on titanium discs in vitro – proof of principle experiment. *J Clin Periodontol* **38**: 956–965.
- Kumar, C.G., and Anand, S.K. (1998) Significance of microbial biofilms in food industry: a review. *Int J Food Microbiol* **42**: 9–27.
- Lademann, J., Ulrich, C., Patzelt, A., Richter, H., Kluschke, F., Klebes, M., *et al.* (2013) Risk assessment of the application of tissue-tolerable plasma on human skin. *Clin Plasma Med* **1**: 5–10.
- LaFleur, M.D., Kumamoto, C.A., and Lewis, K. (2006) *Candida albicans* biofilms produce antifungal-tolerant persister cells. *Antimicrob Agents Chemother* **50**: 3839–3846.
- Laroussi, M., Alexeff, I., and Kang, W.L. (2000) Biological decontamination by nonthermal plasmas. *IEEE Trans Plasma Sci* **28**: 184–188.
- Laroussi, M., Mendis, D.A., and Rosenberg, M. (2003) Plasma interaction with microbes. *New J Phys* **5**: 41.
- Liguori, A., Cochis, A., Stancampiano, A., Laurita, R., Azzi-monti, B., Sorrentino, R., *et al.* (2017) Cold atmospheric plasma treatment affects early bacterial adhesion and decontamination of soft relined palatal obturators. *Clinical Plasma Medicine* **7–8**: 36–45.
- Liu, Y., and Tay, J.H. (2002) The essential role of hydrodynamic shear force in the formation of biofilm and granular sludge. *Water Res* **36**: 1653–1665.
- Lorenzini, M., Simonato, B., Slaghenaufi, D., Ugliano, M., and Zapparoli, G. (2019) Assessment of yeasts for apple juice fermentation and production of cider volatile compounds. *Lwt Food Sci Technol* **99**: 224–230.
- Loureiro, V., and Malfeito-Ferreira, M. (2003) Spoilage yeasts in the wine industry. *Int J Food Microbiol* **86**: 23–50.
- Machala, Z., Chladekova, L., and Pelach, M. (2010) Plasma agents in bio-decontamination by dc discharges in atmospheric air. *J Phys D Appl Phys* **43**: 222001.
- Mafu, A.A., Roy, D., Goulet, J., and Magny, P. (1990) Attachment of listeria-monocytogenes to stainless-steel, glass, polypropylene, and rubber surfaces after short contact times. *J Food Prot* **53**: 742–746.
- Maisch, T., Shimizu, T., Isbary, G., Heinlin, J., Karrer, S., Klampfl, T.G., *et al.* (2012) Contact-free inactivation of *Candida albicans* biofilms by cold atmospheric air plasma. *Appl Environ Microbiol* **78**: 4242–4247.
- Mann, M.S., Schnabel, U., Weihe, T., Weltmann, K.D., and Woedtke, T. (2015) A reference technique to compare the antimicrobial properties of atmospheric pressure plasma sources. *Plasma Med* **5**: 27–47.
- Meireles, A., Borges, A., Giaouris, E., and Simoes, M. (2016) The current knowledge on the application of anti-biofilm enzymes in the food industry. *Food Res Int* **86**: 140–146.
- Misra, N.N., Tiwari, B.K., Raghavarao, K.S.M.S., and Cullen, P.J. (2011) Nonthermal plasma inactivation of food-borne pathogens. *Food Eng Rev* **3**: 159–170.
- Modic, M., McLeod, N.P., Sutton, J.M., and Walsh, J.L. (2017) Cold atmospheric pressure plasma elimination of clinically important single- and mixed-species biofilms. *Int J Antimicrob Agents* **49**: 375–378.
- Mohammed, R.K., and Abas, H.N. (2018) Bactericidal effect of needle plasma system on *Pseudomonas aeruginosa*. *Iran J Sci Technol* **42**: 1725–1733.
- Morata, A., and Loira, I. (2017) *Yeast- Industrial Applications*. London, UK: Intech Open.
- Müller, S., Zahn, R.J., Koburger, T., and Weltmann, K.D. (2010) Smell reduction and disinfection of textile materials by dielectric barrier discharges. *Natural Science* **2**: 1044–1048.
- Niemira, B.A. (2012) Cold plasma decontamination of foods. *Ann Rev Food Sci Technol* **3**: 125–142.
- Nobile, C.J., and Johnson, A.D. (2015) *Candida albicans* biofilms and human disease. *Annu Rev Microbiol* **69(69)**: 71–92.
- Notermans, S., Dormans, J.A.M.A., and Mead, G.C. (1991) Contribution of surface attachment to the establishment of micro-organisms in food processing plants: a review. *J Bioadhesion Biofilm Res* **5**: 21–36.
- Oehmigen, K., Hähnel, M., Brandenburg, R., Wilke, C., Weltmann, K.D., and von Woedtke, T. (2010) The role of acidification for antimicrobial activity of atmospheric pressure plasma in liquids. *Plasma Processes Polym* **7**: 250–257.
- Offerhaus, B., Lackmann, J.W., Kogelheide, F., Bracht, V., Smith, R., Bibinov, N., *et al.* (2017) Spatially resolved measurements of the physical plasma parameters and the chemical modifications in a twin surface dielectric barrier discharge for gas flow purification. *Plasma Processes Polym* **14**: 1600255.
- Pei, X., Lu, X., Liu, J., Liu, D., Yang, Y., Ostrikov, K., *et al.* (2012) Inactivation of a 25.5 μm *Enterococcus faecalis* biofilm by a room-temperature, battery-operated, handheld air plasma jet. *J Phys D Appl Phys* **45**: 165205.
- Pietsch, G.J. (2001) Peculiarities of dielectric barrier discharges. *Contrib Plasma Phys* **41**: 620–628.

1048 O. Handorf et al.

- Pipa, A.V., Andrasch, M., Rackow, K., Ehlbeck, J., and Weltmann, K.D. (2012) Observation of microwave volume plasma ignition in ambient air. *Plasma Sources Sci Technol* **21**: 035009.
- Ramamurthy, T., Ghosh, A., Pazhani, G.P., and Shinoda, S. (2014) Current perspectives on viable but non-culturable (VBNC) pathogenic bacteria. *Front Public Health* **2**: 103.
- Saprykina, M.N., Bolgova, E.S., and Goncharuk, V.V. (2016) Formation of viable noncultural state of *Candida albicans*. *J Water Chem Technol* **38**: 181–185.
- Sarangapani, C., Patange, A., Bourke, P., Keener, K., and Cullen, P.J. (2018) Recent advances in the application of cold plasma technology in foods. *Ann Rev Food Sci Technol* **9**: 609–629.
- Schnabel, U., Andrasch, M., Weltmann, K.D., and Ehlbeck, J. (2014) Inactivation of vegetative microorganisms and *Bacillus atrophaeus* endospores by reactive nitrogen species (RNS). *Plasma Processes Polym* **11**: 110–116.
- Schnabel, U., Handorf, O., Yarova, K., Zessin, B., Zechlin, S., Sydow, D., et al (2019) Plasma-treated air and water-assessment of synergistic antimicrobial effects for sanitation of food processing surfaces and environment. *Foods* **8**: 55.
- Scholtz, V., Pazlarova, J., Souskova, H., Khun, J., and Julak, J. (2015) Nonthermal plasma – a tool for decontamination and disinfection. *Biotechnol Adv* **33**: 1108–1119.
- Scudiero, D.A., Shoemaker, R.H., Paull, K.D., Monks, A., Tierney, S., Nofziger, T.H., et al (1988) Evaluation of a soluble tetrazolium formazan assay for cell-growth and drug sensitivity in culture using human and other tumor-cell lines. *Can Res* **48**: 4827–4833.
- Serra, E., Hidalgo-Bastida, L.A., Verran, J., Williams, D., and Malic, S. (2017) Antifungal activity of commercial essential oils and biocides against *Candida albicans*. *Pathogens* **7**: 15.
- Shekhter, A.B., Serezhenkov, V.A., Rudenko, T.G., Pekshev, A.V., and Vanin, A.F. (2005) Beneficial effect of gaseous nitric oxide on the healing of skin wounds. *Nitric Oxide Biol Chem* **12**: 210–219.
- Simor, M., Creighton, Y., Wypkema, A., and Zemek, J. (2010) The influence of surface DBD plasma treatment on the adhesion of coatings to high-tech textiles. *J Adhes Sci Technol* **24**: 77–97.
- Sladek, R.E.J., Stoffels, E., Walraven, R., Tielbeek, P.J.A., and Koolhoven, R.A. (2004) Plasma treatment of dental cavities: a feasibility study. *IEEE Trans Plasma Sci* **32**: 1540–1543.
- Sladek, R.E.J., Filoche, S.K., Sissons, C.H., and Stoffels, E. (2007) Treatment of *Streptococcus mutans* biofilms with a nonthermal atmospheric plasma. *Lett Appl Microbiol* **45**: 318–323.
- de Souza, I.A., Neto, A.B.D., de Queiroz, J.C.A., Mataromos, E.P., Costa, T.H.D., Feitor, M.C., et al. (2016) Study of the influence of variation in distances between electrodes in spectral DBD plasma excitation. *Mater Res Ibero-Am J Mater* **19**: 202–206.
- Steenackers, H.P., Parijs, I., Dubey, A., Foster, K.R., and Vanderleyden, J. (2016) Experimental evolution in biofilm populations. *FEMS Microbiol Rev* **40**: 980–980.
- Stoffels, E., Flikweert, A.J., Stoffels, W.W., and Kroesen, G.M.W. (2002) Plasma needle: a non-destructive atmospheric plasma source for fine surface treatment of (bio)-materials. *Plasma Sources Sci Technol* **11**: 383–388.
- Sun, Y., Yu, S., Sun, P., Wu, H.Y., Zhu, W.D., Liu, W., et al (2012) Inactivation of candida biofilms by non-thermal plasma and its enhancement for fungistatic effect of antifungal drugs. *PLoS ONE* **7**: e40629.
- Surowsky, B., Schlüter, O., and Knorr, D. (2015) Interactions of non-thermal atmospheric pressure plasma with solid and liquid food systems: a review. *Food Eng Rev* **7**: 82–108.
- Thirumdas, R., Kothakota, A., Annapure, U., Siliveru, K., Blundell, R., Gatt, R., and Valdramidis, V.P. (2018) Plasma activated water (PAW): chemistry, physico-chemical properties, applications in food and agriculture. *Trends Food Sci Technol* **77**: 21–31.
- Tippayawong, N., Chaiya, E., Thanompongchart, P., and Khongkrapan, P. (2015) Sustainable energy from biogas reforming in a microwave discharge reactor. *Proc Eng* **118**: 120–127.
- Traba, C., and Liang, J.F. (2015) The inactivation of *Staphylococcus aureus* biofilms using low-power argon plasma in a layer-by-layer approach. *Biofouling* **31**: 39–48.
- Walker, G.M., and Stewart, G.G. (2016) *Saccharomyces cerevisiae* in the production of fermented beverages. *Beverages* **2**: 30.
- Xu, L., Tu, Y., Yu, Y., Tan, M., Li, J., and Chen, H. (2011) Augmented survival of *Neisseria gonorrhoeae* within biofilms: exposure to atmospheric pressure non-thermal plasmas. *Eur J Clin Microbiol Infect Dis* **30**: 25–31.
- Xu, Z.M., Shen, J., Zhang, Z.L., Ma, J., Ma, R.H., Zhao, Y., et al. (2015) Inactivation effects of non-thermal atmospheric-pressure helium plasma jet on *Staphylococcus aureus* biofilms. *Plasma Processes Polym* **12**: 827–835.
- Xu, Z.M., Shen, J., Cheng, C., Hu, S.H., Lan, Y., and Chu, P.K. (2017) In vitro antimicrobial effects and mechanism of atmospheric-pressure He/O₂ plasma jet on *Staphylococcus aureus* biofilm. *J Phys D Appl Phys* **50**: 105201.
- Yusupov, M., Neyts, E.C., Khalilov, U., Snoeckx, R., van Duin, A.C.T., and Bogaerts, A. (2012) Atomic-scale simulations of reactive oxygen plasma species interacting with bacterial cell walls. *New J Phys* **14**: 093043.
- Ziuzina, D., Boehm, D., Patil, S., Cullen, P.J., and Bourke, P. (2015) Cold plasma inactivation of bacterial biofilms and reduction of quorum sensing regulated virulence factors. *PLoS ONE* **10**: e0138209.

8 Conclusions

Microbial biofilms represent one of the most severe burdens in both industry and health care. Their naturally enhanced tolerance against antimicrobial treatment and the host immunity – primarily caused by the shielding nature of the ECM acting as (diffusion) barrier – makes microbial biofilms nearly impossible to quantitatively eradicate. Thus, there is an urgent need to better understand ECM composition/architecture as well as biofilm physiology to ultimately be able to develop innovative treatment strategies. Consequently, the projects of this thesis addressed these problems from three different perspectives:

(I) We characterized the proteinaceous composition of the ECM formed by one of the most important biofilm-forming pathogen *S. aureus in vitro*. Here, we unraveled that alkaline proteins – primarily ribosomal proteins originating from cell lysis as well as actively secreted virulence factors – accumulate within the ECM and contribute to biofilm stability. Our data led to a model where these proteins get protonated due to the release of organic acids upon fermentation of biofilm-embedded cells, introducing positive charges. These positively charged proteins form an electrostatic network with negatively charged ECM components like eDNA, metabolites and cell surfaces, thereby stabilizing the ECM. Hence, targeting these proteins, e.g. using specific antibodies, proteases, or alkaline substances – eventually in combination with other antimicrobials - might open up new treatment options. Ideally, stabilizing ECM proteins can be inactivated/digested/masked in a first step, breaking down the shielding ECM, so the host immune system and other antimicrobials can eradicate the remaining biofilm cells in a second step. However, it remains to be unraveled if this stabilizing concept can also be observed in *in vivo* settings and among other *S. aureus* strains and biofilm-forming species. It is debatable if this stabilizing concept is an “active”, evolutionarily favorable mechanism, or if this is a passive, “random” accumulation of alkaline proteins within the ECM, which can easily be substituted. To answer these questions, the investigation of the ECM protein repertoire of *in vivo* biofilms, of different *S. aureus* strains, and of other biofilm-forming species would be insightful.

(II) Following the idea of investigating *in vivo* biofilms, we analyzed the microbial metaproteome in sputum samples of CF patients to gain insights into important pathophysiological properties of multi-species biofilms, which are key elements of disease progression. Since this metaproteome analysis is challenging due to various sputum characteristics, we developed an innovative and widely-applicable sputum processing protocol allowing microbial enrichment. Applying this protocol on three proof-of-concept sputum samples, we significantly increased microbial protein coverage and thereby unraveled that microbial proteases and the arginine deiminase pathway so far might have played an underappreciated role in CF research. Since understanding the (patho-)physiology of the multi-species CF community on protein level is

key to understand the disease and to find new treatment options, our results represent a fundamental basis for future studies. Here, the enrichment efficiency might be increased even more, and other protein extraction, purification, and digestion protocols could further improve protein coverage. Doing so could e.g. shed light on antimicrobial resistance mechanisms and might provide insights into new targets for antimicrobial therapy.

(III) Addressing the need for novel biofilm treatment strategies, we further tested the antibiofilm effect of two different nonthermal plasma sources on the important fungal biofilm-former *C. albicans*. Showing a strong inactivation effect, which is surprisingly pronounced on the bottom side of the biofilms, our studies reveal great potential for nonthermal plasma as an antibiofilm weapon in industry and health care. The inactivation of the bottom biofilm side has never been reported before and might open doors for the synergistic combination with other biofilm removal techniques (e.g. mechanical). This, in turn, might be even more effective regarding quantitative biofilm removal and could be of interest for many industrial settings (like the food industry) and health care settings like chronic wound treatment. However, further research is necessary to assess the antibiofilm potential and the applicability of nonthermal plasma to various other surfaces, to *in vivo* biofilms of other species, and to mixed-species biofilms *in vivo*.

9 References

1. **Flemming H-C, Wingender J.** 2010. The biofilm matrix. *Nature Reviews Microbiology* **8**:623–633.
 2. **Høiby N.** 2017. A short history of microbial biofilms and biofilm infections. *APMIS* **125**:272–275.
 3. **O'Toole GA, Kaplan HB, Kolter R.** 2000. Biofilm formation as microbial development. *Annu Rev Microbiology* **54**:49–79.
 4. **Henrici AT.** 1936. Studies of Freshwater Bacteria: III. Quantitative Aspects of the Direct Microscopic Method. *Journal of Bacteriology* **32**:265–280.
 5. **Zobell CE, Allen EC.** 1935. The Significance of Marine Bacteria in the Fouling of Submerged Surfaces. *Journal of Bacteriology* **29**:239–251.
 6. **H Heukelekian AH.** 1940. Relation between Food Concentration and Surface for Bacterial Growth. *Journal of Bacteriology* **40**:547.
 7. **Zobell CE.** 1943. The Effect of Solid Surfaces upon Bacterial Activity. *Journal of Bacteriology* **46**:39–56.
 8. **Donlan RM.** 2002. Biofilms: microbial life on surfaces. *Emerg Infect Dis* **8**:881–890.
 9. **López D, Vlamakis H, Kolter R.** 2010. Biofilms. *Cold Spring Harbor Perspectives in Biology* **2**:a000398–a000398.
 10. **Boudarel H, Mathias J-D, Blaysat B, Grédiac M.** 2018. Towards standardized mechanical characterization of microbial biofilms: analysis and critical review. *npj Biofilms and Microbiomes* 1–15.
 11. **Satpathy S, Sen SK, Pattanaik S, Raut S.** 2016. Review on bacterial biofilm_ An universal cause of contamination. *Biocatalysis and Agricultural Biotechnology* **7**:56–66.
 12. **Jefferson K.** 2004. What drives bacteria to produce a biofilm? *FEMS Microbiol Lett* **236**:163–173.
 13. **Rice KC, Bayles KW.** Death's toolbox: examining the molecular components of bacterial programmed cell death. *Wiley Online Library*.
 14. **Vuotto C, Donelli G.** 2019. Novel Treatment Strategies for Biofilm-Based Infections. *Drugs* 1–21.
 15. **Rumbaugh KP, Sauer K.** 2020. Biofilm dispersion. *Nature Reviews Microbiology* 1–16.
 16. **Vasudevan R.** 2014. Biofilms: Microbial Cities of Scientific Significance. *JMEN* **1**:1–4.
 17. **Berlanga M, Guerrero R.** 2016. Living together in biofilms: the microbial cell factory and its biotechnological implications. *Microbial Cell Factories* 1–11.
-

-
18. **McDougald D, Rice SA, Barraud N, Steinberg PD, Kjelleberg S.** 2011. Should we stay or should we go: mechanisms and ecological consequences for biofilm dispersal. *Nature Reviews Microbiology* **10**:39–50.
 19. **Kostakioti M, Hadjifrangiskou M, Hultgren SJ.** 2013. Bacterial biofilms: development, dispersal, and therapeutic strategies in the dawn of the postantibiotic era. *Cold Spring Harbor Perspectives in Medicine* **3**:a010306–a010306.
 20. **Stoodley P, Hall Stoodley L, Costerton B, DeMeo P, Shirliff M, Gawalt E, Kathju S.** 2013. *Biofilms, Biomaterials, and Device-Related Infections Handbook of Polymer Applications in Medicine and Medical Devices.* Elsevier Inc.
 21. **Otto M.** 2008. Staphylococcal biofilms. *Curr Top Microbiol Immunol* **322**:207–228.
 22. **Donlan RM, Costerton JW.** 2002. Biofilms: survival mechanisms of clinically relevant microorganisms. *Clin Microbiol Reviews* **15**:167–193.
 23. **Graf AC, Leonard A, Schäuble M, Rieckmann LM, Hoyer J, Maaß S, Lalk M, Becher D, Pané-Farré J, Riedel K.** 2019. Virulence Factors Produced by *Staphylococcus aureus* Biofilms Have a Moonlighting Function Contributing to Biofilm Integrity. *Mol Cell Proteomics* **18**:1036–1053.
 24. **Petrova OE, Sauer K.** 2016. Escaping the biofilm in more than one way: desorption, detachment or dispersion. *Current Opinion in Microbiology* **30**:67–78.
 25. **Verderosa AD, Totsika M, Fairfull-Smith KE.** 2019. Bacterial Biofilm Eradication Agents: A Current Review. *Front Chem* **7**:5076–17.
 26. **Brindhadevi K, LewisOscar F, Mylonakis E, Shanmugam S, Verma TN, Pugazhendhi A.** 2020. Biofilm and Quorum sensing mediated pathogenicity in *Pseudomonas aeruginosa*. *Process Biochemistry* **96**:49–57.
 27. **Karygianni L, Ren Z, Koo H, Thurnheer T.** 2020. Biofilm Matrixome: Extracellular Components in Structured Microbial Communities. *Trends Microbiol* **28**:668–681.
 28. **Rabin N, Zheng Y, Opoku-Temeng C, Du Y, Bonsu E, Sintim HO.** 2015. Biofilm formation mechanisms and targets for developing antibiofilm agents. *Future Medicinal Chemistry* **7**:493–512.
 29. **Koo H, Allan RN, Howlin RP, Stoodley P, Hall Stoodley L.** 2017. Targeting microbial biofilms: current and prospective therapeutic strategies. *Nature Reviews Microbiology* **1**–16.
 30. **Orazi G, O'Toole GA.** 2019. “It Takes a Village”: Mechanisms Underlying Antimicrobial Recalcitrance of Polymicrobial Biofilms. *Journal of Bacteriology* **202**:277–18.
 31. **Poulsen LV.** 1999. Microbial Biofilm in Food Processing. *LWT - Food Science and Technology* **32**:321–326.
 32. **Bixler GD, Bhushan B.** 2012. Biofouling: lessons from nature. *Phil Trans R Soc A* **370**:2381–2417.
 33. **Mattila Sandholm T, Wirtanen G.** 1992. Biofilm formation in the industry: A review. *Food Reviews International* **8**:573–603.
-

-
34. **Flemming H-C, Wingender J, Szewzyk U, Steinberg P, Rice SA, Kjelleberg S.** 2016. Biofilms: an emergent form of bacterial life. *Nature Reviews Microbiology* **14**:563–575.
 35. **Handorf O, Weihe T, Bekeschus S, Graf AC, Schnabel U, Riedel K, Ehlbeck J.** 2018. Nonthermal Plasma Jet Treatment Negatively Affects the Viability and Structure of *Candida albicans* SC5314 Biofilms. *Applied and Environmental Microbiology* **84**:1054–15.
 36. **Handorf O, Schnabel U, Bösel A, Weihe T, Bekeschus S, Graf AC, Riedel K, Ehlbeck J.** 2019. Antimicrobial effects of microwave-induced plasma torch (MiniMIP) treatment on *Candida albicans* biofilms. *Microb Biotechnol* **12**:1034–1048.
 37. **Mihai M, Holban A, Giurcaneanu C, Popa L, Oanea R, Lazar V, Chifiriuc M, Popa M, Popa M.** 2015. Microbial Biofilms: Impact on the Pathogenesis of Periodontitis, Cystic Fibrosis, Chronic Wounds and Medical Device-Related Infections. *CTMC* **15**:1552–1576.
 38. **Kovach K, Davis-Fields M, Irie Y, Jain K, Doorwar S, Vuong K, Dhamani N, Mohanty K, Touhami A, Gordon VD.** 2017. Evolutionary adaptations of biofilms infecting cystic fibrosis lungs promote mechanical toughness by adjusting polysaccharide production. *npj Biofilms and Microbiomes* **3**:1–9.
 39. **Lebeaux D, Ghigo J-M, Beloin C.** 2014. Biofilm-related infections: bridging the gap between clinical management and fundamental aspects of recalcitrance toward antibiotics. *Microbiol Mol Biol Rev* **78**:510–543.
 40. **Floyd KA, Eberly AR, Hadjifrangiskou M.** 2016. Adhesion of bacteria to surfaces and biofilm formation on medical devices. *Biofilms and Implantable Medical Devices*. Elsevier Ltd.
 41. **O’Sullivan BP, Freedman SD.** 2009. Cystic fibrosis. *The Lancet* **373**:1891–1904.
 42. **Chmiel JF, Davis PB.** 2003. State of the art: why do the lungs of patients with cystic fibrosis become infected and why can't they clear the infection? *Respiratory Research* **4**:8.
 43. **Ratjen FA.** 2009. Cystic fibrosis: pathogenesis and future treatment strategies. *Respiratory Care* **54**:595–605.
 44. **Rogers GB, Carroll M, Hoffman L, Walker A, Fine D, Bruce K.** 2014. Comparing the microbiota of the cystic fibrosis lung and human gut. *Gut Microbes*, 3rd ed. **1**:85–93.
 45. **Filkins LM, O’Toole GA.** 2015. Cystic Fibrosis Lung Infections: Polymicrobial, Complex, and Hard to Treat. *PLoS Pathogens* **11**:e1005258–8.
 46. **Cystic Fibrosis Foundation.** 2020. 2019 Patient Registry Annual Data Report 1–92.
 47. **Harrison F.** 2007. Microbial ecology of the cystic fibrosis lung. *Microbiology* **153**:917–923.
-

-
48. **Verderosa AD, Totsika M, Fairfull-Smith KE.** 2019. Bacterial Biofilm Eradication Agents: A Current Review. *Front Chem* **7**:5076–17.
 49. **Folkesson A, Jelsbak L, Yang L, Johansen HK, Ciofu O, Molin S.** 2012. Adaptation of *Pseudomonas aeruginosa* to the cystic fibrosis airway: an evolutionary perspective. *Nature Reviews Microbiology* **10**:841–851.
 50. **Goss CH, Muhlebach MS.** 2011. Review: *Staphylococcus aureus* and MRSA in cystic fibrosis. *Journal of Cystic Fibrosis* **10**:298–306.
 51. **Goerke C, Wolz C.** 2010. Adaptation of *Staphylococcus aureus* to the cystic fibrosis lung. *International Journal of Medical Microbiology* **300**:520–525.
 52. **Kluytmans JAJW, vanBelkum A, Verbrugh H.** 1997. Nasal carriage of *Staphylococcus aureus*: Epidemiology, underlying mechanisms, and associated risks. *Clin Microbiol Reviews* **10**:505–.
 53. **Lee AS, de Lencastre H, Garau J, Kluytmans JAJW, Malhotra-Kumar S, Peschel A, Harbarth S.** 2018. Methicillin-resistant *Staphylococcus aureus*. *Nature Reviews Microbiology* **4**:1–23.
 54. **Plata K, Rosato AE, Wegrzyn G.** 2009. *Staphylococcus aureus* as an infectious agent: overview of biochemistry and molecular genetics of its pathogenicity. *Acta Biochim Pol* **56**:597–612.
 55. **Tong SYC, Davis JS, Eichenberger E, Holland TL, Fowler VG Jr.** 2015. *Staphylococcus aureus* Infections: Epidemiology, Pathophysiology, Clinical Manifestations, and Management. *Clin Microbiol Reviews* **28**:603–661.
 56. **Lister JL, Horswill AR.** 2014. *Staphylococcus aureus* biofilms: recent developments in biofilm dispersal. *Front Cell Infect Microbiol* **4**:178.
 57. **Serra R, Grande R, Butrico L, Rossi A, Settimo UF, Caroleo B, Amato B, Gallelli L, de Franciscis S.** 2015. Chronic wound infections: the role of *Pseudomonas aeruginosa* and *Staphylococcus aureus*. *Expert Review of Anti-infective Therapy* **13**:000–000.
 58. **Thomer L, Schneewind O, Missiakas D.** 2016. Pathogenesis of *Staphylococcus aureus* Bloodstream Infections. *Annu Rev Pathol Mech Dis* **11**:343–364.
 59. **Klevens RM, Morrison MA, Nadle J, Petit S, Gershman K, Ray S, Harrison LH, Lynfield R, Dumyati G, Townes JM, Craig AS, Zell ER, Fosheim GE, McDougal LK, Carey RB, Fridkin SK, Investigators AM.** 2007. Invasive methicillin-resistant *Staphylococcus aureus* infections in the United States. *JAMA* **298**:1763–1771.
 60. **Turner NA, Sharma-Kuinkel BK, Maskarinec SA, Eichenberger EM, Shah PP, Carugati M, Holland TL, Fowler VG.** 2019. Methicillin-resistant *Staphylococcus aureus*: an overview of basic and clinical research. *Nature Reviews Microbiology* **1**–16.
 61. **Balasubramanian D, Harper L, Shopsin B, Torres VJ.** 2017. *Staphylococcus aureus* pathogenesis in diverse host environments. *Pathogens Disease* ftx005–13.
 62. **Bien J, Sokolova O, Bozko P.** 2011. Characterization of Virulence Factors of *Staphylococcus aureus*: Novel Function of Known Virulence Factors That Are
-

-
- Implicated in Activation of Airway Epithelial Proinflammatory Response. *Journal of Pathogens* **2011**:1–13.
63. **Plata K, Rosato AE, Wegrzyn G.** 2009. Staphylococcus aureus as an infectious agent: overview of biochemistry and molecular genetics of its pathogenicity. *Acta Biochim Pol* **56**:597–612.
64. **Corrigan RM, Miajlovic H, Foster TJ.** 2009. Surface proteins that promote adherence of Staphylococcus aureus to human desquamated nasal epithelial cells. *BMC Microbiology* **9**:22–10.
65. **Foster TJ, Geoghegan JA, Ganesh VK, Höök M.** 2014. Adhesion, invasion and evasion: the many functions of the surface proteins of Staphylococcus aureus. *Nature Reviews Microbiology* **12**:49–62.
66. **Peschel A, Otto M.** 2013. Phenol-soluble modulins and staphylococcal infection. *Nature Reviews Microbiology* **11**:667–673.
67. **Smith EJ, Visai L, Kerrigan SW, Speziale P, Foster TJ.** 2011. The Sbi protein is a multifunctional immune evasion factor of Staphylococcus aureus. *Infection and Immunity* **79**:3801–3809.
68. **Gaupp R, Ledala N, infection GSFICA.** Staphylococcal response to oxidative stress. *frontiersinorg.*
69. **Olivier AC, Lemaire S, Van Bambeke F, Tulkens PM, Oldfield E.** 2009. Role of rsbU and Staphyloxanthin in Phagocytosis and Intracellular Growth of Staphylococcus aureus in Human Macrophages and Endothelial Cells. *The Journal of Infectious Diseases* **200**:1367–1370.
70. **Proctor RA, Eiff von C, Kahl BC, Becker K, McNamara P, Herrmann M, Peters G.** 2006. Small colony variants: a pathogenic form of bacteria that facilitates persistent and recurrent infections. *Nature Reviews Microbiology* **4**:295–305.
71. **Moormeier DE, Bose JL, Horswill AR, Bayles KW.** 2014. Temporal and Stochastic Control of Staphylococcus aureus Biofilm Development **5**:e01341–14–e01341–14.
72. **Archer NK, Mazaitis MJ, Costerton JW, Leid JG, Powers ME, Shirtliff ME.** 2014. Staphylococcus aureus biofilms. *Virulence* **2**:445–459.
73. **Zapotoczna M, O'Neill E, O'Gara JP.** 2016. Untangling the Diverse and Redundant Mechanisms of Staphylococcus aureus Biofilm Formation. *PLoS Pathogens* **12**:e1005671–6.
74. **Figueiredo AMS, Ferreira FA, Beltrame CO, Côrtes MF.** 2016. The role of biofilms in persistent infections and factors involved in ica-independent biofilm development and gene regulation in Staphylococcus aureus. *Critical Reviews in Microbiology* **43**:602–620.
75. **Foulston L, Elsholz AKW, DeFrancesco AS, Losick R.** 2014. The Extracellular Matrix of Staphylococcus aureus Biofilms Comprises Cytoplasmic Proteins That Associate with the Cell Surface in Response to Decreasing pH **5**:e01667–14–e01667–14.
-

76. **Lindsay AK, Hogan DA.** 2014. *Candida albicans*: Molecular interactions with *Pseudomonas aeruginosa* and *Staphylococcus aureus*. *Fungal Biology Reviews* **28**:85–96.
77. **Lohse MB, Gulati M, Johnson AD, Nobile CJ.** 2017. Development and regulation of single- and multi-species *Candida albicans* biofilms. *Nature Reviews Microbiology* **16**:19–31.
78. **Shak S, Capon DJ, Hellmiss R, Marsters SA, Baker CL.** 1990. Recombinant human DNase I reduces the viscosity of cystic fibrosis sputum. *PNAS* **87**:9188–9192.
79. **López M.** 2019. A Review on Nonthermal Atmospheric Plasma for Food Preservation: Mode of Action, Determinants of Effectiveness, and Applications 1–21.

10 Eigenständigkeitserklärung

Hiermit erkläre ich, dass diese Arbeit bisher von mir weder an der Mathematisch-Naturwissenschaftlichen Fakultät der Universität Greifswald noch einer anderen wissenschaftlichen Einrichtung zum Zwecke der Promotion eingereicht wurde.

Ferner erkläre ich, dass ich diese Arbeit selbstständig verfasst und keine anderen als die darin angegebenen Hilfsmittel und Hilfen benutzt und keine Textabschnitte eines Dritten ohne Kennzeichnung übernommen habe.

Ort, Datum

Unterschrift des Promovenden

11 *Curriculum Vitae*

Due to data privacy, the Curriculum Vitae has been removed.

Due to data privacy, the Curriculum Vitae has been removed.

12 List of Publications

12.1 Peer-reviewed publications

- 08/2021 An innovative protocol for metaproteomic analyses of microbial pathogens in cystic fibrosis sputum
A. C. Graf, J. Striesow, J. Pané-Farré, T. Sura, M. Wurster, D. H. Pieper, M. Lalk, D. Becher, B. Kahl, K. Riedel, *Frontiers in Cellular & Infection Microbiology*
- 09/2019 Antimicrobial effects of microwave-induced plasma torch (MiniMIP) treatment on *Candida albicans* biofilms
O. Handorf, U. Schnabel, A. Bösel, T. Weihe, S. Bekeschus, A. C. Graf, K. Riedel, J. Ehlbeck, *Microbial Biotechnology*
- 03/2019 Virulence factors produced by *Staphylococcus aureus* biofilms have a moonlighting function contributing to biofilm integrity
A. C. Graf, A. Leonard, M. Schäuble, L. M. Rieckmann, J. Hoyer, S. Maaß, M. Lalk, D. Becher, J. Panè-Farrè, K. Riedel, *Molecular and Cellular Proteomics*
- 08/2018 Nonthermal plasma jet treatment negatively affects viability and structure of *C. albicans* SC5314 biofilms
O. Handorf, T. Weihe, S. Bekeschus, A. C. Graf, U. Schnabel, K. Riedel, J. Ehlbeck, *Applied and Environmental Microbiology*

12.2 Oral Presentations

- 07/2018 Nonthermal plasma jet treatment negatively affects viability and structure of *C. albicans* SC5314 biofilms
O. Handorf, T. Weihe, S. Bekeschus, A. C. Graf, U. Schnabel, K. Riedel, J. Ehlbeck, International conference on antimicrobial research, Torremolinos, Málaga
- 05/2018 Panoramic view on *Staphylococcus aureus* biofilm physiology
A. C. Graf, A. Leonard, M. Schäuble, L. M. Rieckmann, J. Hoyer, S. Maaß, M. Lalk, D. Becher, J. Panè-Farrè, K. Riedel
Eingeladener Redner, eingeladen von Dr. Geddes-McAlister und Dr. Cezar Khursigara, Institut für Molekular- und Zellbiologie, Universität Guelph, Kanada
-

04/2018 Panoramic view on *Staphylococcus aureus* biofilm physiology
A. C. Graf, A. Leonard, M. Schäuble, L. M. Rieckmann, J. Hoyer, S. Maaß, M. Lalk,
D. Becher, J. Panè-Farrè, K. Riedel, VAAM-Jahrestagung, Wolfsburg

12.3 Poster Presentations

11/2017 Panoramic view on *Staphylococcus aureus* biofilm physiology
A. C. Graf, A. Leonard, S. Maaß, C. Hirschfeld, J. Hoyer, M. Lalk, D. Becher,
K. Riedel, 1st International Conference on Respiratory Pathogens, Rostock

2014-2017 Panoramic view on *Staphylococcus aureus* biofilm physiology
A. C. Graf, A. Leonard, S. Maaß, C. Hirschfeld, J. Hoyer, M. Lalk, D. Becher,
K. Riedel, VAAM-Jahrestagung, Dresden, Marburg, Jena, Würzburg

09/2016 Panoramic view on *Staphylococcus aureus* biofilm physiology
A. C. Graf, A. Leonard, M. Schäuble, L. M. Rieckmann, J. Hoyer, S. Maaß, M. Lalk,
D. Becher, J. Panè-Farrè, K. Riedel, 3rd International Conference on the
Pathophysiology of Staphylococci, Tübingen

13 Acknowledgements

This thesis would not have been possible without the support of numerous people. Here, I want to offer my most sincere gratitude to all of these people who supported me throughout my Ph.D. thesis.

First of all, I would like to thank my supervisor Prof. Katharina Riedel, who introduced me to the tremendous field of microbial biofilm research and guided me supportively not only throughout my Ph.D. thesis, but already since my Bachelor thesis.

Furthermore, I want to thank Dr. Jan Pané-Farré, my co-supervisor, who phenomenally supported my projects by fruitful discussions, ideas, and advice.

Moreover, I sincerely want to thank Prof. Michael Hecker. Back in the fourth semester of my Bachelor studies, I had the chance to follow his outstanding lectures about microbial physiology, which engaged me so much that these lectures literally paved the way for developing my passion for microbiological research.

The results of this Ph.D. thesis would never have been achieved without the fruitful support of various collaboration partners. Therefore, I am very grateful to Prof. Dörte Becher, Prof. Michael Lalk, Prof. Barbara Kahl, Dr. Jörg Ehlbeck, Prof. Dietmar Pieper, and of course to the members of their respective teams. Here, I especially want to thank Sandra Maaß, Tobias Kroniger, Thomas Sura, Juliane Hoyer, Jürgen Bartel, Anne Leonard, Martina Wurster, Oliver Handorf, Uta Schnabel, and Thomas Weihe.

Also, I would like to thank several (former) members of the Institute of Microbiology, I was able to learn from, who helped me a lot throughout my Ph.D. thesis, and who significantly contributed to the amazing working environment. Especially, I want to thank Susanne Sievers, Christian Lassek, Daniela Zühlke, Jörg Bernhard, Ulf Gerth, Heike Schmidt, Rabea Schlüter, Susanne Gebauer, and Anke Arelt. Moreover, I want to thank Christian Wolff, Anne and Daniel Troitzsch, Madita Brauer, Lars Lilge, Larin Gierse, and Tjorven Hinzke for the wonderful time as Ph.D. students, the help and the vital discussions. Also, I want to thank my former Bachelor and Master students, who significantly contributed to the progress of my Ph.D thesis – I really enjoyed supervising you: Manuel Schäuble, Florentin Holzem, Lisa Rieckmann, Doreen Schultz, Julia Berner, and Johanna Striesow.

Beyond that, I want to deeply thank my family and friends - my parents for giving me “roots to grow and wings to fly”, my little brother for being even more than my best friend, my actual best friends and their families, and – most importantly – my own family. The love I feel for my beautiful wife Anica and my amazing little daughters Lia and Eva, and the love and support I receive from you every day is beyond words.